UNIVERSITY OF MINING AND GEOLOGY
"ST. IVAN RILSKI"

JOURNAL

OF

MINING AND GEOLOGICAL

SCIENCES

Volume 62

Number 3

Sofia 2019

University of Mining and Geology "St. Ivan Rilski"
1, Prof. Boyan Kamenov Str., 1700 Sofia, Bulgaria
http://www.mgu.bg

ISSN 2682-9525 (print)
ISSN 2683-0027 (online)

www.mgu.bg/new/journal

CONTENTS

ANALYSIS OF STRENGTH AND DEFORMATION OF PARABOLIC LEAF SPRINGS FOR TRANSPORT EQUIPMENT

Dobrinka Atmadzhova

Todor Kableshkov University of Transport, 1574 Sofia; atmadzhova@abv.bg

ABSTRACT: Modelling and comparative strength analysis of different structures of parabolic leaf springs are carried out in this paper. They are used in the suspension structures of transport equipment. For example, it includes wagons for transport of ore, coal and other bulk cargo as well as many trucks. Statistical results of many operational observations of the suspension elements of railway wagons and trucks up to their failure status are reflected. The loads and strength characteristics of different types of parabolic leaf springs are described. They were modelled by the Finite Element Method (FEM) and after that a comparative strength analysis using modern software packages is performed.

Keywords: transport equipment, spring suspension, leaf springs, failures in parabolic leaf springs, strength analysis, Finite Element Method

ЯКОСТНО-ДЕФОРМАЦИОНЕН АНАЛИЗ НА КОНСТРУКЦИИ ПАРАБОЛИЧНИ ЛИСТОВИ РЕСОРИ ЗА ТРАНСПОРТНА ТЕХНИКА

Добринка Атмаджова
Висше транспортно училище "Тодор Каблешков", 1574 София

РЕЗЮМЕ: В доклада е извършено моделиране и сравнителен якостен анализ на различни конструкции параболични листови ресори. Те се използват в конструкцията на ресорното окачване на транспортна техника. Например, това са вагони за превоз на руда и други насипни товари, както и много товарни автомобили. Отразени са статистически резултати от експлоатационни наблюдения на елементи от ресорното окачване на железопътни вагони и товарни автомобили, до състоянието им на отказ. Описани са натоварванията и якостните характеристики на различни видове параболични листови ресори. Същите са моделирани по метода на крайните елементи, след което е извършен сравнителен якостен анализ с помощта на съвременни програмни продукти.

Ключови думи: транспортна техника, ресорно окачване, листови ресори, откази в параболични листови ресори, якостен анализ, метод на крайните елементи

Introduction

One of the most important parameters determining the reliability and safety of land vehicles running is the functionality of spring system (SS). The SS failure causes very serious consequences and in many cases leads to derailment. For this reason, the design and reliability of the vehicle SS are subjects of many documents including those related to fault detection and analysis of failures (Mateev, 1971; Fan et al., 2010; Yusuke et al., 2008; Kumbhalkar et al., 2011). The purpose of the above-mentioned studies is to identify potential problems and define constructive and technological solutions for improvement of existing or newly developed types of suspension (Kocev et al., 2018).

Fig. 1. A derailed wagon of Fbd type with spring suspension (leaf springs) owned by Nikola Tesla TPP in Obrenovac, Serbia and used for coal transportation

For example, such a system is the system used for rail coal transportation from Kolubara mining basin to Nikola Tesla Thermal Power Plant (TPP) in Obrenovac, Serbia. The transportation based on Fbd wagons is performed along one of the busiest industrial railway lines in Europe. Due to that and some peculiarities of the SS design based on leaf springs, this type of fractures often leads to derailment (Petrovic et al., 2012; 2014) (Fig. 1).

The consequences of derailments are with huge material damage and considerably reduce railway transport efficiency. Such problems are often encountered along many busy freight rail lines.

Each accident is followed by extensive measures and detailed expert examinations carried out to determine the causes of incident. Based on the results of these studies, relevant regulations are set up to give guidelines for further development of railways and establish relevant measures to prevent incidents and accidents. SS failures, which may be of different nature, are among the dominant causes of rail derailments, especially in freight transportation. The modern approach to avoid any possible risks is based on research to obtain both theoretical and experimental identification of reasons leading to rail vehicle suspension failures (Skrobanski, 2019), such as the quality of leaves used in leaf springs (LS), operation conditions, uniformity of loading, etc. (Nikolov, 2019). Such faults are also observed in the leaf springs of automotive freight vehicles.

Examining the reasons of the Fbd wagon derailment, the following data about fractures of SS components as reflected in Pareto diagram (Fig. 2) have been noticed: fracture of a leaf of leaf spring (1), spring eye (2), spring shackle (3) and centring bushing (4).

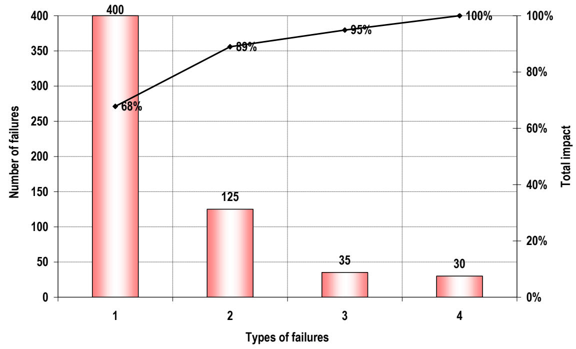

Fig. 2. Pareto diagram of failures of Fbd wagon spring system components

The analysis of the graph in Figure 2 shows that the failures of: leafs of leaf spring are 68%; spring eye – 21%; spring shackle – 6% and centring bushing – of 5%.

The most frequent fractures occur due to destruction of the main leaf and leaves of the multiple packages. In approximately 70% of cases, leaves have been broken in the centre, which is closer to the spring shackle, but in approximately 30% of cases the fracture has appeared in the eye area.

Many conceptual ideas how to reduce failures of leaf springs have been examined (Petrovic et al., 2012). The main idea of solving this problem is to apply parabolic leaf springs (PLS) in SSs (spring systems) of railway wagons and trucks.

Failures of leaf spring structures

Failures or damage of leaf springs include: a crack or breaking of the eye, breaking of the main leaf; breaking of a leaf of the multiple package; corrosion on leaves; a loose U-bolt or loose shackle, a fallen wedge.

The study has been conducted based on statistical data obtained from reports made on repairs or prevention of failures of individual truck suspension elements and the suspension of two-axle freight wagons in a year's period of monitoring.

Concerning the leaf springs of trucks, there are 100 failures registered, distributed in 6 types (groups) while the failures of leaf springs in spring suspension of two-axle freight wagons are distributed into 7 types (groups).

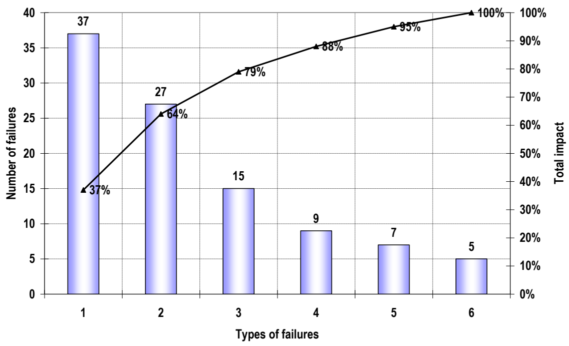

Fig. 3. Pareto diagram of failures of leaf springs for truck spring system

From the Pareto diagram (Fig. 3) it can be determined that the truck leaf springs are characterised with the following six faults (repairs): the main leaf eye (1); the main leaf (2); a leaf of the multiple package (3); a spring suspension component (4); a U-bolt (5); corrosion on leaves (6).

In conclusion, the analysis of failure types shows that the above-mentioned components are the main systems defining (limiting) the reliability of truck suspension. These systems account for 100% of failures. The graph of analysis in Figure 3 shows that failures are due to: the main leaf eye – 37%; the main leaf – 27%; a leaf of the multiple packages – 15%; a U-bolt – 9%; a spring suspension component – 7% and corrosion on leaves – 5%.

From the Pareto diagram (Fig. 4) it can be determined that the leaf springs in spring suspension of two-axle freight wagons include the following seven characteristic faults (repairs): the main leaf eye (1); the main leaf (2); a leaf of the multiple package; (3); a spring suspension component (4); a spring shackle (5); a wedge (6); a spring bushing (7)

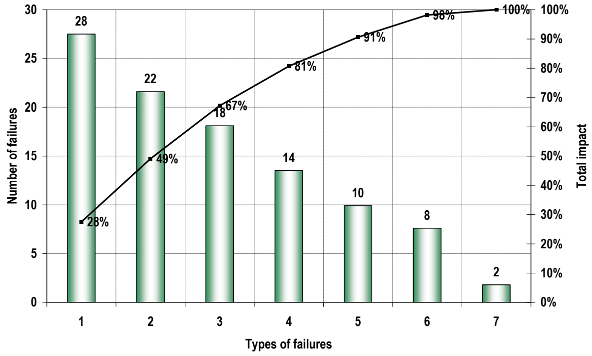

Fig. 4. Pareto diagram of leaf spring failures in spring suspension of two-axle freight wagons

In conclusion, the analysis of failure types shows that the above-listed components are the main systems defining (limiting) reliability of spring suspension of two-axle freight wagons. These systems account for 100% of failures. The graph of analysis in Figure 4 shows that failures are due to: the main leaf eye – 28%; the main leaf – 21%; a leaf of the multiple package – 18%; a spring suspension component – 14%; a spring shackle – 10%; a wedge – 7% and a spring bushing – 2%.

Structures of parabolic leaf springs

PLS of suspension for automotive equipment

Leaf springs are used in suspension of trucks (Tsvetkov, 2011, BDS 2505:1985). Parabolic leaf springs of HST type have been introduced since 1997: for the first time in suspension of Land Rover, Land Cruiser, Suzuki, Daihatsu, etc.

Parabolic springs have leaves of varying profile. Each leaf of parabolic shape has a full multi-leaf spring function - thick in the centre and thinner towards the outer edges.

All springs of HST parabolic type are manufactured according to ISO 9000 standards. The ideal parabolic spring requires only one leaf, but for safety reasons it is necessary to use at least two leaves. The second leaf is of expanded style and it serves as a precautionary measure in case of breaking. Fig. 5-6 shows the computational diagram of a two-leaf parabolic sheet spring.

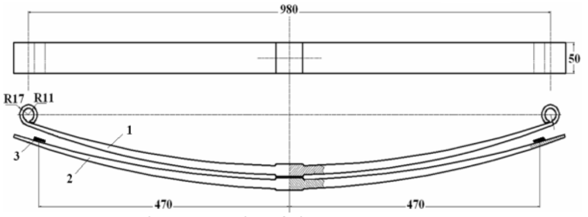

Fig. 5. Diagram of a two-leaf PLS for automotive equipment. 1 – main leaf; 2 – additional leaf and 3 – silencer (limiter)

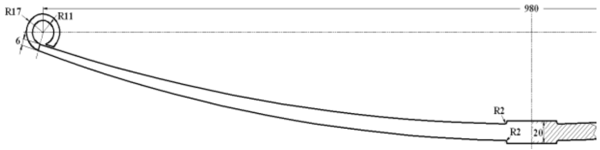

Fig. 6. Dimensions of the main leaf of a two-leaf PLS

Westalia parabolic springs are designed to be 100% compatible with the standard suspension fittings.

The calculations of parabolic leaf springs can be made using MITCalc and simulations can be performed through Solid Works or another software.

Determination of the strength and deformation state of two-leaf PLS using MITCalc software

The calculation of leaf springs using MITCalc software is based on the principle of calculating long rectangular-section beams subjected to bending. They are used as cantilevered beams fixed at one end, or as simple beams fixed at both ends. The leaves of leaf springs can be used independently or in packages (laminated leaf springs).

Results of calculations of a two-leaf PLS – with static load using MITCalc software

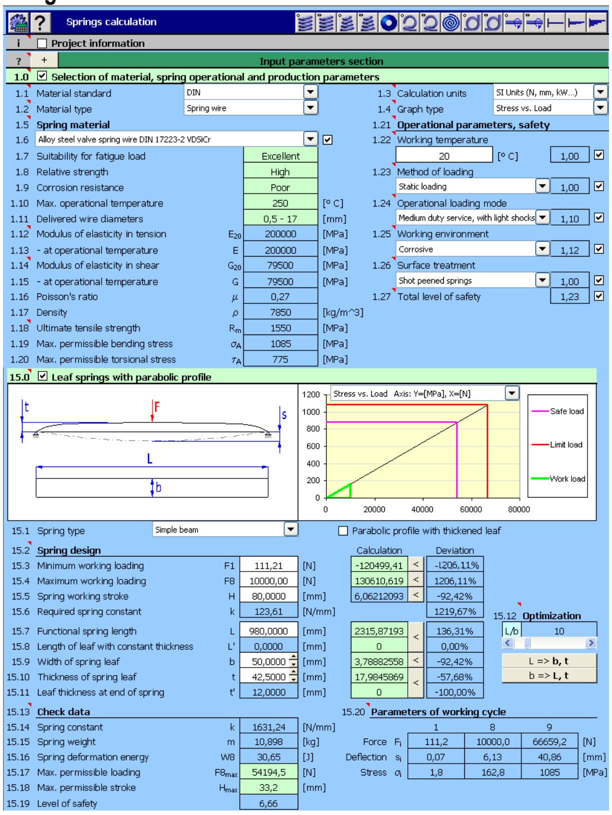

Results of calculations of a two-leaf PLS – with fatigue load using MITCalc software

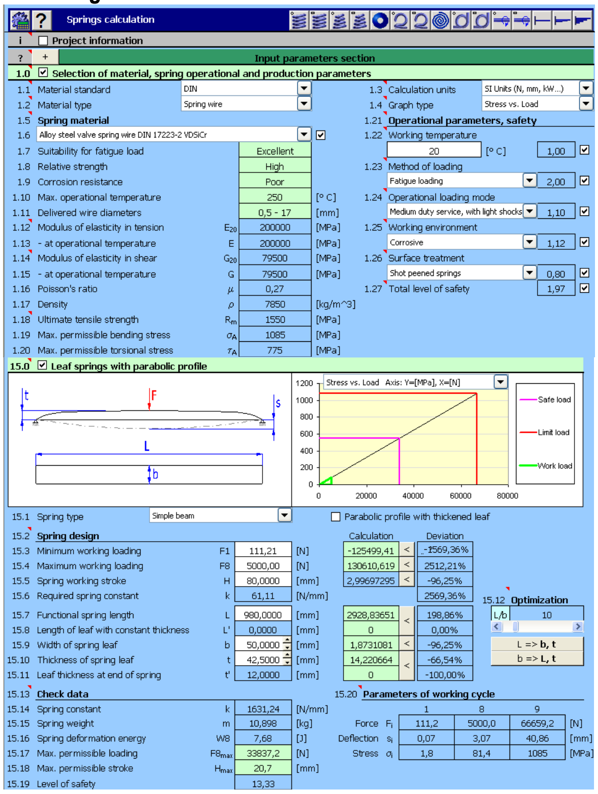

Determination of the strength and deformation state of a two-leaf PLS using Solid Works software

Using SolidWorks software, a two-leaf PLS is modelled as in Figure 5 where the load is in the leaf eye and fixing is in the leaf spring centre. The model contacts are limited except for the contacts between rubber silencers and the main leaf, which are defined as non-friction joints. This type of connection describes the behaviour of a leaf spring in perfect condition where friction between leaves is not desired. The PLS leaf material is according to the manufacturer, SUP 9 (JIS). The standard comparison has shown that SUP 9 spring steel is equal to 55Cr3 by the European standards. Steel fatigue properties are defined in compliance with SAE using the database of Glyph Works material properties. The values for materials by SFS-EN 10089 standard for Glyp Work (SAE5160/SUP 9/55Cr3) materials are as follows: Elastic Modulus, E 207 GPa; Yield Strength, R_{eL} 1250 MPa; Ultimate tensile strength, R_m 1600 MPa; Work Hardening Coefficient, K 1940 MPa; Fatigue Strength Coefficient, Sf 2063 MPa; Cyclic Strength Coefficient K' 2432 MPa; Work Hardening Exponent, n 0.05; Fatigue Strength Exponent, b -0.08; Fatigue Ductility Exponent, c -1.05; Fatigue Ductility Coefficient E_f 9.56; Cyclic Strain-hardening Exponent, n' 0.13; Cut-off, Nc 2,00e+08 Reversals. Silicon material with the following parameters is used for the stops: Elastic Modulus 1.124e+011 N/m^2; Poisson's Ratio 0.28N/A; Shear Modulus 4.9e+010 N/m^2; Density 2330 kg/m^3; Yield Strength 120e+06 N/m^2; Thermal Conductivity 124W/(m·K). Mesh Type: Solid Mesh; Mesher Used: Standard mesh; Automatic Transition: Off; Smooth Surface: On; Jacobian Check: 4 Points; Element Size: 10.88 mm; Tolerance: 0.54402 mm; Quality: High; Number of elements: 11270; Number of nodes: 20763.

At a load of 10000 N in the eyes and fixing in the PLS centre, the maximum stresses equivalent to von-Mises are 439.06 MPa. The maximum stresses are in the area of weakening section in the centre (R2 – Fig. 6) and in the eyes of the main leaf as it can be seen in Figure 7.

With the increase of radius in the main leaf transition from R2 to R5 and the leaf thickness from 6 mm to 7 mm at the eye, it is obtained that the maximum stresses equivalent to von-Mises are175.6 MPa.

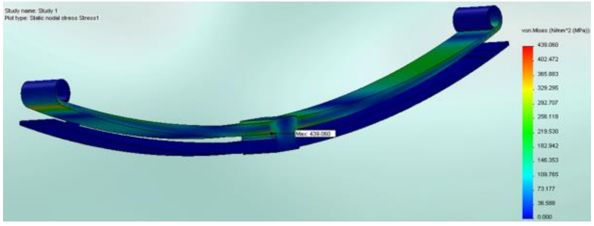

Fig. 7. Stresses in a two-leaf PLS

PLS for suspension of a rail wagon

The parabolic leaf spring (PLS) in compliance with UIC 517 (UIC 517: 2006) (Fig. 8), the main advantage of which is variable stiffness, consists of a main beam of 4 leaves (1 main leaf with eyes and 3 leaves of multiple package) and one additional leaf underneath. Each spring leaf has a section varying in height, which satisfies the condition of having one and the same strength and a line of bending on a vertical plane corresponding to a quadratic parabola. The leaves have equal length, they are connected in a package with a spring shackle. They lean on each other only in the central part and at both ends. A leaf of bigger thickness and a section of variable height is placed at the lower end of the package being mounted with a certain clearance in comparison to the basic package. The latter is calculated for the own mass of a wagon (an empty wagon), and the lower leaf is included in operation with wagon loading. As a result, the spring has a non-linear variable feature as a whole, which makes possible to achieve the necessary flexibility of both an empty and a loaded wagon.

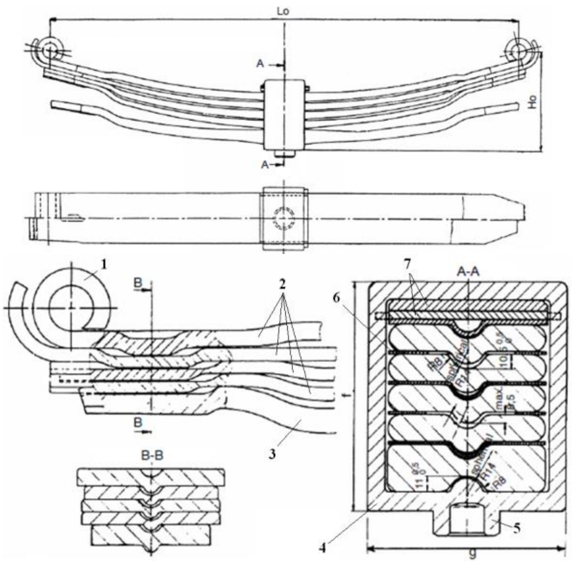

Fig. 8. Diagram of PLS for a railway wagon in compliance with UIC 517

1 – eye; 2 – multiple leaves; 3 –additional leaf; 4 –spring shackle; 5 – a pin of shackle; 6 – metal plates; 7- wedges.

Dimensions: L_0 = 1200mm; H_0 = 227mm; f = 170mm; g = 100 mm. (bxh = 120x21 mm for multiple leaves and bxh = 120x36 mm for the additional leaf)

The spring leafs are made of steels – brands 55 C2 and 60 C2 (GOST 2052-53 and EN BDS 6742-73), 60si7 and 65si7 (DIN 17221) or others, equivalent to them in chemical composition and mechanical properties. The spring shackle is made of steel brand ВСт3 сп, and the spring wedge is made of steel brand АСт3 according to BDS 2592-71.

Determination of railway wagon PLS strength and deformation state using MITCALC software

Results of calculations of a railway wagon PLS – static load using MITCALC software

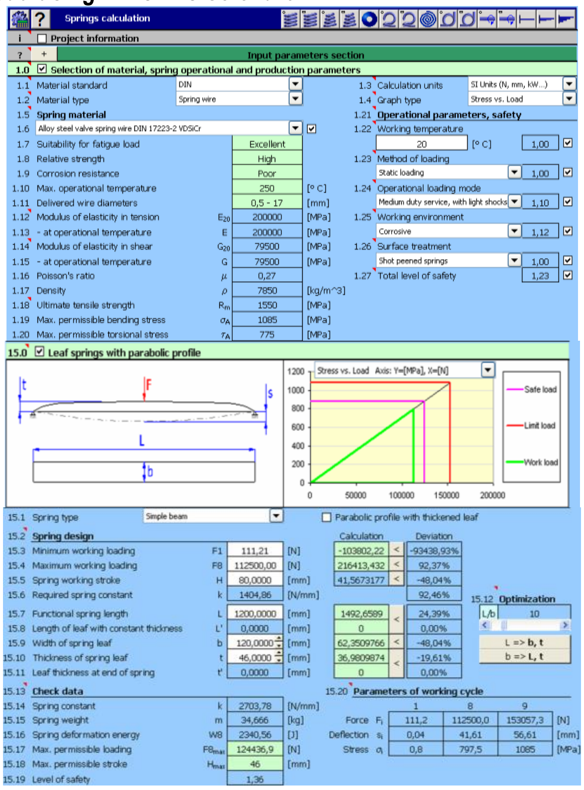

Results of calculations using MITCalc for a railway wagon PLS - at fatigue loading

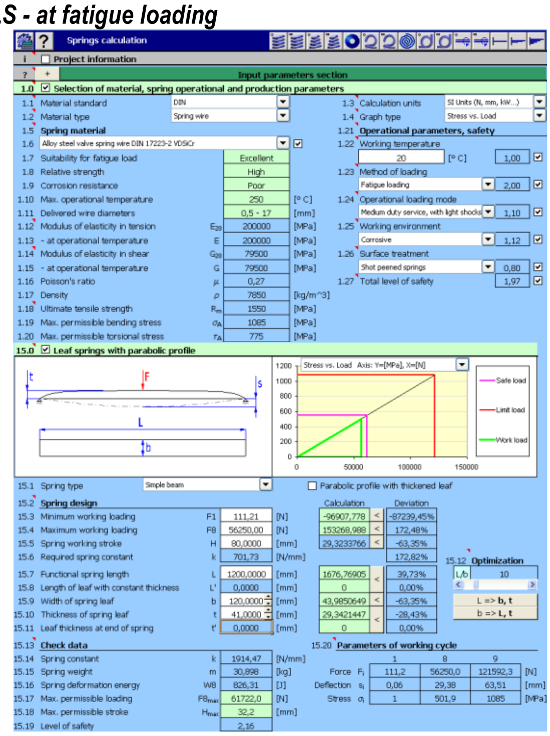

Determination of strength and deformation state of railway wagon PLS using Solid Works software

Using Solid Works software, the PLS is modelled according to Figure 8, with loading in the spring eyes and fixing in the leaf spring centre in spring bushing. Model contacts are limited, except for the contacts of leaves in section B-B, which are defined as non-friction joints of leaves only in longitudinal direction. This type of connection describes the behaviour of a leaf spring in the ideal condition where friction of leaves is not desired. The leaf material of PLS is according to the manufacturer, SUP 11A (JIS).

The standard comparison according to the European standards has shown that UP 11A spring steel is equal to 65Si7 spring steel. The steel fatigue properties are determined according to SAE from the database of Glyph Works material properties. The values of Glyp Works materials (SAE5160 / SUP 11A / 65Si7) SFS-EN according to 10089 standard are as follows: Elastic Modulus, E 200 GPa; Yield Strength, R_{eL} 1196 MPa; Ultimate tensile strength, R_m 1495 MPa; Work Hardening Coefficient, K 1940 MPa; Fatigue Strength Coefficient, Sf 2063 MPa; Cyclic Strength Coefficient K' 2432 MPa; Work Hardening Exponent, n 0.05; Fatigue Strength Exponent, b -0.08; Fatigue Ductility Exponent, c -1.05; Fatigue Ductility Coefficient E_f 9.56; Cyclic Strain-hardening Exponent, n' 0.13; Cut-off, Nc 2.00E+08 Reversals.

Crosslinking is: Mesh Type: Solid Mesh; Mesher Used: Standard mesh; Automatic Transition: Off; Smooth Surface: On; Jacobian Check: 4 Points; Element Size: 7.0018 mm; Tolerance: 0.45726 mm; Quality: High; Number of elements: 303397; Number of nodes: 477934.

At a load of 112.5 kN in eyes (of 56.25 kN per eye) and fixing in the PLS centre, the maximum stresses are 634.7 MPa equivalent to von Mises stress. The maximum stresses are in the centre of the main leaf with eyes in the area of contact with the internal wedge (Fig. 9).

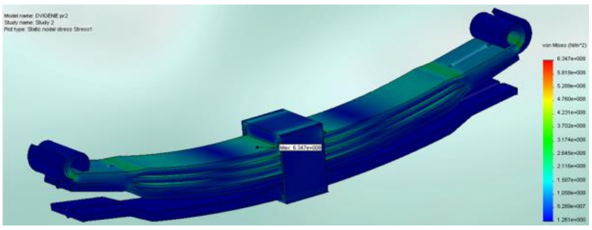

Fig. 9. Stress on a PLS in compliance with UIC 517

Strength analysis of parabolic leaf spring (PLS) structures for transport equipment

Strength analysis of PLS for automotive equipment

The results of modelling and determination of PLS strength and deformation state for automotive equipment using MITCalc and Solid Works software are given in Table 1.

From the results of PLS modelling for automotive equipment, it is established that when applying Solid Works software, stresses are significantly higher – 2.7 times. The maximum stresses are in the area of cross-section weakening in the main leaf centre and eyes. With the radius increase in the main leaf transition from R2 to R5 and the leaf thickness at the eye from 6 mm to 7 mm, the maximum stresses decrease twice and are closer to those obtained by MITCalc software.

Table 1. *Results of PLS modelling for automotive equipment*

MITCALC		
Material	**Stress, MPa**	
	Static load 10000N	**Cyclic load (of fatigue) 5000N**
Modulus of elasticity, E = 200 GPa Ultimate tensile strength, R_m = 1550 MPa Max. permissible bending stress σ_a = 1085 MPa Max. permissible torsion stress τ_a = 775 MPa	**162,8**	**81,4**
SolidWorks		
Material 55Cr3 for leaves	**Stress, MPa**	
	Value	**Area**
Elastic Modulus, E = 207 GPa Yield Strength, R_{eL}=1250 MPa Ultimate tensile strength, R_m = 1600 MPa **Material Silicon for limiters** Elastic Modulus 1.124e+011 N/m^2; Shear Modulus 4.9e+010 N/m^2; Yield Strength 120e+06 N/m^2	**439,06 175,6***	The maximum stresses are in the area of cross-section weakening in the centre (R2 - Figure 6) and in the main leaf eyes.

* Maximum stresses equivalent to von-Mises stress with constructive adjustments.

Strength analysis of PLS for rail wagons

The results of modelling and determination of railway wagon PLS deformation state using MITCalc and SolidWorks software are given in Table 2.

Table 2. *Results of PLS modelling for a railway wagon*

MITCalc		
Materials of elasticity,	**Stress, MPa**	
	Static load 225kN	**Cyclic load (of fatigue) 56.25kN**
E = 200 GPa Ultimate tensile strength, R_m = 1550 MPa Max. permissible bending stress σ_a = 1085 MPa Max. permissible torsion stress τ_a = 775 MPa	**797.5**	**501.9**
SolidWorks		
Material 65Si7	**Stress, MPa**	
	Value	**Area**
Elastic Modulus, E = 200 GPa Yield Strength, R_{eL} = 1196 MPa Ultimate tensile strength, R_m = 1495 MPa	**634.7**	Maximum stress in the main leaf centre in the area of contact with the internal wedge.

Based on the results of rail wagon PLS modelling, it is established that stresses are 25% greater with the application of MITCalc software in comparison to the values obtained by using SolidWorks. The maximum stresses most often occur in the main leaf centre in the area of contact with the internal wedge (Fig. 8).

The results of modelling vehicle and railway equipment for strength and deformation analysis have shown the necessity to apply both MITCalc and SolidWorks software packages. The determination of areas of maximum values gives a possibility for PLS constructive adjustments.

Conclusion

The occurrence of fractures in some spring suspension components of transport vehicle, such as leaf springs of wagons of Fbd type used for coal transportation from Kolubara mining basin to Nikola Tesla TPP in Obrenovac, Serbia, has imposed the necessity of strength and deformation analysis of new construction solutions. The statistical results of operation monitoring on the spring suspension components of railway wagons and trucks up to the state of their failures are considered. The obtained Pareto diagrams reflect the impact of damage types on the components of leaf springs in automotive and railway equipment. The calculations of selected structures of parabolic leaf springs made by the application of MITCalc and Solid Works software packages have confirmed the types of failures in the areas of maximum stresses.

References

Atmadzhova, D., V. Nikolov. 2018. Modelling and comparative structure analysis of different structures of leaf springs for two axle freight wagons. – *Journal Mechanics Transport Communications, 16*, 3/3, VI 27–35 (in Bulgarian with English abstract).

BDS 2505:1985 Automotive leaf springs (in Bulgarian).

Fan, H., X. Wei, L. Jia, Y. Qin. 2010. Fault detection of railway vehicle suspension systems. – *5th International Conference on Computer Science and Education*, 1264–1269.

Ivanov, A. I. 2017. Three Dimensional vibrations of aggregate connected with Elastic Elements. – *Journal Tehnomus*, 37–42.

Ivanov, A. 2011. *Modelling dynamic tasks with MATLAB.* Avangard Prima, Sofia, 100 p. (in Bulgarian)

Kocev, N., L. Lazov, K. Krastanov. 2018. *Mashini za neprekasnat transport.* VTU T. Kableshkov, Sofia (in Bulgarian).

Kostov, K., Ts. Mircheva. 2016. Expert evolution of the technical condition of rail road time after derailment of railway vehicles. – *Journal Mechanics Transport Communications, 14*, 3/3, VI 18–27 (in Bulgarian with English abstract).

Kumbhalkar, M. A., Y. L. Yenarkar, A. K. Grover. 2011. Failure Analysis of Inner Suspension Spring of Railway Engine: A Case Study. – *Proc. of Int. Conf. on Advances in Robotic, Mechanical Engineering and Design*, 12–16.

Mateev, M. 1971. *Mine Locomotive Traction*, Technique, Sofia (in Bulgarian).

Nikolov, V. 2019. Modelling and strength analysis of pivot health from the suspension of the four-axle freight wagon type Tamns. – *Academic journal: Mechanics Transport Communications*, *17*, 3 (in Bulgarian with English abstract).

Petrović, D., M. Bizic. 2012. Improvement of suspension system of Fbd wagons for coal transportation. – *Engineering Failure Analysis*, 25, 89–96.

Petrović, D., D. Atmadzhova, M. Bižić. 2014. Advantage of installation of rubber-metal elements in suspense ion of railway vehicles. – *3rd International Conference on Road and Rail* Infrastructure *CETRA'14*, *28-30 April, Split, Croatia*, 491–497.

Petrović, D., M. Bižić, M. Gasic, M. Savkovic, V. Gajic. 2012. Increasing the efficiency of railway transport by improvement of suspension of freight wagons. – *Traffic&Transportation*, *24*, 6, 487–493.

Skrobanski, B. 2019. *Okonchatelen doklad ot tekhnichesko razsledvane na zhelezopatno proizshestvie – derailirane na tovaren vlak № 30560 v mezhdugarieto Gavrailovo – Shivachevo na 26.01.2019.* MTITC, Sofia 20 May 2019 (in Bulgarian).

Tsvetkov, P. 2011. *Rakovodstvo za kursovo i diplomno proektirane na avtomobilna tekhnika. Í Chast.* VTU „Todor Kableshkov", Sofia (in Bulgarian).

UIC 517:2006 - Wagons – Suspension Gear – Standardisation.

Valkov, R., T. Grozdanov. 2009. Status and Problems of the Construction Elements of the Track. – *Journal Mechanics Transport Communications*, *3*, V 56–61 (in Bulgarian with English abstract).

Vasilev, V., E. Dimitrov, N. Nenov. 2011. Monitoring systems for control of technical state and load of rolling stock, management and synchronisation of access to infrastructure. – *Journal Mechanics Transport Communications*, *1*, BG 2.9–2.22 (in Bulgarian with English abstract).

Yusuke, H., T. Hitoshi, M. Yoshitaka. 2008. Fault detection of railway vehicle suspension systems using multiple model approach. – *Journal of Mechanical Systems for Transportation and Logistics*, *1*, 1, 88–99.

METHODOLOGY FOR DETERMINATION OF THE PARAMETERS OF HYDRAULIC STOKE MECHANISMS

Dimitar Dimitrov

University of Mining and Geology "St. Ivan Rilski", 1700 Sofia; dimitardim61@gmail.com

ABSTRACT. When processing the oscillograms of the operating processes the well-known methodology of B. V. Sudnishnikov is usually used. This requires a large volume of computing work and due to this, only one cycle that is typical for the machine operation, is processed. Thus, the accuracy of the results obtained is reduced. The proposed methodology, based on hydraulic mechanisms of strikes, is designed in order to rationalise this activity and to increase the accuracy.

Keywords: mechanism, hydraulic, oscollogram

МЕТОДИКА ЗА ОПРЕДЕЛЯНЕ НА ОСНОВНИТЕ ПАРАМЕТРИ НА ХИДРАВЛИЧНИТЕ УДАРНИ МЕХАНИЗМИ

Димитър Димитров

Минно-геоложки университет "Св. Иван Рилски", 1700 София

РЕЗЮМЕ. При обработване на осцилограмите на работните процеси обикновено се използва известна методика на Судништиков Б. В. Тази методика изисква извършването на твърде голям обем изчислителна работа, поради което се обработва само един, характерен за работата на машината, цикъл. Това намалява точността на получените резултати. За рационализиране на тази дейност и повишаване точността, на примера на хидравличните ударни механизми, е разработена предложената методика.

Ключови думи: механизъм, хидравличен, осцилограма

Introduction

Over the last decades, the hydraulic drilling and the hammer machines had found an increasingly widespread use, as they have gradually replaced the pneumatic ones. This is due to the exhaustion of the possibilities for further improvement of the performance of pneumatic drilling machines. In the 150-year history of the use of pneumatic drilling machines, they have gone a long way towards their perfection. By the end of the 60s of the last century, it was no longer possible to expect better results from the newly created machines. Some progress has been made only in the period 1955-1965 in a relation with the development of methodologies for recording the internal processes and hence for the optimisation of their structural elements.

The only possibility to increase the power and productivity of pneumatic machines was to increase the diameter of the cylinder, the mass of the machine and the supplied pressure. All this, however, is related to higher operational costs and major reconstruction of the mining pneumatic chattels. The transition to higher pressure (up to 2 - 3MPa) is only appropriate for drilling machines that work together with a mobile compressor.

In both society and technology, when the capabilities of a system, a technology, or a machine are exhausted, a qualitatively new solution to the problem appears. The creation of hydraulic drilling machines is a typical example of such a development of the technique. With the introduction of hydraulic drilling machines due to the much higher operating fluid pressure (up to 25 MPa and even more), the power of the drilling machine has increased many times.

The first hydraulic hammer was developed in 1968 and was introduced in 1970 by the French company MONTAGER. In the next years, other companies began to produce such machines. By the end of the 90s, around 150 models were being produced by 20 companies, and their number has been continuously growing.

The principle of operation of these machines is similar to that of the pneumatic drilling machines. They consist of the same basic parts. Due to the practical non-shrinking mode of the oil, two hydro-accumulators are added – one to the pressure pipe and one to the merging one. The machine is supplied by high pressure oil into the high-pressure pipeline from the oil station. The energy of the oil is transformed into mechanical work in the stroke and the rotation mechanisms. After that the oil, with a reduced pressure in the merging pipeline, returns to the oil station.

The advantages of the hydraulic drilling and the breaking machines are quite important in comparison to the pneumatic ones. The most important of these are:

- Higher power transmitted to the instrument (4 to 5 times)
- Greater drilling speed (2 to 2.5 times);
- Higher efficiency (up to 0.4-0.5);
- Less noise, lack of aerodynamic noise;
- Less air pollution, missing oil aerosols;
- Better shape of the stroke impulse and longer pistons;
- More durability of the drilling tool;

- Better control of the working mode;
- Use of cheaper electricity.

Their disadvantages are of small importance. However, there could be noted:

- Heating of the oil – it is overcome by a cooler of the oil station;
- More complex construction and considerably higher costs;
- Greater requirements for their production;
- Better qualification of the service staff.

The energy carrier for the hydraulic drilling machines is the high pressure oil. The high oil pressure is created by an oil station. It consists of an oil pump coupled with a driving engine. The pump is placed in a tank filled with oil. The oil from the tank is sucked through a filter by the pump, its pressure increases and is fed to the machine through the high pressure hose. Once the energy is delivered, the oil returns to the oil station tank where the cycle is repeated.

Figure 1 shows the general appearance of the hydraulic hammer drill of the company "TAMROCK" - HL-438. The hammer consists of a bore holder 1, a spindle 2, a washing pipe 3, a protective cuff 4, a seal 5, a piston 6, a cylinder 7, a dispenser corpse 8, a shuttle cylindrical distributor 9, a corpse of the stroke mechanism 10, a cylinder 11, a hydraulic motor 12, bearing 13 and gear 14.

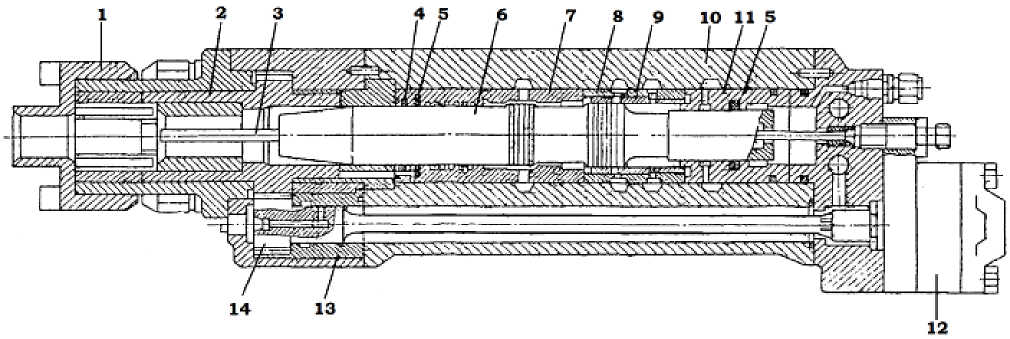

Fig 1. A construction of a hydraulic hammer drill HL-438

Through the shuttle distributor 9, the oil is supplied in series to the two cylindrical chambers. When the piston is moved forward, a strike is applied to the drill. The rotation movement of the tool is accomplished by a hydraulic motor 12 located on the rear cover of the machine. From the engine, because of its high torque, the rotation is transmitted to the instrument by a stage reductor 14. The washing water for the borehole is supplied centrally through a pipe 3.

Exposition

In the laboratory tests of drilling and breaker machines, a significant number of processes are recorded – the displacement, the speed and the acceleration of the piston [Minin I., 2017], the corps and the drilling tool and the compressed air pressure in the machine chamber. These processes are registered in the form of oscillograms or as computer records. The use of the registered records is possible after their preliminary processing. Very often the processing is performed manually by direct measurement and calculation by ordinary means. In such a mode of processing, due to its slow performance, the number of processed cycles is limited and therefore an insufficient accuracy can be achieved.

A methodology for computer registration and processing of recorded oscillograms has been developed in order to rationaliяe this activity. We process a larger number of cycles by determining the parameters we are interested in.

The introduction of the EIT requires changes in the methodology used so far (Sudnishnikov B. V, 1965, Dimitrov D., 1988), along with the introduction of the computer methods (Nedyalkov P., 2010, Stoyanov A., 2016, Ivanov A., 2017). An unlimited number of cycles are processed, the scales of time and power are not set. They are determined by the input parameters. The sequence of processing the oscillograms is as follows:

A section is selected from the oscillogram, where the processes are recorded in quality and the operational mode of the machine is stable. The range of cycles selected for treatment is noted (Fig. 2). The figure shows the operational processes flowchart in a hydraulic stroke mechanism. The methodology will not change significantly for pneumatic stroke machines. The cycles are divided into equal parts along the abscissa, i.e. by the time. The values of the pressure curves in the working chambers are recorded onto the ordinates. The curves P1, P2 and P3 are the recorded pressures acting on the rear part of the cylinder, the operating chamber and the front part of the cylinder, respectively.

The forces F1, F2 and F3 acting on the piston are calculated.

$$F1 = P1\ S1,\ N, \tag{1}$$

$$F2 = P2\ S2,\ N, \tag{2}$$

$$F3 = P3\ S3,\ N, \tag{3}$$

where S1, S2 and S3 are the rear, middle and front work surface areas of the piston, m^2, respectively.

$$R = F1 + F2 + F3,\ N \tag{4}$$

The resultant force R acting on the piston is calculated and it is plotted on the display (Fig. 3).

The resultant force diagram is approximately divided in an operational tp and a reverse to motions.

The surface areas of the impulses I1, I2, I3, I4 and I5 and the static moments of the impulses M1, M2, M3, M4 and M5 are determined. As it is shown in Figure 2 the oscillogram is conditional.

The number of displayed impulses vary depending on the type and design of the machine. In all cases we will have the three impulses I2, I3 and I4, and the impulses I1 and I5 may be missing.

$$I_i = \int_{t_i}^{t_1} R dt, Ns \quad (5)$$

$$M_i = \sum I_i t_i, Ns^2 \quad (6)$$

where I_i is the elementary surface area on which the impulse Ns is broken,

t_i - the distance from the center of the elementary area to the corresponding boundary of the cycle, s.

For the moments M1, M2 and M3, the distances ti are reported toward the ordinate t = 0, i.e. at the start of the cycle, and for M4 and M5 - at the end of the cycle.

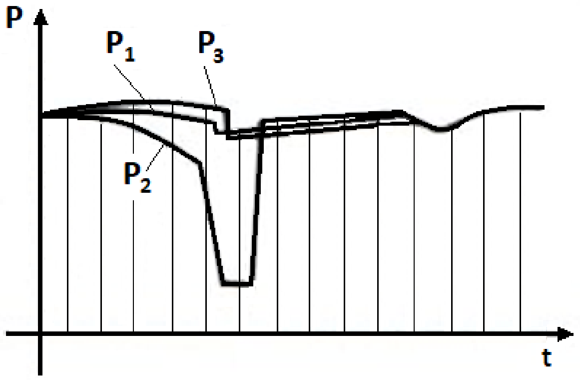

Fig. 2. An oscillogram of the operational cycle of the machine

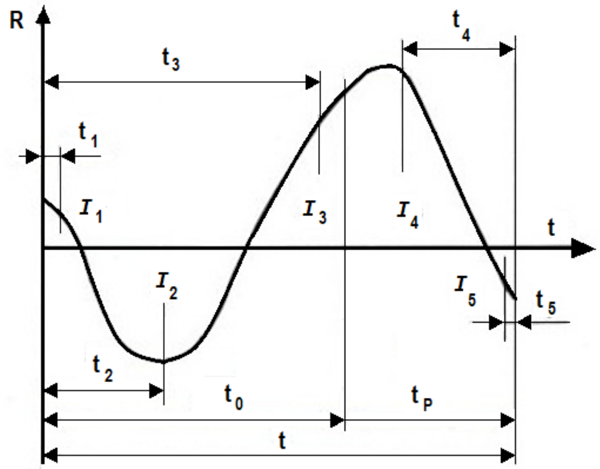

Fig. 3. A diagram for the R-force calculation

The movements made by the piston in the operational and reverse motions are determined.

$$l_0 = \frac{M_1+M_3-|M_2|}{m_6}., \text{m}, \quad (7)$$

$$l_p = \frac{M_4-|M_5|}{m_6}, m \quad (8)$$

where m_6 is the piston mass in kilograms.

In a machine, there is always an equality of the lengths of the operational and the reverse motions. Therefore, if such equality is not achieved, the calculation continues, without an intervention of the operator, until it is balanced at a new location of the distribution line and the size of the impulses I_3 and I_4.

After the equalisation of I_r and I_0, the basic parameters of the investigated machine are determined.

The pre-stroke speed of the piston.

$$V_y = \frac{I_4-|I_5|}{m_6}, m/s \quad (9)$$

The energy of the stroke.

$$A_y = \frac{m_6.V_y^2}{2}, J \quad (10)$$

The same physical laws are valid for the hydraulic hammers, as for the electric machines, i.e. the strokes frequency and the stroke power are in a direct proportionality (Hristova, T. et al., 2018)

$$n = \frac{60}{t_ц}, min^{-1} \quad (11)$$

$$P = \frac{A_y n}{60.10^3}, kW \quad (12)$$

The rebound speed of the tool piston.

$$V_0 = \frac{I_1+I_3-|I_2|}{m_6}, m/s \quad (13)$$

The rebound coefficient.

$$K_0 = \frac{V_0}{V_y}. \quad (14)$$

When performing the computing programme, the piston areas, the cycle time and the three registered pressures are imported. This is done for all sections which the processed cycles were split from.

The cycle is approximately divided into an operational and a reverse motion. The value of the resultant force at the beginning of the cycle is verified by a check-up. If it is higher than 0, I_1 and M_1 are calculated, and if it is less than 0 - I_2 and M_2. Permanent checks are made for the moment when the resultant force will change its character and then the next impulses and their moments are automatically computed. After the static moments and the impulses, the lengths of the operational and the reverse motions are calculated and compared. If any difference is found, as mentioned above, the dividing line is displaced. The programme provides an automatic shifting of the dividing line in one direction or another, depending on the ratio between the operational and the reverse motions. If the values of t_0 and t_r are equalised with the set accuracy, the calculations continue for all the other parameters of the machine. As a final result, the values of all the parameters of the machine are displayed and the resultant force curve is plotted.

The processing of the oscillograms of the operational processes is usually brought to a processing of the indicative pressure diagrams.

This is most common for the machines with a free piston. In the case of drilling machines with a connected piston /with a dependent rotation of the drilling tool/ this methodology does not give enough accurate results. For these machines it is necessary to register and to arrange the operational processes that characterise the movement of the piston, the corps and the drilling tool.

The considered methodology for the processing of the operation oscillograms and the calculation programme made by a model of it are used in the study of a number of pneumatic and hydraulic drilling and breaking machines in the laboratories of the University of Mining and Geology - Sofia. The rationalisation of this activity has been achieved through the elaborated calculation methodology. There is an opportunity for a practical application of the well-known method for processing the oscillograms of the operational processes.

References

Dimitrov, D. 1988. Metodika I programa za obrabotka na indikatornite diagrami na hidrawlichni udarni mehanizmi sas svobodno butalo. – *IV Mladejka konferencia po hidrawlika I pnevmatika*, Kazanlak (in Bulgarian).

Hristova, T., A. B. Yanev, N. Savov. 2018. Determination of the influence of jaw movement frequency of jaw crusher on energy consumption. – *Annals of the University of Petroşani, Electrical Engineering*, 29–36.

Ivanov, A. 2017. Three dimensional vibrations of aggregate connected with elastic elements. – *Journal Tehnomus*.

Minin, I. 2017. *Minni I stroitelni machine.* Zizi Print, Sofia, p.438 (in Bulgarian).

Nedyalkov, P. 2010. Research of milling balls dimensions influence over the characteristics of vibrating comminution mill". – *Annual of University of Mining and Geology "St. Ivan Rilski", 53*, 3, 49–51.

Stoyanov, A. 2016. *Matrichni operacii s MathCAD v Teoretichnata mehanika Statika*. Kineziologia, Sofia, 165 p. (in Bulgarian)

Sudnishnikov, B. V., N. N. Esin. 1965. Elementai dinamiki machine udarnogo deistwia. Novosibirsk, 287 p. (in Russian)

GENERAL AND SPECIFIC REQUIREMENTS FOR THE DEVELOPMENT OF NEW HAMMER DRILLING MACHINES

Dimitar Dimitrov

University of Mining and Geology "St. Ivan Rilski", 1700 Sofia; dimitardim61@gmail.com

ABSTRACT. The paper examines the general and specific requirements for the development of hammer drilling machines. They operate under a strong dynamic regime, so too many requirements must be met when designing them. The study aims to clarify these issues in order to help designers in choosing parameters and constructive schemes. A particular attention is paid on the selection of the air distribution device, the rotation mechanism, the start-up device, the fines removing device, the feed and maintenance device, the fittings and the smoothness classes of the various parts.

Keywords: machine, stroke, hammer

ОСНОВНИ ИЗИСКВАНИЯ ПРИ РАЗРАБОТВАНЕ НА НОВИ ПРОБИВНИ МАШИНИ С УДАРНО ДЕЙСТВИЕ

Димитър Димитров

Минно-геоложки университет "Св. Иван Рилски", 1700 София

РЕЗЮМЕ. В работата са разгледани общите и специфични изисквания при разработване на пробивни машини с ударно действие. Те работят при силно изразен динамичен режим, поради което при конструирането им трябва да се спазват твърде много изисквания. С работата се цели да се изяснят тези въпроси, с което да се подпомогнат конструкторите при избора на параметри и конструктивни схеми. Специално внимание е отделено на избора на въздухоразпределителното устройство, механизмът за въртене, пусковото устройство, устройството за отстраняване на ситнежа, устройството за подаване и поддържане, сглобките и класовете на гладкост на различните детайли.

Ключови думи: машина, удар, чук

Introduction

The process of construction is one of the main activities in the designing of each new product. At the beginning of the design, some basic technical parameters are usually set under operational conditions. The new machines must comply with the normative documents.

Typically, the choice of a constructive solution does not have an unambiguous solution, so these issues should be clarified very well in respect to different types of machines.

In the present paper the basic requirements for the design of new modern hammer drilling machines are examined. These machines include drills and hammers mounted on a manipulator (Mitrev, Minin I., 2017, Nedyalkov P., 2003), submersible pneumatic hammers, rock breaker and pneumatic hammers. The drilling machines operate in a highly dynamic mode. Some of them are used as hand-held machines (Minin I., 2017), others work on manipulators and carriages. Their principle of operation and the way of work set too many requirements on them. It is not enough to know only the general construction requirements of these machines. If the constructor is not well acquainted with the theory and practice of drilling, he cannot create a good drilling machine. In practice, there are many examples for irrelevant constructive decisions due to the lack of knowledge on the problems.

Requirements for machine design

Before the construction, it is necessary to do some research in our and foreign literature sources. The constructions of the drilling machines, implemented and operated in the industry, must be known, their technical level and the possibilities for using the advantages of the new machines should be assessed. It is important to strive for a succession and a unification. New elements must be developed when there is no possibility of using the existing ones and when this leads to an essential improvement of the machine. The hammer drilling machines have been used for more than 150 years and it could be considered that the rational constructive solutions for their individual mechanisms are well known.

The assignment specifies the mass, frequency and energy of the stroke [Minin 2], the relative metal capacity and the energy consumption. These parameters comply with the current standard. The parameters are selected with some reserve in order to fulfil the standard and to provide better qualities of the new machines. The progressiveness of the new construction is mainly determined by the relative metal capacity, the energy consumption and the characteristics of vibration and noise. The rest of the parameters are selected depending on the purpose of the machine and its operational mode. The technical parameters are determined after calculation using the known methodology (1.2).

The choice of the constructive scheme is one of the most important stages of the designing process. The tolerable errors at this point can devalue the construction and make the model morally outdated from the very beginning. We will focus on this problem in more detail, as many errors are made regularly when choosing a constructive scheme.

The air distributor and the rotation mechanism have the greatest influence on the performance of the machine.

As it is known, independent and dependent rotations through front and rear mechanisms are used for the drilling hammers.

An independent rotation should be used on all the machines that work on manipulators and carriages. Only the independent rotation can provide great drilling speed rate. This requirement is often outstepped. A typical example of this are the Russian hammers KC-50 and these of Atlas Copco-BBD-120. They are heavy drilling machines that work on manipulators. The first ones have a rear rotating mechanism and the other ones - a front one. The dependent rotation cannot provide a sufficient torque, an impact power and a drilling speed rate. There are several drilling machines with an independent rotation of the following companies: Permon - Czech Republic, VKS90VM, from Russia – ПК-60, ПК-75, БГА-1, of Atlas Copco – BBE-51 and BBE-53, of USA – PRR-123, PR-143, VS-40M, Ingersol Rand-URD-474, URD-550, Finland, Tamrok-L-400, 500, 800, 1000, 2000, 4000, Germany, Hausherr – ДК7ЕСА and others.

The independent rotation is unsuitable only for manual drilling machines, as thus their mass increases. Some constructions such as these of Atlas Copco, Russia and others are known, but they have not found a widespread application. The independent rotation could find some application in the manual hydraulic drilling machines. Engines and rotation reducers with small sizes and mass are used for the rotation mechanism. The hand-held drilling machine must have a mass up to 25-28 kg, which is not difficult to be achieved with the hydraulic mode.

For the modern hand drilling machines (Djobov, 2017), both types of dependent rotation are used - front and rear. With a rear rotation are almost all of the Russian drilling machines - ПР – 24, ПР – 25, ПР – 27, ПР – 30, ПТ- 29, ПТ- 36, ПП-54В and others, some of the companies Holman - England, Permon - Czech Republic, Ingersol Rand, Tamrok and others. Almost all of the models of Atlas Copco, some models of Flotman, Hausher, Demag, Bohler and others are with a front rotation.

The older drilling machines are predominantly with a rear rotation.

The rear rotation mechanisms set less requirements on the construction, mainly in terms of accuracy classes of surface roughness. The mechanism is not difficult for exploitation and its life-long service is better. This, however, deplete its advantages. Its deficiencies are of great significance. First of all, the excess increase of the drilling machine mass has to be noted - a very important indicator for the hand-held drilling machines. This is due to the filling of the cylinder with many details compiling the rotating mechanism. It is not rational the drilling bore located in the front to be rotated by a mechanism located at the rear of the hammer. It is not necessary to fill the whole distance along the machine length with parts that weigh on, complicate and increase the cost of the construction.

In the case of hammer drills with a front rotation mechanism, the machine consists of fewer details. The details of the rotation mechanism are located at the front of the hammer and have a lightweight and simple construction. Therefore, the mass of the machine is from 5 to 8 kg less.

Another disadvantage of the rear rotation mechanism is the poor design of the stroke mechanism in respect to the power supply. The shape of the piston could not be sustained in energy terms. The piston is of a small length. On the other hand, the requirement for consistence of the piston sectional length could not be complied. To accommodate the rotating chuck at the rear of the piston, its cross section and its mass increase. All of this leads to the occurrence of peak loading rates in the drilling tool when the stroke is transmitted and the duration of the contact between the piston and the tool decreases. For these reasons, at the drilling machines with a rear rotation the drilling tools break more often, and the energy conversion efficiency is smaller.

The front rotation mechanism provides good possibilities to use pistons with a longer length and equal section along the entire length. For the alignment of the cross section, the rear of the piston is straightened up, thus achieving its weight reduction. Additional volume is added with this straightening to the rear chamber, which helps to reduce the rear air buffer and also to reduce vibrations and increase the active motion of the piston.

A ratchet mechanism is used in all constructions with a dependent rotation. For both rotation mechanisms, the constructions are well-worked and should not be changed. In the lighter models, two ratchet tappers are used, and in the medium and heavier ones - four. At an even number of tappers, the number of teeth of the ratchet wheel gear should be odd. Furthermore, the kinematics of the ratchet mechanism need to be designed so that the individual tappers could operate in sequence, not at the same time. This reduces the amount of reverse rotation of the tool at the end of the reverse motion. The novelty that is recommended is the simultaneous coupling of the ratchet tappers, placed oppositely, two by two. Thus, a more symmetrical load on the rotor nodes is achieved, maintaining the coaxiality of the machine, and the piston is moving with a smaller resistance.

The rotation angle of the instrument should be selected depending on the scales in which it will be operated. The optimisation of this parameter is of great importance as it leads to an increase in the drilling speed rate without an additional energy consumption. In a modern construction, this reserve must be used and imposed still into the design. The machine must be produced with several kits of pistons and rotating sleeves. They are identical in design. They differ only on the helical cannels inclines. The machine produced in this way will operate at a different rotation angle of the tool when changing the kits. Depending on the operational conditions, the assembly kits will be ordered to provide the maximum drilling speed rates without any change in the energy consumption. With the optimisation of the rotation angle, an average increase in the drilling speed rate of about 25% and a significant reduction of the consumption of compressed air could be reached. In addition, the presence of the same machine with several sets of pistons and a rotating sleeve will allow the most suitable combination to operate with to be determined for the particular conditions. This idea has not been realized for any construction, neither in Bulgaria nor abroad.

Considering its easy realization, this reserve for improvement of the indicators should be used for each new construction.

The rotation mechanism should provide very light and smooth rotation of the tool for a whole turnover and along the entire length of the cylinder. The rotation should be without retention and with minimal friction loss. This can be achieved by using a soft and heat-treated springs, sufficient smoothness and coaxility of the friction surfaces, an observation of the prescribed assemblies and good lubrication of the parts. The construction of the tappers must be symmetrical and must allow their reversal turning at a wear on the one side. It is best the tapers to be made of rolled material.

Another very important issue to consider when choosing a construction scheme is the type of air distribution device. There are too many studies on this topic, and that is why we will not discuss the problem in detail, as only the most general rules and assessments will be given.

The machine's faultless and economical operation depends on the air distribution device. At its selection, the following issues should be considered: the movement of the distributing element should be small, should not induce throttling of the fluid, the channels should be of sufficient cross-section and without unnecessary bends.

The simplest in construction, safety of operation and with a high energy conversion efficiency is the self-distribution device. This device is becoming more and more applicable. It should be preferred for short-motion fast-impacting machines.

The valve distribution device is relatively simple and safe to operate with. Some of its disadvantages are the presence of a buffer in front of the piston at the end of the working motion and the uneconomic air flow due to the opening of the outlet due to the displacement of the valve. Various designs of valve distribution devices are known. The best features are those in which the valve is supported and does not move the whole. The swinging valve requires the smallest force and moving time, therefore the disadvantages of the valve distribution are minimised. The valve distribution is mainly applicable for different drilling machines.

The slide shutter air distribution is complicated in construction and unsecure for operation. The distributor is in a joint by two or three surfaces, which places a greater demand on the joints and roughness of the surfaces. Closed volumes are formed in the shutter slide box that are not well flowed by the fluid, so the shutter gets dirty quickly. For the new constructions, it is necessary to provide better drainage of all chambers around the shutter, even if some loss of fluid occurs. On the other hand, this distribution provides economical discharge of the compressed air due to the pre-displacement of the slide shutter because of the outlet opening. In addition, at the end of the two motions, the buffer in front of the piston is absent or minimised. The slide shutter air distribution increases the cost of the product, so it is recommended for heavier long-motion machines. The greater cost of the machine in this case is compensated by the lower operating costs.

The design of the distribution device must ensure good lubrication of the machine. It is best to lubricate the details that are up-flown with compressed air. There are problems mainly with the lubrication of the parts of the rotation mechanism and the chuck. They are most easily resolved by diverting a flow-part of the blown air to the front of the machine. This is most easily done by opening the outlet shortly after opening the slit channels. Thus, from the front chamber of the cylinder through the slit slots, a sufficient amount of compressed air will flow out to spread on the front of the machine.

There are less requirements for the rest of the mechanisms of the drilling machines. Let's take a look at them too.

The starting device must have sufficient permeable capacity and density to ensure the normal feeding of the chambers with minimal losses. This is not observed for various constructions. The inlet is narrowed or it does not match well with the opening of the starting faucet and rear cover lid.

The fines removal device is with a central water supply. Various automatic devices are used to start and stop water. During the operation, these devices very quickly get out of order and they are replaced with a shut-off valve. In case of such a problem with the new construction, it is better still at the designing stage to abandon the spectacular but unsafe mechanisms and to predict a simple shut-off valve. Thus, the appearance of the new construction would not worsen. The safety of the machine is of greater importance.

The maintenance and the feeding devices must be selected or constructed together with the drilling machine. For hand-held machines, it is best to use a double-acting stand. Their management can be from the stand itself or from the hammer. The hammer-management is easier. During the operation only one of the worker's hands is occupied. This reduces the harmful impact of vibrations. On the other hand, however, the construction is complicated. Such management may be envisaged if the level of the plant-producer is good enough.

In addition to the specific requirements listed here, the standard requirements must also be observed. Also, standardised, purchased and formerly acquired in the production process products have to be used, to limit the nomenclature of threads, slits, attachment sizes, coatings, assortment of used materials, interchangeability.

It is difficult to accurately calculate the drilling machines. Therefore, the next stages of design are the most important - the manufacturing of the test sample, its testing and the specification of the construction. This is a very important stage and it is worth most in terms of time and costs. No modern design can be created without a precise implementation at this stage.

It is desirable for the design to be as technological as possible and to contain a minimum number of details. The simplicity is an indication of the craftsmanship of the construction. For the drilling machines, it is necessary to exclude any excesses and the efforts need to be focused on increasing the safety of the machine. In this sense, the intention for simplification could not be considered as an indication of an outdated constructive solution. The constructor must also take into account the capabilities of the manufacturer.

The roughness classes and joints are determined by the operating conditions of the mechanisms. For the parts that operate together, the following limits for the roughness classes may be recommended: 0,63 - 0,16 / 0,63 - 0,16 - for couplings cylinder - piston, cylinder - guiding sleeve, cylinder - air distributor, cylinder - ratchet wheel gear: 1,25 - 0,32 / 1,25 - 0,32 - for front body - intermediate body, cylinder - rear cover lid, air distributor - rear cover lid, 1,25 - 0,32 / 2,5 - 0,63, for cylinder - valve box cover lid, cylinder - valve box sleeve.

Joints with guaranteed clearance and tightness are used for the drilling machines. With a guaranteed clearance are the joints between the cylinder and the piston H7-H8 / g6-f7; guiding sleeve- piston, chuck, front body - H7 / f7-e8; front body - intermediate body - H7 - H8 / g6 - h6; cylinder – distribution device corps - H7-H8 / h6-h7; cylinder - valve box cover lid - H7-H8 / f9; cylinder - sleeve of the valve box; cylinder - ratchet wheel gear, cylinder – rear cover lid - H7-H8 / f6-f8; cylinder - intermediate body, cylinder - air distributor, air distributor - rear cover lid - H7 / g6-h6. With a guaranteed tightness are the joints between the body and the guiding sleeve - H7 / r6 and between the chuck and the chuck sleeve - H7 / x6.

As it could be seen from the presented material, the construction designing of drilling machines is a complex task that sets too many questions to the constructor. The design of a modern drilling machine can be done only with a basic knowledge of the drilling technique. This paper is an attempt to clarify the main issues that arise in the design and acquisition of new drilling machines.

Conclusions

1. The frequency and energy of the stroke, the relative metal capacity and the specific energy consumption are set in the design process of new drilling machines. They must comply with the current standards.

2. The air distributor and the rotation mechanism have the greatest influence on the performance of the machine.

3. A possibility for optimisation should be provided for the modern machines through the selection of an appropriate rotating angle of the tool for the various operational conditions.

References

Damyanov, T., E. Assenov, Z. Mihalkov, P. Nedyalkov. 2003. Gallery support manipulator – dynamical research. – *Annual of the University of Mining and Geology "St. Ivan Rilski"*, *46*, III, 1–5.

Dimitrov, D. 1988. Metodika i programa za obrabotka na indikatornite diagrami na hidrawlichni udarni mehanizmi sas svobodno butalo. – *IV Mladejka konferencia po hidrawlika I pnevmatika*, Kazanlak (in Bulgarian).

Djobov, I., I. Koprev. 2017. *Rakovodstvo za uprajnenia po procesi pri otkritia dobiv na polezni izkopaemi.* Sofia, 229 p. (in Bulgarian)

Minin, I. 2017. *Minni i stroitelni machini.* Zizi Print, Sofia, 438 p. (in Bulgarian)

Mitrev, R., I. Minin. 2017. Opredeliane na silovoto natovarvane na mehanitchna konstrukcia na hidravlièn minen, – *Mehanika na machinate*, TU – Varna, 25, 2, 19–29 (in Bulgarian).

VIBRATIONS OF SHAFT CAUSED BY INERTIAL EXCITATIONS

Anastas I. Ivanov

Todor Kableshkov Higher School of Transport, 1574 Sofia; aii2010@abv.bg

ABSTRACT. Small vibrations of a cylindrical shaft caused by inertial excitations are studied in this paper. The shaft is vertically situated. It consists of two sections with different cross sections. It is supported by a spherical and a cylindrical joint. The two supporting devices have horizontal elasticity. Between the two supports, and also at the upper end of the shaft, rotationally movable concentric masses, which are eccentrically situated towards the shaft axis, are mounted. They rotate with a constant angular velocity relative to the rotary axis and they create unfavourable inertial excitations. Due to the elasticity of the shaft, as well as to the elastic horizontal supports, small forced vibrations of the two concentric masses are created in planes perpendicular to the rotary axis. The shaft is modelled as a discrete mechanical system with four degrees of freedom. Differential equations, describing the small vibrations of the system, are derived. A programme of MatLab and Simulink has been compiled and used to integrate numerically derived equations. Calculations have been made for the different unfavourable positions of the concentrated masses relative to a plane perpendicular to the shaft rotary axis. All results are illustrated with appropriate graphs. Some important for the practice conclusions are presented, which can be used in the design of such shafts.

Keywords: shaft, vibrations, inertial excitations, kinematical characteristics

ТРЕПТЕНИЯ НА ВАЛ, ПРЕДИЗВИКАНИ ОТ ИНЕРЦИОННИ СМУЩЕНИЯ

Анастас И. Иванов

Висше транспортно училище "Тодор Каблешков", 1574 София

РЕЗЮМЕ. В статията се изследват малките трептения на цилиндричен вал, предизвикани от инерционни смущения. Валът е разположен вертикално. Състои се от два участъка с различни по размер напречни сечения. Подпрян е със сферична и цилиндрична става. Двете опорни устройства имат хоризонтална еластичност. Между тях, и в най-горния край на вала, са монтирани ротационно движещи се спрямо оста му ексцентрично разположени концентрирани маси. Те се въртят с постоянна ъглова скорост спрямо ротационната ос и създават неблагоприятни инерционни смущения. Поради еластичността на вала, както и поради еластичните в хоризонтално направление опори, се пораждат малки принудени трептения на двете концентрирани маси в равнини, перпендикулярни на ротационната ос. Валът е моделиран като дискретна механична система с четири степени на свобода. Изведени са диференциалните уравнения, които описват малките трептения на системата. Съставена е програма на MatLab и Simulink, с помощта на която са интегрирани числено изведените уравнения. Извършени са изчисления за неблагоприятните взаимни разположения на концентрираните маси спрямо равнина перпендикулярна на оста на вала. Всички резултати са онагледени с подходящи графики. Статията завършва с важни за практиката изводи, които могат да се използват при проектирането на подобен вид валове.

Ключови думи: Вал, трептения, инерционни смущения, кинематични характеристики

Introduction

Many machines and aggregates use different types of shafts. Most often they are examined for torsion and bending because their main purpose is to transmit axial moments (Sevastakiev et al., 1986).

In the presented article, the shaft is examined only on a generalised bending caused by inertial harmonic excitations. Such disturbances are always presented in the rotary machines when unbalanced masses are available (Sergeev et al., 2018).

Harmful vibrations, which are small oscillations with high frequencies and relatively small amplitudes, accompany each machine aggregate as crushers, mills and others (Hristova, et al., 2018). Reducing them to some minimal normative values is the most important engineering problem for solving by any constructor (Petrović, 2017; Sergeev et al., 2018).

For example, the three-dimensional vibrations of a machine aggregate, solved numerically with a suitable program for this purpose, are studied in the paper (Ivanov, 2017).

One of the most important and basic task, the determination of eigen frequencies and eigen forms, is very difficult to solve using only analytical solutions, especially for the systems with many degrees of freedom, (Ivanov, 2017). The engineer needs to make many calculations numerically for multiple variants, which are dependent on a number of parameters. Only then, the optimisation analysis can be made (Cheshankov et al., 2004).

The above-mentioned problems lead to the compilation of the main purpose of this study: to determine the maximum values of the basic kinematical characteristics of a vertical shaft from the most unfavourable inertial excitation.

Mathematical model

A vertically positioned cylindrical shaft, which has two sections, is studied.

The first section has a length l_1 and bending stiffness $E.I_1$, and the second section has length l_2 and bending stiffness $E.I_2$, (Fig. 1).

The shaft is supported at its lower end by a spherical joint, which is equivalent to three simple rod joints. The vertical rod joint is assumed to be perfectly rigid. The two mutually perpendicular and horizontal rod joints are assumed to be ideally elastic with linear stiffness coefficients c_1.

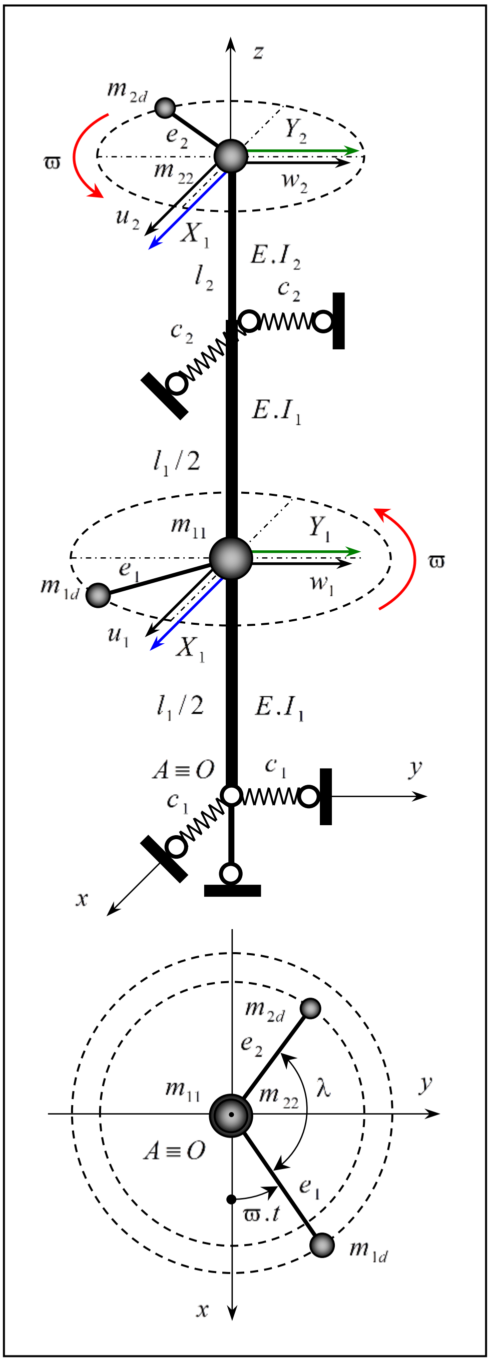

Fig. 1. Dynamical model of the shaft

At the end of the first section and at the beginning of the second one, the shaft is supported by a cylindrical joint. It is equivalent to two horizontal rod joints, which are assumed to be ideally elastic with linear stiffness coefficients c_2.

In the middle of the first section are centrally located a concentrated mass m_{11} and an unbalanced mass m_{1d}, and $m_1 = m_{11} + m_{1d}$. The unbalanced mass m_{1d} is located at a distance e_1 from the shaft axis.

At the upper end of the shaft are centrally located a concentrated mass m_{22} and an unbalanced mass m_{2d} with an eccentricity e_2, and $m_2 = m_{22} + m_{2d}$.

The two unbalanced masses rotate synchronously around the rotary axis Oz with the same angular velocity ϖ and phase difference λ.

Differential equations

The vector of the generalised coordinates, which are determined by the small vibrations of the discrete mechanical system, has the type (Fig. 1):

$$\mathbf{q} = \langle u_1 \quad u_2 \quad w_1 \quad w_2 \rangle^T . \tag{1}$$

The Lagrange differential equations of second gender are used. They have the following matrix form:

$$\frac{\partial}{\partial t}\left(\frac{\partial E_k}{\partial \dot{\mathbf{q}}}\right) - \left(\frac{\partial E_k}{\partial \mathbf{q}}\right) = \mathbf{Q} - \frac{\partial E_p}{\partial \mathbf{q}} . \tag{2}$$

The kinetic energy of the system is a quadratic form of the vector generalised velocities and the mass matrix:

$$E_k = 0{,}50.\dot{\mathbf{q}}^T.\mathbf{M}.\dot{\mathbf{q}} , \tag{3}$$

$$\mathbf{M} = \mathbf{diag}\left(m_1 \quad m_2 \quad m_1 \quad m_2\right). \tag{4}$$

The potential energy of the deformations is the quadratic form of the vector of generalised coordinates and the stiffness matrix:

$$E_p = 0{,}50.\mathbf{q}^T.\mathbf{K}.\mathbf{q} , \tag{5}$$

$$\mathbf{K} = \begin{bmatrix} k_{11} & k_{12} & 0 & 0 \\ k_{21} & k_{22} & 0 & 0 \\ 0 & 0 & k_{11} & k_{12} \\ 0 & 0 & k_{21} & k_{22} \end{bmatrix} . \tag{6}$$

The determination of the stiffness matrix is done by the mathematical dependence:

$$\mathbf{K} = \mathbf{D}^{-1} , \tag{7}$$

where the flexibility matrix has the form:

$$\mathbf{D} = \begin{bmatrix} d_{11} & d_{12} & 0 & 0 \\ d_{21} & d_{22} & 0 & 0 \\ 0 & 0 & d_{11} & d_{12} \\ 0 & 0 & d_{21} & d_{22} \end{bmatrix} , \tag{8}$$

$$d_{11} = \frac{l_1^3}{48.E.I_1} + \frac{c_1 + c_2}{4.c_1.c_2} \quad , \tag{9}$$

$$d_{22} = \frac{l_1.l_2^2}{3.E.I_1} + \frac{l_2^3}{3.E.I_2} + \\ + \frac{l_2^2}{l_1^2}.\frac{c_1+c_2}{c_1.c_2} + \frac{l_1+2.l_2}{l_1}.\frac{1}{c_2} \quad , \tag{10}$$

$$d_{12} = d_{21} = -\frac{l_1^2.l_2}{16.E.I_1} - \frac{l_2}{2.l_1}.\frac{1}{c_1} + \frac{l_1+l_2}{2.l_1}.\frac{1}{c_2} \ . \tag{11}$$

The vector of the generalised non-potential forces is formed by the inertial forces that arise in the two unbalanced masses. This vector has the type:

$$\mathbf{Q} = \left\langle X_1 \quad X_2 \quad Y_1 \quad Y_2 \right\rangle^T , \tag{12}$$

$$X_1 = m_{1d}.e_1.\varpi^2.\cos(\varpi.t) , \tag{13}$$

$$X_2 = m_{2d}.e_2.\varpi^2.\cos(\varpi.t + \lambda_n) , \tag{14}$$

$$Y_1 = m_{1d}.e_1.\varpi^2.\sin(\varpi.t) , \tag{15}$$

$$Y_2 = m_{2d}.e_2.\varpi^2.\sin(\varpi.t + \lambda_n) . \tag{16}$$

The system of differential equations, which describes the small vibrations of the two concentrated masses recorded in a matrix form, has the following type:

$$\mathbf{M}.\ddot{\mathbf{q}} + \mathbf{K}.\mathbf{q} = \mathbf{Q} \ . \tag{17}$$

The upper differential equation system (17) is linear, non-homogeneous, from the second order and it is composed of constant coefficients. It could be integrated analytically (Ivanov, 2017). But when multiple engineering calculations are performed with variations of many parameters, it is advisable to solve it numerically with a suitable program. It can be compiled on the basis of some powerful mathematical package.

Numerical solution

For the numerical solution of the differential equation system (17) in the time area, the MatLab ver. 6.1 and Simulink Toolbox are used.

Eigen frequencies

In order to avoid the dangerous resonance areas, the eigen frequencies were primarily determined.

This task is related to defining the own numbers of the matrix $\mathbf{A}$, which has the following structure:

$$\mathbf{A} = \begin{bmatrix} \mathbf{0} & \mathbf{I} \\ -\mathbf{M}^{-1}.\mathbf{K} & \mathbf{0} \end{bmatrix}_{8\times 8} . \tag{18}$$

Sub-matrices $\mathbf{0} = [0]_{4\times 4}$ and $\mathbf{I} = \mathbf{diag}[1]_{4\times 4}$ are correspondingly zero and unit matrices.

The eigen circular frequencies ω_k, $(k = 1,2,3,4)$, are derived from the own numbers p_k that have the form:

$$p_k = 0 \pm i.\omega_k , \qquad i = \sqrt{-1} \ . \tag{19}$$

Initially, a program file "shaft.m" is created. Then this file is started from the MatLab main command window.

Simulink model file

Initially, the differential equations (17) are presented in the following matrix form:

$$\ddot{\mathbf{q}} = \begin{bmatrix} -\mathbf{M}^{-1}.\mathbf{K} & \mathbf{0} \end{bmatrix}.\begin{bmatrix} \mathbf{q} \\ \dot{\mathbf{q}} \end{bmatrix} + \mathbf{M}^{-1}.\mathbf{Q} \ . \tag{20}$$

A model simulation file "shaft.mdl" is created. This file is started from the Simullink command window.

Numerical results

In order to avoid dangerous resonance areas, the eigen frequencies were originally determined.

The calculations are made using the following numerical parameters:

$E = 2.10^{11}\ Pa$, $m_{11} = 598\ kg$, $m_{22} = 399\ kg$,
$m_{1d} = 2\ kg$, $m_{2d} = 1\ kg$, $c_1 = 5.10^4\ N/m$,
$c_2 = 8.10^4\ N/m$, $I_1 = 1{,}6.10^{-6}\ m^4$, $I_2 = 0{,}8.10^{-6}\ m^4$,
$l_1 = 6\ m$, $l_2 = 2\ m$, $e_1 = 0{,}08\ m$, $e_2 = 0{,}06\ m$,

The following values of the eigen circular frequencies are obtained:

$\omega_1 = 5{,}997\ s^{-1}$, $\omega_2 = 5{,}997\ s^{-1}$, $\omega_3 = 9{,}147\ s^{-1}$,
$\omega_4 = 9{,}147\ s^{-1}$.

The safe frequency areas of the forced circular frequency ϖ for avoidance of resonant phenomena are: $\varpi \le 4\ s^{-1}$ as well as $\varpi \ge 12\ s^{-1}$.

Forced circular frequency $\varpi = 40\ s^{-1}$ is accepted.

The system of differential equations (20) is integrated with a variable step by the selected method ode 113 (Adams) and maximum time duration $t = 5\ s$.

The calculations are made for thirteen values of the phase difference λ_n, namely $\lambda_n = n.\pi/12\ rad$,
$(n = 0,1,2,...,11,12)$.

For each phase difference λ_n, the magnitudes of the displacement of the two masses m_1 and m_2 are determined using the following formulas:

$$A_{1n} = \sqrt{u_{1n}^2 + w_{1n}^2} , \qquad A_{2n} = \sqrt{u_{2n}^2 + w_{2n}^2} \ . \tag{21}$$

For the first mass m_1, the maximum deviation from the shaft axis is obtained with a phase difference $\lambda_0 = 0.\pi/12\ rad$, and it has a value $A_{10} = 0{,}00164\ m$.

For the second mass m_2, the maximum deviation from the axis is obtained with a phase difference $\lambda_{11} = 11.\pi/12\ rad$, and it has a value $A_{211} = 0{,}002027\ m$.

The graphs of functions $A_{10} = A_{10}(t)$ and $A_{211} = A_{211}(t)$ are shown in Figure 2 and Figure 3, respectively.

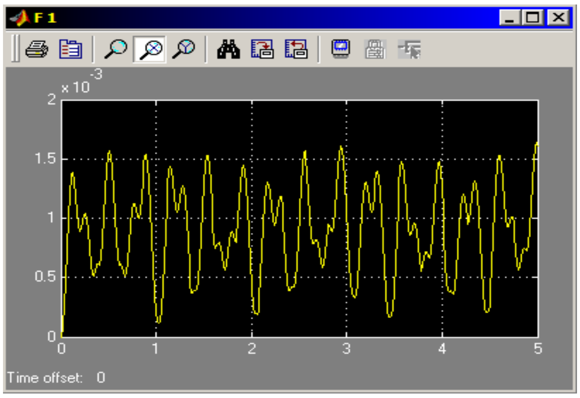

Fig. 2. Displacement of the first mass during the integration time

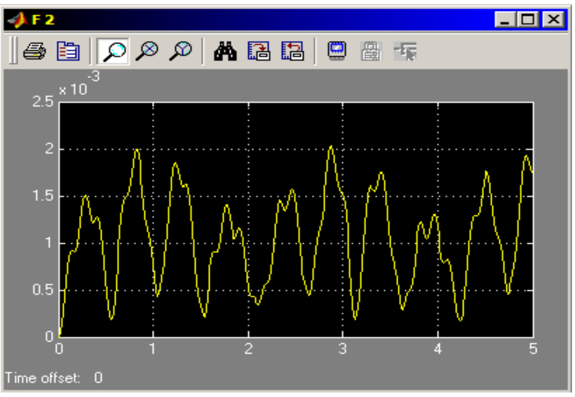

Fig. 3. Displacement of the second mass during the integration time

The prepared model file allows the trajectory traces of each mass in a horizontal plane parallel to the plane Oxy to be visualised.

These trajectory traces of the two masses for the same unfavourable phase differences are shown in Figure 4 and Figure 5, respectively.

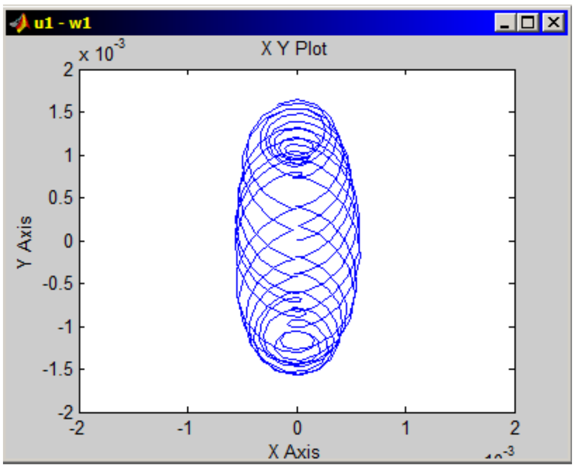

Fig. 4. Trajectory trace of the first mass in the horizontal plane

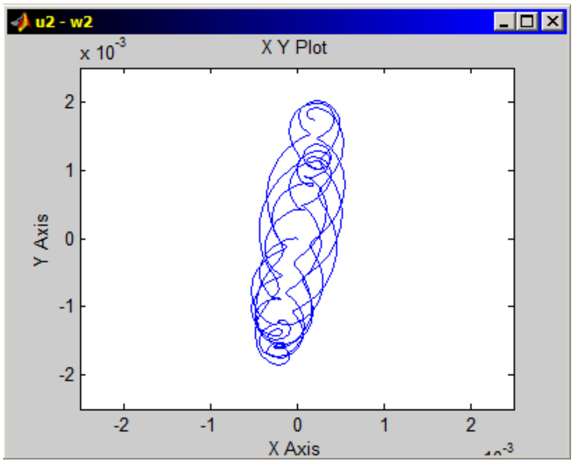

Fig. 5. Trajectory trace of the second mass in the horizontal plane

A study has also been done for the maximum velocities and the maximum accelerations of the two masses.

For each phase difference λ_n the velocity v_n and acceleration a_n of the two masses m_1 и m_2 are determined by the formulas:

$$v_{1n} = \sqrt{\dot{u}_{1n}^2 + \dot{w}_{1n}^2}\ , \qquad v_{2n} = \sqrt{\dot{u}_{2n}^2 + \dot{w}_{2n}^2}\ , \qquad (22)$$

$$a_{1n} = \sqrt{\ddot{u}_{1n}^2 + \ddot{w}_{1n}^2}\ , \qquad a_{2n} = \sqrt{\ddot{u}_{2n}^2 + \ddot{w}_{2n}^2}\ . \qquad (23)$$

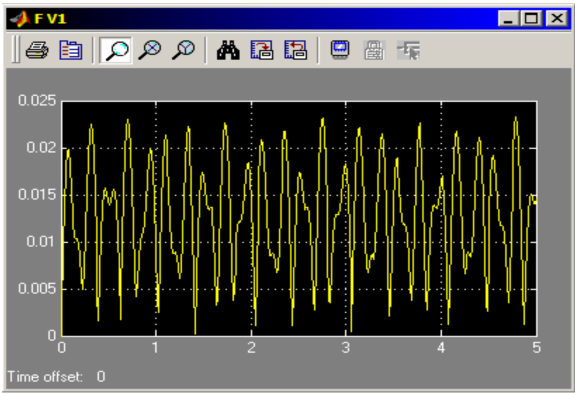

Fig. 6. Velocity of the first mass during the integration time

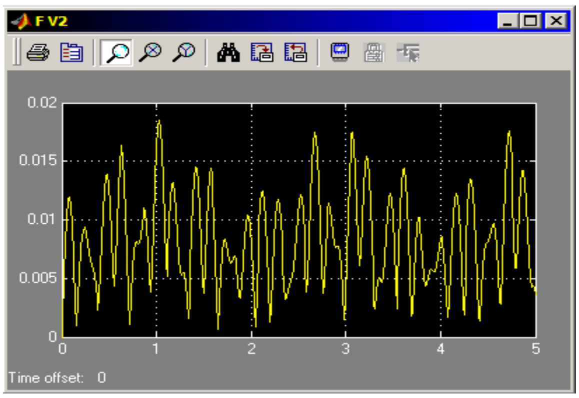

Fig. 7. Velocity of the second mass during the integration time

For the first mass m_1, the maximum velocity is obtained with a phase difference $\lambda_0 = 0.\pi/12\ rad$, and it has a value $v_{10} = 0,0233\ m/s$.

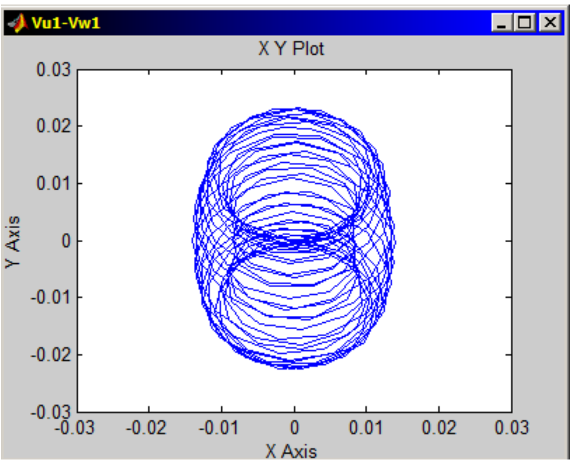

Fig. 8. A trace of velocity vector peak of the first mass in the horizontal plane

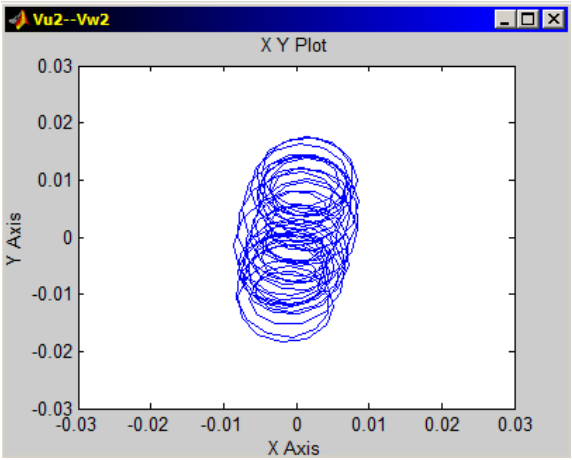

Fig. 9. A trace of velocity vector peak of the second mass in the horizontal plane

For the second mass m_2, the maximum velocity is obtained with a phase difference $\lambda_{11} = 11.\pi/12\ rad$ and it has a value $v_{211} = 0,0185\ m/s$.

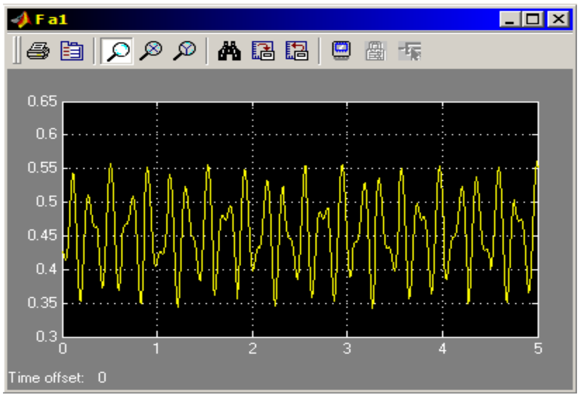

Fig. 10. Acceleration of the first mass during the integration time

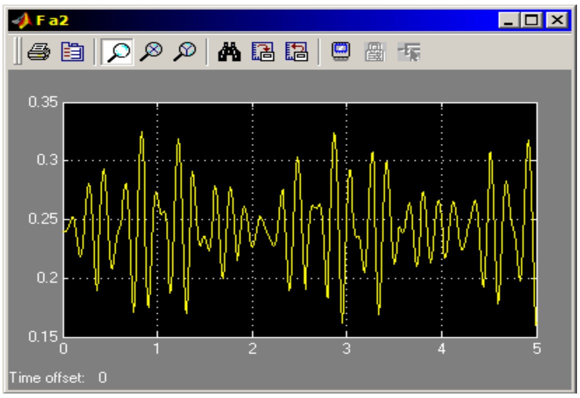

Fig. 11. Acceleration of the second mass during the integration time

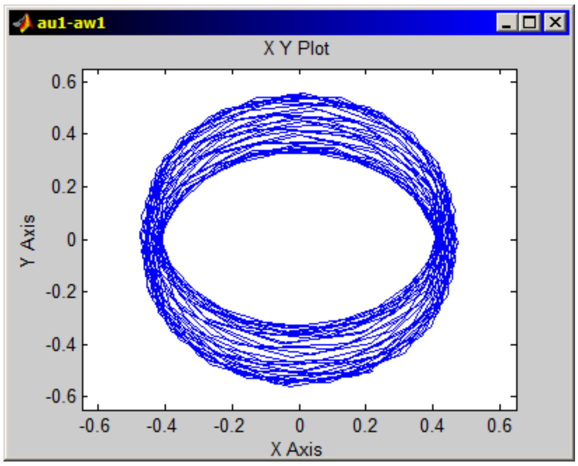

Fig. 12. A trace of acceleration vector peak of the first mass in the horizontal plane

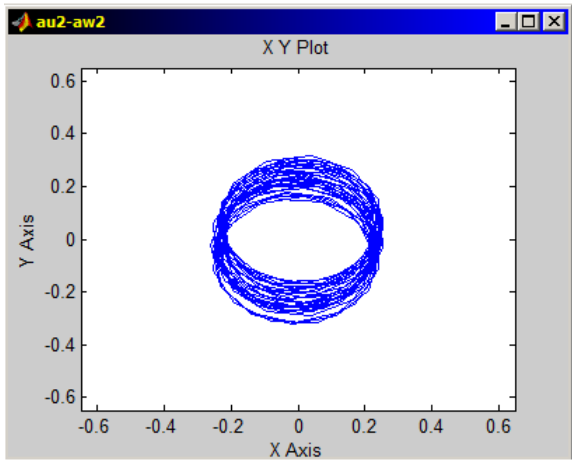

Fig. 13. A trace of acceleration vector peak of the second mass in the horizontal plane

The graphs of functions $v_{10} = v_{10}(t)$ and $v_{211} = v_{211}(t)$ are shown in Figure 6 and Figure 7, respectively.

The trace of velocity vector peaks of the two masses for the correspondingly unfavourable mutual positions are shown in Figure 8 and Figure 9, respectively.

For the first mass m_1, the maximum acceleration is obtained with a phase difference $\lambda_0 = 0.\pi/12\ rad$, and it has a value $a_{10} = 0{,}5606\ m/s^2$.

For the second mass m_2, the maximum acceleration is obtained with a phase difference $\lambda_{11} = 11.\pi/12\ rad$ and it has a value $a_{211} = 0{,}3236\ m/s^2$.

The graphs of functions $a_{10} = a_{10}(t)$ and $a_{211} = a_{211}(t)$ are shown in Figure 10 and Figure 11, respectively.

The trace of acceleration vector peaks of the two masses for the correspondingly unfavourable mutual positions are shown in Figure 12 and Figure 13, respectively.

Conclusion

The main issue is solved.

1. An application program in the area of MatLab ver. 6.1 and in the area of Simulink Toolbox for numerical calculation of free and forced vibrations of a mechanical system with four degrees of freedom is compiled and adapted to this task.
2. The eigen frequencies of this mathematical model of the shaft are determined, and based on these values, a forced circular frequency is selected which is outside the resonant danger zone.
3. The maximum values of the displacements, velocities and accelerations of the two concentrated masses at the correspondingly the most unfavourable mutual position of the two unbalanced masses are determined.
4. All calculated kinematical characteristics are illustrated in detail in Figures 2 to13.
5. This study shows the advantages of the numerical solution compared to the respective analytical solution. These advantages could be summarised as follows:

- Ability to change many input parameters and calculate many variants for a relatively short machine time (Stoyanov, 2018; Stoyanov, 2017).
- Ability to optimise input parameters and the final results using Toolbox Optimisation (Tonchev et al., 2013).

This task provides the basis for further research, complicating the model with the following additions:

1. To take into account the damping in the system.
2. To take into account the effect of horizontal kinematical disturbances that could occur in both supports.
3. To take into account the influence of the distributed mass on the two shaft sections at the bending study.
4. To complicate the dynamical model, taking into account the twist and total bending of the shaft in the two mutually perpendicular planes.

The solved task could be used at the construction of aggregates in the mining industry.

It is also useful for Bachelors, Masters and PhD students who study the Theory of Mechanisms and Machines and Vibrations in Techniques (Sergeev et al., 2018).

The article shows a modern numerical study with the MatLab package (Ivanov, 2011). Such studies can also be performed with other MatLab toolboxes (Marinov et al., 2016), as well as with other mathematical packages such as MathCAD (Stoyanov, 2017, Stoyanov, 2017).

References

Cheshankov B., I. Ivanov, V. Vitliemov, P. Koev. 2004. PCI-method multi-criteria optimisation contracting the set of trade-off solutions. – *15th International Conference on Systems Science*, Wrozlaw, 1–8.

Hristova T. V., A. B. Yanev, N. V. Savov. 2018. Determination of the influence of jaw movement frequency of jaw crusher on energy consumption. – *Annual of the University Petroşani, Electrical Engineering, 20*, 29–36.

Ivanov, A. 2017. Vliyanie na disipaciyata pri izsledvane na svobodnite prostranstveni trepteniya na tvardo tyalo. – *Proceedings of the Annual University Scientific Conference.* Vasil Levski National Military University, Veliko Tarnovo, 234–243 (in Bulgarian with English abstract).

Ivanov, A. 2011. *Modelirane na dinamichni zadachi s MATLAB*. Avangard Prima, Sofia, 100 p. (in Bulgarian)

Ivanov, A. 2017. Three dimensional vibrations of aggregate connected with elastic elements. – *Technomus Journal*, Suceava, 37–42.

Marinov, M., G. Nikolov, E. Gieva, B. Ganev. 2016. Environmental Noise Logging and Calculating. – *IEEE, 39th International Spring Seminar on Electronics Technology (ISSE)*, 425–429.

Petrović, D., M. Bižić, D. Atmadzhova, 2017. Application of rubber elastic elements in suspension of railway vehicles. – *Journal Mechanics, Transport, Communications*, *15*, 3, № 1490. VI-44–VI-51.

Sergeev, Yu. S., S. V. Sergeev, A. A. Dyakonov, E. N. Gordeev. 2018. Improving geometric homogeneity of particles crushed using vibrational drive with modulating properties in machine for crushing brittle materials. – *Journal of Advanced Research in Dynamical and Control Systems*, *13 Special Issue*, 2411–2422.

Sergeev, Yu. S., S. V. Sergeev, A. A. Dyakonov, A. V. Kononistov, G. E. Karpov, A. A. Mikryukov. 2018. Automated monitoring system for self-synchronizing vibrational drives. – *Russian Engineering Research*, *38*, 2, 86–90.

Sergeev, S. V., Yu. S. Sergeev, A. V. Kononistov. 2018. Self-synchronized controlled vibration drive with automated oscillation parameters monitoring system for high-tech equipment. – *ICIE 2018: Proceedings of the 4th International Conference on Industrial Engineering*, 367–374.

Sevastakiev, V., V. Zhivkov, E. Marinov. 1986. *Dinamika i trepteniya na dvigateli s vatreshno gorene*. Tehnika, Sofia, 414 p. (in Bulgarian)

Stoyanov, A. 2017. Solving of statically determined plane truss not built from triangles. – *International Journal of Advancement in Engineering Technology, Management and Applied Sciences (IJAETMAS)*, *4*, 7, 13–22.

Stoyanov, A. 2017. The equilibrium of a body loaded with a spatial system of forces. – *Journal of Mining and Geological Sciences*, *60*, 77–81.

Stoyanov, A. 2017. Research of the equilibrium of a spatial truss with the programming system MathCAD. – *Proceedings of the Annual University Scientific Conference*, Vasil Levski National Military University, Veliko Tarnovo, 214–221 (in Bulgarian with English abstract).

Stoyanov, A. 2018. The movement of a point set in Cartesian coordinates and studied in the MathCAD environment. *Journal of Mining and Geological Sciences*, *61*, 64–69.

Tonchev, Y., V. Vitliemov. 2013. *Optimizaciya s MATLAB. Pragmatichen podhod*. Publising “Angel Kanchev”, Rousse, 250 p. (in Bulgarian)

WEAR OF THE CYLINDER LININGS OF DRUM SAG MILL

Ivan Minin, Simeon Savov

University of Mining and Geology "St. Ivan Rilski", 1700 Sofia; minin_ivan@abv.bg; ss.ss@abv.bg

ABSTRACT. A basic technical parameter of drum mills is the volume of the drum. This parameter changes during operation due to the intensive wear of the mill linings. On the one hand, with the increase of the volume, the productivity of the machine increases too, but on the other this also leads to a change in the speed regime, which affects the grinding quality. The semi-autogenous mills mostly use a cascade and a mixed speed mode motions which depend mainly on the diameter of the drum and the height of the lifters of the cylinder lining. In the present paper an attempt has been made to determine the wear of the lifters of a semi-autogenous mill grinding gold-copper ores with high abrasion and solidity. For this purpose the wear of the mill was periodically measured for several years with a laser scanner, the wear of several cylinder linings of the mill drum was also monitored, while recording the quantity of processed ore and the time of new linings mounting to reach this wear. The necessary number of statistic data has been collected and processed, which, after using the respective computer programmes, presents the quantity of the outworn material from the linings as a function of the grinding time and the quantity of processed ore. For this purpose adequate mathematical models have been obtained, describing the relation between the worn-out steel quantity of the mill linings and the amount of processed ore and the time to achieve to this wear. The results are presented in a graphic manner and the relevant conclusions are made.

Keywords: mill, semi-autogenous, lining, reliability, failure

ИЗНОСВАНЕ НА ОБЛИЦОВКИТЕ НА ЦИЛИНДЪРА НА ПОЛУАВТОГЕННА БАРАБАННА МЕЛНИЦА

Иван Минин, Симеон Савов

Минно-геоложки университет "Св. Иван Рилски", 1700 София

РЕЗЮМЕ. Основен технически показател на барабанните мелници е обемът на барабана. Този параметър се променя по време на експлоатация поради интензивното износване на облицовките на мелницата. От една страна при увеличаване на обема се повишава и производителността на машината но това води и до промяна на скоростния режим който влияе на качеството на смилане. Полуавтогенните мелници използват най често каскаден и смесен скоростен режим които зависят основно от диаметърът на барабана и от височината на лифтерите на облицовката на цилиндъра. В настоящата разработка е направен опит да бъде определено износването на лифтерите на барабанна полуавтогенна мелница смилаща медно златни руди с висока абразивност и здравина. За целта износването на облицовките на мелницата са измервани периодично посредством лазерен скенер в продължение на няколко години, като е проследявано износването на няколко облицовки на цилиндъра на барабана на мелницата и едновременно с това е записвано количеството преработена руда, и времето на поставяне на нова облицовка до достигане на това износване. Събрани са и са обработени необходимия брой статистически данни, които след използване на съответните компютърни програми дават престава за количеството износен от облицовките материал във функция от времето за работа на мелница и количеството преработена руда. За целта са получени адекватни математически модели описващи връзката между износеното количество стомана от облицовките на мелницата и количеството преработена руда и времето за достигане на това износване. Резултатите са показани и графично и са направени съответните изводи.

Ключови думи: мелница, полуавтогенна, облицовка, надеждност, отказ

Introduction

Causes and consequences from the wearing of the lining lifters of a drum mill type SAG 8.5x5.3.

The sliding intensity of the crushing media onto the surface of the drum linings depends mainly on the lining profile and the coefficient of friction between the crushing media and the linings.

It has been proven that the wear of the drum mills linings is greater in mills with high sliding intensity and specific normal contact pressures between the crushing mass and the lining of the drum. It is known that the amount of the grinded by friction product is proportional to the contact area of the friction surfaces. The calculations show that the surface of friction with the balls is only about 2% of the total surface of the balls inside. This allows to claim that the amount of material erased as a result of friction between the grinding bodies and the drum lining is, for example, 2% of the total amount of the grinded product. Thus, it may be concluded that the impact of the linings on the quantitative side of the crushing process because of the friction of grinded mass is negligible. At the same time, the friction significantly increases the wear of the drum linings. As the productivity of the mill for a finished product is proportional to the used useful power, the friction reduction will increase proportionally the mill productivity and the specific energy consumption and lining will be decreased.

If the grinding mass moves without a friction and the speed of the grinding particles, that move on a circle trajectory, is equal to RPMs of the drum $\left(\omega_m = \omega_б\right)$, the power of the drum shaft will be:

$$P_б = M_б . \omega_m , kW \qquad (1)$$

where:

$M_б , N/m$ - torque of the drum.

In the case of movement of the grinding bodies with slippage in order to preserve the initial filling mode, it is necessary to increase the rotation speed of the drum with a value determined by the slippage.

The power of the drum shaft in this case will change and will be defined as:

$$P_{б}^{'} = M_{б} .\omega_{б} ,kW \quad (2)$$

The power, that is lost at the slippage of the ball mass, is:

$$P_{з} = P_{б}^{'} - P_{б} = Mб.\left(\omega_{б} - \omega_{m}\right),kW \quad (3)$$

The power loss at a slippage could be given as:

$$Pз = P_{mp} + P_{U} ,kW \quad (4)$$

where:

P_{Tp} - power loss by the rupture of the lining by friction, kW ;

P_{u} - useful power used to crush material through abrasion in the lining, kW .

The ratio of the values in the above given equation will vary depending on the contact area of the grinding load with the linings of the mill and the resulting pressures at the contact points.

The investigated drum semi-autogenous mill grinds material of high abrasion, hardness and solidity and operates in a mixed speed mode characterised by high slippage intensity of the material on the drum mill linings. Despite the fact that the machine goes out of its operational capacity, with the wear of the drum linings the technological parameters of the machine are gradually changing (Parashkevova, D., Lyubenov, K., 2011). Some of them, such as productivity, are improved due to the increase in drum volume while others, as the yield of the estimated class, are worsened by the change in speed mode and the reduced coefficient of balls fill and large fractions of ore. In addition, the energy consumption and the cost of the final product are increased (Hristova, T., 2018).

The main question that may be posed in this study is whether it is possible to find a relation between the run off of the drum mill linings and the wear rate of the lifters, when measuring and monitoring the wearing of the drum mill linings and using mathematical statistics methods.

This can be used for the proper control of the machine technological parameters with the continuous increase of the drum volume due to the continuous wear of the drum lifters.

Summary

The aim of the present research is to study the patterns of changing the lifters volume of a semi-autogenous drum mill and to obtain an adequate mathematical model, describing the relation of their wear to the mileage of the lining, which can be obtained by means of different programme packages such as MatLab, MuPAD, MathCAD and others (Ivanov. A. 2019). These programmes will serve to create methods and means for predicting the rate of wear under operational conditions.

Investigation on the wear of SAG mill lifters

In order to carry out an investigation of the lifters wear in the lining mileage, it is necessary to choose a method and mode for its measurement.

Due to the complexity of the configuration of the mill linings and the large diameter (Figure 1), it is estimated that the wear of the linings will be monitored and measured using a laser scanner of type “FARO Laser Scanner Focus3DX130” with the following principle of operation and basic parameters:

1. The scanner uses a laser light that is reflected back in the scanner by the object. The distance to 130 m is measured with an accuracy of millimetres through the phase difference between the transmitted and the received light.
2. Vertical scan angle. The mirror deflects the laser light in a vertical direction toward the same object. The maximum angle is up to 270˚ and relies directly to the distance measurement.
3. Horizontal angle. The laser scanner rotates at 360˚ horizontally. The horizontal angle is coded along with the distance measurement.
4. The maximum error in the scanning at 130m is 5mm, as it decreases proportionally for objects nearby.
5. Maximum scanning time for an object - up to 30 minutes.

The scanning takes place under very severe conditions - high temperatures and humidity in the mill drum, because the mill ceases its operation for a short period of time as this is not sufficient for its cooling.

The laser scanner is placed inside the drum on a tripod (Figure 2).

As a result of the scan a cloud of points is obtained (at about 10,000,000 in number) with recorded coordinates, which is a basis for creating a computer model (Figure 3), describing the inside surface of the linings at the exact time of the measurement.

Then, using the software of the scanner, a lining for which the wear of the lifters to be monitored once or twice a month is cropped out.

The results of each scan are overlaid on previous scans for each lining. Finally, cuts in predetermined places are made, to show the wear of the linings throughout their operational life (Figure 4).

Fig. 1. A linings configuration in a drum SAG mill

Fig. 2. The laser scanner during a measurement

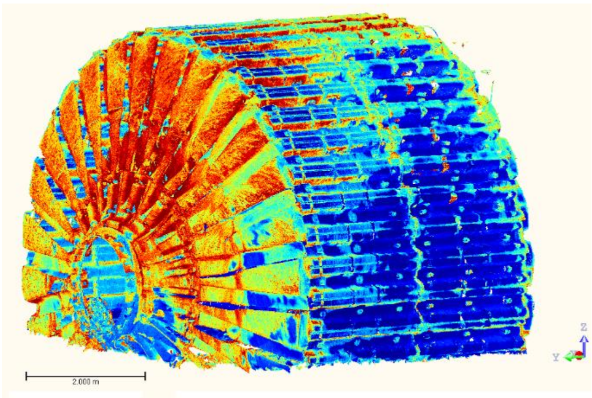

Fig. 3. A model of the scanned inner surface of the mill

Results

By means of the AutoCAD programme, the surface areas of each wear are calculated between two scans (Figure 5). The graphical dependencies of Fig. 4 can also be automatically interpreted using MathCAD (Stoyanov, A., 2016).

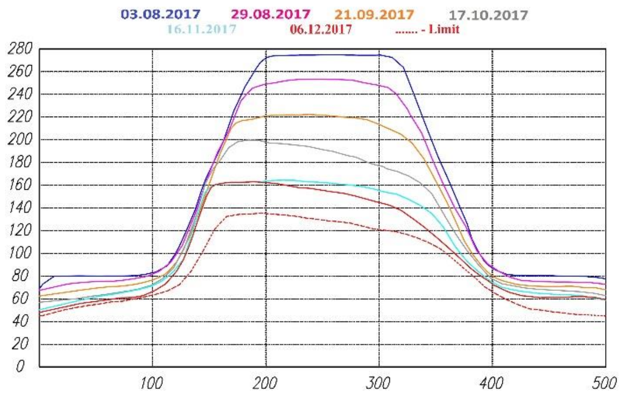

Fig. 4. The linings wear in the middle part of the drum in the period 3rd of August, 2017 – 6th of Dec, 2017

These areas are multiplied by the lining length of each one of the lifters and thus the volume of the worn-out material from the respective lining is obtained. However, in order to obtain the exact volume of the worn material between two scans, it is necessary to subtract the volume of the holes of the clinchers, attaching the lining to the mill drum, from the resulting volume.

For the final calculation of the total volume of the worn out material from the mill drum, the resulting values are multiplied by the number of the lining rows. In order to obtain the quantity of worn material from the mill linings in weight units, the volume is multiplied by the density of the steel.

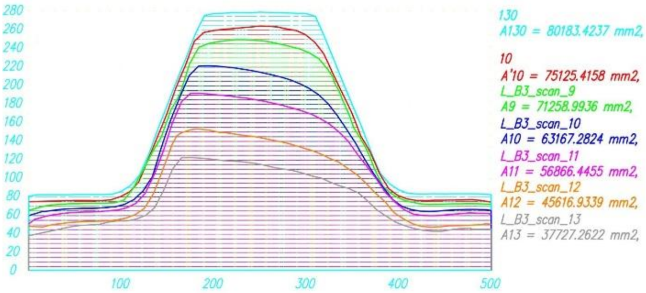

Fig. 5. The linings wear in the middle part of the drum in the period 3rd of August, 2017 – 6th of Dec, 2017

The calculations are drafted by means of the following formula:

$$M = \left[n(A_{NEW} - A), L - V_1\right].\rho, kg \qquad (5)$$

where: M, kg is the calculated mass of the abraded material of the lining due to the wear;

- n - the number of rows of drum linings;
- A_{NEW} - the initial surface area of the section of the new lining;
- A - the measured surface area of the section after the processing of the scan results;
- L - the inner length of the mill drum;
- ρ - the density of the steel of the linings;
- V_1 - the volume of the holes of the clinchers, attaching the lining to the mill drum.

The obtained data, a result of the study, is presented in Table 1.

The last column shows the values of the quantity of the processed ore from the moment of new lining mounting to the moment of the measurement of the linings wearing.

The data processing (the data from Table 1) is performed through a statistical analysis. The whole matrix is processed in order to obtain a mathematical model giving the dependence of the amount of worn material on the tons of processed ore in the mill.

Table 1.

№	$A_{NEW} - A$ m^2	V $m3$	M kg	Q t
1	0.0068	1.010	7928.11	335642
2	0.0094	1.387	10893.56	465570
3	0.0223	3.307	25960.72	586266
4	0.0268	3.982	31260.36	625224
5	0.0364	5.404	42423.77	738401
6	0.0051	0.750	5892.27	105947
7	0.0089	1.324	10396.42	231538
8	0.0170	2.525	19822.78	396555
9	0.0233	3.460	27162.88	572485
10	0.0346	5.129	40267.88	753279
11	0.0425	6.300	49458.88	878000
12	0.0075	1.108	8697.85	167361
13	0.0146	2.172	17056.56	305377
14	0.0197	2.919	22918.92	428799
15	0.0278	4.122	32364.28	562412
16	0.0335	4.968	39005.44	705556
17	0.0468	6.948	54542.27	903122
18	0.0046	0.6796	5335.21	212577
19	0.0103	1.5319	12025.26	381737
20	0.0169	2.5088	19693.71	530653

The results of the experiment were statistically processed using the STATGRAPHICS programme. The programme is suitable for finding target functions to determine the influence factors in stochastic systems. Such are the objects in the mining industry as mills and crushers (Hristova T., 2018, Nedyalkov P., 2010). The results of the statistical analysis of the linings wear are shown in Table 2.

Table 2.

Parameters	**Value**	**Standard error**		**P-value criterion**
Q	0.0269311	0.00631809		0.000
Q^2	3.6136E-9	9.11302E-9		0.000
	Sum of squares of the model	***Degrees of freedom***	***F-value criterion***	***Significance of F***
Model	1.56724E10	2	473,58	0.000
Residual	2.97841E8	18		
Total	1.310446	20		
Multiple correlation coefficient			98.135 %	
Adjusted coefficient of multiple correlation			98.0314 %	
Standard error			4076.76	
Average Absolute Error			3162.78	
Statistics of Durbin - Watson			0.5439	

Thus, 6 models have been obtained, the parameters of which are given in Table 3.

However, it should be taken into consideration that a minimum error is also obtained, caused by the error of the scanner (up to 1 mm) and by the wet mill scanning error. In this case, there is a thin layer of pulp on the linings.

Nevertheless, it can be assumed that the error is within the tolerance limits and is less than 3%.

Table 3

Model №	P criterion	Significance of F	R^2 %	$R^2_{(adj)}$ %
1	<0.05	0	90.28	89.7
2	<0.05	0	96.5	96.5
3	<0.05	0	93.1	92.8
4	0	0	96.2	96.2
5	>0.05	0	93.5	93.3
6	0	0	98.1	98

Among all of the models obtained, the one with the best values of confidence probability is model 6. The multi-correlation coefficient and the corrected multi-correlation coefficient is over 98%.

The value of the confidence probability (P-Value) criterion for the model and the control parameters is below the critical 0.05, i.e., it can be assumed that the model is adequate with a high confidence probability of over 98%.

The equation of the model without a constant in natural variables is:

$$M = 0,027Q + 3,61.10^{-8}Q^2, kg \qquad (6)$$

The relation of the model to the experimental data is shown in Figure 6.

The model is shown in a graphic manner cx Figure 7.

Taking into account the equation of the model and solving it in relevance to m at M = 1kg, it is obtained:

$$3,61.10^{-8}Q^2 + 0,027Q - 1 = 0 \qquad (7)$$

$$Q_{1kg} = \frac{-0,027 + \sqrt{0,027^2 + 4.3,61.10^{-8}}}{2.3,61.10^{-8}} = 37,5t \qquad (8)$$

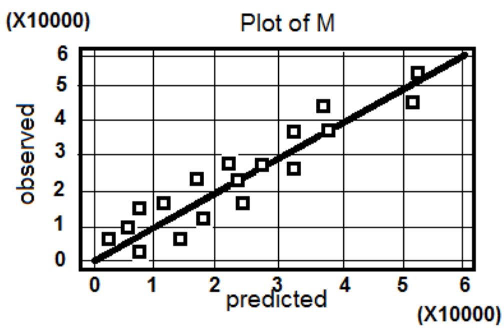

Fig. 6. A compliance of the model with the experimental data

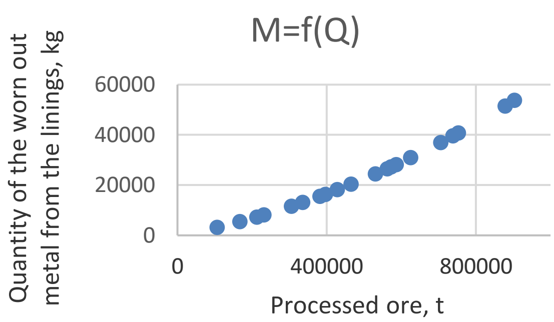

Fig. 7. A graph showing the wear of the linings as a function of the processed ore

Conclusion

As a conclusion, the following statements can be made:

1. There is a functional dependence between the wear of the mill drum linings and the amount of ground ore.

2. The function is parabolic (Figure 3) and this is probably due to the fact that with the wear of the lining lifters the slipping area of the ore onto the inner surface of the mill cylinder increases on the one hand, and on the other, the volume of the mill and the amount of ore in the drum increases, which also leads to an increased wear.

3. The results of the study can be used in the planning of the supply of spare linings of semi-autogenous mills.

References

Hristova, T. 2018. Methodology for determining the replacement period for lifter bars. – *8th International Multidisciplinary Symposium SIMPRO 11-13 October, Petroşani*, 701–706.

Hristova, T., A. Yanev, N. Savov. 2018, Determination of the influence of jaw movement frequency of jaw crusher on energy consumption. – *Annals of the University of Petroşani, Electrical Engineering, 20*, 29–36.

Ivanov, A. 2019. Teoretichno izsledvane na malki vibratsii na dve tvurdi tela s amortizatsiya. – *Sbornik dokladi ot godishna universitetska nautchna konferencia NVU "Vasil Levski"*, 27-28.06.2019, 1555–1565.

Nedyalkov, P. 2010. Research of milling balls dimensions influence over the characteristics of vibrating comminution mill. – *Annual of St. Ivan Rilski University of Mining and Geology*, *53*, III, 49–51.

Parashkevova, D. D., K. Lyubenov. 2011. Avtomatizacia na obogatitelni fabriki. A publishing house „St. Ivan Rilski", Sofia, 190 p. (in Bulgarian)

Stoyanov, A. 2016. *Matrichni operacii s MathCAD v Teoretichnata mehanika Statika*. Kineziologia, Sofia, 165 p. (in Bulgarian)

RELIABILITY AND POSSIBILITY OF FAIL-SAFE OPERATION OF A DRUM MILL TYPE SAG 8,5x5,3

Ivan Minin, Petko Nedyalkov

University of Mining and Geology "St. Ivan Rilski", 1700 Sofia; minin_ivan@abv.bg; petko.nedyalkov@mgu.bg

ABSTRACT. The distribution of failures of an element or machine from a specific technological line is an attempt to describe mathematically their life expectancy. The distribution mode affects the analytical appearance of this distribution. The present paper tries to determine the distribution of failures of the basic elements of a drum semi-autogenous mill used to grind copper and gold ores and to determine the probability of fail-safe operation of this machine. In the present case, the chosen mill has three basic elements, and in case of damage of each one of them it stops working and has to start repair activities for its replacement. That is why, the mill is seen as a system of three elements that are consequently connected. This means that if any one of its components is damaged, there is a failure. The required number of statistics have been gathered and processed, which, after using some elements of the reliability theory, describe the performance regarding the reliability of its separate elements and the mill as a whole. The probability of faultless operation of the whole mill for a given quantity of processed ore is determined by the probability multiplication theorem, thus predicting machine failures and the amount of replacement lining plates necessary for one year ahead. The results obtained after processing the statistics unambiguously prove the right choice of this machine for the exploitation conditions.

Keywords: mill, semi-autogenous, lining, reliability, failure

НАДЕЖДНОСТ И ВЕРОЯТНОСТ ЗА БЕЗОТКАЗНА РАБОТА НА БАРАБАННА МЕЛНИЦА ТИП SAG 8,5x5,3

Иван Минин, Петко Недялков

Минно-геоложки университет "Св. Иван Рилски", 1700 София

РЕЗЮМЕ. Разпределението на отказите на един елемент или една машина от дадена технологична линия е опит да се опише математически продължителността им на живот. Начинът на разпределението се отразява на аналитичния вид на това разпределение. В настоящата разработка е направен опит да бъде определено разпределението на отказите на основните елементи на барабанна полуавтогенна мелница използвана за смилане на медни и златни руди и да бъде определена вероятността за безотказна работа на тази машина. В настоящия случай избраната мелница има три основни елемента, като при повреда на всеки един от тях - спира да работи и започват ремонтни дейности по подмяната му. Ето защо мелницата се разглежда като система от три елемента, които са последователно свързани. Това означава, че който и от елементите й да се повреди, има наличие на отказ. Събрани са и са обработени необходимия брой статистически данни, които след използване на някои елементи от теорията на надеждността, описват поведението по отношение на надеждността на отделните й елементи и на мелницата в съвкупност. Вероятността за безотказна работа на цялата мелница за дадено количество преработена руда е определена от теоремата за умножение на вероятностите, като по този начин могат да бъдат прогнозирани отказите на машината и количеството на резервните облицовъчни плочи необходими за година напред. Получените резултати след обработката на статистическите данни недвусмислено доказват правилният избор на тази машина за условията и на експлоатация.

Ключови думи: мелница, полуавтогенна, облицовка, надеждност, отказ

Introduction

The investigated semi-autogenous tumbling mill type SAG 8.5x5.3 grinds material with high abrasion, hardness and strength. The period of gathering the statistical data was 5 years and shows that the machine went out of service mainly due to wear on the drum linings. They cannot be recovered, but have to be replaced. The drum linings have different wearing in different areas, which depend mostly on the size of the ore fractions in the respective area. The drum of the mill is essentially divided into three elements on which linings are mounted - a feed cover, a cylinder and a discharge cover, as the ore is largest in size in the area of the feed cover and decreases towards the cylinder and the discharge cover of the mill. This also results in quicker wear of the linings of the feed cover than in the other two zones. Figure 1 gives the configuration of the drum linings of a semi-autogenous mill, where 1 shows the lifters of the feed cover linings, 2 – the lifters of the cylinder linings, and 3 - the lifters of the discharge cover of the mill. Figure 2 is a cross-sectional view of a 3D computer model of the overall linings of the mill drum.

The main question that may be set in the present study is how the performance of a machine for the deriving of mineral grains (semi-autogenous drum mill) can be described using the probability and reliability theory and how the failures can be predicted in order to plan the necessary spare parts and upcoming repairs.

The plants in which such machines are in exploitation often are overloaded with spare parts due to the fact that these machines are single and they determine the productivity of the whole company in order to reduce the layovers during the repairs.

The mode of forecasting is reduced to the arithmetic average determination of the required number of nods and elements on the basis of a previous year.

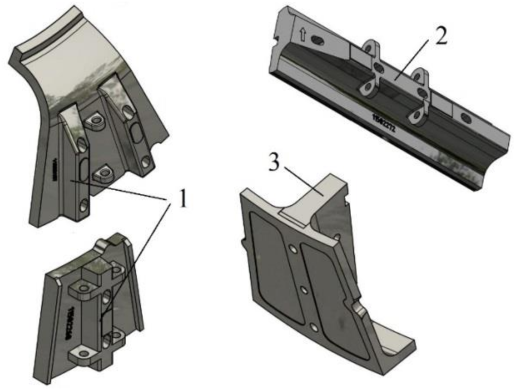

Fig. 1. Configuration of the linings of a mill type SAG

The best solution in this case is to determine the parameters of the machine operational safety based on the reliability theory. A major problem for such a study would appear during the gathering of the statistics when spare parts and nods from different manufacturers and of different quality are delivered for the machine. In the present study this problem is avoided.

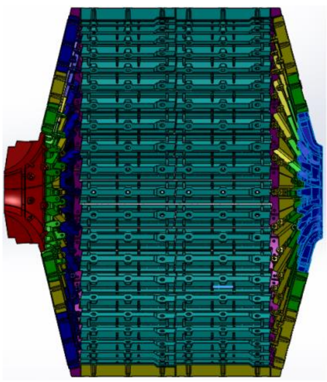

Fig. 2. A cross-section of a 3D computer model of the overall linings of a drum mill type SAG

The present study it is expected to prove the fact that the reliability theory can also be used to solve similar engineering tasks in the mining industry.

The aim of the present study is to investigate the regularities of the alteration of the quality indicators in time by examining the influence of external and internal impacts on the operation of a machine for the deriving of mineral grains - a drum semi-autogenous mill, to create methods and means for prediction of technical conditions and to increase the reliability of such machines under operational conditions.

Theory

The reliability theory widely uses the statistical Weibull distribution function (Waloddi Weibull, 1887 - 1979, KTH Royal Institute of Technology, Stockholm, Sweden) despite the fact that it is based on and uses heavy mathematical and software appliance.

The Weibull probability distribution (density) function /pdf/ is defined as a three parameter function:

$$f(\tau)=\frac{\beta}{\eta}\cdot\left(\frac{\tau-\gamma}{\eta}\right)^{(\beta-1)}\cdot\exp\left[-\left(\frac{\tau-\gamma}{\eta}\right)^{\beta}\right] \quad (1)$$

, where:

- $\beta>0$ - shape (slope) parameter;
- $\eta>0$ - scale parameter;
- $\gamma\in(-\infty,\infty)$ - location parameter, often $\gamma=0$

, and integral (cumulative/CDF/) distribution function is:

$$F(t)=\int_{-\infty}^{t} f(\tau)d\tau=1-\exp\left[-\left(\frac{\tau-\gamma}{\eta}\right)^{\beta}\right], \quad (2)$$

The two parameter Weibull function is derived at zeroing location parameter $\gamma=0$, so the function looks like:

$$f(\tau)=\frac{\beta}{\eta}\cdot\left(\frac{\tau}{\eta}\right)^{(\beta-1)}\cdot\exp\left[-\left(\frac{\tau}{\eta}\right)^{\beta}\right] \quad (3)$$

$$F(t)=\int_{-\infty}^{t} f(\tau)d\tau=1-\exp\left[-\left(\frac{t}{\eta}\right)^{\beta}\right], \quad (4)$$

Survival function *S(t)* or reliability function is defined as admission life period to exceed some time interval *P(T>t)* , so the function is:

$$S(t)=1-P(T\le t)=1-F(t)=exp\left[-\left(\frac{t}{\eta}\right)^{\beta}\right] \quad (5)$$

, and the hazard function is defined by:

$$h(t)=\frac{f(t)}{S(t)}=\frac{f(t)}{1-F(t)}, \quad (6)$$

$$h(t)=\frac{\beta}{\eta^{\beta}}\cdot t^{(\beta-1)} \quad (7)$$

So the reliability functions are defined, but the computational problems appear at the parameter estimation method about Weibull statistics (Weibull 1951, Murthy 2004). One of the easiest method is achieved in median rank regression estimator /**MRE**/ using the equation:

$$\sum_{k=i}^{N}\binom{N}{k}\cdot Z_i^k\cdot(1-Z_i)^{(N-k)} \quad (8)$$

, approximated with Bernard algorithm to:

$$F_T(t_i)\cong Z_i\cong\frac{i-0.3175}{N+0.365} \quad (9)$$

, where:

N, *number* - total number of data;

i - data point ascending rank;
After some transformations shown below:

$$1-F_T(t)=exp\left\{-\left(\frac{t}{\eta}\right)^{\beta}\right\} \quad (10)$$

$$\ln\left\{\ln\left[\frac{1}{S_T(t)}\right]\right\}=\beta\cdot\ln\left(\frac{t}{\eta}\right)=\beta\cdot\left[\ln(t)-\ln(\eta)\right] \quad (11)$$

, one can achieve:

$$y=\beta\cdot x-\beta\cdot\ln(\eta)=A_1\cdot x+A_0 \quad (12)$$

or:

$$\left|\begin{array}{l}\beta=A_1\\ \beta\cdot\ln(\eta)=-A_0\end{array}\right. \Rightarrow \left|\begin{array}{l}\beta=A_1\\ \eta=exp\left(-\dfrac{A_0}{A_1}\right)\end{array}\right. \quad (13)$$

According to these formulas one can easily create non-iterative algorithm in Excel as it is shown in the next section. Usually, the MRE algorithm is represented as a graph of the type on Fig. 3 - 5. The advantage of this method is the ability to work with small amount of data, it is fast and has a simple non-iterative algorithm.

- the mean time to failure /MTTF/ or the expected time to failure as an mathematical expectation:

$$MTTF=E=\eta\cdot\Gamma\left(\frac{1}{\beta}+1\right) \quad (14)$$

, where **Γ** is Gamma function.

Data and results

The particular estimation about parameters of failure data for SAG mill lining plates is described. The data is represented as the point at lining plate changing according cumulative productivity Q_{int} , which is easy to recalculate in relative productivity:

$$Q_i=Q_{Ci}-Q_{Ci-1}, t \quad (15)$$

, respectfully in average hour productivity $Q_h, t/h$ the working hours are:

$$t=\frac{Q_i}{Q_h}, h \quad (16)$$

The median rank is calculated by equation (9), and the parameters regression according equation (13) is shown on Fig.3 - 5 which represent regression:

$$\left|\begin{array}{l}ln(t)\\ ln\left\{ln\left[\dfrac{1}{S(t)}\right]\right\}\end{array}\right. \quad (17)$$

The survival function S(t) and the hazard function h(t) shown on Fig. 6 and 7, are calculated in equidistant points in the observed interval, respectively.

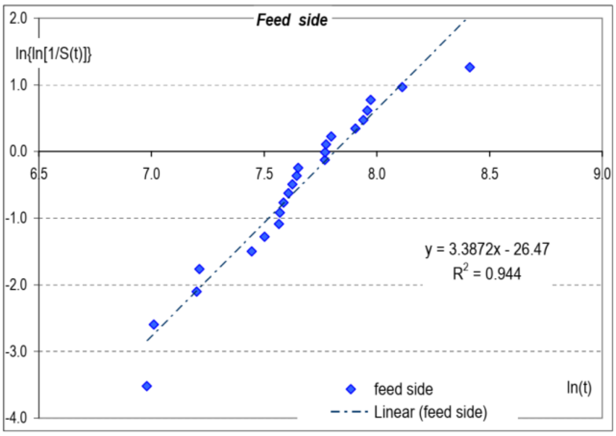

Fig. 3. Feed side maintenance MRE regression

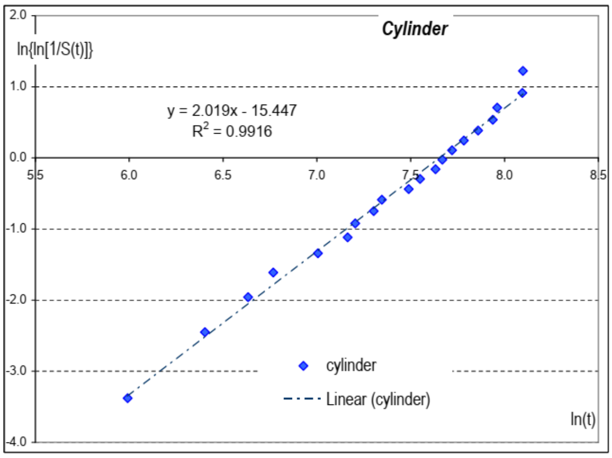

Fig. 4. Cylinder maintenance MRE regression

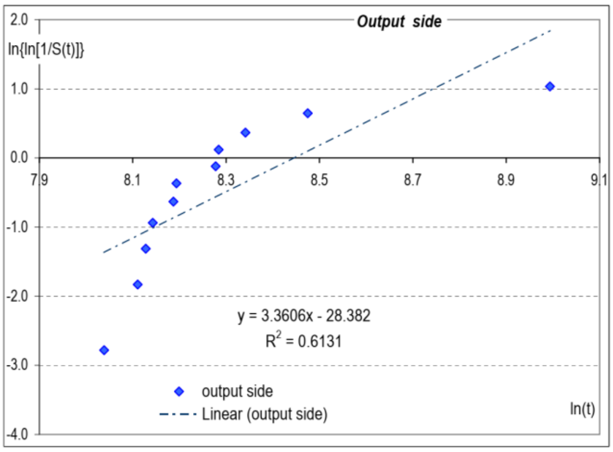

Fig. 5. Output side maintenance MRE regression

Conclusions

So far many researchers (Murthy 2004) found that these dependences follow Weibull models. In comparison with the exponential model (Minin 2017) Weibull fit uses some advantages focused on the reliability over the life cycle of a product. In case of hazard thinking the formula describing hazard function about the maintenance cycle follows formula (6) and it is time dependent in comparison to the time independent hazard function derived from the exponential (Minin 2017) distribution. The derived survival function S(t) is shown on Fig 6, it is clearly seen that probability of survival for all parts of mill liners is dramatically decreasing between 1800 and 4200 working hours. The derived hazard function h(t) from data is shown on Fig. 7.

Table 1. *Parameters results*

	Feed side	Cylinder	Output side
β	3.3872	2.019	3.3606
η	2476.8	2102.4	4654.2
MTTF	2224.66	1862.87	4178.70

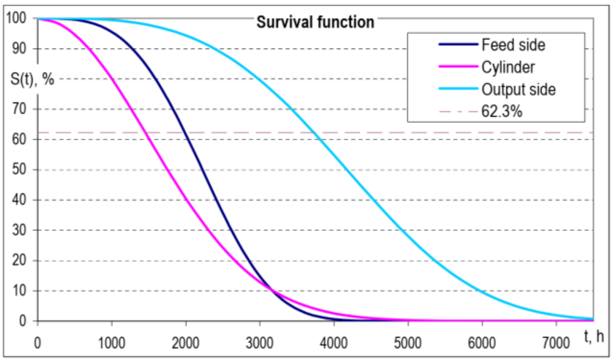

Fig. 6. Survival functions based on fitted Weibull models

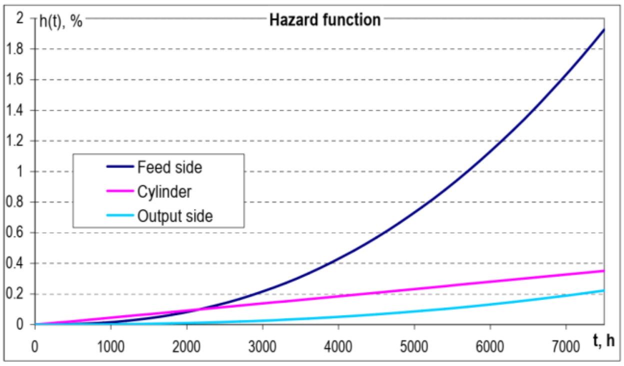

Fig. 7. Hazard functions based on fitted Weibull models

Particular data from SAG maintenance cycles are processed and from them the parameters of Weibull reliability function are estimated. The median regression estimation method with good regression significance is used. The resulting parameters of fitted Weibull function are shown in Table 1.

References

Minin, I., D. Mitev. 2017. Determination of the function of reliability and the possibility of failure-free operation of a jaw crusher type CJ615:01. – *Journal of Mining and Geological Sciences, 60*, III, 11–17.

Murthy, D. P., M. Xie, R. Jiang. 2004. *Weibull Models*. John Wiley and Sons, Inc.

Weibull, W. 1951. A statistical distribution function of wide applicability. – *Journal of Applied Mechanics, 18*, 293–296.

SIMULATION MODELLING OF THE DISCHARGE PLATE OF A JAW CRUSHER

Dimitar Mitev

University of Mining and Geology "St. Ivan Rilski", 1700 Sofia; dimitar_i_radi@abv.bg

ABSTRACT. At present, the application of jaw crushers in the first stage of crushing is most widespread, especially for the purposes of the enrichment industry. During the process, crushing on the jaw crusher elements causes very large mechanical stresses. Determining the magnitude and distribution of deformations and strains in structural elements of mechanical systems is a particularly important engineering task. The application of computer technology has an ever increasing impact in a variety of areas of human knowledge development. This fact is particularly relevant for the heavy machinery industries, one of the main players of which is the enrichment machinery. The main task of this article is to demonstrate the possibilities of modelling, research and analysis (finite element method) of jaw crushers through specialised software products. The object of the study is a real high-performance machine, part of the crushing compartment of a mine situated underground. A simulation computer study of 3D CAD model and CAE analysis was made to obtain the values and the distribution of the deformations and stresses on the model. In this way, it is possible to predict the mechanical damages, the operating time and constructive and other changes in order to optimise the mechanical load and increase safety at work. This article looks at a 3D CAD model of the cut plate. By examining the model of the cut plate the necessary constraints were imposed and it was loaded with the analytically determined forces. From the results of the study, it is clear that the splintered plate is oversized, which is why some suggestions for constructive changes are made.

Keywords: simulation study, movable jaw, jaw crusher

СИМУЛАЦИОННО МОДЕЛИРАНЕ И ИЗСЛЕДВАНЕ НА РАЗПОРНАТА ПЛОЧА НА ЧЕЛЮСТНА ТРОШАЧКА

Димитър Митев

Минно-геоложки университет "Св. Иван Рилски", 1700 София

РЕЗЮМЕ. В настоящия момент прилагането на челюстните трошачки в първи стадий на трошене е най широко разпространено, особено за целите на обогатителната промишленост. По време на процеса трошене върху елементите на челюстните трошачки въздействат много големи механични натоварвания. Определянето на големината и разпределението на деформациите и напреженията в конструкционните елементи от механични системи е особено важна инженерна задача. Основната задача на настоящата статия е чрез специализирани софтуерни продукти да се демонстрират възможностите за моделиране, изследване и анализ (по метода на крайните елементи) на челюстни трошачки. Обект на изследването е реална високопроизводителна машина, част от трошачното отделение на рудник разположен под земята. Направено е симулационно компютърно изследване на 3D-CAD модел и CAE - анализ за да се получат стойностите и разпределението на деформациите и напреженията върху модела. По този начин могат да се прогнозират механичните повреди, експлоатационният срок и извършват конструктивни и др. промени с цел оптимизиране на механичното натоварване и повишаване на сигурността при работа. Тази статия разглежда 3D CAD модел на разпорната плоча. При изследването на модела на разпорната плоча съм наложил необходимите ограничения и съм я натоварил със силите определени по аналитичен път. От резултатите на изследването става ясно, че разпорната плоча е преоразмерена, поради което съм направил предложения за конструктивни промени.

Ключови думи: симулационно изследване, разпорна плоча, челюстна трошачка

Creation of a CAD model of jaw crusher

When creating the model, all dimensions are compiled according to the working drawings of the jaw crusher. This model will be needed in the simulation study of the machine. For this purpose, a CAD model of the jaw crusher was created, according to the original working documentation. For the creation of the current model, a specialised software product for CAD modelling, namely Solid Works, was used. A general view of the 3D model is shown in Figure 1, and Figure 2 presents a sectional view of the model showing the main machine nodes. The simulation analysis was performed on the basis of the three-dimensional model of the crusher with the specialised Solid Works software.

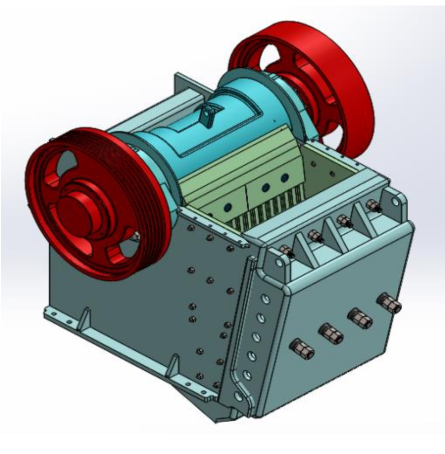

Fig. 1. Jaw crusher type CJ615:01

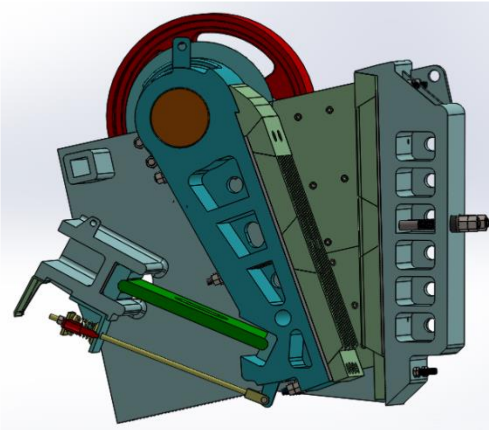

Fig. 2. Jaw crusher type CJ615: 01

The simulation analysis was performed on the basis of the three-dimensional model of the crusher with the specialised Solid Works software. It was chosen to explore the main details - eccentric shaft and moving jaw by neglecting the details that are unrelated to the bearing ability of the structure. The Finite Element method is used with the COSMOS Works software.

Selection of a border condition criterion

The estimation of the stress-strain state of the studied model is a task that has no universal solution for all the cases encountered in practice and is mostly dependent on the material used. On the other hand, the materials can behave as fragile or plastic depending on the temperature, the degree of loading or the way the article is made. All these peculiarities predetermine the choice of one of the following strong theories (Damyanov T., 2009):

- Theory of maximum normal voltages. Valid for fragile materials. It is based on the condition that the boundary of destruction of the material is the same under tension and pressure. This assumption does not correspond to the truth in all cases. For example, most stress concentrators reduce the resistance of the material to tensile loads much more than with a load of stress. According to this theory, the state of frontier occurs when the maximum main voltage reaches the permissible:

$$\sigma_1 \geq [\sigma] \tag{1}$$

- Theory of maximum tangential voltages. Valid for wavy and malleable material. When applied to materials with different mechanical characteristics of tensile and compressive forces, as well as in tensile stress conditions, the obtained results may substantially materially differ from reality. According to the theory, the boundary state criterion is the maximum tangential strain:

$$\tau_{\max} \geq [\sigma] \tag{2}$$

where:

$$\tau_{\max} = \frac{\sigma_1 - \sigma_3}{2} \tag{3}$$

- Energy theory (Von Mises). The theory is based on the appearance of plastic deformations in the masonry materials when equalised with the maximum allowable stress. In most cases the yield limit of the material is given. The results for materials with different mechanical characteristics of tensile and compressive stress are also unsatisfactory. From the point of view of the main stresses, the boundary condition criterion is:

$$\sigma_{VonMises} \geq [\sigma] \tag{4}$$

where:

$$\sigma_{VonMises} = \sqrt{\frac{(\sigma_1-\sigma_2)^2+(\sigma_2-\sigma_3)^2+(\sigma_1-\sigma_3)^2}{2}} \tag{5}$$

- Mor - Columbus Theory. Applicable to brittle materials with different tensile and compressive properties. According to this theory, a border condition occurs when one of the following conditions is met:

$$\sigma_1 \geq [\sigma_{on}] \text{ for } \sigma_1 > 0, \quad \sigma_3 > 0; \tag{6}$$

$$\sigma_3 \geq [-\sigma_{Ham}] \text{ for } \sigma_1 < 0, \quad \sigma_3 < 0; \tag{7}$$

$$\frac{\sigma_1}{[\sigma_{on}]} + \frac{\sigma_3}{[\sigma_{Ham}]} < 1 \text{ for } \sigma_1 \geq 0, \quad \sigma_3 \leq 0 \tag{8}$$

According to the application areas of the studied theories of strength, the theory of maximum tangential strains and energy theory is obviously closest to the conditions typical of the material and the load of the studied structure. It can be summed up that the discharge plate of jaw crusher depends on the type of crushing material and the installed power of the drive motor (Hristova et al., 2012, Christov, Minin, Hristova, 2012).The crushed slag plate 3 is a basic element and serves to close the cementitious crusher chain. At the same time, it acts as a protective element in the extreme load caused by falling into the crushing space of a neutral object. The forces that arise at this point exceed the crushing power 10 times (Minin, 2015), the broken plate is made with special holes thanks to it, which breaks and protects the other crusher elements. It is made of ductile cast iron, bearing its spherical ends in the specially made wedges and frame.

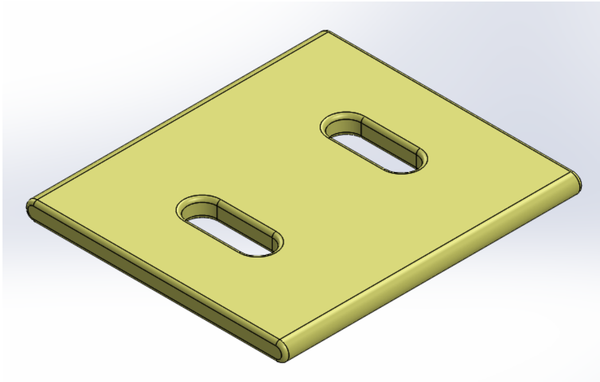

Fig. 3a. Ripped plate

The laser scanner is placed inside the drum on a tripod (Fig. 3).

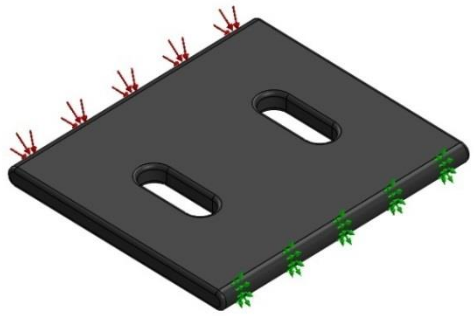

Fig. 3b. Forces and backlash responses

Setting up the sampling tools

The Finite Element Method (FEA) (Nedyalkov 2010) is a numerical method for assessing engineering solutions. For this purpose, the three-dimensional model is divided into small parts of simple-to-form elements, interconnected with common points (nodes). The method determines the behaviour of the model by combining the information obtained from all the forming elements.

Model splicing (discretisation) is one of the most important steps in the study. The large number of elements implies a higher accuracy of the results but also increases the length of the computation process. Conversely, with a small number of endpoints, the calculation time decreases, but this is a prerequisite for network failures and inaccurate results.

Optimal settings for model discretisation are obtained after several dithering attempts.

It is necessary to monitor the time to perform the operations, the size and the number of the final elements obtained, as well as the details in which errors have occurred in their discretion. In some cases, when examining large assembled units containing details of complex shape or relatively small dimensions, the overall reduction in the size of the end elements would lead to an unacceptable increase in their number. In this case, only the problem details are reduced to the size of the end elements, and the overall size is retained at the optimal for the whole model.

In Fig. 4 shows the pattern of the cut plate after sampling in Fig. 5 and 6 show the tensions and security ratios in the jaw crusher plate.

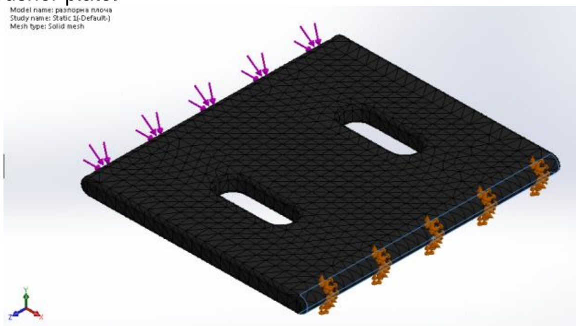

Fig. 4. Discretisation of the plate

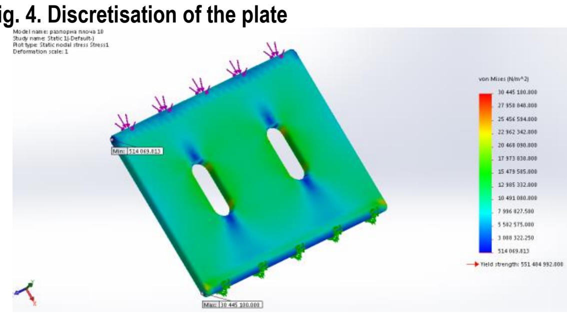

Fig. 5. Distribution of equivalent stresses in the gap plate

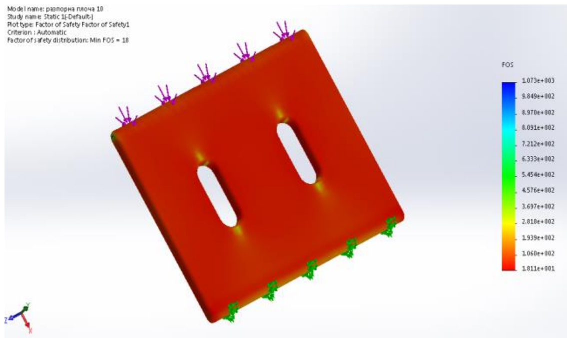

Fig. 6. Distribution of the security factor in the gap plate at normal load

A study of the splintered slab have been done when a neutral object comes in and the crushing power is increased 10 times.

In Fig. 7 and 8 show the stress diagrams and the safety factor for extreme loading of the split plate.

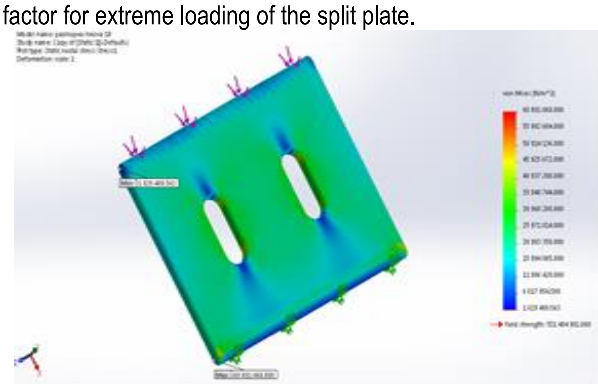

Fig. 7. Distribution of equivalent stresses at extreme load

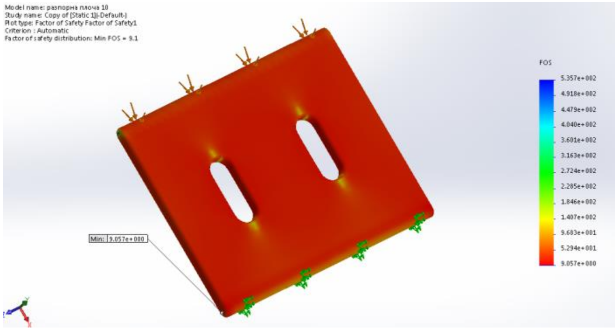

Fig. 8. Distribution of the security factor in the gap plate at extreme crushing strength

During the operation of the crusher, the hydraulic hammer falls and falls into the crushing space, whereby the saw blade does not break and the studs are cut off from the foundation. Due to the resizing of the cut plate constructive changes in its construction have been made.

Two new models on the plate have been made:

- larger openings (Fig. 9).
- with larger openings and two-sided channels (Fig. 10).

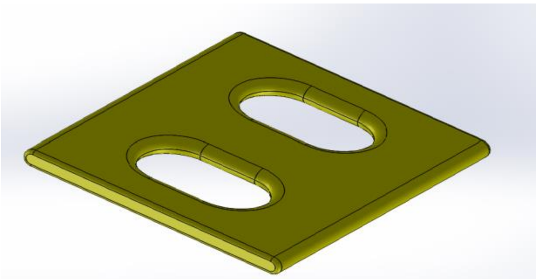

Fig. 9. The laid out a plate with larger openings

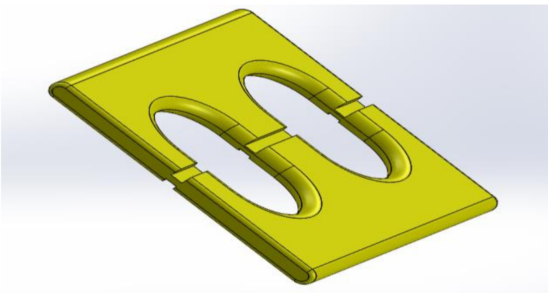

Fig. 10. A slave plate with larger openings and two-sided channels

Fig. 11, 12, 13 and 14 show the voltage and safety ratios in the two jaws of the jaw crusher at extreme stress.

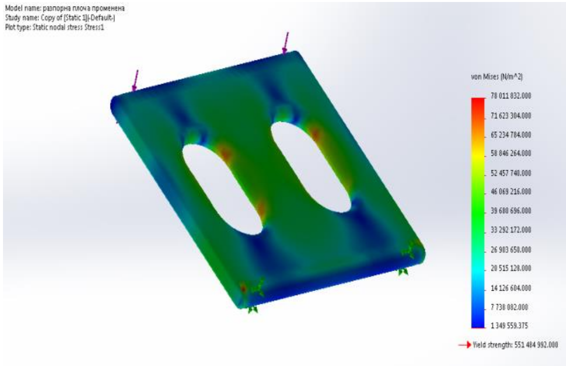

Fig. 11. Distribution of equivalent stresses in the gap with larger openings

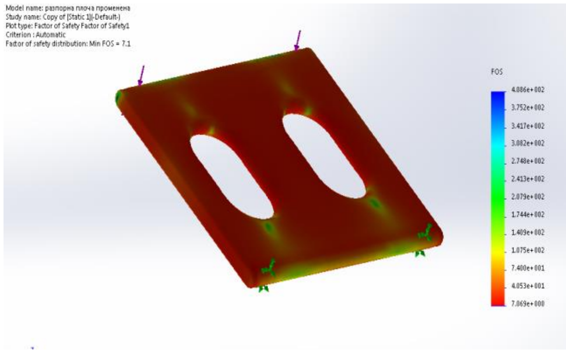

Fig. 12. Distribution of the security factor in the gap with larger openings at extreme load

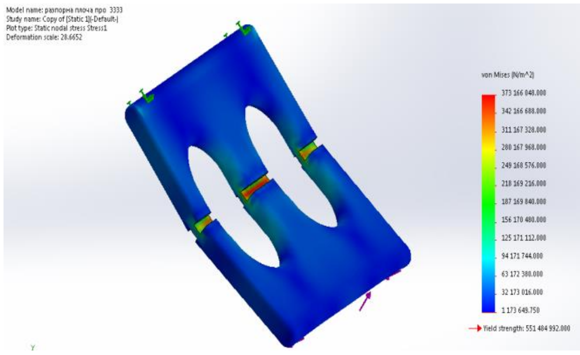

Fig. 13. Distribution of equivalent stresses in the split plate with larger openings and two-sided channels at extreme load

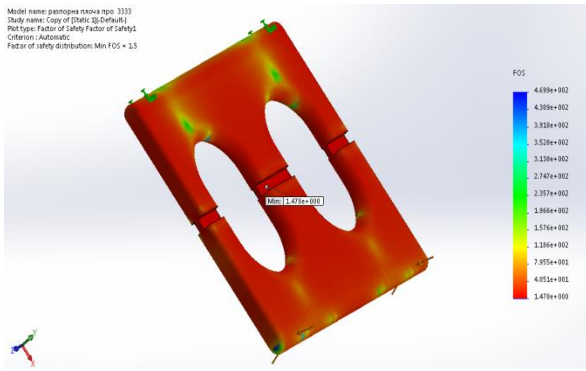

Fig. 14. Distribution of the security factor in the gap with larger openings and two-sided channels at extreme load

Conclusion

1. From the figures and stress diagrams it is clear that the maximum value of 3MPa is located at the end of the edge of the cut plate Fig. 5, where the minimum security factor FOS = 18 Fig. 6 is at normal load, and at extreme load the minimum security factor is FOS = 9.1 (Fig. 8), which is why two more slab plates with a lower security factor have been constructed.

2. A slave plate with enlarged holes in the figures and voltage diagrams makes it clear that the maximum value of 3.9MPa is located at the end of the edge of the cut plate (Fig. 11), where the minimum security factor FOS = 7.1 (Fig. 12) is at normal load.

3. A plate with enlarged holes and two-sided transverse grooves - it is clear from the figures and stress diagrams that the maximum value of 18MPa is located at the end of the edge of the slotted plate (Fig. 13), where the minimum security factor FOS = 1.5 (Fig. 14) is at extreme load, which means that the cavity plate will break at extreme load.

The analysis of the results of the linear static analysis shows that the highest values of strains and deformations do not exceed the permissible ones for the specific case.

References

Christov, V., I. Minin, T. Hristova. 2012. Determination of the engine power of jaw crushers using a neural network. *Annual of University of Mining and Geology “St. Ivan Rilski”, 55*, Sofia, 182–185.

Damyanov, Ts. 2009. *Computer Modelling of Mechanical Systems.* MGU, Sofia.

Hristova T., I. Minin, V. Christov. 2012. Determining the power of crushing engine via neural network with independent input parameters, *Analele Universităţii “Constantin Brâncuşi” din Târgu Jiu, Seria Inginerie, 1*, 160–171.

Minin, I. 2015. Simulation modelling and exploration of a rolling coal mill for crushing copper ores. – *Annual of the University of Mining and Geology "St. Ivan Rilski", 58*, 4, 7–10.

Nedyalkov, P. 2014. FEM modelling and characteristics research of cylindrical journal bearing for cone inertial crusher /KID - 300/*. RECENT, Publ. Transylvania University of Brasov, Romania, 15,* 2(42), 112–116.

RELIABILITY FUNCTION FIT REGARDING ONE JAW CRUSHER LINERS

Petko Nedyalkov

University of Mining and Geology "St. Ivan Rilski", 1700 Sofia; petko.nedyalkov@mgu.bg

ABSTRACT: The paper deals with some formulations in resource assessment function for lining parts in one jaw crusher operating in a Bulgarian gold ore mine. This crusher is operating as a sizing crusher for full ore productivity flow in preventing oversize material fragments to fall on the belt conveyor. In critical view the reliability of that particular crusher influences on the overall mine productivity. Reliability calculations of that machine are based on mathematical assumptions and interpolations using Weibull models. The presented case reviews the modelling with two major interpolation techniques and compares them with estimated data from on-site exploitation. Fitting of the resource function is used in calculation of the reliability, survival and hazard functions for two main lining plates – the lining plate of a moving jaw and the lining plate of a stationary jaw. The research envelopment is the median regression estimation (MRE) method and the maximum likelihood estimation (MLE) method used for density function fitting procedures. The compared fitting procedures are implemented in OpenOffice Calc spreadsheet for MRE and R Studio for MLE algorithm. The fitted functions are compared in a graphical way, and there are some tables presenting the calculated parameter values. Weibull model functions are used to present some diagrams in which it is easy to investigate valuable survival and hazard over time.

Keywords: lining plates, wear, resource, jaw crusher, Weibull reliability function, Weibull model fit

ИЗВЕЖДАНЕ НА ФУНКЦИЯ НА НАДЕЖДНОСТТА ЗА ОБЛИЦОВКИТЕ НА ЧЕЛЮСТНА ТРОШАЧКА

Петко Недялков

Минно-геоложки университет "Св. Иван Рилски", 1700 София

РЕЗЮМЕ: В работата се разглеждат постановки при определяне ресурса и надеждностната функция на облицовките на челюстна трошачка при експлоатационни условия на мина за добив на златна руда в България. Ресурсните изчисления засягащи надеждността обичайно използват математически допускания относно предполагаемият характер на математическата функцията на надеждността, от което се определя и интерполационният метод за извличане на самата функция. В настоящата разработка са използвани два метода за интерполация на функциите на надеждността чрез разпределението на Вейбул. Получени са и са изследвани са функциите на отказите, кумулативната функция на отказите, функцията на надеждността и функция на опасността. На базата на събраните данни са проведени няколко интерполации съгласно статистическото разпределение на Вейбул. Използвано е двупарметрично разпределение на Вейбул като са сравнени два интерполационни метода - с използване на неитеративна интерполация в OpenOffice Calc и итеративна интерполация в RStudio. Представени са резултати в графичен и функционален вид за формения и мащабния параметър на разпределението на Вейбул. Оценката на разпределението е проведена в графичен вид спрямо кумулативните функции на разпределението и плътността на вероятностите на разпределението.

Ключови думи: облицовъчни плочи, износване, ресурс, челюстна трошачка, Вейбул надеждностна функция, Интерполиране на функцията на Вейбул
.

Introduction

Resource calculations, reliability models and their calculations in complex mechanical ore processing machines are multifactor functions. The revealing of adequate mathematical models is a complex job which is usually done by graphical representation. Current research deals with some formulations in resource assessment function for lining parts in one jaw crusher operating in a Bulgarian gold ore mine. The presented method uses mathematical interpolation procedures in comparison with graphical presentation in reveal process.

The jaw crusher (Minin, 2017; Minin, 2012) is a basic machine in first stage ore and rock breakage placed in ore processing and construction material disintegration. That crusher is operating as a sizing crusher for full ore productivity flow in preventing oversize material fragments to fall on the belt conveyor. In critical view the reliability of that particular crusher is influenced by the full mine productivity flow. In case of estimating the product performance regarding the jaw crusher, reliability and recourse calculations are part of its lifecycle and it has to be subjected to its (PLM) product lifecycle management system and maintenance system.

The reliability of the machine is based on some mathematical idealisation and interpolations using some exponential, Gaussian (normal), lognormal, Weibull models and etc. Previous research (Minin, 2017) is focused on the exponential model with its own advantages and disadvantages, and some other researchers (Savov, 2017; Murthy, 2004; Dimitrov, 1994) tend to be using an improved model containing composite exponential function. Widely used are the Weibull models (Weibull 1951, Murthy 2004) in density function fitting, so the presented paper is focused on their application with regard to the reliability of jaw crusher's lining plates.

The presented particular case reviews the case with two major interpolation techniques (Delignette-Muller, 2014; Ricci, 2005) and compares them in estimated data from on-site exploitation. Fitting of the resource function is used in calculation of the reliability, survival and hazard functions for two main lining plates - the lining plate of a moving jaw and the lining plate of a stationary jaw.

THEORY

The reliability theory widely uses the statistical Weibull distribution function (Weibull, 1951) despite the fact that it uses heavy mathematical and software application.

The Weibull probability distribution (density) function /pdf/ is defined as a three parameter function:

$$f(\tau) = \frac{\beta}{\eta} \cdot \left(\frac{\tau-\gamma}{\eta}\right)^{(\beta-1)} \cdot \exp\left[-\left(\frac{\tau-\gamma}{\eta}\right)^{\beta}\right] \quad (1)$$

, where:

- $\beta > 0$ - shape (slope) parameter;
- $\eta > 0$ - scale parameter;
- $\gamma \in (-\infty, \infty)$ - location parameter;

, and integral (cumulative/CDF/) distribution function is:

$$F(t) = \int_{-\infty}^{t} f(\tau)\, d\tau = 1 - \exp\left[-\left(\frac{t-\gamma}{\eta}\right)^{\beta}\right], \quad (2)$$

Often the two parameter Weibull function is derived from a zeroing location parameter $\gamma = 0$ so the function looks like:

$$f(\tau|\gamma=0) = \frac{\beta}{\eta} \cdot \left(\frac{\tau}{\eta}\right)^{(\beta-1)} \cdot \exp\left[-\left(\frac{\tau}{\eta}\right)^{\beta}\right] \quad (3)$$

$$F(t|\gamma=0) = \int_{-\infty}^{t} f(\tau)\, d\tau = 1 - \exp\left[-\left(\frac{t}{\eta}\right)^{\beta}\right], \quad (4)$$

The survival function *S(t)* or reliability function is defined as an admission life period to exceed some time interval *P(T>t)* so the function is:

$$S(t) = 1 - P(T \le t) = 1 - F(t) = exp\left\{-\left(\frac{t-\gamma}{\eta}\right)^{\beta}\right\} \quad (5)$$

, and the hazard function is defined by:

$$h(t) = \frac{f(t)}{S(t)} = \frac{f(t)}{1-F(t)}, \quad (6)$$

$$h(t|\gamma=0) = \frac{\beta}{\eta^{\beta}} \cdot t^{(\beta-1)} \quad (7)$$

The cumulative hazard function is:

$$H(t) = \int_{0}^{t} h(t)\, dt = \int_{0}^{t} \frac{\beta}{\eta^{\beta}} \cdot t^{(\beta-1)}\, dt = \left(\frac{t}{\eta}\right)^{\beta}, \quad (8)$$

or

$$H(t) = -\ln\left[S(t)\right], \quad (9)$$

The reliability functions are defined in upward way, but the computational problems appear at the parameter estimation method about the Weibull statistics (Delignette-Muller, 2014; Ricci, 2005; Murphy, 2004).

One of the easiest method is achieved by median rank regression estimator /**MRE**/ using the equation:

$$\sum_{k=i}^{N} \binom{N}{k} \cdot Z_i^k \cdot (1-Z_i)^{(N-k)} \quad (9)$$

, approximated with Bernard algorithm to:

$$F_T(t_i) \cong Z_i \cong \frac{i-0.3}{N+0.4} \quad (10)$$

, where:

$N, number$ - total number of data;

i - data point ascending rank;

After some transformations shown below:

$$1 - F_T(t) = exp\left\{-\left(\frac{t}{\eta}\right)^{\beta}\right\} \quad (11)$$

$$\ln\left\{\ln\left[\frac{1}{S_T(t)}\right]\right\} = \beta \cdot \ln\left(\frac{t}{\eta}\right) = \beta \cdot \left[\ln(t) - \ln(\eta)\right] \quad (12)$$

, the following equation can be obtained:

$$y = \beta \cdot x - \beta \cdot \ln(\eta) = A_1 \cdot x + A_0$$

or:

$$\left| \begin{array}{l} \beta = A_1 \\ \beta \cdot \ln(\eta) = -A_0 \end{array} \right. \Rightarrow \left| \begin{array}{l} \beta = A_1 \\ \eta = exp\left(-\frac{A_0}{A_1}\right) \end{array} \right. \quad (13)$$

According to these formulas a non-iterative algorithm in spreadsheet can be easily created as shown in the next section. Usually MRE algorithm is represented as values in Table 1 and as a graphical representation of equation (16) in Fig. 1. The advantage of that method is the ability of revealing a small amount of data, despite the fact that it is fast and has a simple algorithm.

Another algorithm is the maximum likelihood estimation /**MLE**/ (Delignette-Muller, 2014) which uses a product of iterative logarithmic and power functions for independent and identical parametrical distributions /iid/ $f(x_i|\theta)$, in which the parameters $\theta_1, ..., \theta_j$ are extracted in function maximisation for:

$$L(\theta) = \prod_{i=1}^{n} f(x_i|\theta) \quad (14)$$

, where:

θ_j - function parameters;

x_i - value for variable x;

n - total count of data x_i and

$f(x_i|\theta)$ - probability density function.

Parameter θ_j extraction uses:

$$\max\left[L(\theta)\right] \Rightarrow \frac{dL(\theta)}{\theta} = 0 \quad (15)$$

or

$$\max\left\{\ln\left[L(\theta)\right]\right\} \Rightarrow \frac{d\ln\left[L(\theta)\right]}{\theta} = 0 \quad (16)$$

, and about particular Weibull distribution:

$$L(t|\beta,\eta) = \prod_{i=1}^{n} f(t_i|\beta,\eta) =$$

$$= \prod_{i=1}^{n}\left[\frac{\beta}{\eta^{\beta}} \cdot t_i^{(\beta-1)} \cdot exp\left\{-\left(\frac{t_i}{\eta}\right)^{\beta}\right\}\right] =$$

$$= \left(\frac{\beta}{\eta^{\beta}}\right)^{n} \cdot \prod_{i=1}^{n} t_i^{(\beta-1)} \cdot exp\left\{-\left(\frac{\sum t_i}{\eta}\right)^{\beta}\right\} \quad (17)$$

The upper function can be simplified by using a logarithm, so:

$$ln\left\{L\left(t\middle|\beta,\eta\right)\right\}=$$

$$=ln\left[\left(\frac{\beta}{\eta^{\beta}}\right)^{n}\cdot\prod_{i=1}^{n}t_i^{(\beta-1)}\cdot exp\left\{-\left(\frac{\sum t_i}{\eta}\right)^{\beta}\right\}\right]=$$

$$=n\cdot ln(\beta)-n\cdot ln\left(\eta^{\beta}\right)+(\beta-1)\cdot\sum_{i=1}^{n}ln(t_i)-\sum_{i=1}^{n}\left(\frac{t_i}{\eta}\right)^{\beta} \qquad (18)$$

The theoretical way is given by those formulas (14 - 18) and the computation way is quite complicated, with implementation of computational iterative algorithm (Delignette-Muller, 2014).

Data and results

The particular estimation about parameters of failure data for jaw crusher's lining plates is described. The data is represented as the point on a lining plate changing according to the cumulative productivity Q_{int}, which is easy to recalculate in relative productivity:

$$Q_i=Q_{Ci}-Q_{Ci-1},\,t \qquad (14)$$

, respectfully in average hour productivity $Q_h, t/h$ working hours are:

$$t=\frac{Q_i}{Q_h},\,h \qquad (15)$$

The median rank is calculated by equation (12), and the regression parameters according to equation (13); Fig.1 and 4 represent the regression:

$$\left|\begin{array}{l} ln(t) \\ ln\left\{ln\left[\dfrac{1}{S(t)}\right]\right\}\end{array}\right. \qquad (16)$$

The survival function *S(t)* and the hazard function *h(t)* are calculated in Table 1 at particular points.

Data extractions represent a real lining plate changing for different plates (Minin, 2017), the first extract (D1) shown in Table 1 is for the lining of a moving jaw, and the second extract (D2) shown in Table 2 is for the lining of a stationary jaw in one and same jaw crusher.

The calculations shown for D1 and D2 and conducted in the same way with the upper formulations give different statistical results. Clearly, the large data (Table 2) quotation gave better MRE regression parameters shown on Fig.4 but there are still issues about the distribution fit.

As shown on Fig. 3 and Fig. 6, the data histogram compared to the fitted distribution shows a difference in the peak height, however, some small shift differences can easily be neglected.

Table 1. *First data extract (**D1**) and MRE calculations*

time	R	time	MR	1/(1-MR)	ln(t)	ln(ln(1/S))		results		
156					5.049	-3.996		*A0*	-19.389	
1235					7.119	1.387		*A1*	2.9702	
608					6.337	-0.557		R^2	0.8595	
	38	*sorted*	MR	1/(1-MR)	ln(t)	ln(ln(1/S))				
h	*№*	*h*								
C	*D*	*E*	*F*	*G*	*H*	*G*		*K*	*L*	*M*
928.6	*1*	155.9	0.0182	1.019	5.049	-4.0		β	2.9702	
607.1	*2*	378.8	0.0443	1.046	5.937	-3.1		η	683.92	
1110.7	*3*	387.6	0.0703	1.076	5.960	-2.6		γ	*0*	
732.1	*4*	391.7	0.0964	1.107	5.970	-2.3		T	1	y
746.4	*5*	391.9	0.1224	1.139	5.971	-2.0		t =	7300	h
475.8	*6*	397.7	0.1484	1.174	5.986	-1.8		S(t)	0.000	
1234.9	*7*	406.1	0.1745	1.211	6.007	-1.7		S(t), %	0	%
522.9	*8*	411.5	0.2005	1.251	6.020	-1.5		h(t)	0.461	
451.0	*9*	451.0	0.2266	1.293	6.111	-1.4		h(t), %	46.1	%
391.9	*10*	456.7	0.2526	1.338	6.124	-1.2		H(t)	4E+08	
482.3	*11*	464.0	0.2786	1.386	6.140	-1.1		T	1/2	y
502.1	*12*	468.7	0.3047	1.438	6.150	-1.0		t =	3650	h
378.8	*13*	474.5	0.3307	1.494	6.162	-0.9		S(t)	0.000	
679.3	*14*	475.8	0.3568	1.555	6.165	-0.8		S(t), %	1.6E-61	%
456.7	*15*	481.5	0.3828	1.620	6.177	-0.7		h(t)	0.118	
489.9	*16*	482.3	0.4089	1.692	6.179	-0.6		h(t), %	11.8	%
527.2	*17*	489.9	0.4349	1.770	6.194	-0.6		H(t)	5.6E+07	
995.2	*18*	502.1	0.4609	1.855	6.219	-0.5		T	1/12	y
406.1	*19*	522.9	0.4870	1.949	6.259	-0.4		t =	608	h
411.5	*20*	527.2	0.5130	2.053	6.268	-0.3		S(t)	0.494	
587.0	*21*	556.8	0.5391	2.169	6.322	-0.3		S(t), %	49.4	%
739.9	*22*	560.3	0.5651	2.299	6.328	-0.2		h(t)	0.003	
397.7	*23*	587.0	0.5911	2.446	6.375	-0.1		h(t), %	0.3	%
468.7	*24*	595.6	0.6172	2.612	6.390	0.0		H(t)	2.719E+05	
938.1	*25*	607.1	0.6432	2.803	6.409	0.0		T	1/24	y
560.3	*26*	658.4	0.6693	3.024	6.490	0.1		t =	304	h
749.2	*27*	679.3	0.6953	3.282	6.521	0.2		S(t)	0.914	
474.5	*28*	732.1	0.7214	3.589	6.596	0.2		S(t), %	91.4	%
556.8	*29*	739.9	0.7474	3.959	6.606	0.3		h(t)	0.001	
387.6	*30*	746.4	0.7734	4.414	6.615	0.4		h(t), %	0.1	%
840.3	*31*	749.2	0.7995	4.987	6.619	0.5		H(t)	3.470E+04	
155.9	*32*	840.3	0.8255	5.731	6.734	0.6		T	3/32	y
658.4	*33*	928.6	0.8516	6.737	6.834	0.6		t =	684	h
481.5	*34*	938.1	0.8776	8.170	6.844	0.7		S(t)	0.368	
464.0	*35*	995.2	0.9036	10.378	6.903	0.9		S(t), %	36.8	%
391.7	*36*	1110.7	0.9297	14.222	7.013	1.0		h(t)	0.004	
595.6	*37*	1136.4	0.9557	22.588	7.036	1.1		h(t), %	0.4	%
1136.4	*38*	1234.9	0.9818	54.857	7.119	1.4		H(t)	3.851E+05	

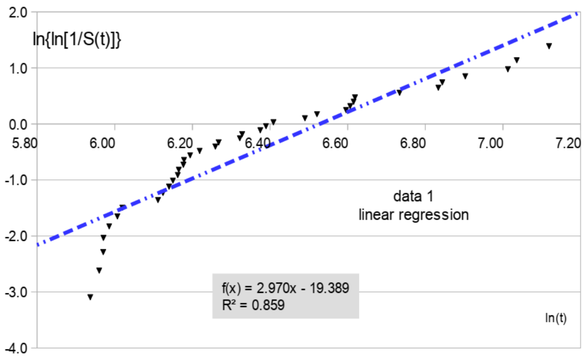

Fig. 1. MRE regression for the second data extract with linear interpolation as shown on the diagram

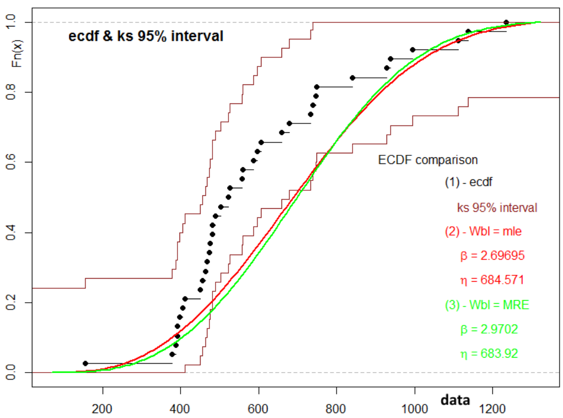

Fig. 2. MRE and MLE fit in comparison with empirical cumulative distribution function

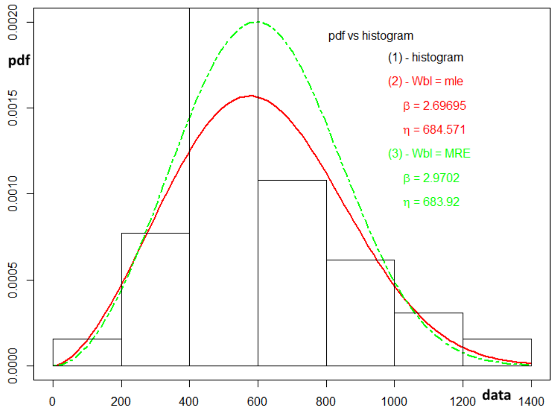

Fig. 3. MRE and MLE fit with histogram for D1

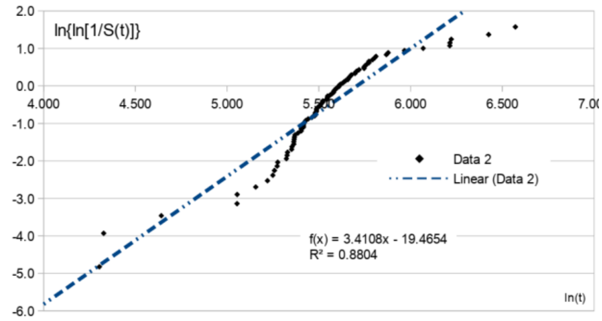

Fig. 4. MRE regression for D2 with linear interpolation

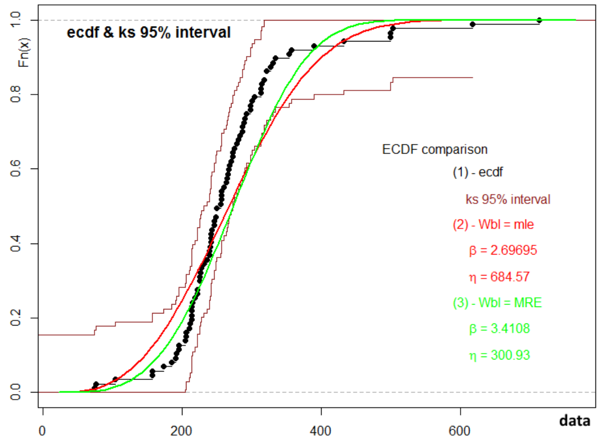

Fig. 5. MRE and MLE fit in comparison with empirical cumulative distribution function for D2

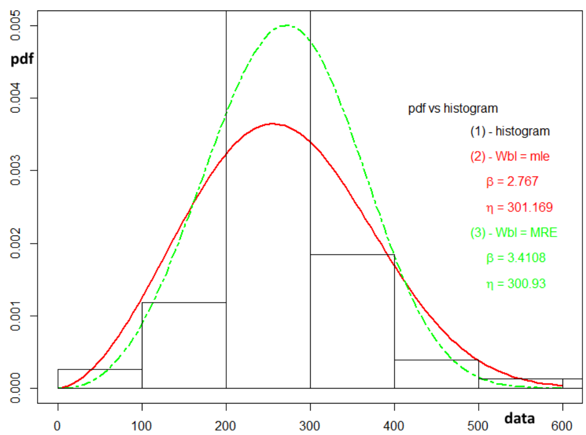

Fig. 6. MRE and MLE fit with histogram for D2

The comparison between the empirical cumulative distribution function /ECDF/ and the estimated cumulative distribution function /CDF/ of fitted distributions is shown on Fig. 2 and 5. The particular plots represented are with 95% Kolmogorov - Smirnov (Ricci, 2005) distance placed in the plot.

Table 2. *Second data extract (**D2**) and MRE calculations*

time	R	time	MR	1/(1-MR)	ln(t)	ln(ln(1/S))	results		
73.99					4.30	-4.82	A0	-19.465	
714.26					6.57	1.57	A1	3.4108	
269.61					5.54	-0.57	R²	0.8804	
	87	sorted	MR	1/(1-MR)	ln(t)	ln(ln(1/S))			
h	№	h							
C	D	E	F	G	H	G	K	L	M
357.1	1	74.0	0.0080	1.008	4.304	-4.8	β	3.4108	
250.0	2	75.7	0.0195	1.020	4.327	-3.9	η	300.93	
432.1	3	103.7	0.0309	1.032	4.641	-3.5	γ	0	
353.6	4	156.7	0.0423	1.044	5.054	-3.1	T	1	y
250.0	5	156.8	0.0538	1.057	5.055	-2.9	t =	7300	h
500.0	6	173.5	0.0652	1.070	5.156	-2.7	S(t)	0.000	
503.6	7	184.9	0.0767	1.083	5.220	-2.5	S(t), %	0	%
321.4	8	190.4	0.0881	1.097	5.249	-2.4	h(t)	0.461	
317.9	9	192.1	0.0995	1.111	5.258	-2.3	h(t), %	46.1	%
278.6	10	195.0	0.1110	1.125	5.273	-2.1	H(t)	4E+08	
321.4	11	195.5	0.1224	1.140	5.276	-2.0	T	1/2	y
239.3	12	205.0	0.1339	1.155	5.323	-1.9	t =	3650	h
240.0	13	205.8	0.1453	1.170	5.327	-1.9	S(t)	0.000	
235.8	14	206.3	0.1568	1.186	5.329	-1.8	S(t), %	0.0E+00	%
327.8	15	210.9	0.1682	1.202	5.352	-1.7	h(t)	0.118	
260.7	16	211.4	0.1796	1.219	5.354	-1.6	h(t), %	11.8	%
239.6	17	213.4	0.1911	1.236	5.363	-1.6	H(t)	5.6E+07	
246.9	18	213.5	0.2025	1.254	5.363	-1.5	T	1/12	y
227.9	19	213.9	0.2140	1.272	5.366	-1.4	t =	608	h
292.4	20	214.2	0.2254	1.291	5.367	-1.4	S(t)	0.000	
314.9	21	214.8	0.2368	1.310	5.370	-1.3	S(t), %	0.0	%
280.7	22	218.5	0.2483	1.330	5.387	-1.3	h(t)	0.003	
75.7	23	222.2	0.2597	1.351	5.404	-1.2	h(t), %	0.3	%
334.0	24	222.3	0.2712	1.372	5.404	-1.2	H(t)	2.72E+05	
195.5	25	225.0	0.2826	1.394	5.416	-1.1	T	1/24	y
225.0	26	225.0	0.2941	1.417	5.416	-1.1	t =	304	h
213.5	27	225.2	0.3055	1.440	5.417	-1.0	S(t)	0.354	
246.4	28	226.4	0.3169	1.464	5.422	-1.0	S(t), %	35.4	%
210.9	29	227.9	0.3284	1.489	5.429	-0.9	h(t)	0.001	
173.5	30	230.8	0.3398	1.515	5.441	-0.9	h(t), %	0.1	%
218.5	31	235.8	0.3513	1.541	5.463	-0.8	H(t)	3.47E+04	
270.4	32	239.3	0.3627	1.569	5.478	-0.8	T	4/97	y
273.2	33	239.6	0.3741	1.598	5.479	-0.8	t =	301	h
248.1	34	240.0	0.3856	1.628	5.481	-0.7	S(t)	0.368	
714.3	35	241.5	0.3970	1.658	5.487	-0.7	S(t), %	36.8	%
304.7	36	241.6	0.4085	1.691	5.487	-0.6	h(t)	0.001	
256.2	37	241.7	0.4199	1.724	5.488	-0.6	h(t), %	0.1	%
617.5	38	243.2	0.4314	1.759	5.494	-0.6	H(t)	3.36E+04	
213.9	39	246.4	0.4428	1.795	5.507	-0.5			
230.8	40	246.9	0.4542	1.832	5.509	-0.5			
211.4	41	248.1	0.4657	1.872	5.514	-0.5			
206.3	42	250.0	0.4771	1.912	5.521	-0.4			
256.7	43	250.0	0.4886	1.955	5.521	-0.4			
195.0	44	255.5	0.5000	2.000	5.543	-0.4			
290.8	45	256.2	0.5114	2.047	5.546	-0.3			
255.5	46	256.7	0.5229	2.096	5.548	-0.3			
298.1	47	256.7	0.5343	2.147	5.548	-0.3			
313.2	48	260.7	0.5458	2.202	5.563	-0.2			
299.0	49	263.1	0.5572	2.258	5.573	-0.2			
283.1	50	265.0	0.5686	2.318	5.580	-0.2			
301.1	51	265.5	0.5801	2.381	5.582	-0.1			
287.2	52	266.8	0.5915	2.448	5.586	-0.1			
273.1	53	268.2	0.6030	2.519	5.592	-0.1			
241.6	54	270.4	0.6144	2.593	5.600	0.0			
331.2	55	273.1	0.6259	2.673	5.610	0.0			
225.0	56	273.2	0.6373	2.757	5.610	0.0			
268.2	57	275.3	0.6487	2.847	5.618	0.0			
289.2	58	278.6	0.6602	2.943	5.630	0.1			
313.2	59	280.7	0.6716	3.045	5.637	0.1			
286.7	60	283.1	0.6831	3.155	5.646	0.1			
263.1	61	286.7	0.6945	3.273	5.659	0.2			
390.3	62	287.2	0.7059	3.401	5.660	0.2			
156.8	63	289.2	0.7174	3.538	5.667	0.2			
74.0	64	290.8	0.7288	3.688	5.673	0.3			
266.8	65	292.4	0.7403	3.850	5.678	0.3			
265.5	66	298.1	0.7517	4.028	5.697	0.3			
214.2	67	299.0	0.7632	4.222	5.700	0.4			
275.3	68	301.1	0.7746	4.437	5.708	0.4			
205.8	69	304.7	0.7860	4.674	5.719	0.4			
243.2	70	313.2	0.7975	4.938	5.747	0.5			
205.0	71	313.2	0.8089	5.234	5.747	0.5			
214.8	72	314.9	0.8204	5.567	5.752	0.5			
241.5	73	317.9	0.8318	5.946	5.762	0.6			
184.9	74	321.4	0.8432	6.380	5.773	0.6			
265.0	75	321.4	0.8547	6.882	5.773	0.7			
222.2	76	327.8	0.8661	7.470	5.792	0.7			
156.7	77	331.2	0.8776	8.168	5.803	0.7			
190.4	78	334.0	0.8890	9.010	5.811	0.8			
226.4	79	353.6	0.9005	10.046	5.868	0.8			
192.1	80	357.1	0.9119	11.351	5.878	0.9			
256.7	81	390.3	0.9233	13.045	5.967	0.9			
222.3	82	432.1	0.9348	15.333	6.069	1.0			
499.7	83	499.7	0.9462	18.596	6.214	1.1			
103.7	84	500.0	0.9577	23.622	6.215	1.2			
225.2	85	503.6	0.9691	32.370	6.222	1.2			
213.4	86	617.5	0.9805	51.412	6.426	1.4			
241.7	87	714.3	0.9920	124.857	6.571	1.6			

Conclusions

A product life cycle usually is described as "the time from the initial concept of a product to its withdrawal from the market". In the case of mechanical damage or wearing the withdrawal point is subordinated to a particular law of quality/quantity decreasing. So far, many researchers (Murthy, 2004; Lazov, 2010) have found that these dependences follow the Weibull models. In comparison with the exponential model (Minin, 2017) the Weibull fit uses some advantages focused on the reliability over the life cycle of a product. The formula describing the hazard function follows the time dependent formula (7) in distinction to the time independent exponential hazard function (Minin, 2017).

Table 3. *Parameters results*

	Data 1		Data 2		
	mle	MRE	mle	MRE	*unit*
β	2.69695	2.9702	2.767	3.4108	
η	684.571	683.92	301.169	300.93	
γ	*0*	*0*	*0*	*0*	
t = η	685	684	301	301	h
F(t)	63.2	63.2	63.2	63.2	%
S(t)	36.8	36.8	36.8	36.8	%
h(t)	0.4	0.4	0.0	0.0	%
t = 2η	1369	1368	602	602	h
S(t)	0.2	0.0	0.1	0.0	%
h(t)	1.3	1.7	3.1	6.0	%

As a particular conclusion from the research the valuated survival for the lining plates can be followed, as shown on Fig. 7. Hence, the repair period has to be multiple to that value. The results in Table 3 give the comparison between the coefficients achieved through the different fit technique and the different data extracts.

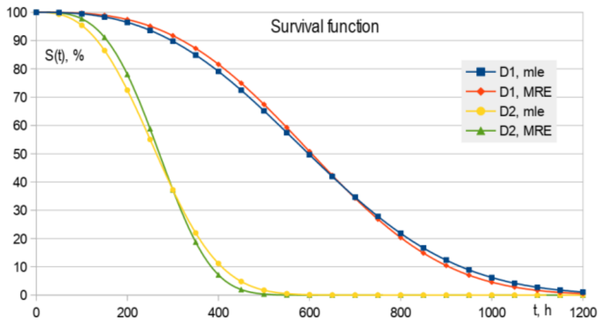

Fig. 7. Survival functions based on fitted Weibull models

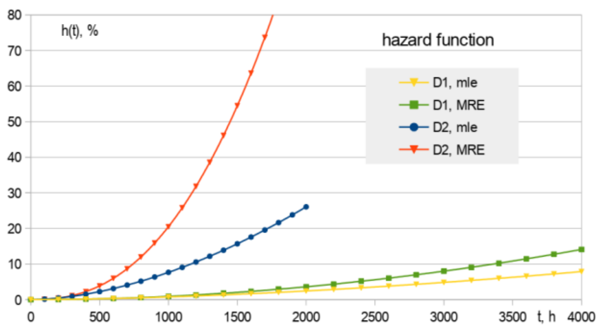

Fig. 8. Hazard functions based on fitted Weibull models

The fitting procedures and the software instruments about distribution functions are in constant development. Many commercial software packages are widely used, and also, many free or under CC and GNU license are applied by the scientific research community. In this research, for the programme calculation and the graph presenting plots the iterative package for R Studio under GNU license is used in comparison with non-iterative calculation made in spreadsheet OpenOffice Calc.

The acceptance of these models is considerable with the graphical instruments shown above. Further implementations should be used with numerical goodness-of-fit test. In the reliability research field the Kolmogorov-Smirnov test, Anderson-Darling test and Chi squared test are preferred.

Some improvement in model fitting can be observed by increasing the data sampling in Fig. 5 in comparison to Fig. 2.

Logically, these conclusions show that the presented Weibull model fit gives an account of the wearing process of jaw crusher's liners with shown values in parameters interpolation. The results and methods should be placed in a modern project design methodology (Lazov, 2010; 2015) with periods' account of the maintenance cycle. It is advisable to expand the research in other interpolation procedures and with different data sampling volume.

References

Delignette-Muller. 2014. Marie Laure and Ch. Dutang, "fitdistrplus": An R Package for Fitting Distributions, October 2014 (revised in July 2018).

Dimitrov, K., D. Danchev. 1994. *Nadezhdnost na stroitelni mashini i sistemi*, Tehnika, Sofia (in Bulgarian).

Jones, O., R. Maillardet, A. Robinson. 2009. *Introduction to Scientific Programming and Simulation Using R*. Chapman and Hall.

Lazov, L. 2010. Simulation study of the wind turbine bearing loads. Bulgarian journal for engineering design. *bjed.tu-sofia.bg, 6, December 2010*, 33–38 (in Bulgarian with English abstract).

Lazov, L. 2015. About the influence of the camber over selection of the main girders cross section of bridge cranes. – *CAx Technologies, 3,* 110–114, (in Bulgarian with English abstract).

Minin, I. 2012. *Technika i technologii za obogatyavane na polezni izkopaemi*. Avangard prima, Sofia (in Bulgarian).

Minin, I., D. Mitev. 2017. Determination of the function of reliability and the possibility of failure-free operation of a jaw crusher type CJ615:01. – *Journal of Mining and Geological Sciences, 60*, III.

Murthy, D. P., M. Xie, R. Jiang. 2004. *Weibull Models*. John Wiley and Sons, Inc.

Savov, S. 2017. *Izsledvane i optimizatsia na tehnologichni parametri pri konusni inertsionni troshachki*. Avangard prima, Sofia (in Bulgarian).

Ricci, V. 2005 Fitting distributions with R. *https://cran.r-project.org/doc/contrib/Ricci-distributions-en.pdf*

Weibull, W. 1951. A statistical distribution function of wide applicability. – *Journal of Applied Mechanics, 18,* 293–296.

SELECTION OF PARAMETERS OF TECHNOLOGICAL EQUIPMENT FOR THE EXTRACTION COMPLEX OF RAW PEAT MATERIALS FROM UNDRAINED DEPOSITS

Irina Khudiakova, Sergey Ivanov

Saint Petersburg Mining University, 199106 Saint Petersburg; irikhudyakova@yandex.ru; lisa_lisa74@mail.ru

ABSTRACT. Expanding the use of peat is strategically aimed at diversifying the country's fuel balance, improving the reliability of energy supply and its energy security. The greatest impact is seen in decentralised energy supply zones, remote and inaccessible areas of the country.
A technology of extraction and quarry processing of raw peat materials without preliminary preparation of the field within the framework of environmental technologies and the selection of the scheme solution of the complex of mining equipment for its implementation are proposed.
The paper presents the operational energy consumption for the schemes of technological mining equipment floating complex for the extraction and processing of raw peat materials. The general structural formula of the complex is given. An algorithm for selecting the main parameters of the complex equipment for the extraction and processing of peat raw materials from an undrained deposit is proposed.

Keywords: raw peat materials, structural scheme, the structural formula, the complex of mining equipment, energy supply

ИЗБОР НА ПАРАМЕТРИ НА ТЕХНОЛОГИЧНО ОБОРУДВАНЕ ЗА КОМПЛЕКС ЗА ДОБИВ НА ТОРФЕНА СУРОВИНА ОТ НЕДРЕНИРАНИ НАХОДИЩА

Ирина Худякова, Сергей Иванов
Санктпетербургски минен университет, 199106 Санкт Петербург

РЕЗЮМЕ. Разширяването на използването на торфа има стратегическо значение за диверсификация на източниците на енергия, подобряване на надеждността на енергийните доставки и енергийната сигурност на страната. Най-голям ефект от този процес се наблюдава в отдалечените и недостъпни райони с децентрализирано електрозахранване.
Предложена е технология за добив и обработка на торфената суровина, без предварителна подготовка на находища, съобразена с изискванията за опазване на околната среда. Предложени са схемно решение на комплекса и необходимото за реализацията му минно оборудване.
В работата са представени оперативните разходите за енергия при различни схеми на технологично минно оборудване на плаващ комплекс за добив и преработка на торфената суровини. Дадена е обща структурна формула на комплекса. Предложен е алгоритъм за избор на основните параметри на цялостно оборудване за добив и преработка на торфената суровина от недренирани находища.

Ключови думи: торфена суровина, структурна схема, структурна формула, комплекс на минно оборудване, електрозахранване

Introduction

At present, the need for extraction of raw peat materials is due to the production of cheap local fuel, agricultural fertilizers to increase soil fertility and to promote the implementation of import substitution programmes in solving the problems of increasing energy, as well as reducing the risks of fires in the waste areas of peat deposits, especially if they are accompanied by preliminary dewatering of territories.

The use of traditional fuels leads to the emission of a large number of toxic substances into the atmosphere and intensifies the processes leading to climate change. Extraction and use of these relatively non-renewable minerals is quite expensive. Many countries, in order to save, use renewable local energy sources, which pollute the environment less. In addition, they do not require large costs for their production, processing and delivery. These resources include peat, and peat raw materials are used as a fuel. For example, in Germany, the Republic of Finland, the Kingdom of Sweden, the Republic of Ireland, the share of fuel derived from peat raw materials accounts for up to 10 % of energy production.

In Russia, this energy source is underestimated, and its share in the country's energy balance is only 0.2%. Meanwhile, there are large peat deposits in 29 regions of the Russian Federation, in fifteen regions the share of peat exceeds 60% of the total potential of renewable energy sources. The total peat reserves are slightly less than $70 \cdot 10^9$ tons of conventional fuel and exceed the energy potential of domestic hydrocarbon reserves. Each year, the peat in Russia is growing by $200 \cdot 10^6$ tons conditional humidity. At the same time, the expansion of peat use is strategically aimed at expanding and reducing the cost of the resource base, diversifying the country's fuel balance in order to increase both the reliability of energy supply and competition in the supply of energy resources, reducing CO_2 emissions and improving the country's energy security.

Analysis of the use of peat raw materials and environmental technologies

Peat is widely used as a fuel in the form of crumbs in thermal power plants, energy-dense fuel in the form of pellets, briquettes and pieces for heating. The cost of heat production from peat briquettes is lower in relation to coal by 17 %, and to fuel oil - by 45 %. In the pyrolysis of peat, a generator gas is produced, which is used as a fuel in both electric power generation and heat power engineering of enterprises. In agriculture, peat raw materials are widely used as fertilizers, for the production of seedlings, composting and substrates. In the chemical industry it is a valuable raw material in the production of ammonium salts, ammonia, wax, fatty acids, oils, paraffins, polymers, alcohols, dry ice, peat-alkaline reagents. Due to its high moisture capacity, heat capacity and adsorption properties, peat raw materials are widely used in medicine as anti-inflammatory and tonic agents, as well as for the manufacture of gels, balms, extracts, filter materials and sorbents for the absorption and fixation of oil spills and oil products, absorption of oils, fuel oils, gasoline, cleaning contaminated surfaces of water and areas of industrial facilities, equipment. Peat is widely used in reclamation of disturbed lands, elimination of landfills and landfills. Peat raw materials are widely used in construction in the form of peat insulation boards, panels, building blocks, concrete additives, components of various coatings, green construction.

When assessing the possibility of developing peat deposits, it is necessary to take into account that they are important elements in the chain of interrelated and interacting components of the natural environment and any anthropogenic impact causes its change.

Within the framework of environmental technologies and environmental management, the authors proposed the technology of extraction and quarry processing of peat raw materials without preliminary preparation of adeposit, excluding hydraulic engineering measures for drainage of adeposit and preparation of production sites, surface layers and production areas (patents RU №2599117, № 2655235, № 2672366).

In the extraction of peat raw materials complexes of mining equipment on the basis of floating platforms it is expected to carry out the production process, both from the surface and from the water. The use of traditional methods of excavation is very effective at depths of up to 4-5 meters. In this case, it is necessary to use modernised equipment that does not allow the erosion of peat raw materials separated from the massif from the working body of the excavating mining machine, or the use of a continuous process of creating a hydro pulp with its delivery to the floating platform by hydro-transport and subsequent centrifugation or extraction of excess moisture, which is more costly than conventional excavation.

The rationale for the choice of an effective structure of complex

The complex of mining equipment is a self-propelled floating platform with mining equipment placed on it and means of autonomous power generation.

Depending on the final commodity product, different circuit solutions of the complex are possible, and its functional structure includes the following blocks: production; separation and crushing of peat-wood raw materials; moulding; drying; production of a commodity product.

The advantages of the proposed technology implemented in the framework of environmental management are presented in Table 1.

Table 1. *Comparison of milling and proposed technologies for the same production volumes*

Milling technology	**Proposed technology**
Cut depth 0.25 m	Excavation depth 2-5 m
Density of peat raw material γ= 500 kg/m3	Density of peat raw material γ= 1040 kg/m3
The area of the production site and its rent per year – 1.0/1.0	The area of the production site and its rent per year – 0.05/0.05
The term of preparation of the field – 3 years	The term of preparation of the Deposit — not required
Range of mining machines for preparing the field: summary of the forests; drainage of fields; preparation of field;	Range of mining machinery for the preparation of the deposit – not required
The technological complex of machinery for processing of peat raw materials and energy is missing	The technological complex of machinery for processing of peat raw materials and energy is provided
Complex machines for the preparation and repair of areas is provided	Complex machines for the preparation and repair of areas – not required
Environmental risks (dust, fires, emissions from internal combustion engines of vehicles, dewatering, destruction of forests and ecosystems)	"Wet technology" – no risk of fire, no dusting, minimised wastage
Reclamation of mined-out areas	No remediation is required. Artificial pond in the framework of environmental technologies.
Seasonality of production and dependence on weather conditions	Production is carried out year-round. Reduced dependence on weather conditions

As can be seen from the table, the use of a floating complex in comparison with the milling method of production will reduce production costs, the timing of a deposit, the range of equipment, their transport component, reduce the risks of man-made disasters, get away from the seasonality of production.

At the same time, it is the primary choice of equipment that determines the entire technological chain of the mining machines of the complex. Figure 1 shows four variants of circuit solutions for the implementation of the complex.

The main mining equipment in the block of extraction of peat raw materials can be: a manipulator with a bucket (reverse shovel); a multi-bucket chain excavator, a vertical screw-cutter; mechanical and hydraulic production.

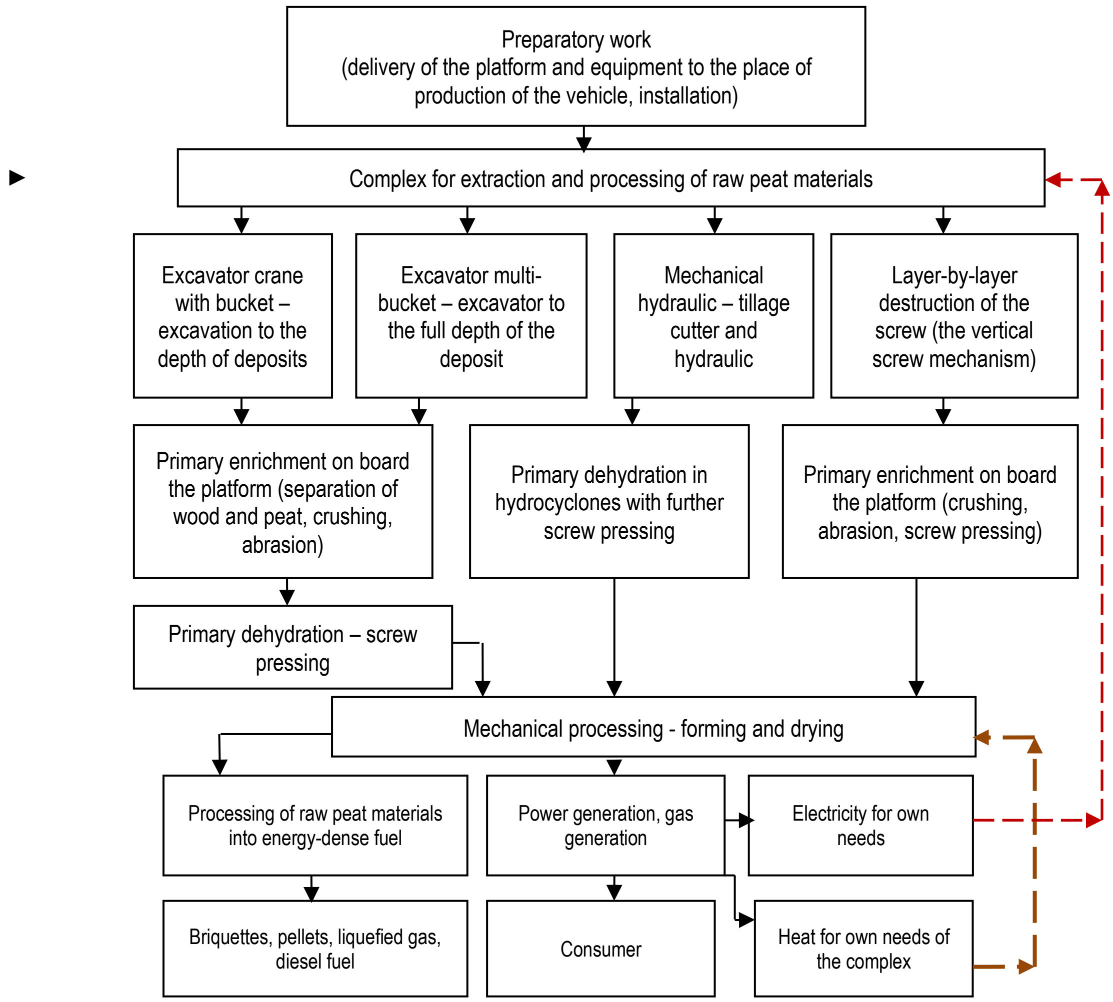

Fig.1. Scheme solutions for extraction and processing of peat raw materials

Depending on the adopted technology of extraction of raw peat materials, further primary enrichment and dehydration are carried out, followed by mechanical treatment on board the complex and generation of thermal and electrical energy.

For each scheme, energy costs were calculated both for the preparation of the field and for the production of 50 thousand tons of peat per year of 45% humidity in the development of a conventional peat deposit. The degree of decomposition of peat was 32%, the stump-1.5, the life of the field – 10 years. The results of calculations are summarised in Table. 2. At the same time, the total energy consumption per 1 ton of 45% moisture of the extracted raw peat materials with the basic milling technology was 8.31 MJ/T45%.

As can be seen from Table 2, the specific energy consumption in the implementation of any of the four circuit solutions of the complex with the installation of existing equipment sizes is lower in comparison with the milling technology of peat extraction. At the same time, the fourth chain of technological mining equipment is the most energy-consuming, the specific energy intensity of which is only 10% lower than the basic one. The least energy-consuming is a chain with a single-bucket excavator, or rather a manipulator. The specific energy consumption in this process chain is 21% lower than the basic one. At the same time, specially designed mining machines for a specific set of equipment can give even greater energy savings to the entire chain of technological mining machines. In any case, the specific energy consumption for the production of a ton of peat products will be lower than in the milling method of production.

Table 2. *Total energy consumption for the schemes of technological mining equipment of the complex for the extraction and processing of peat raw materials with a capacity of 50,000 $T_{45\%}$*

№	Specific energy consumption, MJ/$T_{45\%}$
Scheme I «Manipulator with a bucket»	6.52
Scheme II with «multi-Bucket excavator»	7.0
Scheme III «Mechanical hydraulic method»	7.29
Scheme IV «Using the auger-cutter»	7.47

Having established the fundamental benefits of implementation of environmental technologies for the extraction of raw peat from the flooded deposits with the use of a floating complex, it is necessary to develop theoretical approaches to the evaluation of the energy consumption of the complex, equipped with any set of mining equipment and to provide an opportunity to analyse the structure of such a complex with a unified voice. To do this, we will make a general structural formula of the complex of peat extraction and processing (CPEP) (1):

$$
\begin{aligned}
&CPEP^n=\Sigma\{PB[\Sigma(\Sigma((((M_i+Fg_i)+Fe_i)+I_i\cdot E_i)_i))_j]\\
&+ SB[\Sigma(\Sigma(((M_i+Fe_i)+I_i\cdot E_i)_i))_j]\\
&+ MDB[\Sigma(\Sigma((((M_i+F(e)g)_i+Fe_i)+I_i\cdot E_i)_i))_j]\\
&+ CoB[\Sigma(\Sigma(((M_i+Fe_i)+I_i\cdot E_i)_i))_j]\\
&+ DrB[\Sigma(\Sigma((((M_i+Fg_i)+Fe_i)+I_i\cdot E_i)_i))_j]\\
&+ 5TrB[\Sigma(\Sigma(((M_i+Fe_i)+I_i\cdot E_i)_i))_j] + EPB[\Sigma(\Sigma((((Ge_i\\
&+M_i)+Fe_i)+I_i\cdot E_i)_i))_j]\} + I\cdot E \quad (1)
\end{aligned}
$$

In the general case, the complex of mining equipment can be represented by the following blocks: production (DB)=PB, separation (SB), mechanical dewatering (MDB), drying (DrB), commercial products (CoB), power generation (EPB), transportation (TrB), united into a single chain by means of links providing for: only the harmonisation of the (-) connection (+) or the combination (•). In this case, by changing the parameters of each individual machine, module, unit, one can analyse the performance and optimise the parameters of the whole complex and its components.

Taking into account that a single complex of equipment on a floating platform for the extraction and processing of peat raw materials requires significant areas, it is advisable to leave only a complex of mining equipment for extraction, separation and primary dehydration on the floating platform, and to concentrate the bulk of the equipment for processing and energy generation on the shore, delivering primary dehydrated peat raw materials by floating shuttle containers operating in the shuttle mode, which will contribute to improving the efficiency of the entire complex.

Conclusions

The study found that the use of floating complex mining equipment for the extraction and processing of raw peat materials from the undrained deposits in modern conditions is more effective than the extraction of milling peat, while such complexes successfully fit into environmental technologies and, contributing to the development of energy potential of remote areas of the country, increase its energy security.

Within the framework of the study, a number of circuit solutions are proposed that determine the structure and composition of floating complexes for the extraction and processing of raw peat materials, and a complex of mining equipment in its composition is determined.

The algorithm of the choice of parameters of the mining equipment of a complex is offered, its realization in electronic model allows a simulating process of career processing of peat raw materials, providing the maximum efficiency of joint work of the equipment.

References

Grevtsev, N. – In: A. G. Samarov. 2009. System principles of choice of technology for extraction and processing of peat and man-made materials. News of universities. *Mining Journal, 8,* 14–20.

Kashinskaya, T. Ya., A. P. Gavrilchik, I. V. Ageychik. 2011. On the choice of environmentally compatible technologies for the development of peat deposits. – *Nature management,* 19, 144–149.

KhudyakovaI, N. et al. 2017. The formation of the structure of the main technological equipment of the autonomous complex for the extraction of peat from undrained deposits. – *Internet-journal "Science of Science", 9*, 3.

Mikhailov, A. V., S. L. Ivanov, V. V. Gabov. 2015. Formation and effective use of the machine park of peat mining companies. Vestnikpnipu. Geology. Oil and gas and mining. Perm. 14, 82–91.

Rodionov, V. Z. 2017. Development of peat deposits in the Leningrad region (problems and solutions). – *Regional ecology*, 3(49), 59–64.

Shtin, S. M. 2011. Application of peat as fuel for small power engineering. – *Mining industry*, 7, 82–96.

Timofeeva, S. S., G. R. Mingaleeva. 2014. Prospects of peat use in regional power engineering. – *Proceedings of Tomsk Polytechnic University. Equipment and technologies in the energy sector, 325,* 4, 46–55.

Titova, G. D. 2016. The Concept of ecological debt: development and possible applications in practice. *Regional ecology,* 1(43), 7–14.

Vagapova, E. A., S. L. Ivanov, I. N. Khudyakova. 2017. Assessment of energy consumption of technological equipment of an Autonomous modular complex for extraction and processing of peat raw materials from an untreated field. – *Socio-economic and environmental problems of mining, construction and energy: 13th international conference on mining, construction and energy. In 2 t. T. 1: the proceedings of the conference*. Izd-voTulgu, Tula, 156–163.

DETERMINATION OF THE LOADS ACTING ON THE SLEWING SUPPORT OF A TRUCK MOUNTED CRANE AND SELECTION OF A SLEWING SUPPORT

Hristo Sheiretov

University of Mining and Geology "St. Ivan Rilski", 1700 Sofia; sheiretov@abv.bg

ABSTRACT. The loads, acting on the slewing support of a truck mounted crane are determined - the resultant vertical force, the resultant horizontal force and the unbalanced moment of the forces acting on the slewing part of the crane. The mass of the counterweight is determined in advance using the condition of equality of the arms of the resulting forces to the rotation axis at the two endmost positions of the boom. Four cases are considered - at maximum and minimum length of the boom and at maximum and minimum angle of inclination of the boom. From the calculations it can be seen that the heaviest loads are obtained at minimum boom length and minimum boom inclination, because the unbalanced moment is the greatest. On the basis of the obtained forces and moments a slewing support is selected from the diagrams of the serially produced supports for the heaviest case of loading. A concrete example for the crane KC-45717, mounted on the truck chassis KamAZ, is solved.

Keywords: truck mounted crane, slewing support, unbalanced moment

ОПРЕДЕЛЯНЕ НА НАТОВАРВАНИЯТА ВЪРХУ ВЪРТЯЩАТА СЕ ОПОРА НА АВТОМОБИЛЕН КРАН И ИЗБОР НА ВЪРТЯЩА СЕ ОПОРА

Христо Шейретов

Минно-геоложки университет "Св. Иван Рилски", 1700 София

РЕЗЮМЕ. Определени са натоварванията върху въртящата се опора на автомобилен кран - резултантната вертикална сила, резултантната хоризонтална сила и неуравновесения момент от силите, действащи върху въртящата се част на крана. Предварително е определена масата на противотежестта от условието за равенство на рамената на равнодействащите сили спрямо оста на въртене за двете крайни положения на стрелата. Разгледани са четири случая - при максимална и минимална дължина на стрелата и при максимален и при минимален ъгъл на наклон на стрелата. От направените изчисления се вижда, че най-тежкия случай на натоварване е при минимална дължина на стрелата и минимален наклон на стрелата, тъй като при него се получава най-голям неуравновесен момент, действащ върху опората. Въз основа на получените натоварвания е избрана въртяща се опора от диаграмите на серийно произвеждани опори, за най-тежкия случай на натоварване. Решен е конкретен пример за кран КС-45717, монтиран на автомобилно шаси КамАЗ.

Ключови думи: автомобилен кран, въртяща се опора, неуравновесен момент

Introduction

The aim of the present study is to determine the loads acting on the slewing support of a truck mounted crane at different lengths and angles of the inclination of the boom and to select a standard slewing support. A concrete example is solved for the crane КС-45717 (Kran strelovoy avtomobilnyiy КС45717К-1), mounted on the truck chassis KamAZ.

The slewing support of the crane КС-45717 (fig. 1) consists of the crown 1, the ring 6 and the balls 7, situated between them. The outgoing gear of the slewing mechanism meshes with the crown 1. The crown is fixed to the crane support frame by the bolts 2. The ring 6 is fixed to the slewing platform by the bolts 8.

Input data

The input data for the determination of the loads acting on the slewing support are (Kran strelovoy avtomobilnyiy КС45717К-1):

- length of the boom L = 9÷21 m;
- angle of inclination of the boom β = 5÷75°;
- maximum capacity of the crane (at stretched side supports, L = 9 m and β = 75°) Q = 25 t;
- capacity of the crane at stretched side supports, L = 9 m and β = 5° Q_1 = 6.35 t;
- capacity of the crane at stretched side supports, L = 21 m and β = 75° Q_2 = 6.35 t;
- capacity of the crane at stretched side supports, L = 21 m and β = 5° Q_3 = 0.9 t;
- capacity of the crane at unstretched side supports, L = 9 m and β = 5° Q_4 = 1.15 t;
- mass of the boom m_c = 1.99 t;
- mass of the slewing platform m_o = 5.1 t;
- mass of the block with the hook $m_{рб}$ = 306 kg.

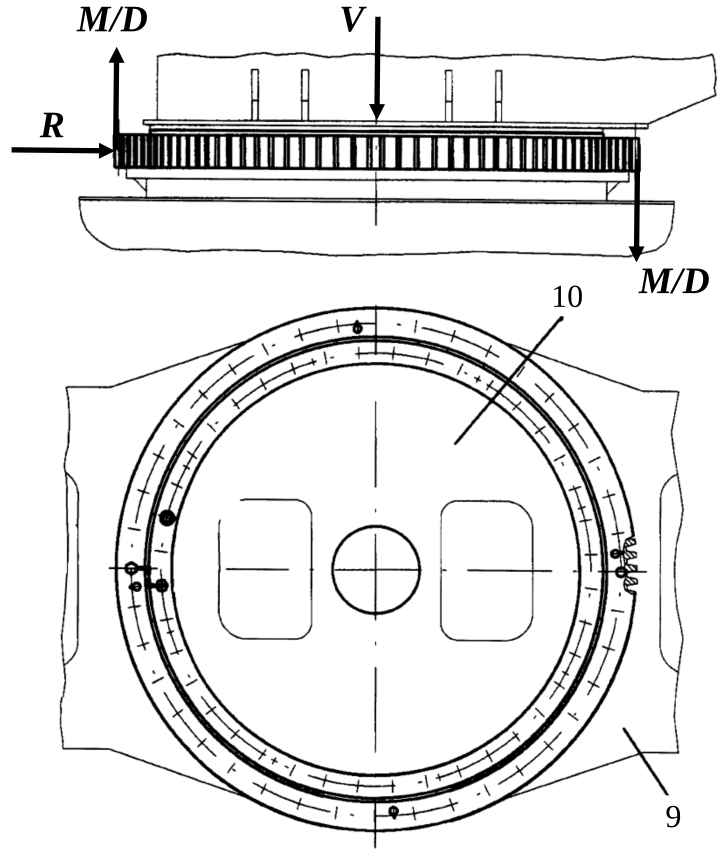

V - vertical force, acting on the support

R - radial (horizontal) force, acting on the support

M/D - couple of forces from the unbalanced moment *M* of the forces, acting on the slewing platform

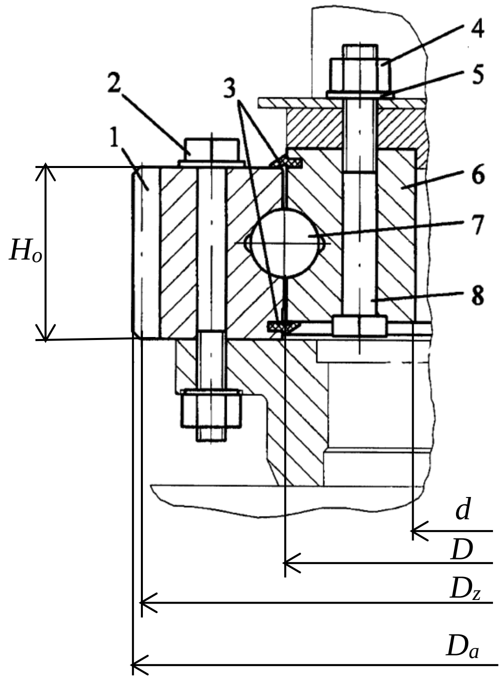

1 - crown;
2 - bolt for fixing to the unslewing part of the crane;
3 - sealing;
4 - nut;
5 - washer;
6 - inner ring;
7 - ball;
8 - bolt for fixing to the slewing part of the crane;
9 - support frame of the crane;
10 - slewing platform

d - inner diameter
D - diameter of the circuit over which the balls are rolling
D_z - centre diameter of the crown
D_a - outer diameter of the crown

Fig. 1. Scheme for the determination of the dimensions of the slewing support and the forces acting on the support

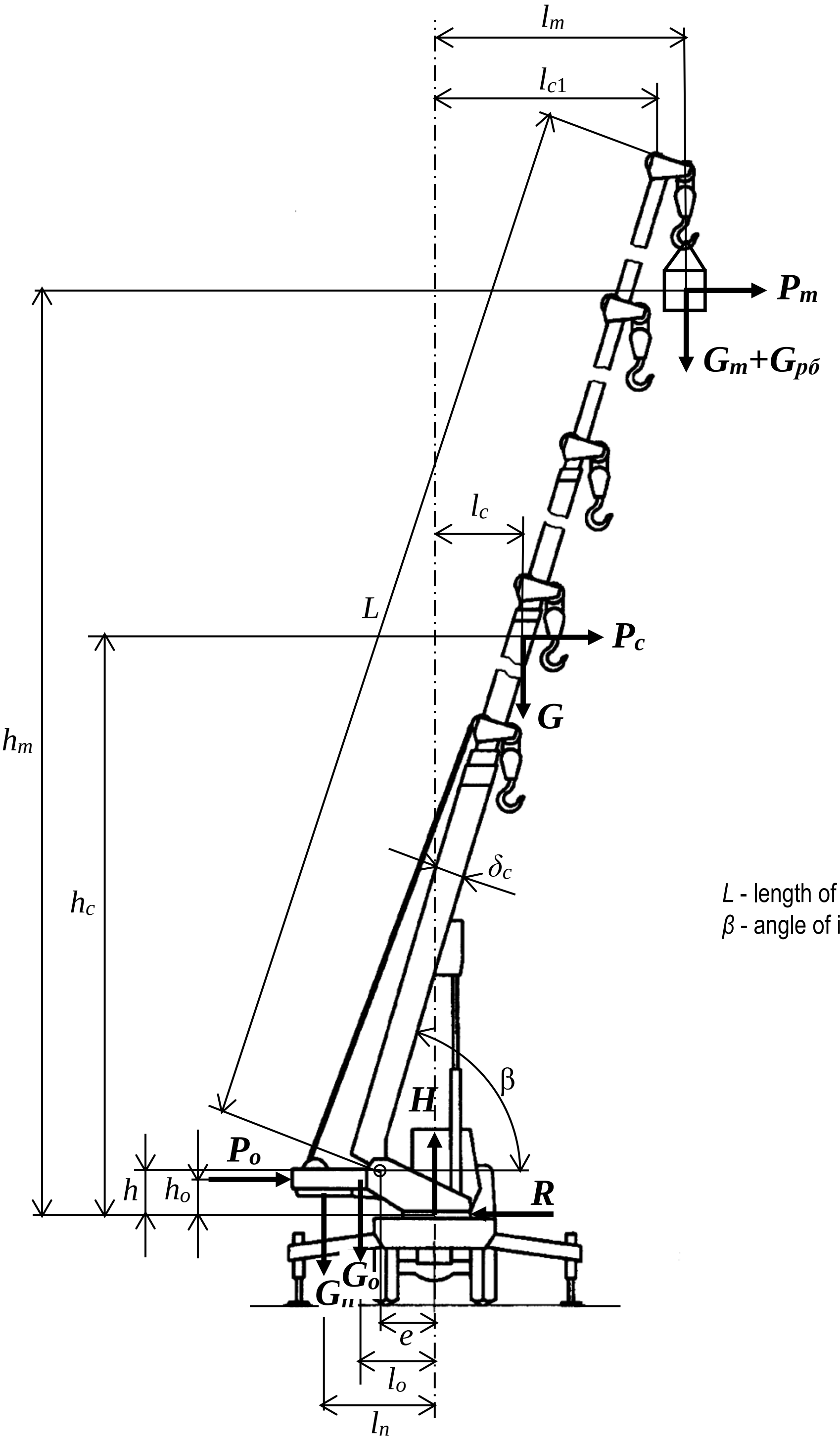

L - length of the boom
β - angle of inclination of the boom

Fig. 2. Scheme for the determination of the mass of the counterweight and the forces and moments acting on the slewing support

G_m, $G_{рб}$, G_c, G_o, G_n - gravity forces of the load, the block with the hook, the boom and the slewing platform and force of the counterweight
P_m, P_c, P_o - wind forces over the load, the boom and the slewing platform
l_m, l_c, l_o, l_n - arms of the gravity forces toward the axis of rotation
h_m, h_c, h_o - arms of the wind forces toward the centre of the slewing support
e - distance between the suspension point of the boom and the axis of rotation; *h* - distance between the suspension point of the boom and the centre of the slewing support; l_{c1} - distance between the end of the boom and the axis of rotation; δ_c - height of the side wall of the boom
H, R - vertical and horizontal resultant forces acting on the slewing support

Mass of the counterweight

The mass of the counterweight m_n [kg] is determined by the condition for the equality of the arms of the resultant vertical forces toward the axis of rotation for the two endmost positions of the boom (at maximum angle of inclination of the boom with load and at maximum angle of inclination of the boom without load) at unstretched side supports. The mass m_n is assumed in such a way, that the arms l_p and l'_p, determined by the formulae (1) and (8), are equal (I set different values for m_n and calculate l_p and l'_p, until the received values coincide l_p=l'_p=0.98 m).

After the accomplished calculations it is obtained that the mass of the counterweight must be m_n = 357 kg.

Arm of the resultant vertical force towards the axis of rotation at *L*=9 m, *β*=5° and Q_4=1,15 t

$$l_p = \frac{\left(G_m + G_{pб}\right).l_m + G_c.l_c - G_o.l_o - G_n.l_n}{G_m + G_c + G_o + G_n} = 0.98 \text{ m}, \qquad (1)$$

where: G_m, $G_{pб}$, G_c, G_o, G_n [kN] - gravity forces of the load, the block with the hook, the boom, the slewing platform and the counterweight (fig.2) (they are determined by formulae (2÷6));
l_m, l_c, l_o, l_n [m] - arms of the gravity forces toward the axis of rotation (fig.2) (l_m and l_c are determined by formulae (7) and (8), l_o and l_n are checked by the drawing of the slewing platform, l_o=1.3 m; l_n=2.2 m);

$$G_m = Q_4.g = 11.3 \text{ kN} \qquad (2)$$

$$G_{pб} = 0.001.m_{pб}.g = 3 \text{ kN} \qquad (3)$$

$$G_c = m_c.g = 19.5 \text{ kN} \qquad (4)$$

$$G_o = m_o.g = 50 \text{ kN} \qquad (5)$$

$$G_n = 0.001.m_n.g = 3.5 \text{ kN} \qquad (6)$$

$$l_m = L.cos\beta - e + 0.3 = 8.1 \text{ m} \qquad (7)$$

$$l_c = 0.5.L.cos\beta - e = 3.3 \text{ m} \qquad (8)$$

e [m] - distance between the suspension point of the boom and the axis of rotation (fig.2) (e=1,15m - it is checked by the drawing of the slewing platform).

Arm of the resultant vertical force toward the axis of rotation at *L*=9m, *β*=75° and *Q*=0t (without load)

$$l'_p = \frac{G_o.l_o + G_n.l_n - G_c.l'_c}{G_c + G_o + G_n} = 0.98 \text{ m}, \qquad (9)$$

where:

$$l'_c = 0.5.L.cos\beta - e = 0.01 \text{ m} \qquad (10)$$

Determination of the loads acting on the slewing support

The slewing supports are selected via graphs (Fig. 3) according to the resultant vertical force, acting on the support V [kN], the resultant horizontal force, acting on the support R [kN], and the unbalanced moment of the forces, acting on the slewing part of the crane toward the centre of the slewing support M [kN.m] (Fig. 1, Fig. 2). Four cases are considered for the fourth endmost positions of the load. The calculation results are given in a table.

In the formulae up to the end of the calculations, the values for the case for L = 9 m, β = 5° and Q_1 = 6.35 t are substituted, and for the leaving three cases only the results will be given in the table.

Resultant vertical force acting on the slewing support

$$V = G_m + G_{pб} + G_c + G_o + G_n = 135 \text{ kN}, \qquad (11)$$

where:

$$G_m = Q_1.g = 62.3 \text{ kN} \qquad (12)$$

Resulting horizontal force acting on the slewing support

$$R = P_m + P_c + P_o = 1.2 \text{ kN}, \qquad (13)$$

where: P_m, P_c, P_o [kN] - wind forces over the load, the upper wall of the boom and the back surface of the slewing platform (Fig. 2) (they are determined by formulae (14÷16));

$$P_m = A_m.q.k_3.c.k_h = 0.9 \text{ kN} \qquad (14)$$

$$P_c = A_c.q.k_3.c.k_h = 0.03 \text{ kN} \qquad (15)$$

$$P_o = A_o.q.k_3.c.k_h = 0.2 \text{ kN}, \qquad (16)$$

where: A_m [m^2] - wind-beaten area of the load (it is assumed from table 1 according to the crane capacity). At Q = 6,35 t I check A_m = 8 m^2;
q [kPa] - wind pressure at normal loading in working condition (case of loading I) (q = 0.09 kPa);
k_3 - filling coefficient of the construction (for loads and whole-wall constructions k_3 = 0.2÷0.6). For the calculated truck crane k_3=1;
c - aerodynamic coefficient (c=1.4 for the boom; c=1.2 for the load);
k_h - height coefficient (it is assumed from table 2 according to the height of the position of the load). At h_m=0.9m I check k_h=1;
A_c [m^2] - wind-beaten area of the upper wall of the boom (it is determined by formula (17));
A_o [m^2] - wind-beaten area of the back surface of the slewing platform (it is checked by the drawing of the platform, A_o=2.1m^2);

Table 1. *Wind-beaten area of the load A_m according to the crane capacity Q*

Q [t]	5	6,3	8	10	12,5	16	20	25
A_m [m^2]	7.1	8	9	10	12	14	16	18

Table 2. *Height coefficient*

h_m [m]	0÷10	10÷20	20÷40	40÷60
$k_в$	1	1.25	1.55	1.75

h_m [m] (fig.1) - see the explanations in formula (18)

$$S_c = L.b_c.sin\beta = 0.3 \text{ m}^2 , \qquad (17)$$

where: b_c [m] - width of the boom (it is checked by the drawing of the boom, b_c=0.43m).

Unbalanced moment of the forces acting on the slewing part of the crane toward the centre of the slewing support

$$M = (G_m+G_{pб}).l_m + G_c.l_c - G_o.l_o - G_n.l_n + P_m.h_m + P_c.h_c + P_o.h_o = 498 \text{ kN.m} , \qquad (18)$$

where: h_m [m] - arm of the wind force over the load P_m in relation to the centre of the slewing support (Fig. 2) (it is determined by formula (19));
h_c [m] - arm of the wind force over the boom P_c in relation to the centre of the slewing support (Fig. 2) (it is determined by formula (20));
h_o [m] - arm of the wind force over the platform P_o in relation to the centre of the slewing support (Fig. 2) (it is checked from the drawing of the platform, h_o=0.8 m);

$$h_m = h + L.sin\beta - 1 = 0.9 \text{ m} \qquad (19)$$

$$h_c = h + 0.5.L.sin\beta = 1.5 \text{ m} , \qquad (20)$$

where: h [m] - distance between the suspension point of the boom and the horizontal plane, passing through the middle of the slewing support (figr.2) (it is checked from the drawing of the platform, h=1,1 m).

Selection of a slewing support

In table 3 the calculation results for V, R and M for the fourth positions of the load are given.

Table 3.*Calculation results for the vertical force V, horizontal force R and the unbalanced moment M of the forces acting on the slewing platform for the fourth positions of the load*

	L [m]	β [°]	Q [t]	A_m [m²]	k_h	V [kN]	R [kN]	M [kN.m]
1	9	75	25	18	1.25	318	3.4	315
2	9	5	6.35	8	1	135	1.2	498
3	21	75	6.35	8	1.25	135	2.4	270
4	21	5	0.9	2.5	1	82	0.3	286

The toughest case of loading is at position 2, because the unbalanced moment M is determinative for the selection of the slewing support. According to the graphs in Fig. 3 a slewing support size 04 is chosen, which at V = 135 kN and R = 1.2 KN ≈ 0 kN has a permissible unbalanced moment M = 620 kN.m > 498 kN.m.

A single row ball support type KC size 04 with externally generated teeth (Fig. 1) is selected from Table 4 with the following parameters:

- number of the teeth z=123;
- module of the teeth m=12 mm;
- centre diameter of the crown D_z=$m.z$=12x123=1476 mm;
- outer diameter (to the top of the teeth) D_a=$mz+2xm$=12x123+2x12=1500 mm;
- inner diameter d=1175 mm;
- diameter of the circuit over which the balls are rolling D=1320 mm=1.32 m;
- height H_o=100 mm;
- maximum permissible speed of rotation n_{max}=2,5 min^{-1};
- maximum permissible radial loading R_{max}=59 kN;
- material of the rings - steel 50 Mn;
- mass – 460 kg.

Table 4. *Characteristic of the single row ball slewing supports with externally generated teeth* (Kolarov, 1986)

№	1	2	3	4
D_a [mm]	1000	1150	1300	1500
D [mm]	880	1012	1144	1320
m [mm]	6	8	8	12
z	164	142	160	123
D_z [mm]	984	1136	1280	1476
H_o [mm]	60	80	90	100
Mass [kg]	145	210	345	460

№	5	6	7	8
D_a [mm]	1900	2250	2650	3150
D [mm]	1672	1980	2332	2772
m [mm]	12	12	16	16
z	156	184	163	194
D_z [mm]	1872	2208	2608	3104
H_o [mm]	130	145	170	195
Mass [kg]	900	1320	2200	3700

D_a - outer diameter; D - diameter of the circuit, over which the balls are rolling; m - module of the teeth of the crown; z - number of the teeth of the crown; D_z =$m.z$ - centre diameter of the crown; H_o - height

Conclusions

1. From the calculations for the fourth endmost positions of the load the greatest resultant vertical force V, acting on the slewing support, is obtained at position 1 (minimum range of the crane, i.e. minimum boom length L and minimum angle of inclination of the boom β). The smallest vertical force is obtained at position 4 (minimum range of the crane, i.e. maximum boom length and minimum angle of inclination of the boom).

2. The greatest resultant horizontal force R, acting on the platform, is obtained at position 1, and the smallest - at position 4.

3. The greatest unbalanced moment M toward the centre of the slewing support is obtained at position 2 (minimum boom length and minimum angle of inclination of the boom). The smallest unbalanced moment is obtained at position 3 (maximum boom length and maximum angle of inclination of the boom).

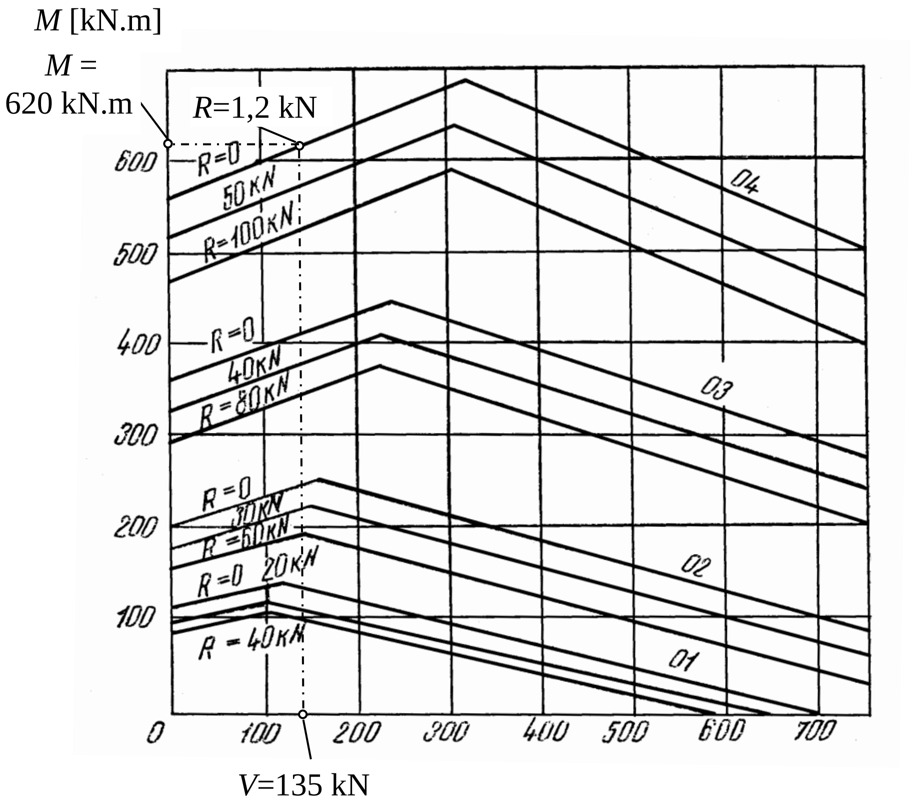

M - unbalanced moment of the forces acting on the platform toward the centre of the slewing support; *V, R* - resultant vertical and horizontal forces acting on the slewing support

Fig. 3. Graphs for the selection of the slewing support

4. The toughest case of loading of the slewing support is at position 2 (minimum boom length and minimum angle of inclination of the boom), because the unbalanced moment is determinative in the selection of the slewing support.

5. For the calculated truck mounted crane the slewing support is correctly selected, because the dimensions of the mounted support coincide with the dimensions of the selected support.

References

Gohberg, M. M. 1988. *Spravochnik po kranam. Tom 2.* Mashinostroenie, Leningrad, 453 p. (in Russian)

Kolarov, I. G., M. N. Prodanov, P. D. Karaivanov. 1986. *Proektirane na tovaropodemni mashini*. Tehnika, Sofia, 386 p. (in Bulgarian)

Kran strelovoy avtomobilnyiy KS45717K-1. Rukovodstvo po ekspluatatsii (in Russian).

COMPARISON OF THE METHODOLOGIES FOR THE DETERMINATION OF THE BELT TENSIONS AND THE REQUIRED DRIVE POWER OF THE BELT CONVEYORS

Hristo Sheiretov

University of Mining and Geology "St. Ivan Rilski", 1700 Sofia; sheiretov@abv.bg

ABSTRACT. Four methodologies are discussed: short and precise methodology of the Design, Science and Research Institute for Industrial Transport (Protransniiproekt), Russia; short and precise methodology according to the German calculation standard for belt conveyors DIN 22101.
The calculations are accomplished using the four methodologies for a concretely solved example - a stationary all-purpose belt conveyor with assigned layout profile, type and characteristic of the transported material, capacity, belt width and belt velocity, linear mass of the material, the belt and the idlers. In the calculations an equal coefficient of motional resistance and an equal coefficient of friction between the belt and the drive pulley are assumed. The belt tensions at start-up and at steady state working and the required drive power are determined.
The following conclusions are drawn: 1. Approximately equal values are obtained for the required drive power; 2. Smaller values are obtained for the belt tensions in the precise methodology in comparison with the short methodology. 3. Higher values are obtained for the belt tensions in the DIN methodology in comparison with the Protransniiproekt methodology. The reason is the difference in the methods for determination. 4. It should be noticed that the coefficient of motional resistance in the Promtransniiproekt methodology is recommended to be taken greater in comparison with the DIN methodology, which will lead to the increase of the belt tensions.

Keywords: belt tensions, drive power, methodology

СРАВНЯВАНЕ НА МЕТОДИКИТЕ ЗА ОПРЕДЕЛЯНЕ НА СИЛИТЕ НА ОПЪН В ЛЕНТАТА И МОЩНОСТТА НА ЗАДВИЖВАНЕТО НА ЛЕНТОВИТЕ ТРАНСПОРТЬОРИ

Христо Шейретов
Минно-геоложки университет "Св. Иван Рилски", 1700 София

РЕЗЮМЕ. Разгледани са четири методики: приблизителна и уточнена методика на проектанстския и научно-изследователски институт за промишлен транспорт (Промтрансниипроект), Русия; приблизителна и уточнена и методика по немския стандарт за изчисляване на лентови транспортьори DIN 22101.
Направени са изчисления по четирите методики за конкретно решаван пример - стационарен общопромишлен транспортьор със зададени профил на трасето, вид и характеристика на транспортирания материал, производителност, ширина и скорост на лентата, линейни маси на материала, лентата и ролковите опори. При изчисленията е приет еднакъв коефициент на съпротивление при движението на лентата и еднакъв коефициент на триене между лентата и задвижващия барабан. Определени са силите на опън в лентата при пусков и установен режим и необходимата мощност на задвижването.
Направени са следните изводи: 1. За необходимата мощност на задвижването се получават близки по значение стойности; 2. За силите на опън в лентата при уточнената методика се получават по-малки стойности в сравнение с приблизителната методика; 3. За силите на опън в лентата по двете уточнени методики при методиката на DIN се получават по-големи стойности. Причина за това е разликата в начина им на определяне; 4. Трябва да се отбележи, че по методиката на Промтрансниипроект се препоръчва коефициентът на съпротивление при движение да се приема по-голям в сравнение с методиката на DIN, което ще доведе до увеличаването на силите на опън.

Ключови думи: сили на опън в лентата, мощност на задвижването, методика

Introduction

There are different methodologies for the calculation and the design of the belt conveyors - the American standards ISO and CEMA, the German standard DIN, Russian methodologies, etc. Because of the differences in the methods for the determination of some parameters it will be useful tohave a comparative evaluation of the calculation results using these methodologies.

The present research is a continuation of a previous research, in which the calculation results of the material cross section area and the capacity of the belt conveyor using three methodologies are compared (Journal of Mining and Geological Sciences, 2018).

The calculations in the present paper are accomplished using the following methodologies: the methodologies of the Design, Science and Research Institute for Industrial Transport Promtransniiproekt, Russia - short and precise methodology (Posobie po proektirovaniyu konveyernogo transporta,1988); the methodologies according to the German standard for belt conveyor design DIN 22101 - short and precise methodology (Dunlop conveyor belt design and calculation, Phoenix conveyor belt design fundamentals, 2004).

The aim of the present research is to calculate the belt tensions at start-up and at steady state working and the required drive power using the four methodologies and to compare the results. A concrete example is solved for a conveyor with a given layout profile, type and characteristic of the transported material, capacity, belt width and belt velocity, linear masses of the belt, the material and the idlers. In the calculations an equal coefficient of motional (primary) resistance and an equal friction coefficient between the belt and the drive pulley are assigned.

Determination of the belt tensions and the required drive power using the different methodologies

Input data for the design

The calculations in the present research are accomplished for a stationary belt conveyor with the following parameters: length of the horizontal projection of the conveyor L_r = 200m; lifting height H = 24 m; transported material limestone with density ρ = 1,5 t/m^3; belt width B = 800 mm; belt velocity v = 1.6 m/s.

Determination of the geometric parameters of the layout profile of the conveyor (according to Fig.1)

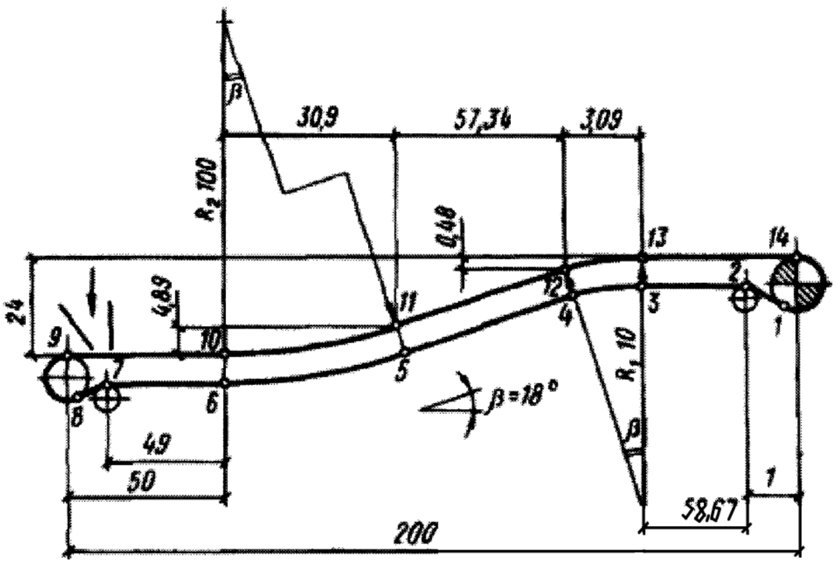

Fig.1. Scheme of the layout profile of the conveyor

Initially it is assumed: angle of inclination of the conveyor β = 18° (the maximum permissible angle for the transportation of limestone); radius of the concave curve R_2 = 100 m (the minimum permissible radius at belt width B = 800 mm); radius of the convex curve R_1 = 10 m (the minimum permissible radius at B = 800 mm and an angle of inclination of the side rollers λ = 30°); length of the horizontal section $l_{9\text{-}10}$ = 50 m; length of the horizontal projections of the sections $l_{r1\text{-}2} = l_{r7\text{-}8}$ = 1 m.

The lengths of the horizontal projections $l_{ri\text{-}j}$ and the lifting heights $h_{i\text{-}j}$ of the other sections are:

$$l_{r10\text{-}11} = l_{r5\text{-}6} = R_2.sin\beta = 30.9\ \text{m} \tag{1}$$

$$h_{10\text{-}11} = h_{5\text{-}6} = R_2 - R_2.cos\beta = 4.89\ \text{m} \tag{2}$$

$$l_{r12\text{-}13} = l_{r3\text{-}4} = R_1.sin\beta = 3.09\ \text{m} \tag{3}$$

$$h_{12\text{-}13} = h_{3\text{-}4} = R_1 - R_1.cos\beta = 0.48\ \text{m} \tag{4}$$

$$h_{11\text{-}12} = h_{4\text{-}5} = H - h_{10\text{-}11} - h_{12\text{-}13} = 18.63\ \text{m} \tag{5}$$

$$l_{r11\text{-}12} = l_{r4\text{-}5} = \frac{h_{11\text{-}12}}{tg\beta} = 57.34\ \text{m} \tag{6}$$

$$l_{13\text{-}14} = L_r - l_{r10\text{-}11} - l_{r11\text{-}12} - l_{r12\text{-}13} = 58.67\ \text{m} \tag{7}$$

$$l_{6\text{-}7} = l_{9\text{-}10} - l_{7\text{-}8} = 49\ \text{m} \tag{8}$$

$$l_{2\text{-}3} = l_{13\text{-}14} - l_{1\text{-}2} = 57.67\ \text{m} \tag{9}$$

The length of the conveyor is:

$$L = l_{9\text{-}10} + \frac{2.\pi.\beta.R_2}{360} . \frac{l_{r11\text{-}12}}{cos\beta} + \frac{2.\pi.\beta.R_1}{360} + l_{13\text{-}14} = 203.5\ \text{m} \tag{10}$$

Short methodology of Promtransniiproekt

Required peripheral forces of the drive pulley at start-up and steady state working

$$P = k_\partial.k'_\partial.L_r.w.\left(q_м + q'_p + q''_p + 2.q_л\right) + q_м.H = 24370\ \text{N} \tag{11}$$

$$P_n = k_\partial.k'_\partial.L_r.w_n.\left(q_м + q'_p + q''_p + 2.q_л\right) + q_м.H = 26780\ \text{N}, \tag{12}$$

where: k_∂ - coefficient of the additional resistances from belt bending (it is chosen from Table 1 according to the conveyor length L; at $L \approx$ 200 m k_∂ = 1.45);
k_∂' - correction coefficient (at horizontal conveyors and at inclined conveyors with length L < 100 m k_∂' = 1; at inclined conveyors with length $L \geq$ 100 m k_∂' is chosen from Table 2; at $L \approx$ 200 m and n = 5 k'_∂ = 1.15);
w, w_n - coefficients of motional resistance during the belt movement at start-up and at steady state movement (at normal

conditions of exploitation they are assumed to be $w = 0.020$ and $w_n = 0.026$);
$q_м$ - linear gravity force of the material ($q_м$ = 681 N/m at conveyor capacity Q = 400 t/h and belt velocity v = 1,6 m/s);
q_p', q_p'' [dN/m] - linear gravity forces of the rotating parts of the carry and return idlers (they are assumed to be q_p' = 179 N/m and q_p'' = 64 N/m at belt width B = 800 mm, density of the material ρ = 1.5 t/m^3 and idler pitches l'_p = 1 m и l''_p = 2.2 m);
$q_л$ [dN/m] - linear gravity force of the belt (it is assumed to be $q_л$ = 140 dN/m at B = 800 mm).

Table 1. *Coefficient of additional resistances $k_д$*

L [m]	10	20	30	50	60	80	100
$k_д$	4.5	3.2	2.6	2.2	2.1	1.91	1.75

L [m]	120	140	160	180	**200**	250	300
$k_д$	1.7	1.6	1.55	1.5	**1.45**	1.38	1.32

L [m]	350	400	500	700	800	1000
$k_д$	1.28	1.24	1.19	1.12	1.095	1.087

Table.2. *Correction coefficient $k_д'$*

L [m]	100	150	**200**	300	500	≥ 800
n = 3 - **5**	1.04	1.13	**1.15**	1.3	1.42	1.53
n = 6 - 10	1.21	1.31	1.42	1.54	1.66	1.81

L - length of the conveyor; n - number of belt bending over the drive and non-drive pulleys and the convex sections of the conveyor. For the solved example (Fig.1) n = 5.

Belt tensions in the points of entering and leaving of the drive pulley at start-up and steady state working

$$S_{вл} = S_{14} = \frac{e^{\mu.\alpha}.P}{(e^{\mu\alpha} - 1)} = 33740 \text{ N} \tag{13}$$

$$S^n_{вл} = S^n_{14} = \frac{e^{\mu.\alpha}.P_n}{(e^{\mu\alpha} - 1)} = 37080 \text{ N} \tag{14}$$

$$S_{изл} = S_1 = S_{вл} - P = 9370 \text{ N} \tag{15}$$

$$S^n_{изл} = S^n_1 = S^n_{вл} - P_n = 10300 \text{ N} \tag{16}$$

where: μ - coefficient of friction between the belt and the drive pulley (it is assumed μ = 0.35 at rubber lagged pulley and dry surfaces);
α - wrap angle of the belt (α = 210° = 3.66 rad).

Required power on the shaft of the drive pulley

$$N_б = \frac{P.v}{1000} = 39 \text{ kW} \tag{17}$$

Precise methodology of Promtransniiproekt

Belt tensions

The belt tensions are determined using the method of going round of the contour. The resistances of the sections $W_{i\text{-}j}$ are added consecutively to the belt tension in the point of leaving from the drive pulley $S_1 = S_{изл}$ and the remaining tensions are obtained. For the solved example for the start-up period it is obtained (according to the scheme of Fig.1):

$$S^n_1 = S^n_{изл} \tag{18}$$

$$S^n_2 = S^n_1 + W^n_{1\text{-}2} = S^n_1 + 0{,}02.S^n_1 \tag{19}$$

$$S^n_3 = S^n_2 + W^n_{2\text{-}3} = S^n_2 + \left(q_л + q''_p\right).w_n.l_{2\text{-}3} \tag{20}$$

$$S^n_4 = S^n_3 + W^n_{3\text{-}4} = S^n_3 + \left[S^n_3 + \left(q_л + q''_p\right).R_1\right].\beta.w_n \tag{21}$$

$$S^n_5 = S^n_4 + W^n_{4\text{-}5} = S^n_4 + \left(q_л + q''_p\right).w_n.l_{г4\text{-}5} - q_л.h_{4\text{-}5} \tag{22}$$

$$S^n_6 = S^n_5 + W^n_{5\text{-}6} = S^n_5 + \left(q_л + q''_p\right).w_n.l_{г5\text{-}6} - q_л.h_{5\text{-}6} \tag{23}$$

$$S^n_7 = S^n_6 + W^n_{6\text{-}7} = S^n_6 + \left(q_л + q''_p\right).w_n.l_{6\text{-}7} \tag{24}$$

$$S^n_8 = S^n_7 + W^n_{7\text{-}8} = S^n_7 + 0{,}02.S^n_7 \tag{25}$$

$$S^n_9 = S^n_8 + W^n_{8\text{-}9} = S^n_8 + 0{,}04.S^n_8 \tag{26}$$

$$S^n_{10} = S^n_9 + W^n_{9\text{-}10} = S^n_9 + \left(q_м + q_л + q'_p\right).w_n.l_{9\text{-}10} \tag{27}$$

$$S^n_{11} = S^n_{10} + W^n_{10\text{-}11} = S^n_{10} + \left(q_м + q_л + q'_p\right).w_n.l_{г10\text{-}11} + \left(q_м + q_л\right).h_{10\text{-}11} \tag{28}$$

$$S^n_{12} = S^n_{11} + W^n_{11\text{-}12} = S^n_{12} + \left(q_м + q_л + q'_p\right).w_n.l_{г11\text{-}12} \tag{29}$$

$$S^n_{13} = S^n_{12} + W^n_{12\text{-}13} = S^n_{12} + \left[S^n_{12} + \left(q_м + q_л + q'_p\right).R_1\right].\beta.w_n \tag{30}$$

$$S^n_{14} = S^n_{вл} = S^n_{13} + W^n_{13\text{-}14} = S^n_{13} + \left(q_м + q_л + q'_p\right).w_n.l_{13\text{-}14} = 1{,}097.S^n_1 + 22231 \tag{31}$$

On the other hand:

$$S^n_{14} = S^n_1.e^{\mu.\alpha} = 3.61.S^n_1 \tag{32}$$

When the equations (31) and (32) are solved together, the tension S_{1n} is obtained:

$$1.097.S^n_1 + 22331 = 3.61.S^n_1 \tag{33}$$

$$S^n_1 = 8870 \text{ N} \tag{34}$$

Using the formulae (19)÷(31) the remaining tensions are obtained. The tensions at steady state of working are obtained by analogy, but the coefficient of motional resistance is taken w = 0.020 instead of w_n = 0.026. The results from the calculations of the belt tensions at start-up and at steady state working are given in Table 3.

Table 3. *The results from the calculations of the belt tensions at start-up and at steady state working*

Formula for calculation (w_n=0.026)	Belt tensions [N]	
	Start-up w_n=0.026	Steady state w = 0.020
S_1^n = 8870	S_1^n = 8870	$S_1 = S_{изл}$=8250
S_2^n = 1.02. S_1^n	S_2^n = 9050	S_2 = 8420
S_3^n = 1.02. S_1^n + 306	S_3^n = 9350	S_3 = 8660
S_4^n = 1.036. S_1^n +358	S_4^n = 9370	S_4 = 8650
S_5^n = 1.036. S_1^n - 2048	S_5^n = 7070	S_5 = 6280
S_6^n = 1.036. S_1^n - 2567	S_6^n = 6550	S_6 = 5720
S_7^n = 1.036. S_1^n - 2307	S_7^n = 6810	S_7 = 5920
S_8^n = 1.056. S_1^n - 2354	S_8^n = 6940	S_8 = 6030
S_9^n = 1.098. S_1^n - 2448	S_9^n = 7210	S_9 = 6270
S_{10}^n = 1.98. S_1^n + 1148	S_{10}^n = 8510	S_{10} = 7270
S_{11}^n = 1.098. S_1^n + 3662	S_{11}^n =13320	S_{11} = 11890
S_{12}^n = 1.098. S_1^n + 20457	S_{12}^n =30110	S_{12} = 28340
S_{13}^n = 1.11. S_1^n + 20706	S_{13}^n =30430	S_{13} = 28580
S_{14}^n = 1.11. S_1^n + 22231	S_{14}^n =31960	$S_{14} = S_{вл}$= 29750

Required peripheral force on the drive pulley

$$P = \frac{S_{вл} - S_{изл}}{\eta_б} = 23120 \text{ N} \tag{35}$$

where: $\eta_б$ - coefficient of efficiency of the drive pulley (it is determined by formula (36))

$$\eta_б = \frac{1}{1 + w_б.\left(2.\frac{e^{\mu.\alpha}}{e^{\mu\alpha}-1} - 1\right)} = 0.93 \tag{36}$$

where: $w_б$ - coefficient of resistance of the drive pulley taking an account of the belt bending (it is assumed to be $w_б$=0.04).

Required power on the shaft of the drive pulley

$$N_б = \frac{P.v}{1000} = 37 \text{ kW} \tag{37}$$

Short methodology according to the standard DIN 22101

Required drive power

$$P_T = P_1 + P_2 + P_3 = 35.8 \text{ kW} \tag{38}$$

where: P_1 [kW] - required power for the belt and the material moving on the rollers (it is determined by formula (39));
P_2 [kW] - required power for the material lifting (it is determined by formula (40));
P_3 [kW] - sum of the required additional powers for the trippers, side boards and unloading ploughs (when there are no trippers boards and ploughs P_3=0);

$$P_1 = \frac{c_B.v + Q_m}{c_L.k_f} = 9.7 \text{ kW} \tag{39}$$

$$P_2 = \frac{H.Q_m}{367} = 26.1 \text{ kW} \tag{40}$$

where: c_B - coefficient depending on the belt width and the density of the transported material (it is determined by Table 4; at B = 800 mm and ρ = 1.5 t/m^3 it is assumed c_B = 126);
c_L - coefficient depending on the conveyor length (it is determined by Table 5; at L = 203,5 m after interpolation it is assumed c_L = 62);
k_f - coefficient depending on the working conditions (it is determined by Table 6; at medium (normal) working conditions k_f = 1).

Table 4. *Coefficient c_B depending on the belt width*

ρ [t/m^3]	Belt width B [mm]					
	650	**800**	1000	1200	1400	1600
< 1	81	108	133	194	227	291
1-2	92	**126**	187	277	320	468
> 2	103	144	241	360	414	644

ρ - density of the material

Table 5. *Coefficient c_L depending on the conveyor length*

L [m]	10	20	32	50	80	100	150	**200**
c_L	417	286	222	167	119	103	77	**63**

100	150	200	250	300	500	800	1000	2000
103	77	63	53	47	31	20	17	9

Table 6. *Coefficient k_f depending on the working conditions of the conveyor*

Working conditions	k_f
Light Good belt centering, small belt velocity	1.17
Medium (normal, standard)	**1**
Heavy Dusty atmosphere, low temperatures, overloading, high belt velocity	0.87 – 0.74

Precise methodology according to the standard DIN 22101

Belt tensions at steady state working

According to the scheme of Fig.1 the correspondence of the belt tensions is: T_2 to S_1, T_3 to S_8, T_4 to S_9 и T_1 to S_{14}.

$$T_2 = F_U.c_2 = 8910 \text{ N} \tag{41}$$

$$T_3 = T_2 + F_u - F_{Stu} = 6330 \text{ N} \tag{42}$$

$$T_4 = T_3 ; \qquad T_1 = T_4 + F_N + F_o + F_{Sto} = 32070 \text{ N} \tag{43}$$

where: F_U - total peripheral force on the drive pulley (it is determined by formula (44));
c_2 - drive factor for the determination of the belt tension in point of leaving from the drive pulley (it is determined by formula (45));
F_o, F_u - primary resistances in the carry and the return run (from the belt and material movement, rotation of the rollers, bending of the belt, strike of the belt to the rollers, inner friction of material etc. (they are determined by the formulae (46) and (47));

F_{Stu}, F_{Sto} - gradient resistances in the carry and the run side (they are determined by the formulae (48) and (49));
F_N - total secondary resistance (from the bending of the belt around the pulleys, friction in the pulley bearings, resistances in the loading and cleaning devices, etc. (it is determined by the formula (50)).

$$F_U = F_H + F_N + F_{St} = 23170 \text{ N} \quad (44)$$

$$c_2 = \frac{1}{e^{\mu.\alpha} - 1} = 0.3846 \quad (45)$$

$$F_o = f.L.g.\left[m'_{Ro} + \left(m'_G + m'_L\right).cos\delta\right] = 3910 \text{ N} \quad (46)$$

$$F_u = f.L.g.\left(m'_{Ru} + m'_G\right).cos\delta = 790 \text{ N} \quad (47)$$

$$F_{Sto} = H.g.\left(m'_G + m'_L\right) = 19710 \text{ N} \quad (48)$$

$$F_{Stu} = H.g.m'_G = 3370 \text{ N} \quad (49)$$

$$F_N = (C - 1).F_H = 2120 \text{ N} \quad (50)$$

where: f - coefficient of motional (primary) resistance (it is assumed $f = w = 0.02$);
m'_{Ro}, m'_{Ru} - linear masses of the rotating parts of the idlers in the carry and the return run (they are assumed according to the previously chosen q'_p = 179 N/m and q''_p = 64 N/m - m'_{Ro} = 18.3 kg/m and m'_{Ru} = 6.5 kg/m);
m'_G, m'_L - linear masses of the belt and the material (they are assumed according to the previously chosen $q_л$ = 140 N/m and $q_м$ = 681 N/m - m'_G = 14.3 kg/m and m'_L = 69.4 kg/m);
δ - angle of inclination of the conveyor ($\delta = \beta = 18°$);
C - coefficient of secondary resistance (corresponds to the coefficient $k_д$; it is assumed $C = k_д$ = 1.45 from Table 1);
F_H - total primary resistance (it is determined by the formula (51));
F_{St} - total gradient resistance (it is determined by the formula (52)).

$$F_H = f.L.g.\left[m'_{Ro} + m'_{Ru} + \left(2.m'_G + m'_L\right).cos\delta\right] = 4710 \text{ N} \quad (51)$$

$$F_{St} = H.g.m'_L = 16340 \text{ N} \quad (52)$$

Belt tensions at start-up

$$T_{A2} = F_A.c_{2A} = 10590 \text{ N} \quad (53)$$

$$T_{A3} = T_{A2} + F_u - F_{Stu} + F_{au} = 10020 \text{ N} \quad (54)$$

$$T_{A4} = T_{A3} = 10020 \text{ N} \quad (55)$$

$$T_{A1} = T_{A4} + F_N + F_o + F_{Sto} + F_{ao} = 45750 \text{ N} \quad (56)$$

where: c_{2A} - drive factor at start-up (it is determined by the formula (57));
F_{au}, F_{ao} - acceleration forces in the carry and return run (they are determined by the formulae (58) and (59));

$$c_{2A} = \frac{1}{e^{\mu_A.\alpha} - 1} = 0.3009 \quad (57)$$

$$F_{ao} = L.a_A.\left(0.9.m'_{Ro} + m'_G + m'_L\right) = 9990 \text{ N} \quad (58)$$

$$F_{au} = L.a_A.\left(0.9.m'_{Ru} + m'_G\right) = 2010 \text{ N} \quad (59)$$

where: μ_A - coefficient of friction between the belt and the pulley at start-up (it is determined by the formula (60));
a_A - acceleration of the conveyor at start-up (it is determined by the formula (61));

$$\mu_A = \mu + 0.05 = 0.4 \quad (60)$$

$$a_A = \frac{F_A - F_U}{L.\left(0.9.m'_{Ro} + 0.9.m'_{Ru} + 2.m'_G + m'_L\right)} = 0.49 \text{ m/s}^2 \quad (61)$$

where: F_A - peripheral force on the drive pulley at start-up (it is determined by the formula (62)).

$$F_A = k_A.F_U = (1.2 \div 1.5).F_U = 1.3.F_U = 35200 \text{ N} \quad (62)$$

Correction of the belt tensions at the steady state working according to the kind of the tension device

A condition is used that the belt tensions in the point, where the tension weight is put (in this case on the return pulley), at start-up and steady state working are equal. This means that $T_{A4} = T_4$. Then for the belt tensions at steady state working after the correction with the value of $\Delta T = T_{A4} - T_4$ it is finally obtained:

$$T_{A4} = T_4; \quad \Delta T = T_{A4} - T_4 = 3690 \text{ N} \quad (63)$$

$$T_1 = T_1 + \Delta T = 35760 \text{ N} \quad (64)$$

$$T_2 = T_2 + \Delta T = 12600 \text{ N} \quad (65)$$

$$T_3 = T_4 = T_3 + \Delta T = 10020 \text{ N} \quad (66)$$

Required drive power

$$P_T = \frac{F_U.v}{1000} = 37 \text{ kW} \quad (67)$$

Conclusions

The results of the calculations are generalised in Table 7.

Table 7. *Comparative results of the calculations of the belt tensions and the required drive power*

Methodology	1	2	3	4
T_1 (S_{14}, $S_{вл}$) [N]	33740	29750	-	35760
T_2 (S_1, $S_{изл}$) [N]	9370	8250	-	12600
T_3 (S_8) [N]	-	6030	-	10020
T_4 (S_9) [N]	-	6270	-	10020
T_{A1} (S_{14}^n) [N]	37080	31960	-	45750
T_{A2} (S_1^n) [N]	10300	8870	-	10590
T_{A3} (S_8^n) [N]	-	6940	-	10020
T_{A4} (S_9^n) [N]	-	7210	-	10020
P_T ($N_б$) [kW]	39	37	35,8	37

1 - Promtransniiproekt short; 2 - Promtransniiproekt precise;
3 - DIN 22101 short; 4 - DIN 22101 precise.

The following conclusions can be drawn from the calculations using the four discussed methodologies:

1. Approximately equal values are obtained for the required drive power P_T ($N_б$). The highest is the value obtained by methodology 1 and the smallest - by methodology 3.

2. a Smaller values are obtained for the belt tensions according to the precise methodology (methodology 2) in comparison with the short methodology (methodology 1).

3. Higher values are obtained for the belt tensions using the precise methodologies (2 and 4) according to methodology 4 in comparison with methodology 2. The reason is the difference in the methods for their determination. In methodology 2 the belt tensions at start-up are determined in the same way as at steady state working, but a higher coefficient of motional resistance is assumed. In methodology 4 the acceleration forces at start-up are considered.

4. Higher values are obtained for the belt tensions at steady state working using the precise methodologies in methodology 4. The reason is the correction (increase) of the tensions in accordance with the condition, that in the point where the tension weight is put the tensions at start-up and steady state working are equal.

5. The calculations are accomplished at equal coefficients of motional (primary) resistance f (w). It should be noticed, that in methodologies 1 and 2 it is recommended to take higher coefficients of motional in comparison with methodologies 3 and 4. This will lead to the increase of the belt tensions, determined by methodologies 1 and 2.

References

Conveyor Handbook. Conveyor belt technique. Design and calculation. 2009. Fenner Dunlop.

Oreshkin, V. L., V. K. Dyachkov, O. V. Zelenskiy. 1988. *Posobie po proektirovaniyu konveyernogo transporta. Lentochnyie konveyeryi.* Stroyizdat, Moscow (in Russian).

Phoenix conveyor belt design fundamentals. DIN 22101. 2004. Hamburg.

DETERMINATION OF A 3D STRUCTURE'S EXTERNAL REACTIONS UNDER THE ACTION OF APPLIED LOADS WITH COMPLEX CONFIGURATION

Asen Stoyanov

University of Mining and Geology "St. Ivan Rilski", 1700 Sofia; assendragomirov59@gmail.com

ABSTRACT. In this paper a numerical solution is suggested by using the package MathCAD 15. The solution determines the rods' force reactions, which support the homogeneous plate. A homogeneous body, which is loaded unilaterally with wind pressure, is lying on this plate. Sometimes routine and labour-intensive calculations complicate the calculated process. The research shows that the difficulties are due to the complicated spatial configuration of the homogeneous body. They influence both the determination of the body's volume (impossible accurate dual integration of complicated functional dependence $z = f(x, y)$) and the determination of the surface (the "shadow" of the body over the plane Oxz) loaded with wind. The study demonstrates the application of the numerical methods in mechanics and the spatial visualisation of complicated functional dependencies.

Keywords: centre of gravity, 3D structure, surface plot, MathCAD

ОПРЕДЕЛЯНЕ НА ВЪНШНИТЕ РЕАКЦИИ НА 3-D СТРУКТУРА, ПОД ДЕЙСТВИЕТО НА ПРИЛОЖЕНИ ТОВАРИ СЪС СЛОЖНА КОНФИГУРИРАЦИЯ

Асен Стоянов

Минно-геоложки университет "Св. Иван Рилски", 1700 София

РЕЗЮМЕ. Статията предлага числено решение с MathCAD 15. Решението определя прътовите усилия в пръти, които подпират хомогенна плоча. Върху нея лежи хомогенно тяло, натоварено едностранно с вятър. Понякога рутинни и трудоемки пресмятания усложняват изчисленият процес. В показаното изследване, трудностите поизтичат от сложната пространствена конфигурация на хомогенното тяло. Те влияят както за определяне обема (невъзможно точено двойно интегриране на сложна функционална зависимост $z = f(x, y)$) на тялото, така и за определяне повърхнината („сянката" на тялото върху равнината Oxz) натоварена от вятър. Изследването демонстрира приложението на числените методи в механиката, а също и пространствената визуализация на сложни функционални зависимости.

Ключови думи: център на тежестта, 3D структура, повърхностен участък, MathCAD

Calculation of 3D structure through the package MathCAD

The three dimensional structure is shown in Fig.1. It is supported by six rods anchored with ball-and-socket connections at points A, B and C. The rods are loaded with the weights of homogeneous plate and body as well as the wind.

The load from a body is unevenly distributed over the surface of the plate according to the law $z = f(x, y)$ – see Figures 1. 2 and 3. The wind direction is the same as the axis y – see Figures 1 and 2.

The input data for the problem are as follows:

$$a = 3{,}5m;\ b = 3m;\ c = 6m;\ w = 3kN/m^2;\ q = 4kN/m^3;$$
$$g = 6{,}8kN/m^3;\ h = 0{,}2m;$$
$$z = f(x, y) = y.\sin[(0{,}8.x)^2] + 2 + 0{,}5.y.\sin(2.y)\ .$$

The following symbols are used:

- $a,\ b\ and\ h$ – Dimensions of the plate;
- $a,\ b\ and\ z = f(x, y)$ – Dimensions of the body – see Figures 1 and 2.

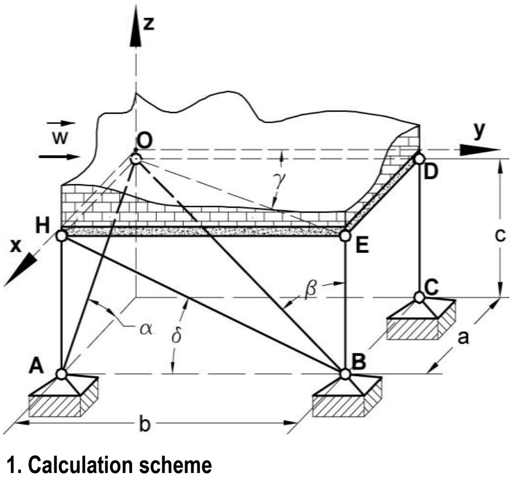

Fig. 1. Calculation scheme

- w – Intensity of a wind load – see Fig.1;
- q – Volumetric weight of the homogeneous body;

- g – Volumetric weight of the homogeneous plate;
- $\vec{e}_p$ – Unit vector in the "p" direction – see Fig.3.

The functional dependence $z = f(x, y)$ is illustrated graphically in Fig.2.

All reactions in the support rods are determined.

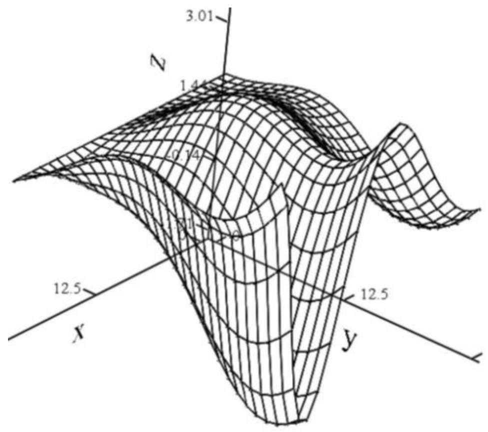

Fig. 2. 3G graphics of the function $z = y.\sin[(0{,}8.x)^2] + 2 + 0{,}5.y.\sin(2.y)$

A similar problem is published in Doev and Doronin study (2016), but this article complements and expands the solution.

<u>*Algorithm of the solution:*</u>

1) *Data introduction. The weight* $\vec{G}_{pl}$ *and the centre of gravity* C_{pl} *of the plate are determined – see Figures 2 and 3.*
2) *Determination of the body's volume* V_b *– see Figures 1, 3 and 6;*
3) *Determination of the body's weight* $\vec{G}_b$ *– see Figures 2 and 3;*
4) *Determination of the body's centre of gravity* $C_b\,(x_{cb}; y_{cb})$ *– see Figures 2. and 3;*
5) *Graphic visualisation with MathCAD of the projection (or "shadow") of the body over the coordinate plane* Oxz *– see Fig.3;*
6) *Determination of the equivalent concentrated load* $\overrightarrow{P_w}$ *over the body, which is subjected to the distributed load from the wind, as well as the centre of gravity of the loaded area – see Figures 2 and 3;*
7) *Determination of the external reactions of the supported plate;*
8) *Checking the solution.*

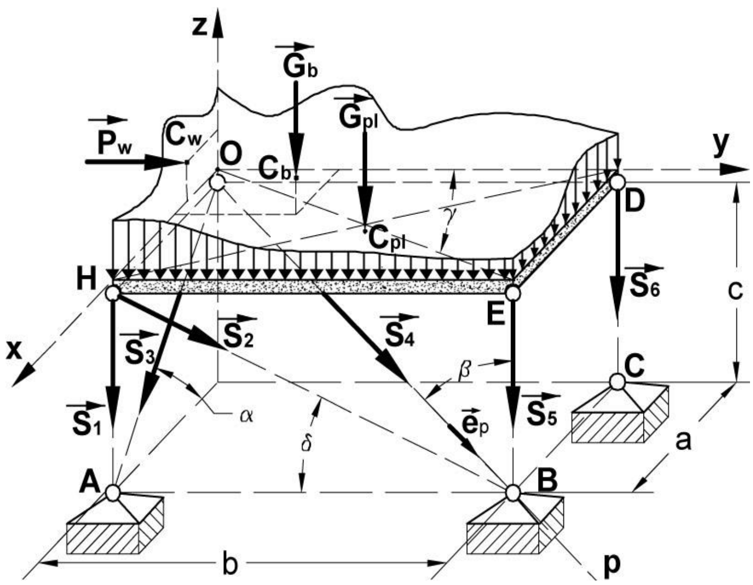

Fig. 3. External reactions of the supported plate loaded with concentrated forces which are equivalent to the distributed loads

The projection of the body (or "shadow") over the plane Oxz is graphically visualised in Fig.4.

The input data, boundaries of amendment, as well as the variable steps, are introduced in Fig.5.

On the same figure, the weights of the plate and body, as well as the gravity body centres and projections over the plane Oxz , are determined.

The determination of the external plate reactions, as well as their verifications, are shown in Fig.6.

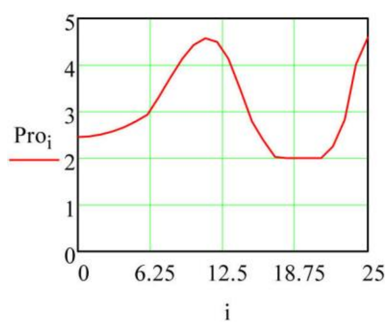

Fig. 4. Projection of the body over the plane Oxz

$$a := 3.5 \quad b := 3 \quad c := 6 \quad w := 3 \quad q := 4 \quad g := 6.8 \quad h := 0.2$$

$$f(x,y) := y \cdot \sin\left[(0.8 \cdot x)^2\right] + 2 + 0.5 \cdot y \cdot \sin(2 \cdot y) \quad Gpl := g \cdot a \cdot b \cdot h \quad N := 25$$

$$dx := \frac{a}{N} \qquad dy := \frac{b}{N} \qquad i := 0..N \qquad j := 0..N \qquad x_i := dx \cdot i$$

$$y_j := dy \cdot j \qquad M_{i,j} := f\left(x_i, y_j\right) \qquad Vb := \int_{y_0}^{y_N} \left(\int_{x_0}^{x_N} f(x,y)\,dx \right) dy$$

$$Gb := Vb \cdot q \qquad Vb = 21.808 \qquad Gb = 87.23 \qquad Gpl = 14.28$$

$$xcb := \frac{\int_{y_0}^{y_N} \left(\int_{x_0}^{x_N} f(x,y) \cdot x\,dx \right) dy}{Vb} \qquad ycb := \frac{\int_{y_0}^{y_N} \left(\int_{x_0}^{x_N} f(x,y) \cdot y\,dx \right) dy}{Vb}$$

$$xcb = 1.632 \qquad ycb = 1.38 \qquad i1 := 1..N$$

$$Pro_i := \max\left[\left(M^T\right)^{\langle i \rangle}\right] \quad F_{i1} := Pro_{i1} \cdot \left(x_{i1} - x_{i1-1}\right) \quad Pw := w \cdot \left(\sum_{i1=1}^{N} F_{i1} \right)$$

$$xcw := \frac{\sum_{i1=1}^{N} \left[F_{i1} \cdot \frac{\left(x_{i1} + x_{i1-1}\right)}{2} \right]}{\sum_{i1=1}^{N} F_{i1}} \qquad zcw := \frac{\sum_{i1=1}^{N} \left(F_{i1} \cdot \frac{Pro_{i1}}{2} \right)}{\sum_{i1=1}^{N} F_{i1}}$$

$$zcw = 1.674 \qquad xcw = 1.736$$

$$s\alpha := \frac{c}{\sqrt{a^2 + c^2}} \qquad c\alpha := \frac{a}{\sqrt{a^2 + c^2}} \qquad s\beta := \frac{\sqrt{a^2 + b^2}}{\sqrt{a^2 + b^2 + c^2}}$$

$$c\beta := \frac{c}{\sqrt{a^2 + b^2 + c^2}} \qquad s\gamma := \frac{a}{\sqrt{a^2 + b^2}} \qquad c\gamma := \frac{b}{\sqrt{a^2 + b^2}}$$

$$s\delta := \frac{c}{\sqrt{b^2 + c^2}} \qquad c\delta := \frac{b}{\sqrt{b^2 + c^2}}$$

$$A := \begin{pmatrix} 0 & 0 & c\alpha & s\beta \cdot s\gamma & 0 & 0 \\ 0 & c\delta & 0 & s\beta \cdot c\gamma & 0 & 0 \\ -1 & -s\delta & -s\alpha & -c\beta & -1 & -1 \\ 0 & 0 & 0 & 0 & -b & -b \\ a & a \cdot s\delta & 0 & 0 & a & 0 \\ 0 & c\delta \cdot a & 0 & 0 & 0 & 0 \end{pmatrix} \qquad |A| = -3.283$$

Fig. 5. Determination of the body gravity centre and the wind loaded area centre as well as the analytical expressions of trigonometric functions and matrix A

$$B := \begin{bmatrix} 0 \\ -Pw \\ Gb + Gpl \\ Gpl\cdot .5\cdot b + Gb\cdot ycb + Pw\cdot zcw \\ -(.5\cdot a\cdot Gpl + Gb\cdot xcb) \\ -Pw\cdot xcw \end{bmatrix} \qquad S := A^{-1}\cdot B \qquad S = \begin{pmatrix} -37.06 \\ -35.9 \\ 37.776 \\ -41.149 \\ -7.12 \\ -86.282 \end{pmatrix}$$

$$S1 := \begin{pmatrix} 0 \\ 0 \\ 37.06 \end{pmatrix} \qquad S2 := \begin{pmatrix} 0 \\ -35.9\cdot c\delta \\ 35.9\cdot s\delta \end{pmatrix} \qquad S3 := \begin{pmatrix} 37.776\cdot c\alpha \\ 0 \\ -37.776\cdot s\alpha \end{pmatrix}$$

$$S4 := \begin{pmatrix} -41.149\cdot s\gamma\cdot s\beta \\ -41.149\cdot c\gamma\cdot s\beta \\ 41.149\cdot c\beta \end{pmatrix} \qquad S5 := \begin{pmatrix} 0 \\ 0 \\ 7.12 \end{pmatrix} \qquad S6 := \begin{pmatrix} 0 \\ 0 \\ 86.282 \end{pmatrix}$$

$$Gpl := \begin{pmatrix} 0 \\ 0 \\ -14.28 \end{pmatrix} \qquad Gb := \begin{pmatrix} 0 \\ 0 \\ -148.291 \end{pmatrix} \qquad Pw := \begin{pmatrix} 0 \\ 32.37 \\ 0 \end{pmatrix}$$

$$ep := \begin{pmatrix} s\gamma\cdot s\beta \\ c\gamma\cdot s\beta \\ -c\beta \end{pmatrix} \qquad ep = \begin{pmatrix} 0.463 \\ 0.396 \\ -0.793 \end{pmatrix}$$

$$ep\cdot(S1 + S2 + S3 + S4 + S5 + S6 + Gpl + Gb + Pw) = -1.153 \times 10^{-3}$$

Fig. 6. Determining the external reactions and their verification

Conclusion

The contemporary teaching of mechanics in the universities is related to using the most advanced mathematical packages such as MatLab, MathCAD, MuPAD and others, (Bertyaev, 2005; Doev et al., 2016; Ivanov, 2015; Stoyanov, 2016). In this case, the presented study is a continuation of the ideas published in the works (Ivanov et al., 2017; Stoyanov, 2017), where all calculations are made by using mathematical packages.

The traditional solution of the problem, solved in this paper, is related to some difficulties. The volume of the body V_b cannot be defined directly. In this case, it is necessary a function of two variables to be numerically integrated. But this action is associated with a large volume of calculations when it is executed by hand. The problems associated with determining the body shadow area on the plane Oxz are similar.

These difficulties are easily overcome by using the mathematical package MathCAD. In this case, the programme MathCAD can be used to check the problem solved in the traditional way.

We have a similar problem in the determination of the stability of excavators during their operation when a large piece of ore is loaded and the centre of gravity of the bucket has to be found (Minin, 2013).

The paper demonstrates a fast solution and excellent graphical visualisation - see (Bertyaev, 2005; Doev et al., 2016; Ivanov, 2017; Stoyanov, 2017).

References

Bertyaev, V. 2005, *Teoreticheskaya mehanika na baze MathCAD praktikum.* BHV-Peterburg, Sankt-Peterburg, 739 p. (in Russian)

Doev, V. S., F. A. Doronin, 2016. *Sbornik zadaniy po teoreticheskoy mehanike na baze MathCAD*, Lany, Sankt-Peterburg, Moscow, Krasnodar, 585 (in Russian).

Ivanov, A. I. 2015. Svobodni nezatihvashti prostranstveni trepteniya na nesimetrichno tvardo tyalo vurhu elastichna osnova. – *Sbornik nauchni trudove na RU Angel Kunchev, 54,* 2, 38–42 (in Bulgarian with English abstract).

Ivanov, A. I., P. C. Petkov. 2017. Izsledvane prinudenite prostranstveni trepteniya na mashinen agregat “Elektrodvigatel-kompresor”. – *Mehanika, Transport, Komunikacii, 15, 3, №1484*, VI-7 – VI-12 (in Bulgarian with English abstract).

Minin, I. 2013. Metodika za opredelyane koeficienta na ustoychivost na hidravlichnite ednokofovi bageri po vreme na rabota, – *Godishnik na MGU ”St. Ivan Rilski”, 56*, 3, 16–20 (in Bulgarian with English abstract).

Stoyanov, A. 2016. *Matrichni operacii s MathCAD v teoretichnata mehanika Statika*, Kineziologiya BG, Sofia, 165 p. (in Bulgarian)

Stoyanov, A. 2017. Survey of the relationship between the efforts in the bars and geometrical parameter on tree-dimensional truss. – *XVII International scientific conference VSU’2017 8-9 June*, Sofia, 103–111 (in Bulgarian with English abstract).

GRAPHICAL DETERMINATION OF 2D FRAME REACTIONS UNDER THE ACTION OF CONCENTRATED FIXED LOADS AND SLOWLY MOVING EVENLY DISTRIBUTED LOAD

Asen Stoyanov

University of Mining and Geology "St. Ivan Rilski", 1700 Sofia; assendragomirov59@gmail.com

ABSTRACT. A study of the equilibrium of a 2D structure of the frame type was performed. One of the applied loads (evenly distributed load) moves very slowly along the roadway of the frame. The intermediate joint at point C of the frame is replaced by an N-release. This non-standard constructive solution helps to analyse the change in the bending moment at point C for arbitrary position of the moving load. The study ends with an analysis of the results obtained.

Key words: slowly-moving evenly distributed load with constant intensity, frame, MathCAD

ГРАФИЧНО ОПРЕДЕЛЯНЕ НА РЕАКЦИИТЕ НА 2D РАМКА, ПОД ДЕЙСТВИЕТО НА КОНЦЕНТРИРАНИ НЕПОДВИЖНИ ТОВАРИ И БАВНО ДВИЖЕЩ СЕ РАВНОМЕРНО РАЗПРЕДЕЛЕН ТОВАР

Асен Стоянов

Минно-геоложки университет "Св. Иван Рилски", 1700 София

РЕЗЮМЕ. Проведено е изследване на равновесието на 2D структура от типа рамка. Един от приложените товари (равномерно разпределен товар) се премества много бавно по пътното платно на рамката. Междинната става в т.С на рамката е заменена с N-апарат. Това нестандартно конструктивно решение помага да се анализира промяната на огъващия момент в т.С за произволно положение на движещия се товар. Изследването завършва с анализ на получените резултати.

Ключови думи: подвижен равномерно разпределен товар, рамка, MathCAD

Introduction

The article presents an alternative method for calculating a bridge structure of a frame type, which carries an evenly distributed load moving very slowly along the roadway of the frame.

The classical method for solving these problems requires knowledge related to the influence lines for the external and internal support reactions of the statically determinate structure.

When the calculations are not automated, the variation of the reactions in the different positions of an evenly distributed load requires too much routine and monotonous work, which in turn is a prerequisite for making mistakes.

The shown example is solved with matrix operations in graphical form through the mathematical package MathCAD.

The presented programme can be used to study the same frame using Q-release in the intermediate joint. In addition, in order to optimise the 2D structure, combinations of N-release and Q-release in the external supports are possible as well as changes in its dimensions.

Solution of the problem by MathCAD package

Fig.1 presents the solution for the frame if it supports the shown external load.

The evenly distributed load is mobile. It moves very slowly along the roadway (ED) of the frame. The geometric dimensions and load of the structure are as follows:

$$a = 2\,m;\ b = 5\,m;\ c = 4\,m;\ d = 2\,m;\ e = 6\,m;$$

$$f = 4\,m;\ l = 2{,}8\,m;\ \alpha = \frac{\pi}{3};\ \beta = \frac{\pi}{4};\ P_1 = 20\,kN;$$

$$P_2 = 50\,kN;\ M = 25\,kN.m;\ q = 60\,\frac{kN}{m}.$$

Solution:

Let a coordinate „x” be accounted from the left end of the distributed load (Fig.1).

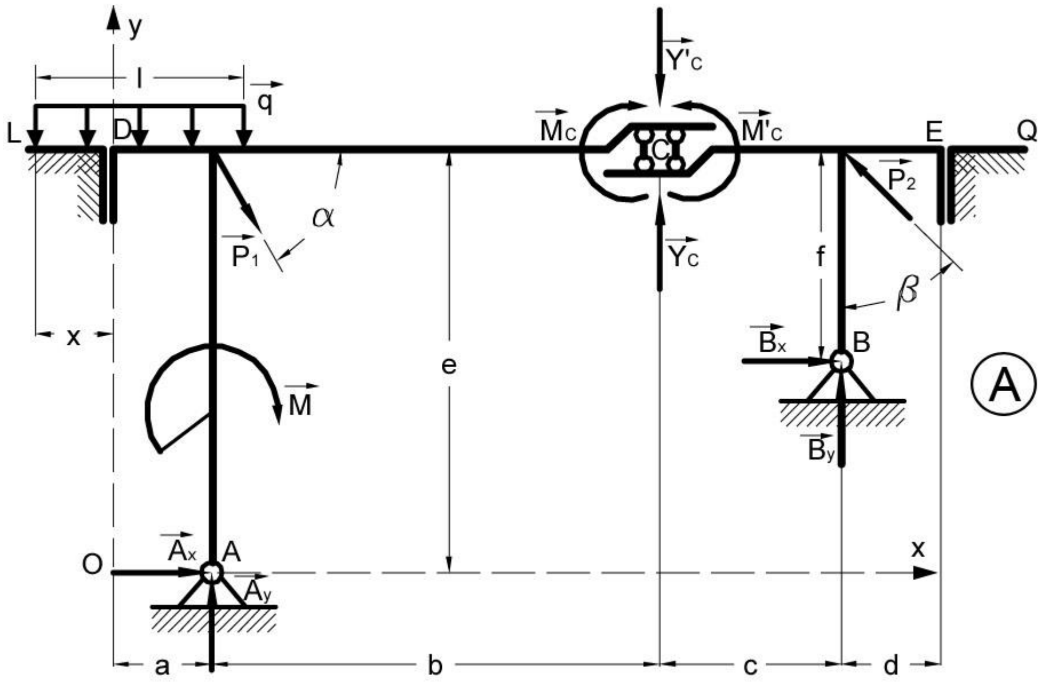

Fig. 1. Calculation scheme. The distributed load as it is moving in the section $-l \le x < 0$ - case A)

We dismember the frame and draw the free-body diagram Fig.1.

The unknown reactions are determined by the six equilibrium equations:

$$\sum M_{Ci} = 0;\ \text{for a left side}$$

$$A_x.e - A_y.b + P_{1y}.b - M +$$
$$+q.(l + x).[a + b - 0{,}5.(x + l)] = 0; \quad (1)$$

$$\sum M_{Bi} = 0;\ \text{for all construction}$$

$$A_x.(e - f) - A_y.(b + c) - M - P_{1x}.f +$$
$$+P_{1y}.(b + c) + q.(l + x).[a + b + c - 0{,}5.(x + l)] +$$
$$+P_{2x}.f = 0; \quad (2)$$

$$\sum M_{C'i} = 0;\ \text{for a right side}$$

$$B_x.f + B_y.c + P_{2y}.c + M'_C = 0; \quad (3)$$

$$\sum M_{Ai} = 0;\ \text{for all construction}$$

$$-B_x.(e - f) + B_y.(b + c) + P_{2y}.(b + c) +$$
$$+P_{2x}.e - P_{1x}.e - M +$$
$$+q.(l + x).[a - 0{,}5.(l + x)] = 0; \quad (4)$$

$$\sum P_{yi} = 0;\ \text{for a left side}$$

$$A_y + Y_C - P_{1y} - q.(l + x) = 0; \quad (5)$$

$$\sum M_{Ai} = 0;\ \text{for a left side}$$

$$Y_C.b - M_C - P_{1x}.e - M +$$
$$+q.(l + x).[a - 0{,}5.(l + x)] = 0. \quad (6)$$

These equations refer to the case shown on Fig.1 and are in effect for $x \in [-l, 0)$.

For the cases in Fig.2 other equilibrium equations are valid. They express the dependence between reactions and the position of the distributed load on the members of the structure.

Hence, it becomes clear that the solution of such a problem "by hand" is a difficult and monotonous process.

Generally, each system from linear equations can be presented in a matrix form –

$$A.R = P_i(x) \quad (7)$$

Where:

- A - a square matrix from the coefficients in front of the unknowns;
- $P_i(x)$ - a vector from the free members of the system (the known values move to the right parts of the equations);
- R - The vector with the unknowns.

In this case it is convenient to use any of the following software applications: Matlab, MathCAD or Maple (Doev et al. 2016; Bertyaev 2005; Stoyanov 2016; Ivanov 2011, 2017). Here the problem is solved with the MathCAD package.

The solution of the problem is demonstrated on Figures 3 and 4.

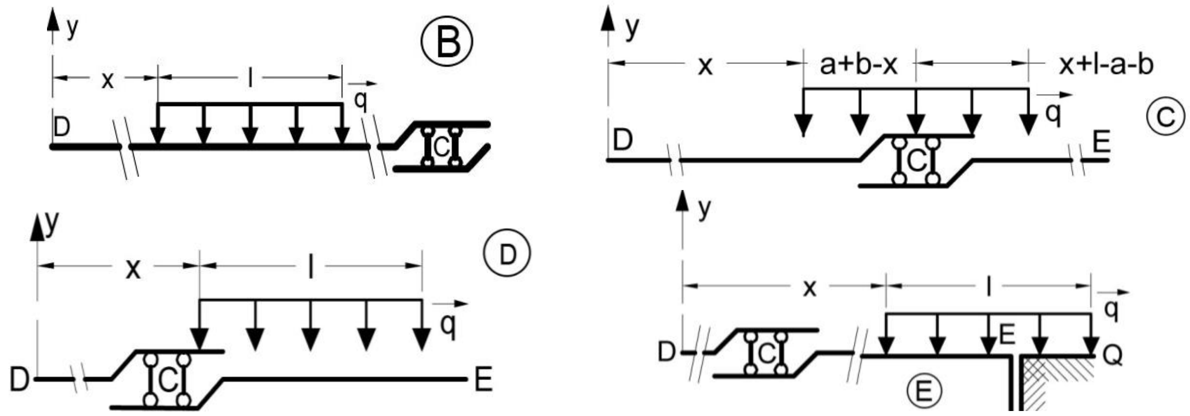

Fig. 2. A movement of the distributed load on the roadway of a structure: case B) - $x \in [0, a+b-l]$; **case C) -** $x \in (a+b-l, a+b)$; **case D) -** $x \in [a+b, a+b+c+d-l]$; **case E) -** $x \in (a+b+c+d-l, a+b+c+d)$;

$$a := 2 \quad b := 5 \quad c := 4 \quad d := 2 \quad e := 6 \quad f := 4 \quad l := 2.8$$

$$\alpha := \frac{\pi}{3} \quad \beta := \frac{\pi}{4} \quad P1 := 20 \quad P2 := 50 \quad M := 25 \quad q := 60$$

$$A := \begin{bmatrix} e & -b & 0 & 0 & 0 & -1 \\ e-f & -(b+c) & 0 & 0 & 0 & 0 \\ 0 & 0 & f & c & 0 & 1 \\ 0 & 0 & -(e-f) & (b+c) & 0 & 0 \\ 0 & 1 & 0 & 0 & 1 & 0 \\ 0 & 0 & 0 & 0 & b & -1 \end{bmatrix} \quad \begin{array}{l} P1x := P1\cdot\cos(\alpha) \\ P1y := P1\cdot\sin(\alpha) \\ P2x := P2\cdot\sin(\beta) \\ P2y := P2\cdot\cos(\beta) \\ |A| = 2.376\times10^{3} \end{array}$$

$$R1(x,l) := q\cdot(x+l) \;\; k1(x,l) := [a+b-.5\cdot(x+l)] \;\; k2(x,l) := [a+b+c-.5\cdot(x+l)]$$

$$k3(x,l) := [a-.5\cdot(l+x)]$$

$$R2(l) := q\cdot l \quad k4(x,l) := (a+b-x-.5\cdot l) \;\; k5(x,l) := (a+b+c-x-.5\cdot l)$$

$$k6(x,l) := (a-x-.5\cdot l)$$

$$R3(x) := q\cdot(a+b-x) \;\; k7(x) := (a+b-x)\cdot.5 \;\; k9(x) := [a-x-.5\cdot(a+b-x)]$$

$$R4(x,l) := q\cdot(x+l-a-b) \;\; k8(x,l) := (x+l-a-b)\cdot.5$$

$$P11(x,l) := \begin{bmatrix} -P1y\cdot b + M - R1(x,l)\cdot k1(x,l) \\ M + P1x\cdot f - P1y\cdot(b+c) - R1(x,l)\cdot k2(x,l) - P2x\cdot f \\ -P2y\cdot c \\ -P2y\cdot(b+c) - P2x\cdot e + P1x\cdot e + M - R1(x,l)\cdot k3(x,l) \\ P1y + R1(x,l) \\ P1x\cdot e + M - R1(x,l)\cdot k3(x,l) \end{bmatrix}$$

$$P12(x,l) := \begin{bmatrix} -P1y\cdot b + M - R2(l)\cdot k4(x,l) \\ M + P1x\cdot f - P1y\cdot(b+c) - P2x\cdot f - R2(l)\cdot k5(x,l) \\ -P2y\cdot c \\ -P2y\cdot(b+c) - P2x\cdot e + P1x\cdot e + M - R2(l)\cdot k6(x,l) \\ P1y + R2(l) \\ P1x\cdot e + M - R2(l)\cdot k6(x,l) \end{bmatrix}$$

Fig. 3. Solution of a frame with the MathCAD package

$$P13(x,l) := \begin{bmatrix} -P1y \cdot b + M - R3(x) \cdot k7(x) \\ M + P1x \cdot f - P1y \cdot (b+c) - P2x \cdot f - R2(l) \cdot k5(x,l) \\ -P2y \cdot c + R4(x,l) \cdot k8(x,l) \\ -P2y \cdot (b+c) - P2x \cdot e + P1x \cdot e + M - R2(l) \cdot k6(x,l) \\ P1y + R3(x) \\ P1xe + M - R3(x) \cdot k9(x) \end{bmatrix}$$

$$P14(x,l) := \begin{bmatrix} -P1 \cdot b + M \\ M + P1x \cdot f - P1y \cdot (b+c) - P2x \cdot f - R2(l) \cdot k5(x,l) \\ -P2y \cdot c + R2(l) \cdot (-k4(x,l)) \\ -P2y \cdot (b+c) - P2x \cdot e + P1x \cdot e + M - R2(l) \cdot k6(x,l) \\ P1y \\ P1x \cdot e + M \end{bmatrix}$$

$$R5(x) := q \cdot (a+b+c+d-x) \quad k10(x) := .5 \cdot (a+b+c+d-x) - d$$

$$k11(x) := -.5 \cdot (a+b+c+d-x) + d + c \quad k12(x) := -.5 \cdot (a+b+c+d-x) + b + d + c$$

$$P15(x,l) := \begin{bmatrix} -P1y \cdot b + M \\ P1x \cdot f + M - P1y \cdot (b+c) - P2x \cdot f - R5(x) \cdot k10(x) \\ -P2y \cdot c + R5(x) \cdot k11(x) \\ -P2y \cdot (b+c) - P2x \cdot e + P1x \cdot e + M + R5(x) \cdot k12(x) \\ P1y \\ P1x \cdot e + M \end{bmatrix}$$

$$L1(x,l) := A^{-1} \cdot P11(x,l) \quad L2(x,l) := A^{-1} \cdot P12(x,l) \quad L3(x,l) := A^{-1} \cdot P13(x,l)$$

$$L4(x,l) := A^{-1} \cdot P14(x,l) \quad L5(x,l) := A^{-1} \cdot P15(x,l) \quad x := -2.8, -2.799 .. 13$$

$$L(x,l) := \left| \begin{array}{ll} L1(x,l) & \text{if } -l < x < 0 \\ L2(x,l) & \text{if } 0 \le x \le a + b - l \\ L3(x,l) & \text{if } b + a - l < x < b + a \\ L4(x,l) & \text{if } a + b \le x \le a + b + c + d - l \\ L5(x,l) & \text{if } a + b + c + d - l < x < a + b + c + d \end{array} \right.$$

$$Ax(x,l) := L(x,l)_0 \quad Ay(x,l) := L(x,l)_1 \quad Bx(x,l) := L(x,l)_2 \quad By(x,l) := L(x,l)_3$$

$$YC(x,l) := L(x,l)_4 \quad MC(x,l) := L(x,l)_5$$

Fig. 4. Continuation of the solution of the frame with the MathCAD package

A similar example is discussed in (Doev et al., 2016).

Analysis of the results obtained

The position of the distributed load does not influence the magnitude of the reactions A_x *and* B_x - see Fig.5.

The module of the support reaction A_y increases to $x = 0$, and after that decreases to $x = 10{,}19\,m$ according to a linear law. The same reaction A_y changes its size according to a quadratic law in the section $10{,}19 \le x \le 13\,m$ and it reaches a minimum module at $x = 11\,m$ Fig.5.

The support reaction B_y changes by module and direction. In a section $-2{,}8 \le x \le 0\,m$ the change of a module is according to a quadratic law, and after that according to linear laws, respectively. In the coordinates $x = 2{,}84\,m$ and $x = 12{,}42\,m$ the direction of the support reaction B_y changes and has a zero value (Fig.5).

The module of the internal support reaction C_y also changes. For a coordinate $x = 4{,}15\,m$ it gets a maximum value, and for $x = 6{,}95\,m$ - respectively minimum. Besides, it changes its direction four times (Fig.5).

The change of the module of the reactive moment at a point C is associated with three local extremums. They appear near $x = -0{,}63\,m$, $x = 5{,}28\,m$ and $x = 11{,}02\,m$ respectively (Fig.5).

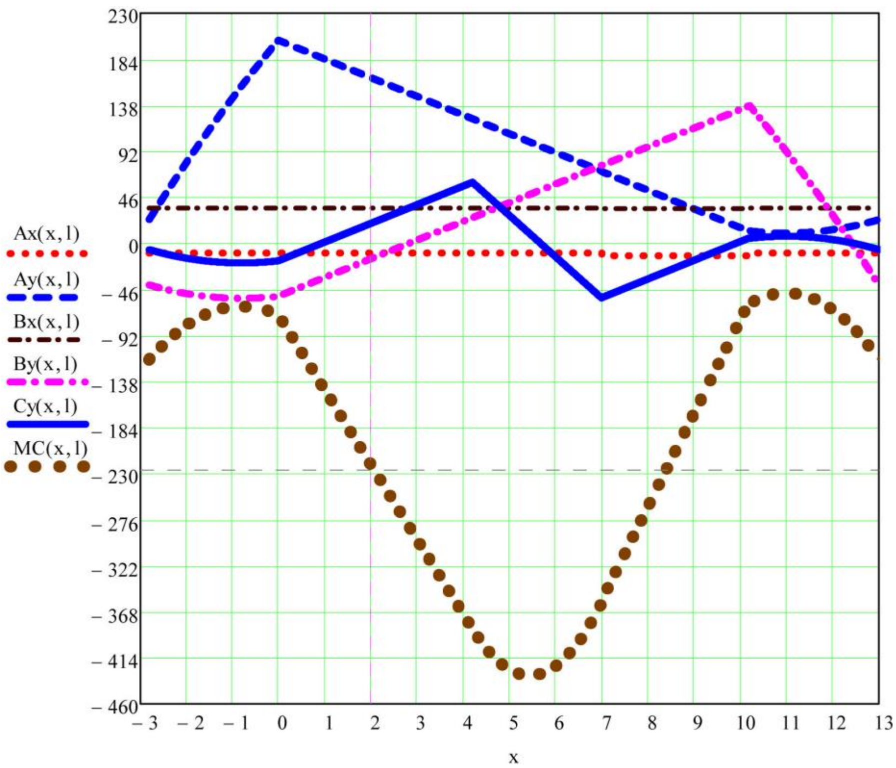

Fig. 5. Amendments of the external and internal reactions depending on the position of the evenly distributed load along the roadway of the frame

Conclusion

The study offers an opportunity to optimise the structure in geometrical attitude, as well as to choose the support reaction devices.

It demonstrates the easy use of MathCAD's graphical interface to analyse the results of the solution.

The shown example can be used in the engineering practice to automate the solution for a wide range of problems. It can be applied in problems related to transport bridges and more specific in the automation of their design (Minin 2013; Hristova et al. 2018).

References

Bertyaev, V. 2005. *Teoreticheskaya mehanika na baze MathCAD praktikum,* BHV-Peterburg, Sankt-Peterburg, 739 p. (in Russian)

Doev, V. S., F. A. Doronin. 2016. *Sbornik zadaniy po teoreticheskoy mehanike na baze MathCAD*, Lany, Sankt-Peterburg, Moscow, Krasnodar, 585 (in Russian).

Hristova, T. V., A. B. Yanev, N. V. Savov. 2018. *Determination of the influence of jaw movement frequency of jaw crusher on energy consumption*, *Annals of the University of Petroşani,Electrical Engineering*, 20, 29-36 p.

Ivanov, A. 2011. *Modelirane na dinamichni zadachi s MATLAB*, Avangard Prima, ISBN 978-954-323-837-8, Sofia, 100. (in Bulgarian)

Ivanov, A. 2017. Three dimensional vibrations of aggregate connected with elastic elements. – *Journal Tehnomus*, May, 37–42.

Minin, I., D. Dimitrov. 2013. *Minni mashini.* Avangard Prima, Sofia, 378 p. (in Bulgarian)

Stoyanov, A. 2016. *Matrichni operacii s MathCAD v teoretichnata mehanika Statika*, Kineziologiya BG, Sofia, 165 p. (in Bulgarian)

DEVELOPMENT OF AN ALGORITHM FORECASTING THE GENERATION OF ELECTRIC ENERGY BY A WIND DIESEL COMPLEX

Daria Batueva

Saint Petersburg Mining University, 199106 Saint Petersburg; dasha-batueva4@rambler.ru

ABSTRACT. There are a large number of autonomous sources of power supply, which provide electricity to industrial enterprises and regional power regions in the Arctic zone operating in isolation from the united power system. Their power supply is carried out mainly from autonomous diesel power plants. Load schedule of remote areas in which there are industrial enterprises will directly depend on the cycles of electrical equipment. However, when using a wild-diesel complex as one of the sources of power supply, it is necessary to take into account the effect of climate change on the operation of a wind power plant and to predict it, together with the forecast of energy consumption of an electrical object. The data shown on the wind maps do not allow to determine the location of wind power plants in the Arctic, because, firstly, they do not take into account all the necessary parameters, secondly, the work should be based on the study of dynamic maps, the data in which are processed and analysed in real time based on neural networks and machine learning. The article develops an algorithm for optimising the software package; upon receipt of data on meteorological conditions, the programme will calculate the electricity generated by the wind power plant. When planning the load schedule of an enterprise for days or hours in advance, the ratio of electric power output of wind power stations, diesel power stations and accumulation or output of electric power from batteries will be determined.

Keywords*:* Wind-diesel complexes, reliability of power supply, load schedule, energy consumption forecasting

РАЗРАБОТВАНЕ НА АЛГОРИТЪМ ЗА ПРОГНОЗИРАНЕ НА ГЕНЕРИРАНЕТО НА ЕЛЕКТРОЕНЕРГИЯ ОТ ВЯТЪРНО-ДИЗЕЛОВ КОМПЛЕКС

Дария Батуева

Санктпетербургски минен университет, 199106 Санкт Петербург

РЕЗЮМЕ. Има голям брой автономни източници на електрозахранване, които осигуряват електроенергия на промишлени предприятия и регионални енергийни райони в арктическата зона, работещи в изолация от общата енергийна система. Захранването им се осъществява главно от автономни дизелови електроцентрали. Графикът на натоварване на отдалечените райони, в които има промишлени предприятия, ще зависи пряко от циклите на електрическото оборудване. Въпреки това, когато се използва вятърно-дизелов комплекс като един от източниците на електрозахранване, е необходимо да се вземе предвид ефектът от изменението на климата върху работата на вятърна електроцентрала и да се прогнозира, заедно с прогнозата за потреблението на енергия на електрически обект. Данните, показани на вятърните карти, не позволяват да се определи местоположението на вятърните централи в Арктика, защото, първо, не отчитат всички необходими параметри, второ, работата трябва да се основава на проучването на динамичните карти, данните, в които се обработват и анализират в реално време въз основа на невронни мрежи и машинно обучение. Статията разработва алгоритъм за оптимизиране на софтуерния пакет; след получаване на данни за метеорологичните условия програмата ще изчисли електроенергията, генерирана от вятърната електроцентрала. При планиране на графика за натоварване на предприятието за дни или часове напред, ще се определи съотношението на изходната мощност на вятърните електроцентрали, дизеловите електроцентрали и натрупването или произведената електрическа енергия от акумулатори.

Ключови думи: вятърно-дизелови комплекси, надеждност на електрозахранването, график на натоварване, прогнозиране на консумацията на елекрическа енергия

Introduction

Today, the development of the Arctic territories of Russia requires reliable sources of electricity, and the region needs new solutions and technologies, one of which may be wind-diesel complexes operating in parallel to cover the peaks of the electrical load.

"Ensuring the country's energy security, including through reliable and high-quality power supply in a number of remote regions and regions with low consumer density," is one of the main targets of state policy reflected in the energy strategy of Russia until 2035. About 70% of the territories of the Russian Federation are decentralised power supply zones and non-electrified zones.

Today, the energy supply of the Arctic regions is mostly isolated, due to the fact that the energy areas are far from each other and the energy complex cannot be used efficiently; because of this the reliability of providing electricity to the consumers is reduced. Energy supply is carried out separately in each district at the expense of diesel power stations and the fuel for them comes once a year for northern delivery. As a rule, these are diesel power plants that have low efficiency and high production costs of electricity, which reach to 80-120 rubles per kilowatt-hour, taking into account the fact that diesel fuel for them has to be delivered once a year during winter delivery. At the same time, if we take the average price of electricity in the zone of centralised power supply in the country, it will be 3-4 rubles per kWh for the end user. Wind turbine complexes will significantly reduce the cost of electricity (due to the fuel component), ensure a payback period of the project of 3-5 years, and achieve a reduction in emissions of pollutants and CO_2.

The development of the Arctic territories of Russia requires reliable sources of electricity, and in connection with the geographical features of the region, new solutions and technologies are needed.

It is necessary to plan not only the modernisation and expansion of the existing electric grid complex, but also to use distributed generation, including renewable energy sources, to increase the efficiency of the energy complex.

For settlements that do not have industrial enterprises, the curve of electrical load is largely determined by the pumps of the village heating system - boiler plants operating on wood, fuel oil or coal. This determines the significant seasonal uneven energy consumption of such settlements. The deviation of real energy consumption from the curve of the day's workload is from 11 to 56%, with the maximum deviation occurring in the summer months. This is because there are consistently low air temperatures in winter and the average temperature changes significantly every month in the spring, summer and autumn periods, which entails a shift in the load curve. As a result, the deviation of real loads from the energy balances used in calculations for the summer regime day can be 40-50%.

As for remote areas in which there are industrial enterprises, the load schedule will directly depend on the electrical equipment operation cycles. However, when using a wind-diesel complex as a power source, the question of the impact of climate change on the operation of wind turbines remains, which also needs to be predicted in the system together with the energy consumption forecast of an electrical object.

Baseline Territory Data

The parameters that must be considered during the construction of a wind farm on the territory of the Arctic practically do not differ from the parameters for the territories in the middle lane. However, it is necessary to pay special attention to some of them, due to extreme and unstable weather conditions. Below is a complete list of parameters that are important when choosing a place:

1. Average wind speed.
2. Wind direction
3. Minimum wind speed.
4. Maximum wind speed.
5. Power density.
6. Average temperature.
7. Average humidity.
8. Average pressure.
9. Altitude above sea level.
10. Distance to water.
11. Height difference.
12. Smooth height differences.
13. The maximum difference in the area of 5-10 km.
14. Percentage of trees or plants in the area (roughness).
15. Distance to the settlement.
16. The distance of the pre-industrial facility.
17. The average number of inhabitants in the area.
18. Distance to the road (sea, air).
19. Distance to the electricity network.
20. Protected areas: reserves, etc.

Operation mode of the wind turbine and diesel generator

Characteristic of system

The wind-diesel complex should incorporate an automatic system that will take into account external climatic changes (this work takes into account only the change in wind speed) and change the operating modes of the diesel generator and wind turbines. The change in power of wind and diesel generator sets depending on the change in wind speed is shown in Figure 1.

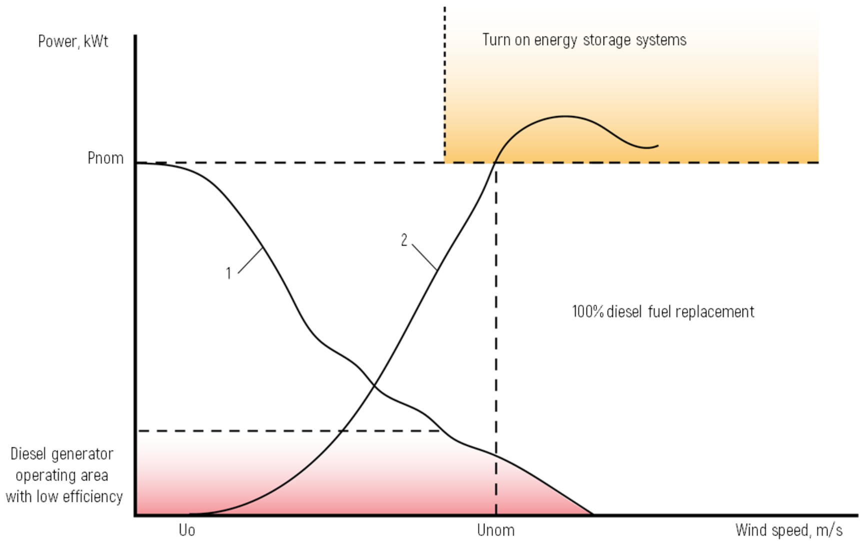

Fig. 1. Operation mode of the wind turbine and diesel generator

Algorithm for choosing the mode of operation

The procedure is described in the form of an algorithm, on the basis of which the automatic system will make a decision on the choice of the operating mode of a wind-diesel complex under changing climatic conditions. The algorithm is based on the presence of a wind turbine, a diesel generator set and a battery in the system, wind speed readings. After selecting the mode of operation of the power supply sources for the object of research, the production and consumption of electricity as well as how much energy is accumulated in the battery are calculated. The algorithm is shown in Figure 2.

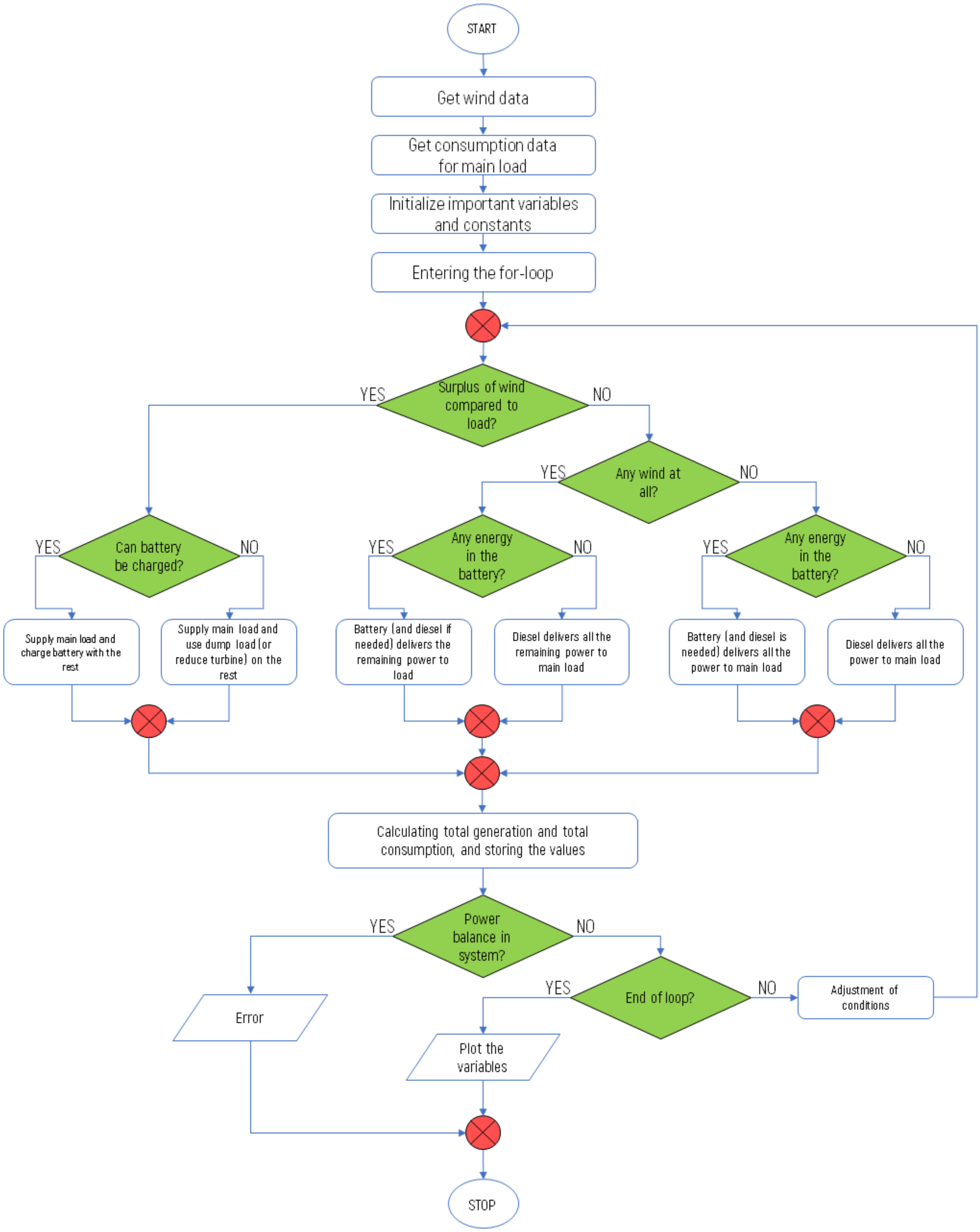

Fig. 2. Algorithm for choosing the mode of operation of wind turbines and diesel generator

Neural network prediction

The next step in the study will be to create a model based on neural networks. The databases of statistical data from the points indicated in the chapter earlier will be used to forecast the generation by the wind-diesel complex. A simplified structure of the model is presented in Figure 3.

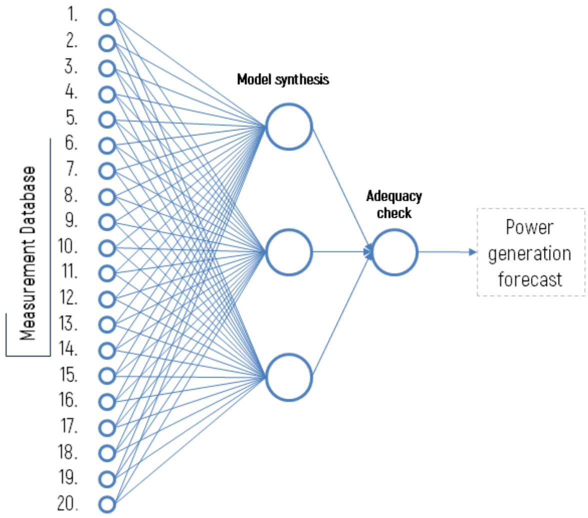

Fig. 3. Model of neural network prediction

It should be noted that the more factors will be taken into account, the more accurately it will be possible to form a forecast of electricity generation. Knowing the projected graphs of loads of objects that are supplied from the wind-diesel complex, it will be possible to determine with high precision the operating modes of the wind-diesel complex and batteries for energy storage.

Conclusion

The article describes the main problems of areas with decentralised power supply, including dependence on the supply of expensive fuel and high specific fuel consumption at diesel power plants, as well as the deviation of real energy consumption from the load schedules of the day.

A description of the algorithms that will allow to predict and automatically select the operating modes of wind-diesel complexes to cover the peaks of the electrical load is presented.

The necessary information is indicated, on the basis of which it is possible to analyse and identify the dependence of electricity consumption on climate change and predict the operating modes of the wind-diesel complexes to cover the peaks of the electrical load.

References

Batueva, D. E., J. E. Shklyarskiy. 2019. Increasing efficiency of using wind diesel complexes through intellectual forecasting power consumption. – *Proceedings of the 2019 IEEE Conference of Russian Young Researchers in Electrical and Electronic Engineering, ElConRus*.

Beloborodov, S. S. 2018. Reducing CO2 emissions: the development of cogeneration or the construction of renewable energy sources. – *Energosovet*, 1 (51).

Karapetyan, K. G., O. V. Denisova. 2017. Advanced technologies of microlenses production for robot system camcorders. – *IOP Conference Series: Earth and Environmental Science, IOP Science, 87,* 1–4.

Popiel, A. S., S. V. Kiseleva, M. O. Morgunova. 2015. The use of renewable energy sources for energy supply to consumers in the Arctic zone of the Russian Federation. *Arctic: ecology and economics, 1,* 64–69.

Sosnina, E. N., A. Yu. Kechkin, D. A. Filatov. 2014. Power supply issues for consumers remote from the network infrastructure. – *Proceedings of the Nizhny Novgorod State Technical University. R.E. Alekseeva,* 5 (107), 100–104.

The Draft Energy Strategy of Russia for the Period up to 2035. 2014. Moscow.

The Strategy for the development of the Arctic zone of the Russian Federation and national security for the period up to 2020. 2010. Moscow, 241 p.

Zhukovskiy, Y. L., V. V. Starshaia, D. E. Batueva, A. D. Buldysko. 2018. Analysis of technological changes in integrated intelligent power supply systems. – *Innovation-Based Development of the Mineral Resources Sector: Challenges and Prospects, 11th Conference of the Russian-German, Raw Materials*, 249–258.

EVALUATION OF TECHNOLOGICAL SOLUTIONS, GIVEN THE RISKS OF DEVIATION OF INTEGRAL DESIGN INDICATORS

Inna Bondarenko, Igor Temkin

National University of Science and Technology MISiS, 119049 Moscow; innasbondarenko@gmail.com

ABSTRACT. The article deals with the choice of technological solutions for conducting underground works that most adequately meet the conditions of the construction site. At the initial stages of project development the proposed methodology for comparative assessment of integral indicators of the project allows evaluating and selecting a technological solution that enhances the efficiency and safety of the construction of an underground structure. The structure of the methodology includes fuzzy models and algorithms that provide processing of large amounts of information, form the significance of environmental factors (organisational, mining and geological, construction site factors), design and technological parameters of the project and allow the main relationships and interdependencies between them to be identified.

Key words: technological solution, project, underground structure, risk, fuzzy model

ОЦЕНКА НА ТЕХНОЛОГИЧНИ РЕШЕНИЯ, КАТО СЕ ВЗЕМАТ ПРЕДВИД РИСКОВЕТЕ ОТ ОТКЛОНЕНИЕ НА ИНТЕГРАЛНИТЕ ИНДИКАТОРИ НА ПРОЕКТА

Инна Бондаренко, Игор Темкин

Национален университет за наука и технологии “МИСиС”, 119049 Москва

РЕЗЮМЕ. Статията разглежда избора на технологични решения за провеждане на подземни работи, които най-адекватно отговарят на условията на строителната площадка. Предложената методология за сравнителна оценка на интегралните показатели на проекта позволява на началните етапи на разработване на проекта да се оцени и избере такова технологично решение, което да повиши ефективността и безопасността на изграждането на подземна конструкция. Структурата на методологията включва размити модели и алгоритми, които осигуряват обработка на големи количества информация, формират значението на факторите на околната среда (организационни, минни и геоложки, фактори на строителната площадка), проектни и технологични параметри на проекта и позволяват да се идентифицират основните отношения и взаимозависимостите между тях.

Ключови думи: технологично решение, проект, подземна структура, риск, размит модел

Introduction

The construction of underground structures includes a number of geotechnical risks, for which the project participants, funding and performing the construction, require qualitative and quantitative analysis. The adoption of a decision depends on many objective and subjective conditions and factors. It is not always possible to consider all conditions and factors, and then influence them actively, i.e. there is uncertainty of the forecasting situation.

In most cases, the security is provided by the normative models and coefficients that apply to groups of corresponding structures. The project security can be achieved by processing the standards documents for the use of the project. They take into account unusual and random loading: earthquakes, floods, mudslides, strong winds, fires in tunnels, etc. But it is important to perform this analysis during the project preparation stage and choose the design option based on the assessment of uncertainties and their impact on the construction project.

Methodology

At the initial stages of design, comparison of the project options is impossible without its formalised presentation, including the development of each of the possible technological solutions in the form of engineering design schemes, engineering topological plans, etc. It is a lengthy and not rational procedure for all project participants. It`s extremely important to choose a method for describing the structure of a construction project, provided that, on the one hand, the problem of choosing a design solution is effectively solved, and on the other hand, allowing to take into account the characteristic qualitative features of its constituent elements.

Based on the above conditions for the implementation of construction projects of communication tunnels and analysis of project documentation, a parametric description of the project will be further provided.

Earlier, in scientific papers on the laying of engineering structures (Kulikova et al., 2005; Krivonozhko et al., 2016) the most significant environmental factors were identified, which included the parameters of mining and geological conditions, the parameters of the ground and underground characteristics of the urban environment. They were considered in accordance with the issues related to this problem. As a result, 9 main parameters were identified, and the attributes describing them were also determined (Temkin et al., 2012)

From the entire set of mining and geological conditions (U_1), the parameters were identified. The strength of the host rocks (P_1) and the water saturation of soils (P_2) are the most important parameters in the development of the underground space.

The underground conditions (U_2) of the construction site are characterised by the density (P_3) of already existing underground utilities and facilities at the construction site. When evaluating the density of the underground structures, three informal categories are usually distinguished: “high”, “medium” and “low”, depending on the ratio V_{ps} / V_{ob} × 100%, where V_{ps} is the volume of the underground facilities already in the construction area, V_{ob} is the total volume of the underground space construction of communication tunnels.

The ground conditions (U_3) include the most significant parameters for underground construction, the density of the ground structures, road load, environmental condition, type of territory, historical and cultural value. Further, it is necessary to develop algorithms for evaluating the integral parameters that allow comparing design solutions, detailed structuring and model representations of the construction project.

To describe the project, 6 parameters characterising the constructive solution of communication tunnels and route (S) were identified: the diameter of the communication tunnel, the laying depth, the total length of the route, the geometry of the route, the slope of the route, the shape of the section of the tunnel, category (Temkin et al., 2012).

The main tunnelling technologies (G) were also identified: the mining method (manual labour + combined technology), the semi-mechanised shield, the mining method (manual labour + combined technology), mechanised shield, puncture, punching, directional drilling, microtunnelling (Bondarenko, 2011).

In the construction projects of underground structures an indicator of reliability and safety is the expert assessment of the level of possibility of mutual influence of the developed design solutions and the specific external environment for their implementation.

When implementing a project in real conditions the projected values of the terms and costs may often differ from the actual ones, $\Delta T = | T_f - T_{pr} |$ and $\Delta C = | C_f - C_{pr} |$.

It is impossible to directly relate the Δ value to such characteristics as “project reliability”, “project environmental safety”. However, for expert designers, the obvious paradigm is that “the project is better, the smaller | Δ |”, i.e. in a formalised language: E ⟶ max at ΔT, ΔC ⟶ min; E ⟶ min at ΔT, ΔC ⟶ max.

Now, based on the foregoing, each project option (Di) can be represented as the following information structure:

$$Di \{U_{1i}, U_{2i}, U_{3i}, S_i, G_i, C_i, T_i, E_i\} \quad (1)$$

where:

U_{1i}, U_{2i}, U_{3i} - the set of parameter values characterising a particular construction site;

S_i - design parameters of the communication tunnel;

G_i - the technology or technologies that form the basis of the project;

C_i, T_i, E_i - integral indicators of the project: project cost, terms of its implementation, reliability and safety of implementation.

In this task more detailed description of the technologies is not required, because calculations of the parameters of the methods of sinking are in the engineering field. In addition, the most modern technologies have established assessment criteria, regardless of the internal parameters.

When considering engineering and technological features of the construction of communication tunnels, and especially the environment of the project (major city, dense underground and surface development, high population density, etc.) such factors as the geological uncertainty factor (F_1), the factor of uncertainty of site conditions (F_2) and the structural uncertainty (F_3) should be identified.

Assessment of the impact of the uncertainty factors F_1,F_2,F_3 on the integrated project performance K_j (C - the cost of construction, T - construction period, E - reliability and safety implementation) is solved as a comprehensive evaluation of the fuzzy risk (R)) in the context of the problem.

In this case the fuzzy risk is defined as the subjective probability that is the result of the influence of uncertainty factors. F_1,F_2,F_3 will occur as a deviation of the design value of the integral indicator K_j^* of the total actual $\widetilde{K}_j$.

Evaluation of the fuzzy risk is a combination of the influence (V) of uncertainty factors for integral indices and the degree of this effect (Z).

The possibility of influence of uncertainties on the integral parameters of the construction site`s project under the same conditions is different for the different structural solutions, and the degree of influence of uncertainties on integrated indicators will be different for the different versions of the project implemented under the same conditions, only when these variants differ in construction technology. Thus, it can be argued that there is some dependence of V on the design parameters of the project, and dependence of Z on the technology used and the conditions in which the construction of the communication tunnel is performed:

$$V_{F_iK_j} = f(S); \quad (2)$$

$$Z_{F_iK_j} = f(U, G). \quad (3)$$

In the conditions of the given problem it is not possible to construct an accurate model of dependence because there are no objective estimates and sufficient statistics, so it is only applicable to expert evaluation methods.

According to all uncertainties for all integral indices a comprehensive risk assessment of the design option will be found on the basis of the values of the matrix elements' components of the expert assessment of influence and impact:

$$V = \begin{bmatrix} v_{F_1K_1} v_{F_2K_1} v_{F_3K_1} \\ v_{F_1K_2} v_{F_2K_2} v_{F_3K_2} \\ v_{F_1K_3} v_{F_2K_3} v_{F_3K_3} \end{bmatrix}, Z = \begin{bmatrix} z_{F_1K_1} z_{F_2K_1} z_{F_3K_1} \\ z_{F_1K_2} z_{F_2K_2} z_{F_3K_2} \\ z_{F_1K_3} z_{F_2K_3} z_{F_3K_3} \end{bmatrix} \quad (4)$$

where: $v_{F_iK_j}$– value of influence of the i-th element of uncertainty to the j-th integral parameter; $z_{F_iK_j}$ – the value of the degree of influence of the i-th element of uncertainty to the j-th integral parameter.

To assess the impact of these factors on the integral characteristics of the construction project (such as, for example, the depth of the tunnel lining, slope, alignment, diameter, etc.) the expert rules and the methodology for project evaluation were developed based on the calculation of the influence $V_{F_iK_j}$ of the uncertainty factor (Fi) and the degree of influence $Z_{F_iK_j}$ of the uncertainty factor (Fi) on the integral indicator (Kj) (Temkin et al., 2013) .

When the expert rules are used to describe the parameters and their estimates, it is proposed to use fuzzy formalisms. Each of the rule elements is described using several Boolean variables (3÷5): "high," "upper average", "average", "below average", "low". Figure 1 shows an example of a membership function for linguistic variable "high," "medium" and "low" for the rock strength.

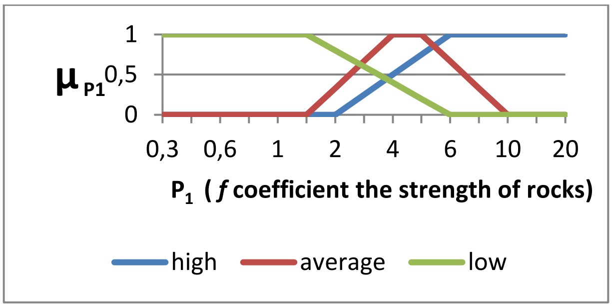

Fig. 1. The membership functions of linguistic variables "high", "average" and "low" for the rock strength

Thus, the model of fuzzy risk (R), integral index K_j of the construction project of a communication tunnel is determined by calculating a fuzzy risk for each uncertainty factor, which, in turn, is obtained by evaluating the influence and impact of uncertainty on K_j:

$$\left.\begin{array}{l} V_{F_1K_j} \wedge Z_{F_1K_j} \rightarrow R_{F_1K_j} \\ V_{F_2K_j} \wedge Z_{F_2K_j} \rightarrow R_{F_2K_j} \\ V_{F_3K_j} \wedge Z_{F_3K_j} \rightarrow R_{F_3K_j} \end{array}\right\} R_{K_j} \qquad (5)$$

Figure 2 shows the general scheme of the fuzzy risk assessment model for the integral index of the project in the form of a block diagram.

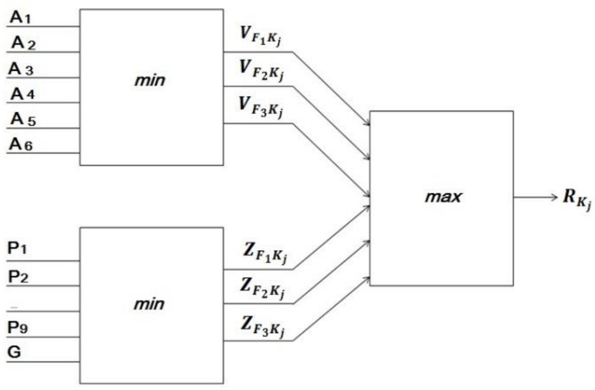

Fig. 2. The general scheme of the model of fuzzy risk assessment for the integral indicator of the construction project of CT

Identifying the impact of factors on the overall risk to the integral index is based on the fuzzy associative matrix (Table 1).

Table 1. *The possibility and degree of influence factor*

The possibility of the influence factor	high	average	average	above average	high	high
	above average	below average	average	average	above average	high
	average	below average	below average	average	average	above average
	below average	low	below average	below average	average	average
	low	low	low	low	below average	average
The degree of influence factor		low	below average	average	above average	high

In the future, when the rule will be difficult to operate with facts that are represented in linguistic form, it will be needed to encode the original set of the rules and generate the source of inductive table.

According to the chosen risk factors based on a formalised description of the project, a training table was developed for building a fuzzy rule base, where on the basis of expert opinions the possibility of the influence of the uncertainty factor (F_i) on the integral indicator (K_j) – $V_{F_iK_j}$ (table 2) and the degree of influence of the uncertainty factor (Fi) on the integral indicator (K_j) - $Z_{F_iK_j}$ (Table 3) will be determined.

Table 2.*The estimation of the influence of the uncertainty factor (F_i) on the integral indicator (K_j)*

LS	A_1	…	A_6	$V_{F_iK_j}$
1	a_{11}	…	a_{61}	$V_{LS\ 1}$
2	a_{12}	…	a_{62}	$V_{LS\ 2}$
…	…	…	…	…
n	a_{1n}	…	a_{6n}	$V_{LS\ n}$

Table 3. *Assessment of the degree of influence of the uncertainty factor (F_i) on the integral indicator (K_j)*

LU	P_1	…	P_9	h_{GFi}	$Z_{F_iK_j}$
1	p_{11}	…	p_{91}	h_1	$z_{LU\ 1}$
2	p_{12}	…	p_{92}	h_2	$z_{LU\ 2}$
…	…	…	…	…	…
z	p_{1z}	…	p_{9z}	h_z	$z_{LU\ n}$

where:
LS_x – line training table, by definition;
$P_{F_iK_j}$ (= 1 rule), $x = \overline{1, n}$;
LU_y – line training table, by definition, $Z_{F_iK_j}$ (= 1 rule), $y = \overline{1, z}$;
h_{GFi} - resistant technology to the uncertainty factor F_i, defined by the experts.
The number of training tables (i×j)×2.

Results from the calculations

The example of expert reasoning can serve as the following rules assessment of the geological influence factor on the construction time:

LS 1:	If the diameter is<2 and depth[3-8] and track length>600 and geometry of the route (number of turns)>3 and slope of the route (number of turns in the cut)[1-3] and shape sections III,IV => V_{F_1T}→average
LU 1:	If the fortress[3-6] and water saturation<0.1 and the density of underground structures [high], and the density of surface facilities [average] traffic load [high] and the environment [normal] view site [residential] and historical and cultural value [is] complex and the significance of the [required] and hGFi [low] => Z_{F_1T}→ below average

Conclusion

Thus, each rule is built on a set of formal parameters and the project gives an expert estimation of the influence and degree of influence of the uncertainty factor (F_i) on the integral indicator (K_j) for each possible combination of values for these parameters.

As an example of the use of this mechanism, the choice of two design options for the construction of a communication tunnel (D1 and D2) was considered based on risk assessment of the uncertainty geological factor (F1) for the integral indicator of "construction time" (T) for the conditions of the construction site of a sewer tunnel under the Moscow railway, Savelovsky direction on the site "Reconstruction of Lianozovsky passage from Dmitrovsky sh. to Cherepovetskaya street".

From the calculations, the following results were obtained:

$V_{F_1T}(D_1) = 1.55$ and $Z_{F_1T}(D_1) = 6.59$ → RT(D1)=3.63
$V_{F_1T}(D_2) = 1.79$ and $Z_{F_1T}(D_2) = 4.76$ → RT(D2)=2.74

These results show that the risk for deviation of the actual value of the integral indicator (timing of implementation) from the design value under the given conditions of the construction site for the second project is smaller, i.e., the risk that they will violate the terms of project implementation is smaller than in the case of chosen technological solution D2.

The study was implemented under a grant by the Russian Scientific Foundation (project No. 17-11-01353).

The resulting model provides a choice of the design options for the construction of the tunnel communication in conditions of uncertainty for many integrated indicators (economic, organisational, technological), which is implemented with minimum risk.

References

Belopushkin, V. I., I. S. Bondarenko. 2008. The method of choosing the optimal technology for the construction of a communication tunnel. – *Software products and systems, 3*, 10–13.

Bondarenko, I. S. 2011. The methodology of choosing the technology for driving the collector tunnel. *Mountain Information and Analytical Bulletin, 6*, 108–114.

Bondarenko, I. S. 2015. Ecological-economic analysis of project solutions in the construction of communication tunnels based on the methodology of the assessment of deviations of integral indicators of the project. – *Materials 11-th International Conference on Problems of Mining, Construction and Energy. Socio-economic and environmental problems of mining, construction and energy. Tula-Minsk-Donetsk*, 268–279.

Granichin, O. N., V. I. Comedy. 2008. Information technology in management. *INTUIT,* Moscow.

Kaufman, L. L. 2009. Geotechnical risks in underground construction. – *Nord-Press,* Donetsk.

Krivonozhko, V. E., F. Forsund, A. V. Lychev. 2016. Improving the Frontier in DEA Models. – *Mathematics*, *94,* 3, 715–719.

Kulikova, E. Yu., A. V. Korchak, A. N. Levchenko. 2005. Strategy risk management in urban underground construction. – *Moscow State Mining University,* Moscow.

Temkin, O. I., S. I. Bondarenko. 2013. Risk assessment of the construction of communication tunnels based on expert analysis of design decisions. – *Heavy machinery,* 9, Moscow, 38–40.

Temkin, I. O., I. S. Bondarenko, I. V. Barannikova. 2012. Evaluation of the integral parameters of the project based on the neural network models for forecasting the cost and timing of the project. – *Mountain Information and Analytical Bulletin* 6, 95–101.

INFLUENCE OF THE BALL LOAD ON THE SPECIFIC POWER CONSUMPTION OF BALL MILLS

Kiril Dzhustrov

University of Mining and Geology "St. Ivan Rilski", 1700 Sofia; justrov@mgu.bg

ABSTRACT. The mill's output, and hence the specific power consumption, depend on the correct selection of the ball load. Both the increased and the decreased ball load lead to decreasing the mill's output which induces increase of the specific power consumption. At the optimum ball load of the mill, working in a closed loop, an increase in the circulating load can be allowed with a simultaneous increase in the mill's output, lowering the specific power consumption and improving the performance. To analyse the impact of the ball load on the specific power consumption, three-month data from 10 ball mills were processed. Experimental tests were also carried out for one mill to determine the specific power consumption when filling the mill with grinding bodies.

Key words: ball mills, optimum ball load, specific power consumption

ВЛИЯНИЕ НА ТОПКОВИЯ ТОВАР ВЪРХУ СПЕЦИФИЧНИЯ РАЗХОД НА ЕЛЕКТРОЕНЕРГИЯ НА ТОПКОВИ МЕЛНИЦИ

Кирил Джустров

Минно-геоложки университет "Св. Иван Рилски", 1700 София

РЕЗЮМЕ. От правилния избор на топковия товар зависи производителността на мелницата и следователно специфичния разход на електроенергия. Както завишения, така и занижения топков товар води до намаляване на производителността на мелницата, което предизвиква повишаване на специфичния разход на електроенергия. При оптимален топков товар на мелницата, работеща в затворен цикъл, може да се допусне повишение на циркулационния товар при едновременно увеличение на производителността на мелницата, снижавайки специфичния разход на електроенергия и подобрявайки технологичните показатели. За анализ на влиянието на топковия товар на специфичния разход на електроенергия са обработени данни за три месеца от работата на 10 топкови мелници. За една мелница са направени и експериментални изследвания за определяне на специфичният разход на електроенергия от запълването на мелницата със смилащи тела.

Ключови думи: топкови мелници, оптимален топков товар, специфичен разход на електроенергия

Introduction

By increasing the ball load the power consumption increases to maximum capacity (extremum) and after that lowers gradually (Fig. 1). This explains the fact that after increasing the ball load, the extremum, centre of load of grinding bodies is moving closer to the axle of rotation of the machine.

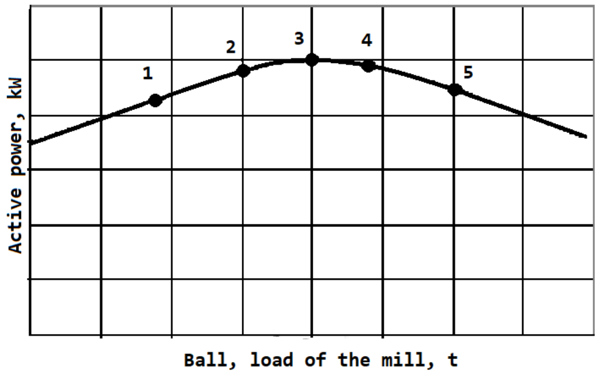

Fig.1. Dependence of the extracted active power on the ball load of the mill

It is well known that the waterfall mode of operation in the ball mill, the useful power *Po* includes the power to increase the grinding environment and to transfer the needed kinetic power.

$$P_0 = Mw \text{ , } W; \tag{1}$$

Where: *M* is the momentum, created by the grinding environment by the rotation of the drum, Nm;

w – actual angular velocity rad/s

$$M = G_{cм} . I \text{ ,} \tag{2}$$

Where *Gсм* – the weight of the milling environment, N;

l – the distance between the centre of the load and the milling environment and the axis rotation of the drum, *m*.

The modes of work in (1) and (2) at (Fig. 1) are with unbalanced circulating load due to the lack of ball load.

It is typical of this section of the curve that with the increase of the ball load, the power gained by the electric motor increases.

In (3) the mill is supposed to work with stable circulating load and the ball load in this section of dependence is optimal.

The operation of the mill in later stages of ball load in (4) and (5) leads to a mode that is unstable circular load due to the overage of ball load and lowers the kinetic power of the grinding environment.

For this section of the curve it is specific that with the increase of the ball load, the active power produced by the electric motor decreases.

Experimental Tests

It is well known that the specific electricity consumption for ball mill grinding is closely connected with the technical process and depends on a number of factors: the weight of the ball mill, the size of the mill, the speed of rotation, the density of the pulp, the size of the end material, the lining of the mill, physical and mechanical properties of the ore, the efficiency of the mill, etc. Based on experimental tests, it was found that the main power in the ball mill is being consumed for lifting the ball load – approximately 80%. The increase of productivity of the mill leads to insignificant increase of exhausted power. The aim for increasing the productivity of the mills is apparent, and hence, the increase of the specific power consumption.

The productivity of the mill depends on the correct choice of ball load. Increasing and decreasing of the ball load leads to lowering the productivity of the mill and from there to increasing the specific power consumption. The size of the grinding bodies (balls) has to be taken under consideration in the productivity of the mill. The specific electrical consumption in the process of grinding of the ore can be determined most accurately by the electrical specifications.

Figure 2 shows the curves, determining the dependence between the size of the ball load and the exhausted power from the electric motor of a mill for a period of 12 days.

The data on the hourly distribution and the volume of the ball load for building the curve were taken by the SCADA system in the enterprise. After calculating the results from the measurements of the ball load, the hourly consumption norm of the balls was determined in relation to the alternation of the ball load in the mill during that time. In the same period data was extracted about the consumption of the electric motor of the mill, active power, recorded in the network analyser FLUKE. The curves in Fig.2 show that after every load with balls there is an active power jump registered. The increase of the active power is with approximately 9 kW per ton balls. During the work, the balls wear out, the electric load lowers and the used-up active power from the electric motor decreases. It is certain that if the ball dosage machine works and loads consistently the balls in the mill, the load schedule of the active power will be levelled which leads to economic power consumption.

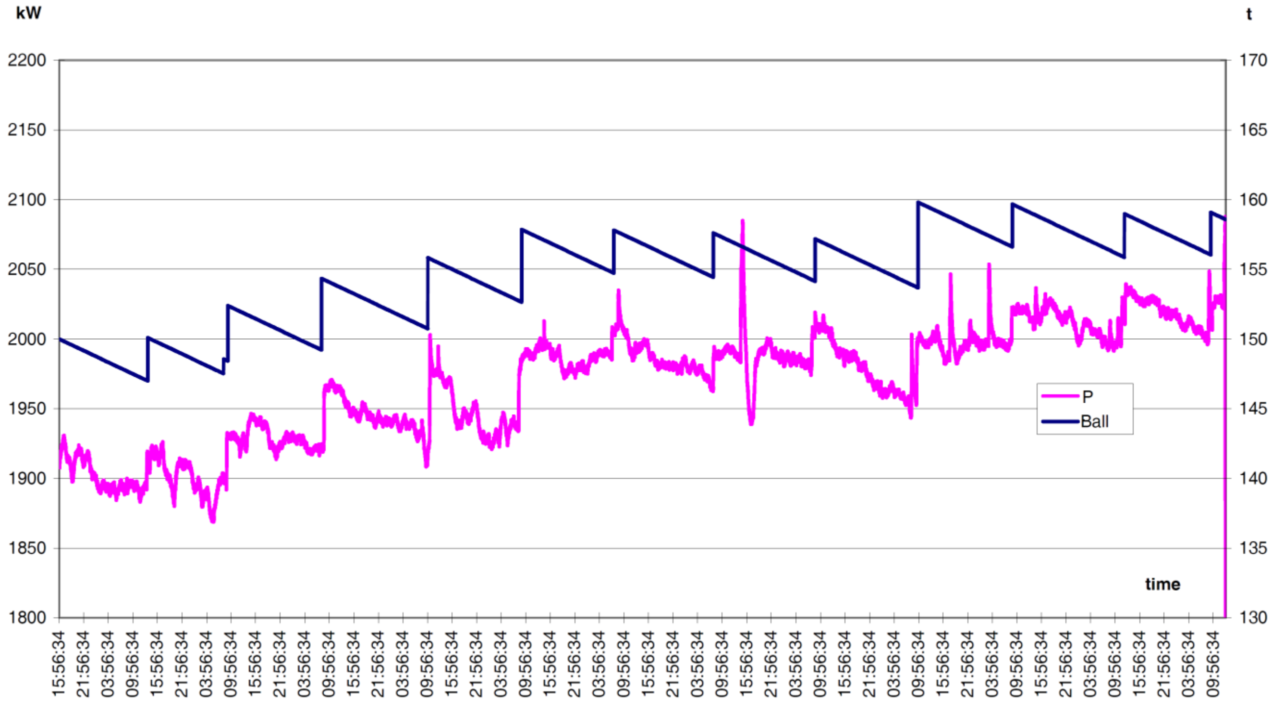

Fig. 2. Dependence of the active power consumed by the engine on the amount of ball load in the mill

Evidently, the perceived criteria for controlling ball dosage machines, namely the stator currant of synchronised electric motor averaged over a 30-minute interval, is not the most appropriate solution. In this sense, the stator current is not a unique criterion for loading the mill with balls or ore. The unique criterion for loading is the active power, consumed by the synchronised electric motor.

It is proposed that the control over the ball loading machines is to be provided when active power is monitored. In small intervals (the smaller the better) the active power is compared with the one that is set. The ball loading machine is turned on and loads the mill with portion of balls only if the ball load is in the left part of the extremum (3) of the curve, shown in graph 1. In approximately even load of ore this mode of control of the ball load, the work of the mill is ensured with optimal ball load (around the extremum in the curve in Graph 1) and will also decrease the power consumption.

The curves of active power and the ball load when starting the M4 mill after changing the lining are displayed in Fig. 3.

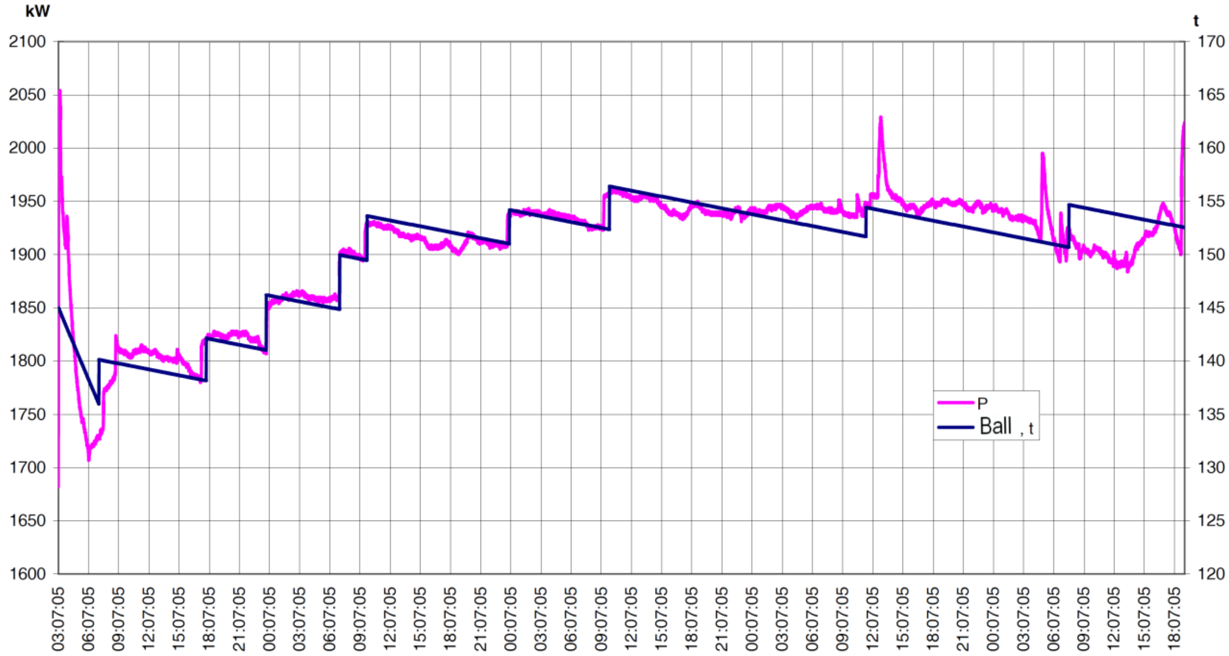

Fig. 3. Dependence of the active power consumed by the engine on the amount of ball load in the mill after changing the lining

At first there are rapid reduction engine's active power drop awey as a result of the filling of the lining of the mill with balls. The short intervals can also be seen during loading the ball load in the beginning in order to increase the effective balls involved in grinding. A period of set ball load is followed, around 155 tonnes (accepted 4514 in m^3 – Minin and other, 2014). After the last shown load of balls it is obvious that the ball load has exceeded the optimal (point (3) in Graph 1) and lower power can be seen. Because of the proximity of the centre of gravity towards the axis of the drum, the mill does not reduce the active power, and the balls go into mixed speed mode with partial rewind and partial flight of the grinding bodies.

Afterwards due to the wearing out of the balls the circuit gradually increases. From this experiment the optimal ball load and the relevant active power can be determined. For mill unit M4, which is with new lining, the optimal ball load is 155 tonnes and the corresponding active power is 1950 kW.

Such dependence with expressed extreme exist and between the power from the electric motor and the quantity ore with consistent ball load.

The hourly load of the ore mill and the average hourly power with constant ball load are compared on Fig. 4. The fact registered by previous measurements is also confirmed - that with the increase of the load of the mill, the power drawn by the electric motor decreases. This shows that for the duration of measurements the working mode of the mill is after the extremum of the function P= F(Gсм), which means that the ball load is optimal or exceeds the optimum.

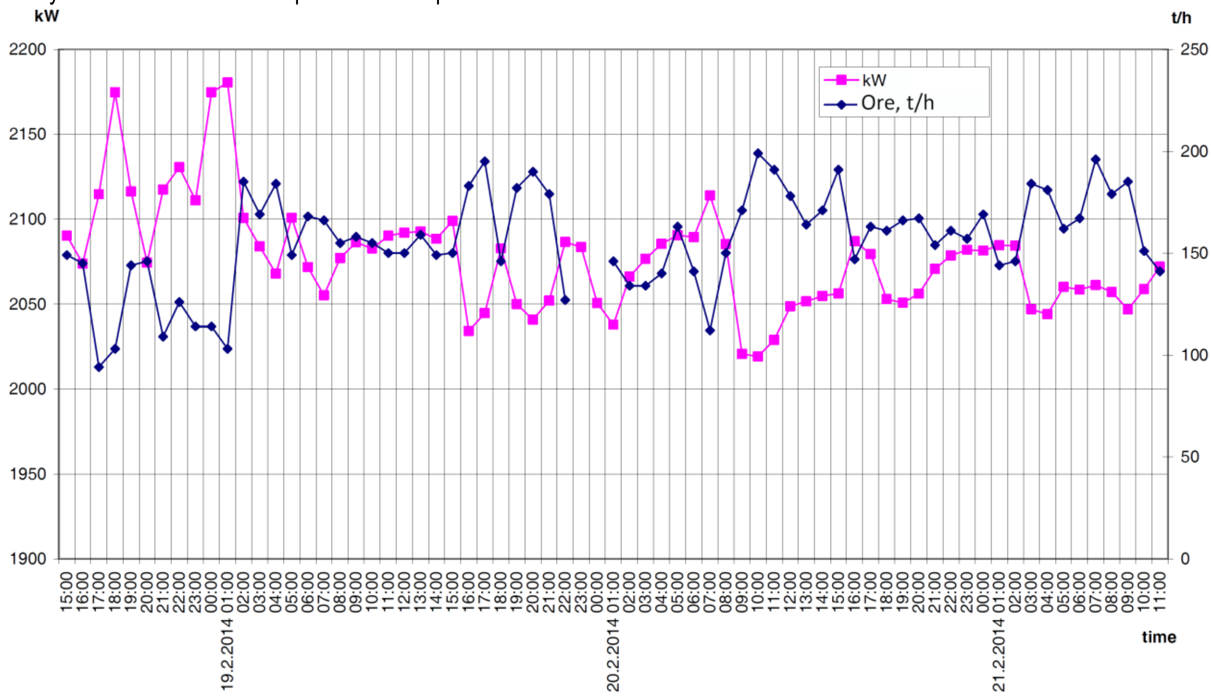

Fig. 4. Dependence between the exhausted active power and ore load

In order to analyse the influence of the ball load, the specific expense of electricity data has been processed in a period of 3 months across 5 mills. The end results are shown in Table 1.

Table 1.

Mill/ type balls	Monthly consumption of balls, t			Measurements 2013, bucket			Total balls	Ore from line	Ore	Produc-tivity	Time worked	Ball consum-ption	Energy	Average special cost	Hour power
	IV	V	VI	IV	V	VI	t	t	t	t/h	h	t/h	kWh	kWh/t	kWh
3 - steel	150	143	133	6	4	5	426	59000	220923	124.3	1777	0.2398	3357333	15.2	1889
4 - steel	141	138	143	11	4	9	422	69806	283141	148.6	1905	0.2215	3812398	13.5	2001
5 - steel	138	153	140	5	12	0	431	29817	219571	114.6	1915	0.2250	3744141	17.1	1955
6 - BU	114	123	136	0	6	4	373	46636	230906	127.7	1808	0.2063	3380748	14.6	1870
7 - BU	124	152	125	0	5	0	401	78940	288367	158.7	1818	0.2206	3521223	12.2	1937

The calculated average values of the specific electricity consumption based on the three month period confirm completely the results calculated during determining the energy performance. The lowest specific cost can be observed in mill №7, followed by №4. Mill №5 has the worst energy performance.

For the whole three-month period, a single ball measurement was performed at mill №7, with 31.5 % filling with balls, or 125 t balls (when 4650/m³). For the period between 1st of April and 15th of May the consumption was between 200t balls and approximately the same amount also was added, which means that the mill for the period worked with 31.5% filling with grinding bodies. 20 tonnes were added, which means that the filling became 36.8%. The average specific cost for electricity during the three-month period is 12.2 kWh/t. Mill №7 has the biggest productivity (158.7 t/h) compared to the rest.

For the month of April four control measurements were conducted for mill №4, during which the mill was with fulfilment 35,9; 35,6; 35,9 and 37,4 % (between 141 and 148 t). The second place in terms of good energy consumption was mill №4 which also worked with a fill factor of less than the optimal 38%. For the period the specific power consumption was 13.5 kWh/t at an average output of 148.6 t/h.

Based on the above described dependence of the extracted power on the size of the ball load, it can be assumed that for the studied period, grinder №4 has the optimum ball load, since it has the highest hourly output (2001 kWh) and very good energy indicators.

Mill №5 is with the worst energy performance on 10th of April, on 12th of May control measurements were conducted on the ball load. The filling of the mill with grinding bodies was 35% (140 t) and 12t were added. In both cases a 38% fill is maintained with the added balls. For the tested period specific energy consumption of 17.1 kWh/t was recorded and the production rate was 114.6 t/h.

The comparison of the energy consumption of mill 5 and the maintained ball load allows the assumption that mill №5 worked with an excess of ball load during the testing.

Fig. 5 shows a comparison between the average power per hour and the specific power consumption during the hourly ball consumption.

Based on the analysis of the results the following assumptions can be made:

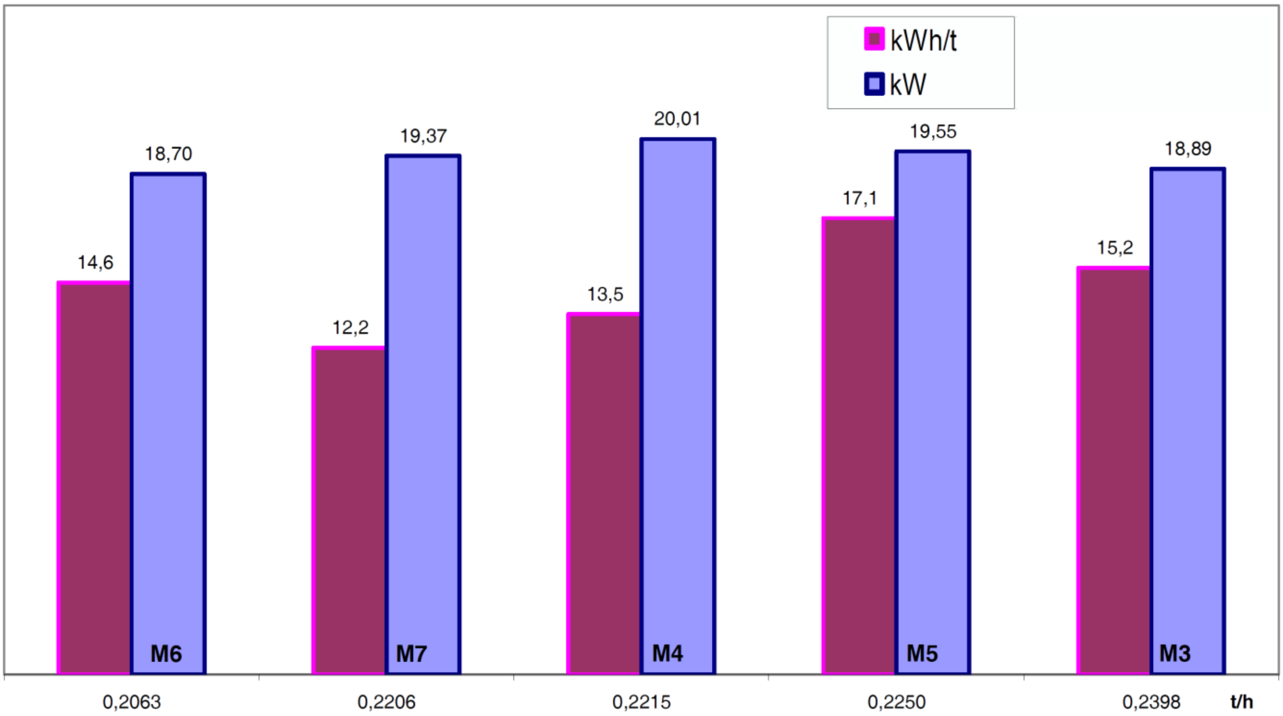

Fig. 5. Dependence between the specific consumption and hourly power of the balls consumption

1. Mill №7 worked very fast with optimal ball load and minimal ball load shortage.
2. Mill №6 worked with significant ball shortage. On 15th of May a control measurement was conducted on the balls in mill №6. The results showed the following: diameter 430 cm and height of the balls – 290 cm. This corresponds to 28,3 % filling or 114 t balls. This gives reason to assume that mill №6 has worked with an insufficiently balanced circulating load which, at roughly the same hourly working time, has led to nearly 20% lower production than mill №7 and increased the specific power consumption by 2,4 kWh/t.
3. Mill №5 has worked with an excess of ball load, average hourly power decreases due to the displacement of the centre of gravity of the grinding medium relative to the axis of rotation, the degree of equilibration of the circulation load is disturbed due to a decrease in kinetic energy. This has led to reduced productivity and increased specific electricity consumption.
4. Mill №3 like mill №5 worked with an excess of ball load and bad electric measurements. The measurements conducted in mill №3 on 29th of April and on 15th of May led to additional 24 t of balls on the first day with which the percentage and the fill rate was 37,1% and 16 t by the second day, which led to an increase of 37,6%.

The conducted analysis on the influence of the ball load of the energy parameters of the milling aggregates gives reason to conclude that in order to achieve good energy indicators, a research to optimise the ball load is needed. In this sense, we believe that the aove-mentioned experiment proposed by us will lead to significant positive results.

From the table above it can also be seen that the consumption of ball load of the type BU is lower than the oneused in type "Steel" with average 0,0153 t/h.

Conclusion

The results from the conducted experiments give reason to make the following conclusions.

- The drawn active power of the ball mill electric motor is not a unique indicator of the mill load;
- In the continuous operation of the mill, the balls in it are worn out and their quantity is reduced. As a result, the electricity consumption and mill performance are altered;
- The wear of the balls is a reduction of the diameter and shape under the abrasion of the ground ore. As a result of this process, the balls in the mill are of different size and the grain size of the ball filling greatly affects the work of the mill;
- The size the grinding bodies directly affects the power consumption of the mill's motor. With the change in the structure of the ball filling, the centre of gravity of the grinding medium, and respectively, the resistance moment, which must overcome the electric motor, also change.

References

Minin, I., I. Savov, T. Hristova. 2014. Determining the influence of size of steel balls on the spending power of engine drum ball mills at a constant duty cycle. – *Geologia i mineralni resursi,* 6, 30–32 (in Bulgarian with English abstract).

THE APPLICATION OF SEARCH METHODS FOR SOLVING OPTIMISATION PROBLEMS IN GEODESY

Nadezhda N. Eliseeva, Andrey V. Zubov

Saint Petersburg Mining University, 199106 Saint Petersburg; nadezhda.eliseeva.1994@mail.ru; zaw@spmi.ru

ABSTRACT. As a rule, excessive data is used to solve any problem in practice. When it happens, the problem has several solutions (or, in some cases, a possibly infinite number thereof). As a result, a problem arises of how to optimise the solution process.
The purpose of the optimisation problem is to find a solution in accordance with any objective function (such as the criterion of efficiency or quality). Most practical problems are nonlinear in nature, i.e. the objective function and /or the connections between the parameters are nonlinear. The following algorithms of search optimisation have been developed for solving optimisation nonlinear problems: genetic algorithms, the method of simple search with a variable step size, the parabolic optimisation method. The paper describes the results of running search algorithms in Visual Basic for Applications (VBA) for solving optimisation problems in geodesy.
Search methods are very effective in solving optimisation nonlinear problems due to their advantages:
- a great variety of mathematical algorithms which have already been developed;
- the possibility of combining these algorithms with each other and with other methods of nonlinear programming;
- ease of programming;
- independence from the accuracy of the preliminary values of the parameters defined;
- there is no need to formulate error-correction equations or constraint equations or use a system of normal equations and solve them.

Search methods are convenient in programming and a large number of already existing methods along with the development of new search algorithms makes it possible to adapt them to solving any problems. This article discusses the possibility of using search methods in solving optimization nonlinear geodetic problems using the example of approximation of the results of measurements of a circle. To significantly speed up the search process, the algorithm for determining the minimum parabola is considered.

Keywords*:* optimisation; convex programming; search methods; parabolic optimisation

РЕШАВАНЕ НА ОПТИМИЗАЦИОННИ ЗАДАЧИ В ГЕОДЕЗИЯТА ЧРЕЗ МЕТОДИ НА ТЪРСЕНЕТО

Надежда Н. Елисеева, Андрей В. Зубов

Санктпетербургски минен университет, 199106 Санкт Петербург

РЕЗЮМЕ. Обикновено решаването на практическите задачи се извършва в условията на излишък от данни. Когато това се случи, задачата има няколко решения, (а в някои случаите са безкрайно много на брой). В резултат на това възниква въпросът как да се оптимизира процеса на търсене на решение. Целта на оптимизацията е да се намери решение в съответствие с всяка целева функция (като критерия за ефективност или качество). Повечето практически оптимизационни задачи са нелинейни по своята същност, т.е. целевата функция и/или връзките между параметрите са нелинейни. Разработени са множество алгоритми за търсенето на оптимално решение при нелинейни оптимизационни задачи: генетични алгоритми, метод на просто търсене с променлив размер на стъпката, метод за параболична оптимизация. В статията са описани резултатите от работа с алгоритми за търсене, реализирани във Visual Basic for Applications (VBA) за решаване на оптимизационни задачи в геодезията. Методите за търсене са много ефективни при решаване на нелинейни задачи за оптимизация поради следните предимства:
- голямо разнообразие от математически алгоритми, които вече са разработени;
- възможността за комбиниране на тези алгоритми помежду им и с други методи на нелинейно програмиране;
- лесни за програмна реализация;
- независимост на точността от предварителните стойности на параметрите;
- не е необходимо да се формулират уравнения за корекция на грешки или уравнения на ограниченията или да се използва система от нормални уравнения, които да се решават.

Методите за търсене са удобни за използване, а големият брой вече съществуващи методи, заедно с разработването на нови алгоритми за търсене, дават възможност за адаптирането им към решаване на всякакви проблеми. В тази статия се разглежда възможността за използване на методи за търсене при решаване на оптимизационни нелинейни геодезически задачи, използвайки примера на апроксимацияна резултатите от измерванията на окръжност. За значително ускоряване на процеса на търсене се разглежда алгоритъм за минимизация по парабола.

Ключови думи: оптимизация; изпъкнало програмиране; методи на търсене; оптимизация по парабола

Introduction

Modern measuring tools allow to get a lot of information about an object, for example, when scanning millions of points. Due to the overabundance of data, the required parameters can be obtained many times (many solutions). Optimisation is understood as the process of choosing the best solution of the problem from all possible (Turchak L.I., 1987). Currently, optimisation problems arise in various fields of scientific and industrial activity. The purpose of optimisation is to find a solution in accordance with any objective function (criterion of efficiency, quality, accuracy, reliability, etc.).

Among non-linear optimisation of surveying and geodetic applications, we can mention:
- strain prediction;
- finding communication parameters between different coordinate systems;
- reconciliation of non-linear engineering structures;
- combining digital images;
- equalisation of planned and spatial networks, etc.

The methods of solving optimisation problems are quite diverse and have a branched classification (Kuznetsov A.V., 1994). At present, there is a possibility for widespread implementation of search methods for solving such problems. These methods are very effective because of their advantages, including:
- wide variety of already developed mathematical algorithms;
- possibility of combining these algorithms with each other and with other methods of nonlinear programming;
- easy software implementation;
- independence from the accuracy of the preliminary values of the determined values (you can take values that are far from true, and the decision process is not violated);
- need to create an equation of the amendments or the equation of the relationship, to move to a system of normal equations and solve them;
- there is no need even for the first analogue derivatives in the linearisation of the calculation process.

Development of a method of optimisation of a parabola

In the previous publication on this topic (Zubov A.V., Eliseeva N.N., 2017) the algorithm of the simplest search with variable step is considered. It consists of a sequential multiple calculation of the objective function and each time one or more variables are changed in one direction or another until its minimum is reached.

The algorithm was used to solve the problem of approximation of measurements of a circle (Zubov A.V., Eliseeva N.N., 2017), and the following results are obtained: $x = 100.036\ m$, $y = 10.488\,m$, $r = 1.674\,m$, $f_{end} = 0.012436$, $n = 224$ (x, y - the coordinates of the centre of the circle, r - circle radius, f_{end} - the final value of the objective function $[VV] = \min$, n - the number of cycles required to solve the problem).

The answers were tested in MathCAD, the difference of the results did not exceed 0.5 mm (Zubov A.V., Eliseeva N.N., 2017). Thus, the correctness of the algorithm of simple search and the reliability of the results of calculations are confirmed.

The main disadvantage of this method is the large number of iterations. This article describes an algorithm for significantly accelerating the search engine optimisation method, especially at the initial stage of approximation.

Figure 1 shows a graph of the change of the function $[VV]$ from the argument x in some area. It is seen that this is a parabola, i.e. a graph of convex quadratic functions of the form (1):

$$y = a \cdot x^2 + b \cdot x + c, \tag{1}$$

where x, y - are variables; a, b, c - are given numbers $(a \neq 0)$.

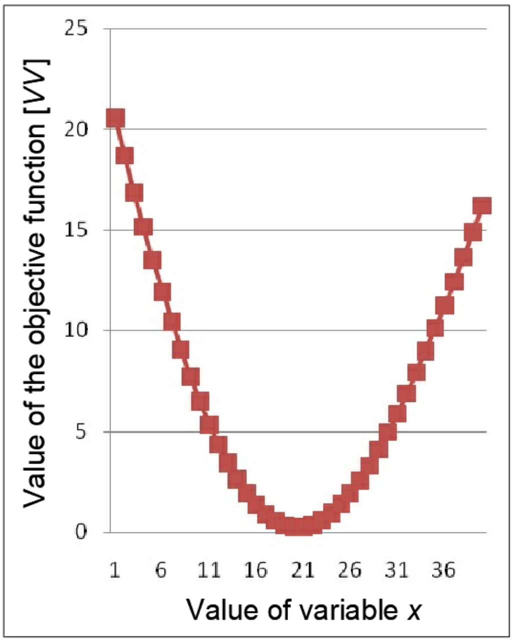

Fig. 1. Graph of the target function change from the variable *x*

The following theory is proposed: it is possible to get to the minimum of the objective function in one «global step» by constructing optimisation parabolas for each variable.

Let's check this theory with the example of an already considered problem of approximation of results of measurements of a circle. In determining the method of the least squares coordinates of the circle's centre (x and y) and its radius r on the coordinates of the points measured on the circle (x_i and y_i), the objective function has the form (2):

$$F(x, y, r) = \sum_{i=1}^{n}\left[\sqrt{(x_i - x)^2 + (y_i - y)^2} - r\right]^2 = \min. \tag{2}$$

Any function of linear or nonlinear form can be taken as a target function, for example, the sum of the squares of the corrections to the measurement results $[V^2] = \min$ or the sum of the correction modules $[|V|] = \min$. It is important that it is a reliable criterion of efficiency in solving the optimisation problem.

Let's set the initial value of the parameter x_0 and a small enough step to change this parameter k. Arguments y and r remain unchanged. Calculate three values of the objective function $F(x_{-1}, y, r)$, $F(x_0, y, r)$, $F(x_{+1}, y, r)$ for the arguments $x_{-1} = x_0 - k$, x_0 and $x_{+1} = x_0 + k$. The optimisation parabola for the parameter x is shown in Figure 2.

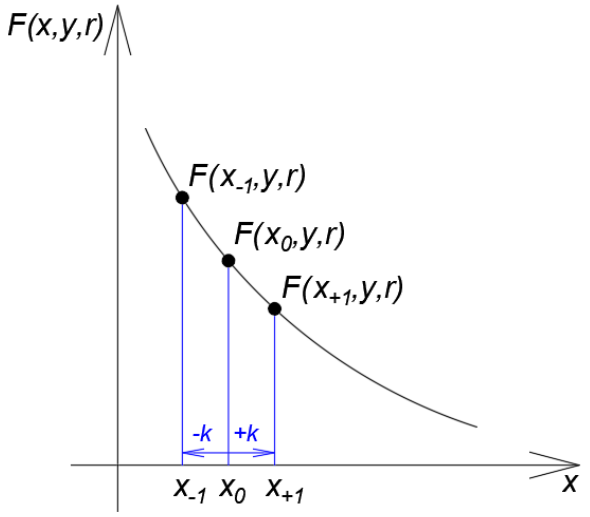

Fig. 2. Fragment optimisation of the parabola for *x*

The conclusion of the «global step» will begin with the compilation of a system of three equations:

$$\begin{cases} a \cdot x_{-1}^{\ 2} + b \cdot x_{-1} + c = F_{-1}; \\ a \cdot x_{0}^{\ 2} + b \cdot x_{0} + c = F_{0}; \\ a \cdot x_{+1}^{\ 2} + b \cdot x_{+1} + c = F_{+1}. \end{cases}$$

Write down the determinants:

$$\Delta = \begin{vmatrix} x_{-1}^{\ 2} & x_{-1} & 1 \\ x_{0}^{\ 2} & x_{0} & 1 \\ x_{+1}^{\ 2} & x_{+1} & 1 \end{vmatrix}, \qquad \Delta_1 = \begin{vmatrix} F_{-1} & x_{-1} & 1 \\ F_{0} & x_{0} & 1 \\ F_{+1} & x_{+1} & 1 \end{vmatrix},$$

$$\Delta_2 = \begin{vmatrix} x_{-1}^{\ 2} & F_{-1} & 1 \\ x_{0}^{\ 2} & F_{0} & 1 \\ x_{+1}^{\ 2} & F_{+1} & 1 \end{vmatrix},$$

$$a = \frac{\Delta_1}{\Delta}, \qquad b = \frac{\Delta_2}{\Delta}.$$

The minimum of the parabola is determined by the derivative (3), equating it to zero:

$$F'(x) = \lim_{\Delta x \to 0} \frac{\Delta F}{\Delta x} = 2 \cdot a \cdot X_{optimal} + b = 0, \tag{3}$$

where $X_{optimal}$ - value of the parameter x, which falls within the region of the parabola minimum.

From the last equation follows (4):

$$X_{optimal} = -\frac{b}{2 \cdot a} = -\frac{\Delta_2 \cdot \Delta}{\Delta \cdot 2 \cdot \Delta_1} = -\frac{\Delta_2}{2 \cdot \Delta_1}. \tag{4}$$

We introduce the value of h and write down the equation (5):

$$x_0 + h = X_{optimal}, \tag{5}$$

where h - the "big" (or "global") step for parameter x.

Thus, on the basis of equations (4) and (5) after the transformations, the formula for calculating the «global» step is derived (6):

$$h = \frac{k \cdot (F_{-1} - F_{+1})}{2 \cdot (F_{-1} - 2 \cdot F_0 + F_{+1})}. \tag{6}$$

Then "global" steps for other variables are calculated. Figure 3 shows the parabola of the optimisation parameter x.

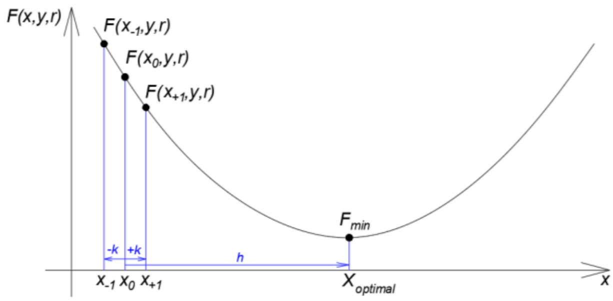

Fig. 3. Optimisation parabola in the parameter *x*

The developed algorithm was implemented in the Visual Basic for Applications programme and was called «Optimisation parabola method».

Thus, acting on the principle «from simple to complex», the transition from the method of simple search with a variable step to the method of optimisation parabola was made. The results obtained did not differ from those obtained by other methods, while the developed algorithm is not final and requires detailed study of other more complex practical problems. However, even at the initial stage, the main advantage of the optimisation parabola method is revealed, namely, the approximation to the minimum of the objective function for the first approximation.

Therefore, the developed method can be used at the initial stage of solving optimisation problems, namely to determine the minimum area of the objective function. Table 1 shows the results of solving the problem of approximating the circle by different methods. This algorithm can be used to create a programme for determining the roll of chimneys and cylindrical copra, when reconciling rotary kilns, etc.

Table 1. *Results of solving the problem of approximation by a circle*

The solution method of the optimisation of the parabola			The solution by the method of simple search with variable step	Solution in MathCAD using the Minimise function
Initial parameter values	The parameter values of the **first approximation**	Final parameter values		
$x_0 = 50\,m$	$x = 99.260\,m$	$x = 100.036\,m$	$x = 100.036\,m$	$x = 100.036\,m$
$y_0 = 5\ m$	$y = 10.562\ m$	$y = 10.489\,m$	$y = 10.488\,m$	$y = 10.489\,m$
$r_0 = 1\ m$	$r = 1.803\ m$	$r = 1.674\ m$	$r = 1.674\ m$	$r = 1.674\ m$
		The final value of the objective function		
		$f = 0.01243$	$f = 0.01244$	$f = 0.01243$

Conclusion

The optimisation parabola method can be applied to solve a wide range of nonlinear surveying problems.

The use of search methods is not limited to the implementation of existing algorithms. Round non-linear surveying and geodetic tasks are quite broad. Production tasks are not of the same type and sometimes they are even unique. Therefore, it is not always possible to solve them «by templates» by traditional methods. In turn, search methods are more convenient for software implementation, and a large number of existing and the development of new search algorithms can adapt them to solve any problems.

References

Kuznetsov, A. V., V. Sakovich, N. Kholodyu. 1994. *Vysshaya matematika: Matematicheskoye programmirovaniye.* Vysshaya shkola, Misk, 286 p. (in Russian)

Turchak, L. I. 1987. *Osnovy chislennykh metodov.* Nauka, Moscow, 320 p. (in Russian)

Zubov, A. V., N. Eliseeva. 2017. Resheniye marksheydersko-geodezicheskikh zadach poiskovymi metodami. – *Marksheyderskiy vestnik, 5,* 35–38 (in Russian).

TECHNOLOGICAL ASPECTS AND APPLICATIONS OF LARGE POWER SWITCHED RELUCTANCE MOTORS IN MINING

***Yassen Gorbounov*[1], *Hao Chen*[2]**

[1] *University of Mining and Geology "St. Ivan Rilski", 1700 Sofia; y.gorbounov@mgu.bg*
[2] *China University of Mining and Technology; hchen@cumt.edu.cn*

ABSTRACT. The switched reluctance motors (SRM) are known from about the beginning of the 19th century. They are in fact amongst the first rotating electrical machines ever, firstly called electromagnetic engines. Being synchronous salient poles motors they have very simple construction but are difficult to control due to the highly nonlinear magnetic circuit. With the fast development of the power electronics and the computational abilities of the nowadays microcontrollers and field programmable gate arrays SRMs has gained growing popularity especially in fields like the mining industry. This is possible due to their ability to work in heavily polluted and harsh environments and their fault-tolerant operation and control. In the paper the technological aspects of the SRMs are introduced and some typical applications of large power switched reluctance motors in mining are pointed out.

Keywords: switched reluctance motors, electrical drives, nonlinear magnetic circuit, mining, fault tolerant control

ТЕХНОЛОГИЧНИ АСПЕКТИ И ПРИЛОЖЕНИЕ НА МОЩНИТЕ ПРЕВКЛЮЧВАЕМИ РЕАКТИВНИ ЕЛЕКТРОДВИГАТЕЛИ В МИННАТА ПРОМИШЛЕНОСТ

***Ясен Горбунов*[1], *Хао Чен*[2]**
[1] *Минно-геоложки университет "Св. Иван Рилски", 1700 София; y.gorbounov@mgu.bg*
[2] *China University of Mining and Technology; hchen@cumt.edu.cn*

РЕЗЮМЕ. Превключваемите реактивни двигатели (ПРД) са известни още от началото на 19-ти век. Всъщност те са сред първите въртящи се електрически машини изобщо, наричани първоначално електромагнитни двигатели. Като синхронни двигатели с явнополюсна структура те имат много проста конструкция, но са трудни за управление поради силно нелинейната си магнитна верига. С развитието на силовата електроника и изчислителните възможности на днешните микроконтролери и програмируеми логически схеми, популярността на ПРД силно нараства, особено в области като минната индустрия. Това става възможно благодарение на тяхната способност да работят в силно замърсени и тежки среди и тяхната отказоустойчива работа и управление. В статията са представени технологичните аспекти на ПРД и са показани някои типични приложения на превключваемите реактивни двигатели с голяма мощност в минното дело.

Ключови думи: превключваеми реактивни двигатели, електрозадвижване, нелинейна магнитна верига, минно дело, отказоустойчива работа

Introduction

The Switched Reluctance Motors (SRM) are one of the earliest rotating electric machines ever. Their origins lie in the Sturgeon's electromagnet (Sturgeon, 1825) and they were initially called electromagnetic engines (Miller 1993). They were originally used in locomotive drives but due to their poor performance and the lack of proper electronic control at that time they lost popularity for almost 100 years. With the fast development of the power electronics switches, the computational abilities of the nowadays microcontrollers (MCU) and the field programmable gate arrays (FPGA) SRMs popularity, especially in fields like the mining industry, is continuously growing.

The SRM technology development worldwide, in both practical and theoretical terms, can be seen from the number of patents received and the number of publications over the years. In 1972 Burnice Bedford received 2 patents. According to Fleadh Electronics (Watkins, 2016) 67 patents were published before 1976 and over 1775 patents were published until 1999. The articles on this topic were 11 before 1976 and over 1847 until 1999. According to official data of the United States Patent and Trademark Office (USPTO 2013), patent applications filed for the period 1980-2010 were a total of 5936. The data presented clearly show the increasing interest in SRM technology and its augmented applicability in practice.

The major distinctive property of the SRM is the strong non-linearity of the magnetic circuit, which predetermines the difficulties in their modelling and control. This problem leads to increased torque ripples and to higher acoustic noise as a consequence. Although their manufacturing is greatly facilitated due to the full absence of rotor windings and mechanical commutator, and also the lack of impregnating resins for the coils, the requirements for mechanical precision are significantly higher than for most other types of electric motors. A higher computational speed is required that often poses a demand for the implementation of parallel algorithms that can be performed in real time. On the other hand, the construction simplicity, the lack of collector sparking, the large power and the extremely increased fault tolerance in terms of both operation and control, makes SRMs more and more popular in heavily polluted and harsh environments such as in mining.

Principle of operation

The switched reluctance motor has a simple salient pole construction with a passive rotor. Both the rotor and the stator armature are made of laminated steel. The windings are located at the poles of the yoke. For each phase, they are located at opposite poles and are coupled in pairs to form the phase sections of the inductor. Furthermore, the windings are connected so that the total magnetic flux is increased. The motor is called "switched" because it commutates the poles with a common magnetic flux of the stator compared to those of the rotor. It is called "reluctance" because of the tendency of the rotor to move to a position with less reluctance, i.e. minimal magnetic resistance. There is no current flowing into the rotor.

In order to produce a starting torque it is necessary the rotor teeth to be displaced with regard to the stator teeth, i.e. to be in an unaligned position. That is why, the rotor poles are generally less in number than those of the stator (DiRenzo, 2000; Wach, 2011). The control signal is not a sine-wave voltage, it consists of current pulses fed in a certain sequence, for which the current direction is irrelevant. The aftereffect of this is the reduced hysteresis loss.

The most common SRM types are shown in Fig. 1.

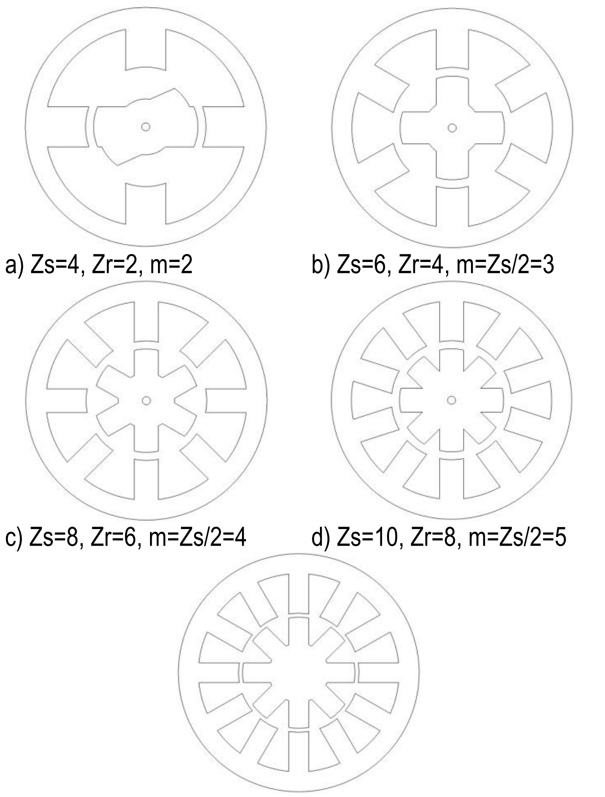

Fig. 1. Basic stator-rotor configuration of the SRM

The main characteristic is the combination of stator poles - *Zs* and rotor poles - *Zr*. The number of phases *m* is equal to the number of stator teeth *Zs* divided by the pairs of poles *2p*. When the number of pairs of poles 2p = 1, the number of phases is 2 because the diametrically opposed teeth of the stator are simultaneously excited by the same current when the windings are connected in series. For the most common SRM 2p = Zs-Zr. The angular distance between the closest stator and rotor poles (from the unaligned to the aligned position) is given by the expression (1).

$$\varepsilon = \frac{2.\pi}{p} = \left(\frac{1}{Z_r} - \frac{1}{Z_S} \right) = \frac{2.\pi}{p} \frac{2.p}{Z_S.Z_r} = \frac{2.\pi}{m.Z_r} \qquad (1)$$

This is the angle by which one phase can be excited. For SRM6-4 this angle is ε=30°, for the SRM8-6 it is ε=15° and it is the same for the SRM12-8, etc.

Although SR motors with 72-48 poles configuration (Elhomdy et al., 2018) exist, the most common large power motor configuration is of type 12-8. The greater the number of poles, the higher the switching frequency, and the more the torque ripples are smoothed but the losses in the steel are greater. At the same time, the mechanical design of the motor and the control electronics become more complicated. Increasing the number of teeth per pole results in an increase in output power (Finch et al., 1984; Qishan et al., 1988) which results in a reduction in the rotational period in which the transformation of energy takes place. For the classical SRM, each stator pole consists of only one tooth. The doubling of the number of teeth can be achieved without substantially reducing the maximum inductance at the aligned position of the rotor and stator teeth. In this way the motoring torque can be almost doubled by using two teeth per one stator pole. Increasing the number of teeth requires a proportional increase in sensor resolution. An increased count of pole teeth is used in the Vernier Reluctance Motors (Harris et al., 1982) where the three-phase coils are mounted on a salient pole stator. For this type of motors the control voltage is sinusoidal and the energising of all of the phases is done simultaneously. At least two phases are required to ensure starting of rotation, whereas at least three phases are required to ensure a desired starting direction. A number of methods exist for reducing the torque ripples which are divided into two groups, namely by control parameters adjustment and by changing the geometry of the poles. The first method is generally preferred as it is the most flexible – for example, phase overlay or phase current profiling can be done. In SRM drives the average torque and the torque ripples are affected by the turn-on and turn-off angles. The SRM torque characteristic can be optimised by applying appropriated pre-calculated turn-on and turn-off angles in function of the motor current and speed.

The mechanical characteristic of the SRM is shown in Fig. 2. It is hyperbolic in nature and is very similar to that of the serially excited DC motor (DiRenzo, 2000; Wach, 2011).

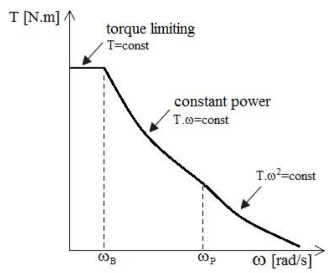

Fig. 2. Mechanical characteristic of the SRM

The torque production in the SRM is dependent on the change of the stored magnetic energy in the phase winding as a function of the rotor position. The maximal torque is related to the maximal current flowing through the winding of the machine. The speed ω is limited by the supply voltage. The speed may be increased over its nominal value but at the expense of the torque reduction.

The instantaneous power equation of the SRM is (2).

$$\begin{aligned} U.I &= R.I^2 + I.\frac{d\Psi}{dt} = \\ &= R.I^2 + L(I,\theta).I.\frac{dI}{dt} + I^2.\frac{dL(I,\theta)}{dt} \end{aligned} \quad (2)$$

The left side in the equation represents the instantaneous electric power delivered to the motor. The first term on the right side reflects the active losses. The second term on the right side of the equation includes the sum of the mechanical power and the power that is stored in the magnetic field.

Sometimes it is more appropriate for the torque to be expressed by the magnetic flux, and sometimes by the current through the windings. For this reason in the literature (Balazovic, 2002; Pavlitov, 2005) it is often considered the energy of the magnetic field Wf (3) and the co-energy Wc (4).

$$W_f = \int_0^{\Phi} I(\theta, \Phi).d\Phi \quad (3)$$

$$W_m \equiv W_c = \int_0^{i} \Phi(\theta, I).dI \quad (4)$$

The graphical representation is given in Fig. 3.

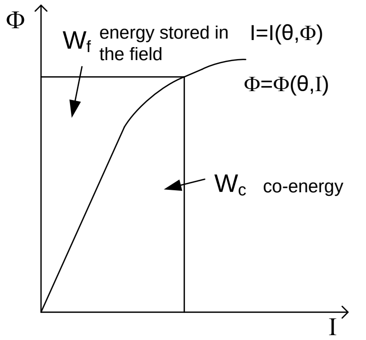

Fig. 3. Graphical interpretation of the energy and co-energy of the magnetic field

In the absence of magnetic saturation the curve will be a straight line and then at any angle the co-energy and the stored magnetic energy will be equal. It can be easily seen that the inductance is highly nonlinear and depends on both the position of the rotor and of the current through the stator. This is due to the salient pole structure of the SRM and the saturation effects. For the same reason the magnetic flux is also dependent on the position of the rotor and the current through the winding.

Several inverter topologies are suitable for driving the SRM (Miller, 1993; Miller, 2001; Ellabban et al., 2014; Murthy et al., 2014). The most appropriate one that is convenient for large power motors like the ones used in mining is shown in Fig. 4. A single phase is shown for clarity but it is being expanded over all phases depending on the exact SRM motor type.

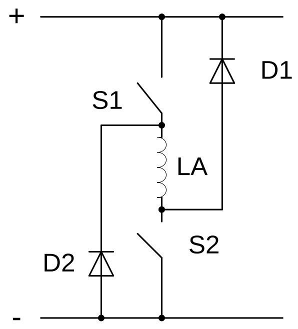

Fig. 4. Single phase part of the asymmetric bridge

As the torque is independent on the current polarity, the inverter needs to contain at least one power switch per phase. This is in contrast with the induction motor that requires at least two power switches. Moreover, the coils of the asynchronous motor are not serially connected to the switches, which can lead to irreparable short circuit faults. In the SRM the winding is always connected in series with the switch. That means that no shoot-though is possible and no dead-time is needed thus making it possible to increase the commutation frequency. In addition, the phases are independent of each other, which is why, even with reduced power, a continuous operation is feasible in a case of one or more disconnected or faulty phases. The mutual inductance between the phases is negligible, which makes phase commutation completely independent but also requires some measures to be taken to dissipate the stored magnetic energy. This is done with the diodes D1 and D2 in the figure. An exhaustive classification and a more detailed analysis of the power inverters for SR motors is given in (Krishnan, 2001).

Modelling and control

Due to the highly nonlinear profile of the stator inductance the mathematical modelling of SR motors is a tough task. A typical inductance profile as a function of the stator current is shown in Fig. 5 a) while the dependence of the normalised inductance as a function of the rotor position is shown in Fig. 5 b). for the sake of simplicity the numerical values are omitted.

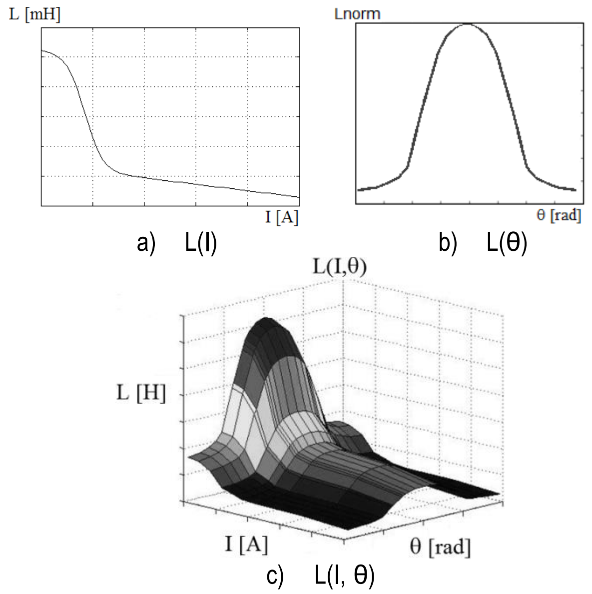

Fig. 5. Stator inductance as a function of two variables

Fig. 5 c) represents the inductance profile as a function of the two variables. In fact the actual inductance depends also on the temperature of the copper coil but in most of the cases this effect is negligible.

The precise mathematical description plays a crucial role for the effectiveness of the control because it permits to determine the right turn-on and turn-off angles for the phase switching and thus to achieve optimal control in terms of speed, torque ripples reduction and efficiency. Many methods exist for solving this task. The mathematical products such as Matlab (Chen, 2001, Ramasamy, 2005, Chen, 2009), Mathcad (Staudt, 2015, Stoyanov, 2016; 2017), Ansys Maxwell (Karim, 2016), Modelica (Bals, 2011) and PC-SRD (Miller 1990) are often used. The mathematical methods can be categorised into two major categories namely numerical methods and analytical methods. The mathematical modelling of non-linearity is most often based on the Finite Element Method (FEM) (Ohyama, 2006; Srinivas, 2005), which is a numerical method for finding approximate solutions for partial differential equations and requires great computational power. This is a very accurate method for static and dynamic modelling, but it is quite complex and time-consuming. Numerical methods are related in general with some difficulties in the implementation of the control algorithms. They also demand knowledge of the physical dimensions and the material of the motor. On the other hand, the analytical methods can be subdivided into:

- linear methods – they usually do not consider the edge and saturation effects and therefore the inductance curve cannot be expressed as a function of the current;
- quasi-linear methods – they represent a piecewise linearization of the magnetic curves in aligned position of the rotor and stator poles;
- nonlinear methods – they include various mathematical approaches for modelling the nonlinearities and are very perspective. At first, there is the Fourier decomposition (Hur 2003) which is made possible because the shape of the inductance is a periodic function and therefore it can be expressed as an endless sum of sinusoids. A fully dynamic model can be build using the Flux lookup table method (Torrey et al., 1995) and the intelligent approach of the Artificial Neural Networks (ANN) (Pavlitov et al., 2009). The last method is an innovative one and is being applied where the formal analysis is very difficult or even impossible.

Applications in mining

SR motors are widely accepted in mining and the trend of their increased usage is sustainable (Arunava, 2012, Chen, 2009, Ptakh, 2015, Szklarski, 2013). This is due mainly to their substantial advantages such as explosion safety because of the lack of a commutating device, as well as a reduced amount of heating; high reliability due to the possibility of working with one or more broken phases; increased starting torque; high overloading capability; inability to short-circuit the inverter; easy maintenance since there are no impregnating resins, and the change of a coil is a matter of removing and reinserting the new winding on the stator tooth. In the mining industry SRMs are mainly used in belt and armoured face conveyors, drilling machines, traction systems and pumps.

A world leader in the research and development of SR motors is the Japan-based Nidec Motor Corporation and its subsidiaries – the U.S. Motors (USA), Emerson Motor (USA) and SR Drives Ltd (UK). In 2012 Nidec acquired Avtron Industrial Automation Inc. (USA) and in 2014 - the China Tex Mechanical and Electrical Engineering Co. Ltd company. Other major players on the market include Ametek, VS Technology, Shandong Kehui Power Automation, Maccon GmbH, Rongjia Motor Co. Ltd, Shandong Desen, Huayang, Heliad, Rocky Mountain Technologies and some others. The global SRM market is assessed at over 440 million USD for 2018 and it is expected to reach 670 million USD by the end of 2025 (Ptakh, 2015).

A 150 kW SR motor manufactured by SR Drives Ltd is shown in Fig. 6. It is installed by the company on a 2300 m belt conveyor (Nidec 2015).

Fig. 6. The 150 kW Diamond drive system of SR Drives Ltd. (image courtesy of SR Drives Ltd. UK)

A major Canadian potash mining company has upgraded its existing load out conveyor with two 200 kW SRM449TN-180 motors on each end of the conveyor pulley after consulting the SR drive made by Synergy Engineering Ltd in cooperation with Nidec (IMJ 2015) – see Fig. 7. The needs of the drive system are for starting the conveyor 35 times/h, 20 hours/day, 350 days a year and 1000 m under the ground for a 30 years lifespan.

Fig. 7. The two-SRM Synergy Engineering drive system

A mining locomotive with a parallel drive system comprised of two three-phase 7.5kW SRM6-4 motors used in a coal mine in China (Chen, 2001) is shown in Fig. 8. The locomotive has a thrust of 7.1kN, a maximum speed of 10km/h and a braking distance of 14m.

Fig. 8. A mining locomotive with a parallel drive system of two 3-phase SRM6-4

The new Cat988KXE is a wheel loader offered by Caterpillar which employs the SR technology. It has a payload of 14.5 t and its efficiency is increased by 25% overall and by up to 49% in face-loading applications. It is shown in Fig. 9.

Fig. 9. The Caterpillar's Cat 988K XE wheel loader

The world's largest wheel loader is the P&H L-2350 manufactured by Le Tourneau (now part of Komatsu Mining Corp.). It is included in the Guinness Book of Records. This wheel loader weighs 266 tons and has an operating capacity of more than 72 tons. Its fuel consumption is about 45% less than comparably sized mechanical drive wheel loaders which is made possible by using an SR Hybrid drive system. Additional advantage is that the SR motor allows for full utilisation of all braking energy during the loading cycle and the service interval is increased to 20000 hours. The P&H L-2350 is shown in Fig. 10 below.

Fig. 10. The Le Torneau P&H L-2350 wheel loader uses a 400 kW SRM

The UK registered Chinese company Kehui International Ltd. is a manufacturer of SR motors of up to 400 kW. A coal shearer by Kehui is shown in Fig. 11. It benefits from the low starting current and a high torque (30% of rated current gives starting torque of up to 150%) provided by the SR motor.

Fig. 11. The Le Torneau P&H L-2350 wheel loader uses a 400 kW SRM

Conclusions

The technology, modelling, control, and applications of large power switched reluctance motors in mining are introduced in the paper. SR motors have indisputable advantages such as simple construction and robustness of the motor, fault tolerant operation and control, high starting torque, high overload capabilities and many more that make them an emerging alternative to the other large power motors used in the mining industry at present. Some keystone examples from the top manufactures worldwide are briefly introduced that prove the intense SRM penetration into the mining industry. It is obvious that despite some peculiarities related to their control the tendency of their increased usage is quite sustainable. The usage of the SR technology on hybrid, geared and direct drive systems is a premise for a more ecological industry.

Acknowledgements. The support for this work is provided by the bilateral Chinese-Bulgarian scientific project of the National Science Fund of the Ministry of Education and Science with contract No KP-06-China/2 D-83/2018 between the China University of Mining and Technology and the University of Mining and Geology "St. Ivan Rilski", Sofia.

References

Arunava, M., A. Emadi. 2012. On the suitability of large switched reluctance machines for propulsion applications. – *IEEE Transportation Electrification Conference and Expo (ITEC), USA*, 49–54.

Balazovic, P., R. Visinka. 2002. *Three-Phase Switched Reluctance Motor Control with Encoder Using DSP56F80x.* Application Note AN1937, Motorola Inc.

Bals, J., Y. Ji. 2011. Physical modelling of switched reluctance motors using modelica. – *Proceedings of the International MultiConference of Engineers and Computer Scientists (IMECS), 2*, Hong Kong.

Chen, H., C. Pavlitov. 2009. Large power analysis of switched reluctance machine system for coal mine. – *Mining Science and Technology Journal, Elsevier*, *19*, 5.

Chen, H., X. Guilin. 2001. The parallel drive system of the double srm for locomotive traction application. – *27th Annual Conference of the IEEE Industrial Electronics Society*.

DiRenzo, M. 2000. *Switched Reluctance Motor Control – Basic Operation and Example Using the TMS320F240*. Application Report SPRA420A, Texas Instruments Inc.

Elhomdy, E., G., Li, J. Liu, S. Bukhari, W. Cao. 2018. Design and Experimental Verification of a 72/48 Switched Reluctance Motor for Low-Speed Direct-Drive Mining Applications. – *Energies*, *11*, 192.

Ellabban, O., A. Haitham. 2014. Switched reluctance motor converter topologies: A review. – *IEEE International Conference on Industrial Technology (ICIT)*.

Finch, J., M. Harris, A. Musoke, H. Metwally. 1984. Variable Speed Drives using Multitooth per pole Switched Reluctance Motors. – Proceedings of the Thirteenth Annual Symposium on Incremental Motion Control Systems and Devices, 293–301.

Fulton, N., P. Greenhough. 1991. Switched Reluctance Drives for Applications in Hazardous areas. – Fifth International Conference on Electrical Machines and Drives, London, UK, 11–15.

Greenhough, P. 1996. Switched reluctance variable speed drives—a focus on applications. – *Mining Technology*, 107–110.

Harris, M., V. Andjargholi, P. Lawrenson, A. Hughes, B. Ertan. 1982. Vernier reluctance motor. – *IEE Proceedings B - Electric Power Applications, 129*, 1, 43–44.

Hur, J., C. Kim, D. Hyun. 2003. Modelling of switched reluctance motor using Fourier series for performance analysis. – *Journal of Applied Physics*, *93*, 10, 871–878.

IMJ - International Mining Journal. 2015. International Mining Team Publishing Ltd, Hertfordshire, England, Issue November, 66–67.

Karim, K., N. Abdullah, M. Othman, R. Firdaus, Z. Zulfattah, N. Zainal. 2016. Quick design of switched reluctance motor and effect of switching angle ansys maxwell. – *Journal of Telecommunication, Electronic and Computer Engineering, 8,* 7.

Krishnan, R. 2001. *Switched Reluctance Motor Drives: Modelling, Simulation, Analysis, Design, and Applications*. CRC Press LLC.

Miller, T., M. McGilp. 1990. Sizing software for electrical machines. – *IEE Colloquium on Heavy Current CAD Applications*, 6/1–6/5, Glasgow, UK, INSPEC 3381075.

Miller, T. 1993. Switched reluctance motors and their control (Monographs in Electrical and Electronic Engineering). Magna Physics, Clarendon Press, Oxford.

Miller, T. 2001. *Electronic control of switched reluctance machines.* Reed Educational and Professional Publishing Ltd.

Murthy, V., S. Tulasiram, J. Amarnath. 2014. A new converter topology for switched reluctance drive with reduced active switching devices. – *International Journal of Recent Technology and Engineering (IJRTE), 2*, 3.

Nidec SR Drives Ltd. 2015. Nidec Motor Corporation, http://www.srdrives.com/mining-drives.shtml (online, last access June 2019).

Ohyama, K., M. Nashed, K. Aso, H. Fujii, H. Uehara. 2006. Design using finite element analysis of switched reluctance motor for electric vehicle. – *2nd International Conference on Information and Communication Technologies,* ICTTA, Damascus, Syria.

Pavlitov, C. 2005. *Technical Report for contract No IF-02-66*. Sofia (in Bulgarian).

Pavlitov C., H. Chen, Y. Gorbounov, T. Georgiev, W. Xing, Z. Xiaoshu. 2009. Artificial neural network identification model of SRM 12-8. – *Proc. Earth and Planetary Science, 1*, 1, 1301–1311.

Ptakh, G. 2015. Switched reluctance drive medium and high power: foreign and domestic experience (in Russian). Russian Internet Journal of Electrical Engineering, 2, 3.

Ramasamy, G., R. Rajandran, N. Sahoo. 2005. Modelling of switched reluctance motor drive system using Matlab/Simulink for performance analysis of current controllers. – *International Conference on Power Electronics and Drives Systems, Kuala Lumpur, Malaysia.*

Qishan, G., E. Andresen, G. Chun. 1988. Airgap permeance of vernier-type, doubly-slotted magnetic structures. – *IEE Proceedings, 135*, pt. B, 1, 17–21.

Srinivas, K., R. Arumugam. 2005. Analysis and Characterization of Switched Reluctance Motors: Part II - Flow, Thermal, and Vibration Analyses. – *IEEE Transactions on Magnetics, 41*, 4, 1321–1332.

Staudt, T. 2015. *Brushless doubly-fed reluctance machine modelling, design and optimization*. PhD thesis, Université Grenoble Alpes.

Stoyanov, A. 2016. *Matrix operations with MathCAD in the theoretical mechanics.* Statics, Kinesiology, Sofia, 165 p. (in Bulgarian)

Stoyanov, A. 2017. Survey of the relationship between the efforts in the bars and geometrical parameter on tree-dimensional truss. – *Proceedings of the XVIIth International Scientific Conference, Sofia, Bulgaria*, 103–111.

Sturgeon, W. 1825. Improved Electromagnetic Apparatus. – Trans. Soc. Arts, Manufacturers and Commerce, *XLIII*, 37–52.

Szklarski, L. 2013. *Underground Electric Haulage*. Elsevier.

Torrey, D., X. Niu, E. Unkauf, 1995, Analytical modelling of variable-reluctance machine magnetisation characteristics. – *IEE Proceedings on Electric Power Applications, 142*, 1, 14–22.

United States Patent and Trademark Office (USPTO). 2013, (http://www.uspto.gov).

Wach, P. 2011. *Dynamics and Control of Electrical Drives,* Springer.

Watkins, S. 2016. *Fleadh Electronics Ltd*. Leeds, UK (http://fleadh.co.uk/).

ANALYTICAL STUDY OF THE ENERGY CONSUMPTION OF DRUM MILLS ACCORDING TO THEIR SIZE

Teodora Hristova

University of Mining and Geology "St. Ivan Rilski", 1700 Sofia; teodora@mgu.bg

ABSTRACT. In the design of processing factories, the main problem is the choice of the sizes of the drum mills. The factors influencing the choice of a mill are several, each meeting different requirements. One of the main ones is the possibility to supply the technological scheme with a minimum number of mills. This leads to the choice of large-scale machines with the highest price and repair costs. The result of such a choice can be the unnecessary high cost of the milling process. Therefore, the second factor in the choice is the energy consumption of each machine per tonne of processed ore. Various types of drum ball mills were investigated in the paper and their energy consumption was calculated under the same conditions according to the known methodologies. An automatic calculation programme was developed according to the shown methodology. Based on the results obtained, some conclusions are drawn.

Keywords: ball mill, energy consumption, size, power of engine, relative power consumption

АНАЛИТИЧНО ИЗСЛЕДВАНЕ НА ЕНЕРГОРАЗХОДА НА БАРАБАННИ ТОПКОВИ МЕЛНИЦИ СПОРЕД ТИПОРАЗМЕРА ИМ

Теодора Христова

Минно-геоложки университет "Св. Иван Рилски", 1700 София

РЕЗЮМЕ. При проектиране на обогатителни фабрики основен проблем е изборът на типоразмери на барабанните мелници. Факторите, влияещи на избора на мелница са няколко, като всеки от тях удовлетворява различни изисквания. Един от основните е възможността за удовлетворяване на технологичната схема е с минимален брой мелници. Това води до избора на едрогабаритни машини с най-висока цена и разходи за ремонт. Резултатът от такъв избор може да е излишно оскъпяване на процеса смилане. Затова втори фактор при избора е енергоразходът на всяка машина за тон преработена руда. В статията са изследвани различни типоразмери барабанни топкови мелници, изчислен е техният енергоразход при еднакви условия според известна методика. Разработена е програма за автоматично изчисление, според показаната методика, и въз основа на получените резултати са направени съответните изводи.

Ключови думи: топкова мелница, мощност на двигател, енергоразход, размер, специфичен енергоразход

Introduction

According to the Sustainable Development Paradigm, social, economic and environmental issues are accepted to be considered in a complex way in every human and productive activity. In recent years, manufacturers have become aware of the relationship between production operations, the quality of the environment and the welfare and health of employees (Rosen, Kishawy, 2012). Naturally, the sustainability criteria apply to the different stages of existence of industrial sites - designing, renovating, building, operations. The achievement of these complex objectives is also important in the mining and processing sector, which puts producers and engineers in front of four key environmental objectives: 1) Human extinction, 2) Sustainable development, 3) Conservation of biodiversity, 4) Aesthetic wealth [A. Szekeres, 2016]. In this aspect, the impact assessment of the mining and processing sector is best considered not only for the entire life cycle but also for the full range of activities involving the product (ERP), process (ERP), facility (ERF), service (ERS) and infrastructure (ERI). Due to the need to meet the sustainability criteria under changed requirements, standards, regulations and laws, it is often necessary to change technological lines or to build new enterprises.

Relative power consumption for technological processes

The factor of relative power consumption as part of the objectives for achieving sustainable development in the choice of mills for the mining sector is considered in the article. In the life cycle of production, this is one of the most energy-intensive processes not only for the mining sector, but also for other economic activities. From the reference of literature sources it has been found that mills in the light industry and in particular in the food industry have relatively high energy consumption in the production cycle. Rice mill engines consume between 80 and 85% of total energy in the life cycle from flaking to packing rice (Pachanawan, 2017). Similar are the statistics data for other sectors of the food industry like sugar cane production, where mainly roll crusher or roller mills are used (Ștefan, Voicu, 2013).

For the mining sector, 50% of the electricity consumed was found to be the crushing and milling process in the full production cycle of the four parts of the chain: exploration, extraction, processing and recycling (Jeswiet, 2016). It is estimated that approximately 60% of this energy is consumed in the milling process. The data from foreign sources overlap with those for Bulgarian mining enterprises, where 60% of the consumption is of synchronous engines (SM) driving the mills, and 40% is from asynchronous engines in the crushing process (Kurtzelin et al., 2009). Under the sustainability criteria, scientists are analysing these issues not only in order to save both the electrical energy and resources. The reason is that the quality of the product at the output of a particular process has an effect on the quality and consumption of energy and raw materials in the next one.

Energy saving approaches can be either theoretical or experimental, performed by machine operators. The latter are very expensive and usually do not lead to optimal results (Jafarzadeh, Khodaygan, 2019). To achieve synergy, it is necessary to reduce the energy consumption while preserving the quality of the resulting product, for which optimisation of the processing parameters is necessary. Research has recently been done to achieve targeted features such as maximising tool life, maximising material removal rate (MRR), maximising surface quality of grain size while minimising energy consumption or material consumption, compensating for energy losses in propulsion synchronous motors through change of supply voltage (Kurtzelin et al., 2009), determination of vibrations at maximum MRR and others (Jafarzadeh et al., 2019). Various methods, algorithms, mathematical apparatus (Mryankov, 2007), machine algorithm for calculation, neural networks, etc. are used to achieve the optimal parameters of the surveyed objects. In order to achieve the target function, it is good to compare several methods and select the one with the smallest error (Singh Nain, 2019).

All of these studies lead to an increase in energy performance, but from a lifecycle aspect of production, it is first necessary to theoretically choose the appropriate machines for each technology.

With this purpose, a point system has been proposed that can be used to evaluate types of mills against the indicators: energy consumption; quantity of material and quantity of gaseous, solid and liquid waste; public needs (Jeswiet, 2016). However, it is not possible to compare different machine sizes of the same type on the basis of energy consumption, quantity of waste and produced products and others.

In the presented problem, it is most expedient to determine the energy per unit of product produced or the so-called relative power consumption at a selected mill type. Therefore, the article examines the problem of choosing the size of drum mills in the design of processing factories versus the lower energy consumption factor. The necessity of the study arises because many scientists study the energy consumption of already installed and operating mills according to the properties of the material to be milled - hardness, size, content and etc. The literature emphasises only the reasons for choosing a type of mill in the design and construction of a technological line by a classical or point method. The choice of type of mill according to size must be guided by the cost of building and maintaining the machinery, the leading criterion being the energy consumption of each machine per tonne of processed ore. Such a condition is fully consistent with sustainable development criteria because lowering energy consumption will lead to improvements in some of the energy efficiency criteria.

Structure of the object to be analysed

When designing a technological line in the mining and processing industry according to the technological requirements, a certain type of mill is chosen. Classification of mills can be done according to different criteria:

- depending on the drum design, they are cylindrical or cylindrical conical;
- according to the discharge, with central discharge or pouring; discharging through a grate; outlet through a peripheral grate;
- according to the type of grinding media they are ball, bar, gravel, autogenous and semi-autogenous;
- according to the number of cameras they are single-chamber or multi-chamber (Minin, 2012).

In processing factories one chamber drum mills are used as milling equipment. For the study, MTP machines (ball mill with grating) are chosen. This model has a low pulp level which results in increased efficiency due to increased impact of the grinding media. They are also known as grate discharging. This is achieved by placing a grid in the semi-receptive chamber between the grating and the bottom of the drum. When the mill is rotated, the milled product passes through it, rises out of the elevator and they outflow from the discharge port. The particles that have reached the required particle size pass through the holes of the grate and enter the semi-receiving chamber from where they are unloaded.

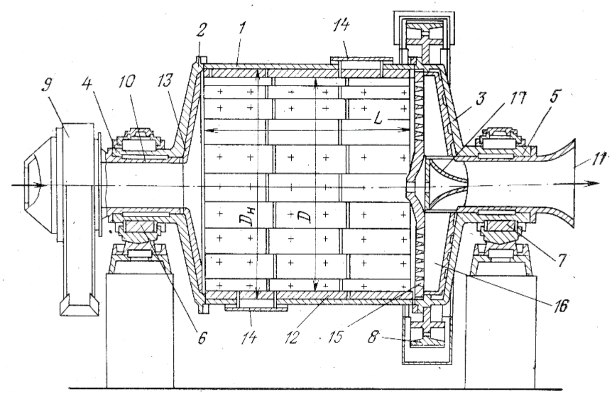

Fig. 1. Drum ball mill with grate
1 - drum; 2 - bottom; 3 - discharge chamber; 4,5-discharge trunnions; 6.7 – bearing seats; 8 - tooth gearing; 9 - combined feeder device; 10,11 - supply and discharge bushings; 12 - drum linings; 13 - lining of the bottoms; 14 - hatch; 15 - discharging grate; 16 - elevator; 17 - unloaded cone; 18-pinion; 19 – shaft

The drum selected for analysis is visualised in Figure 1. It consists of a drum (1) and side bottoms (2). The rotation of the mill is accomplished by means of bearings (6, 7) which are attached to the grippers on the lateral bottoms. On rotation, the material fed in the drum is lifted by the lifter bars of the lining (12), then dropped and milled by impact, grinding and crushing under the action of the grinding media. The milled material is continuously discharged from the discharge port (3), and ore grindings are fed through the feeder port (9) in accordance with a certain technologically chosen filling factor. The performance of the mill, of course, depends directly on the volume of the drum.

The relative power consumption analysis against an appropriate type size is based on the following metrics: engine power, output, energy consumption and cost. For engineering evaluation, the following type sizes were selected for comparison: MTP 4.5x6, MTP 4.5x5, MTP 4x5, MTP3.6x5 and MTP 3.6x4.

Method for determining the productivity of a drum ball mill

For comparison of the defined criteria, the productivity of the selected by size mills must be calculated. In some studies, the energy consumption is determined according to the electricity paid per unit of product (A. Pachanawan, 2017, GH Voicu, 2013), but in this case it is more correct to use a classical methodology for calculating engine power. This is the method used by engineers to determine the basic technological parameters and forces, which includes the steps described below in the text (I. Minin, 2012, Minin et al., 2010).

The light drum diameter is determined using the formula:

$$D_1 = D_\delta - 2\delta, mm \qquad (1)$$

where:
- D_δ – is the drum diameter;
- δ - the thickness of the lining, being between 0.15 ÷ 0.17 mm for the different sizes of mills.

The critical angular speed of the drum is calculated as follows:

$$\omega_{cr} = \sqrt{\frac{2g}{D_1}}, \text{ rad/s}, \qquad (2)$$

where D_1 is the light drum diameter.

The actual angular velocity of the drum is given according to the expression:

$$\omega = \frac{\pi n}{30}, \frac{rad}{s}, \qquad (3)$$

where n is the rotation speed of the drum.

The relative angular speed of the rotation of the drum Ψ is determined by the ratio of the drum speed to the actual angular velocity and the critical angular velocity.

$$\Psi = \frac{\omega}{\omega_{cr}}.100\% \,. \qquad (4)$$

The working volume of the drum for each mill is determined according to the expression:

$$V_1 = \pi R_1^2.L, m^3, \qquad (5)$$

where:
$R_1 = \frac{D_\delta - 2\delta}{2}, m$ - is the drum radius without the lining;
L - drum length.

The mass of the balls is determined according to:

$$M_T = \rho_T V_1 \varphi, \qquad (6)$$

where:
- ρ_T – is the density of the balls;
- φ - fill factor with grinding bodies, which is selected in this case 0,4.

To determine the mass of the balls, their density should be chosen. By known methods the density of the balls is selected according to their diameter, but from a theoretical study it has been found that the balls are of different wear and do not stand symmetrically in the mill drum. It is estimated that the density of the balls is about 4514kg/m^3 and this density does not depend on their diameter (Minin et al., 2014).

The weight of grinding media in the mill is determined according to the dependence:

$$C_T = g.M_T \qquad (7)$$

where g is the Earth's acceleration.

Table 1. *Specification table of the selected type mills*

Parameters	MTP-3600x4000	MTP-3600x5000	MTP-4000x5000	MTP-4500x5000	MTP-4500x6000
the thickness of the lining,mm	110	110	110	120	120
the light drum diameter,mm	3600	360	4000	4500	4500
drum length,mm	4000	5000	5000	5000	6000
the working volume of the drum,m^3	36	45	55	71	85
the rotation speed of the drum, min^{-1}	18,1	18,1	17,4	16,5	16,5
% of the critical angular speed	78,7	78,7	79,9	80,4	80,4
the mass of balls,t	74	93	115	148	177
the weight of grinding media in mill,t	216	238	333	395	-
the weight of the drum,Mmill,t	160	165	265	300	320
power of engine,kW	1000	1250	2000	2500	2500

The weight of the drum is:

$$C_б = g.M_б, N \qquad (8)$$

where $M_б$ – the mass of the drum, the value being taken from the enclosed grinder specification table, Table 1.

The idle power is determined with the equation:

$$N_{idle} = 0{,}5\mu C_6 \omega d \quad (9)$$

where:

- μ – the coefficient of friction in the bearings;
- *d* – the diameter of the collar of the mill bearings.

The extra power depends on the weight of the milling media and is calculated with the expression:

$$N_{add} = 0{,}5.\mu.C_T.\omega.d, W, \quad (10)$$

where μ is the coefficient of friction in the bearings and its value is 0.008.

The next step is determining the power to raise the balls in the drum:

$$N_G = \rho_T.g.L.\omega_{cr}.\Psi^3.R_1^3\left[(1-k_2^4) - \frac{2}{3}\Psi^4(1-k_2^6)\right], W \quad (11)$$

where: k_2 – is the relative radius for the innermost layer of the balls, which is taken according to the values in the tables referenced in the literature. The value is 0.606.

The power to transmit the kinetic energy of the balls is:

$$N_e = 0{,}125\rho_T L.\omega_{cr}^3 R_1^4(1-k_2^4), W \quad (12)$$

Calculated power values are used to calculate the engine power required to drive the mill. In these mills, synchronous motors are used for propulsion and for each type of dimension it is required that drive power is to be calculated according to the formula:

$$N_{engine} = \frac{N_{idle}+N_{add}+N_G+N_e}{1000\eta_\mu}, \text{W} \quad (13)$$

where η_μ is the mechanical coefficient of efficiency of the drive.

The total productivity of the drum mill versus the starting product is determined according to the dependence:

$$Q = qV_1, kg/h \quad (14)$$

where q is the specific productivity of the mill.

The specific performance of the mill is determined by the factors on which it depends: grinding mode, type of grinding medium, size of the output and final product, physico-mechanical properties of the grinding material, mill diameter, grinding medium, relative angular velocity of the mill and others. Their impact is accounted for by correction factors, the values of which are established by the practice. They are:

Correction coefficient for the influence of the size of the outcoming ore:

$$K_d = \sqrt[4]{\frac{dh}{25}} = 0{,}83, \quad (15)$$

where dh is the maximum size of the outcoming ore, mm.

Correction factor for the influence of the diameter of the drum:

$$K_D = \sqrt{\frac{3}{D_6}}, \quad (16)$$

where 3 - drum diameter of a reference mill, m.

Correction coefficient for the influence of the relative velocity:

$$K_\Psi = \frac{75}{\Psi} \quad , \quad (17)$$

Correction coefficient for the effect of the amount of the milling media:

$$K_\varphi = \frac{75}{\varphi} \quad (18)$$

Correction coefficient for the influence of the size of the milled product:

$$K_\beta = 3.4d_k, \quad (19)$$

where d_k - nominal diameter of the finished product.

Coefficient considering the type of mill chosen $K_{mill} = 1$ if the mill has a grate (in this case) or $K_{mill} = 0.87 \div 0.8$, if the mill is centrally unloaded.

Coefficient for calculating the influence of the digestibility of the ore on the mill performance. This factor is counted from graphic and accepted $K_T = 0.85$.

After determining all the coefficients, the specific productivity of each mill by source product can be calculated according to the dependence:

$$q = \frac{q_0 K_T K_\beta K_{mill}}{K_d K_D K_\Psi K_\varphi}.\frac{\rho_H}{16000}, kg/m^3 \quad (20)$$

where:

- q_0 - reference specific productivity (assumed $q_0 = 2200\, kg/m^3h$);
- ρ_H – a coefficient of bulk density of the ore;
- 1600 – reference bulk density.

Results

Based on the methodology, the productivity (Q/ t) of different types of mills was calculated. The results obtained are shown in Figure 2. It can be seen that reducing the size of the drum also reduces the performance.

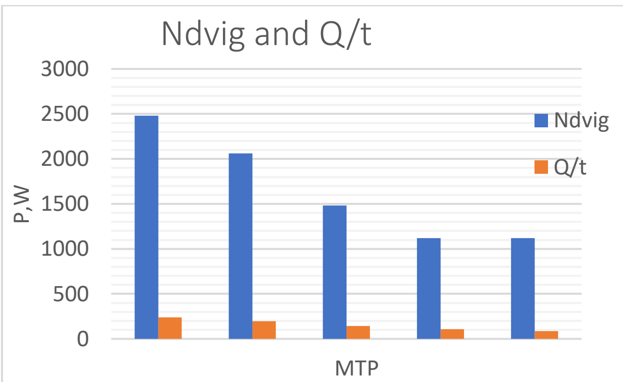

Fig. 2. Productivity and power of engine of the surveyed MTP

Comparison of different types of mills based on relative power consumption

The concept of relative power consumption is introduced because the consumed electricity does not provide an objective estimate of the costs of the processed ore. The relative power consumption $E, kWh/t$ is the ratio of the calculated power of the mill engine to the productivity of the mill per finished product per unit of time. Changing this value depends on the load of the engine with different loads. Energy efficiency can therefore be used to determine effective operation regimes when changing qualitative characteristics of the incoming ore. The relative power consumption is obtained using the formula:

$$E = \frac{N_{engine}}{Q}, kWh/t \qquad (21)$$

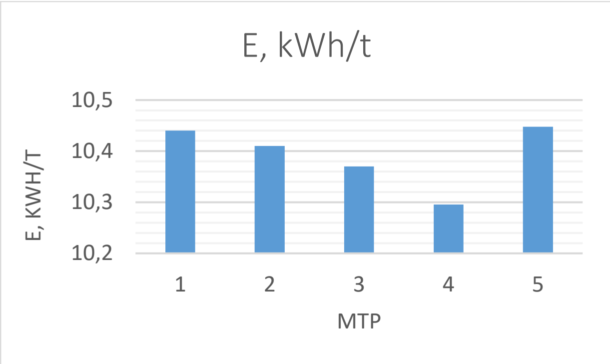

Fig. 3. Relative power consumption of Types MTP

It can be seen that the relative power consumption depends on the size of the mills. In a given order, the energy consumption decreases when the volume decreases, but with excessive volume decrease it increases. The reason is that the mass of the parts of the smaller machines is close to that of the larger machines, resulting in increased idling energy consumption and hence increased energy consumption of small mills. This is visualised in Figure 4, and to achieve the symmetry of the graphs the data on the weight of the mill are divided into 10000.

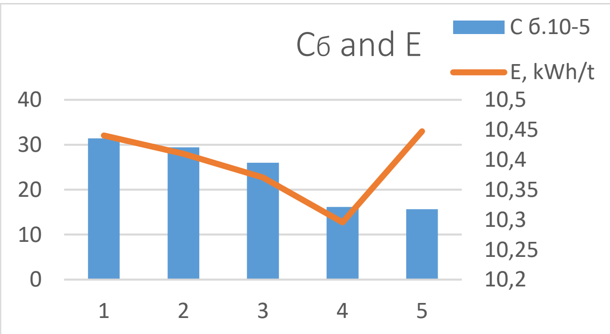

Fig. 4. Drum weight and relative power consumption of types MTP

When deciding on the choice of a type-sized mill aiming to rationalise the electricity consumption, the result obtained should be taken into account. The price factor is not insignificant and can also be included. The price is determined according to the dependence:

$$P = prM_{mill}, euro \qquad (22)$$

where pr – the price per unit weight, given conditionally 6 euro per kilogram

– M_{mill} – the mass of the mill.

It can be seen that the reduction of the mill's mass decreases the price, respectively the repair costs, as well as the quantity of the produced product. However, Figure 5 shows that energy consumption increases as the volume of the mill drum decreases, while the productivity is almost unchanged, and this is the key factor in deciding on the size of mills.

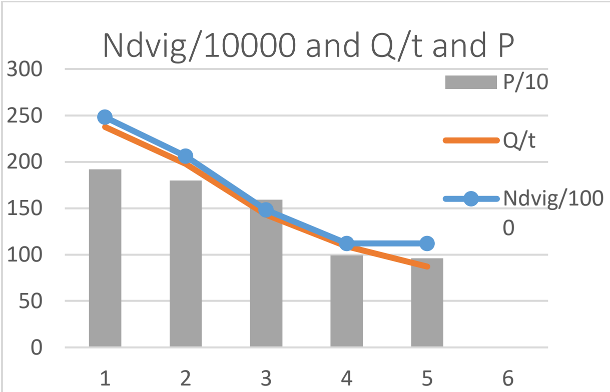

Fig. 5 Engine power, productivity, cost of MTP

After choosing a type-sized mill and building a processing line, it is necessary to define the operating modes. In determining their economic efficiency, it is necessary to analyse the technological mode of the processing plant, according to the boundary conditions of the equipment and the characteristics of the material to be milled, such as grain size, changing the trajectory of the particles (Stoyanov, 2015), the humidity, the hardness, etc. (Assawamartbunlue, 2018). This is related to determining the impact of each of these factors on the energy consumption by measuring and subsequently processing and analysing the data.

Conclusion

It is important that the mills are selected according to their relative power consumption, because in this way it is possible to save not only energy, but also costs for parts, repair, and maintenance. Worldwide, there is an emphasis on choosing a larger machine rather than a few smaller ones, such as rice flour mills. The theoretical study proves this trend.

However, the choice of the type of mill and its size should not only be the relative power consumption of the grinding process, but that of the whole technological line. To achieve a synergic effect from all the phases of processing the ore, it is necessary to analyse the change in energy consumption when changing the production technology. For example, the use of an additional reagent to the mill in order to increase the efficiency of the next flotation process (Boteva, 2002). This action will not lead to a reduction in the mill's relative power consumption, but only to the flotation process. Finally, this will generally improve the energy performance of the whole life cycle due to the increased amount of the extracted metal. This is a future topic of research.

References

Assawamartbunlue, K., N. Kunrapeegayson, P. Limwattana. 2018. Specific Energy Consumption of Sugar Cane Mills in Thailan. – *Chemical Engineering Transactions*, *70.*

Boteva, A., B. Vladkova. 2002. New selective collector for flotation of sulfide ores. – *Annual of the University of Mining and Geology "St. Ivan Rilski", 45,* 2, 67–70.

Jafarzadeh, E., S. Khodaygan, A. Sohani. 2019. A new method for multi-objective optimal design of milling parameters by considering chatter vibrations. – *SAE Technical Paper 2019-01-5043.*

Jeswiet, J., A. Szekeres. 2016. Energy Consumption in Mining Comminution. – *23rd CIRP Conference on Life Cycle Engineering Jack Jeswiet.*

Kurtzelin, E., N. Minekov, R. Istalianov, I. Mladenova. 2009. Study of the influence of the voltage at loss of electricity in synchronous electric motors. – *Annual of the University of Mining and Geology "St. Ivan Rilski", 52,* III, 91-94 (in Bulgarian with English abstract).

Minin, I., S. Savov, T. Hristova. 2014. Opredelyane vliyanieto na edrinata na stomanenite topki vurhu izrazhodvanata moshtnost ot dvigatelya na barabannite topkovi melnitci pri postoyanen koefitsient na zapulvane. – *Geology of Mineral Resources, 6*, 30–32 (in Bulgarian).

Minin, I. 2012. *Tehniki I tehnologii pri obogatiyavane na polezni izkopaemi - Part I*. Avangard Prima, Sofia, (in Bulgarian).

Minin, I., P. Nedyalkov. 2010. Study of relative productivity of tumbling nall mill type 4,5X6 working under the conditions of processing plant "ELACITE". – *Annual of the University of Mining and Geology "St. Ivan Rilski", 53*, III, 44–48 (in Bulgarian with English abstract).

Mryankov, I., A. Ivanov. 2007. Izsledvane na prostranstvenite treptenya na vibratsionna melnitsa. – *Mehanika na machinite, XV, 68,* 2, 130–133 (in Bulgarian).

Pachanawan, A., S. Chuan-Udom, K. Saengprachatanarug, S. Wongpichet. 2017. Electrical Energy Consumption and Energy Conservation of Rice Mills in the Northeastern of Thailand. – *Engineering Journal, 21,* 4.

Rosen, M. A., H. A. Kishavy. 2012. Sustainable Manufacturing and Design: Concepts, Practices and Needs. – *Sustainability, 4(2),* 154–174.

Singh Nain, S., R. Sai, P. Sihag, S. Vambol, V. Vambol. 2019. Use of machine learning algorithm for the better prediction of SR peculiarities of WEDM of Nimonic-90 superalloy. – *Archives of Materials Science and Engineering, 1(95),* 12–19.

Ştefan, Gh. Voicu, G. Ipate, G. A. Constantin. 2013. Mathematical model to estimate the energy consumption at the wheat grinding with roller mills. – *41. International Symposium on Agricultural Engineeringp*, *Actual Tasks on Agricultural Engineering At: Opatija, Croatia I.*

Stoyanov, A. 2015. A task for the movement of a rigid body with the fixed point. – *Annual of the University of Mining and Geology "St. Ivan Rilski", 58,* 3*,* 119–121 (in Bulgarian with English abstract).

ALGORITHM FOR IoT-SENSOR DESIGN AND MAINTENANCE SERVICE

Mila Ilieva-Obretenova, Elena Blagoeva, Boiko Karkov

University of Mining and Geology "St. Ivan Rilski", 1700 Sofia; mila.ilieva@mgu.bg; elena.blagoeva@mgu.bg; boiko.karkov@mgu.bg

ABSTRACT. Internet of Things (IoT) is the extension of Internet to physical devices and everyday objects. Embedded with electronics, Internet connectivity, and other forms of hardware (such as sensors), these devices can communicate and interact with others over the Internet, and they can be remotely monitored and controlled. The paper offers an algorithm for IoT-sensor design and Maintenance Service with a high level of detail. It is intended for students and junior designers. The hypothesis is the following: unambiguous steps are defined by the usage of appropriate methods. The methodology includes a theory for: semiconductor devices, Wheatstone bridge, analogue-to-digital conversion with successive approximation, finite elements method, unified modelling language (UML) and programming language Verilog. The algorithm is illustrated by an example for a pressure sensor. The result is an algorithm in two parts: simulation design and service design. The simulation design includes hardware design and simulation elements calculation. The service design includes definitions of Managed Objects classes with names, attributes, operations and methods. With the chosen detail level, the algorithm is a good base for designing a system with two sensors (e.g. a pressure sensor and a temperature sensor) and for experiments in specific working environment (e.g. underground mine).

Keywords: IoT-sensor, pressure sensor, temperature sensor, simulation, service

АЛГОРИТЪМ ЗА ПРОЕКТИРАНЕ НА IoT -СЕНЗОР И ОБСЛУЖВАНЕ НА ПОДДЪРЖАНЕТО

Мила Илиева-Обретенова, Елена Благоева, Бойко Кърков
Минно-геоложки университет "Св. Иван Рилски", 1700 София

РЕЗЮМЕ. IoT (Internet of Things) е разширението на интернет към физически устройства и обекти за ежедневна употреба. Снабдени с електроника, интернет свързаност и други форми на хардуер (като сензори), тези устройства могат да комуникират и да взаимодействат с други чрез интернет и могат да бъдат дистанционно наблюдавани и контролирани. Предлага се алгоритъм за проектиране на IoT-сензор и обслужване на поддържането с висока степен на детайлизация. Предназначен е за студенти и младши проектанти. Хипотезата е следната: Еднозначност на стъпките се постига чрез използване на подходящи методи и средства. Методологията за проектиране включва теории за: полупроводникови елементи, Уитстонов мост, аналогово-цифрово преобразуване с последователна апроксимация, метод на крайните елементи, унифициран език за моделиране (UML) и език за програмиране Verilog. Алгоритъмът се илюстрира с пример за сензор за налягане. Резултатът се състои от алгоритъм в две части: проектиране на симулация и проектиране на обслужване. Проектирането на симулацията включва: проектиране на хардуер и изчисляване на елементите на симулацията. Проектирането на обслужването съдържа класове управлявани обекти с имена, атрибути, операции и методи. С избраната степен на детайлизация алгоритъмът представлява добра основа за проектиране на система с два сензора (например сензор за налягане и сензор за температура) и за експерименти в специфична работна среда (например подземен рудник).

Ключови думи: IoT-сензор, сензор за налягане, сензор за температура, симулация, обслужване

Introduction

IoT (Internet of Things) is the extension of Internet to physical devices and everyday objects. Embedded with electronics, Internet connectivity, and other forms of hardware (such as sensors), these devices can communicate and interact with others over the Internet, and they can be remotely monitored and controlled. The recent developments are represented in articles with low level of detail (Miller, 2018) or represent concepts of very high level (Ruh, 2018; Perera et al., 2018). This article offers an algorithm for IoT-sensor design and Maintenance Service with high level of detail. It is intended for students and junior designers. Unambiguous steps are defined by the usage of appropriate methods.

Methodology

The design methodology includes the application of the theory for: semiconductor devices (Lienig, 2017), Wheatstone bridge (Ekelof, 2001), analogue-to-digital conversion with successive approximation (Baker, 2010), finite element method (Logan, 2011), Unified Modelling Language – UML (Fowler, 2004) and programming language Verilog (Bergeron, 2012). The algorithm is illustrated with a pressure sensor.

Results

Simulation design

Hardware design. 1. Block-diagram design: Fig.1 shows a block-diagram of a monitoring system for the liquid level. It contains a sensor, an amplifier, an analogue-to-digital converter (ADC), a microcontroller, a RF-transmitter, a gateway, a power supply and a clock.

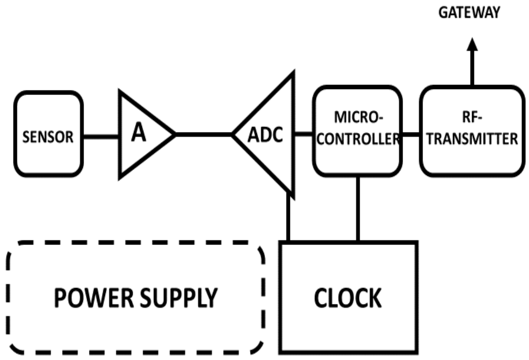

Fig. 1. Block-diagram of a monitoring system for the liquid level

2. Measure scheme for sensor resistance: Fig. 2 shows a measure scheme for sensor resistance with a Wheatstone bridge and an amplifier.

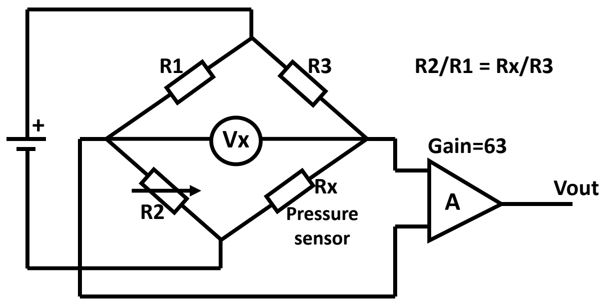

Fig. 2. Measure scheme for sensor resistance

3. Detailed block-diagram of ADC: Fig.3 shows a detailed block-diagram of ADC with successive approximation, where SAR is the Successive Approximation Register, Vref is the Reference Voltage, DAC is the Digital-to-analogue converter, Vin is the Input Voltage, S/H is the sample and hold circuit and EOC is the End of Conversion.

The operation of ADC with successive approximation is the following: SAR is initialised so that the most significant bit (MSB) is equal to a digital 1 (Vref). This code is fed into the DAC, it is converted to the analogue equivalent and is fed into the comparator circuit for comparison with the sampled input voltage Vin. If this analogue voltage exceeds Vin, the comparator causes the SAR to reset this bit (turns it to 0). Otherwise, the bit is left as 1. Then the next bit is set to 1 and the same test is done. The binary search continues until every bit in the SAR has been tested. The resulting code is the digital approximation of the sampled input voltage and is finally the output by the SAR at the end of the conversion. Fig.4 shows the operation of ADC with successive approximation for the binary digit 00000001.

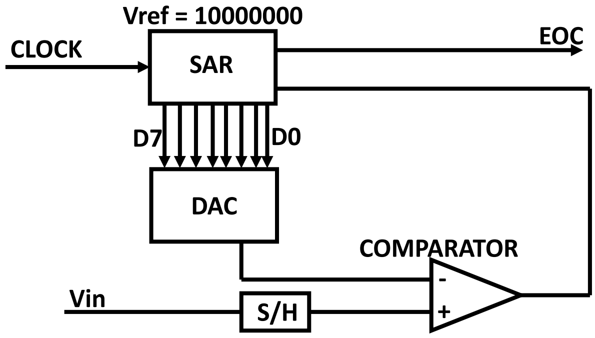

Fig. 3. Detailed block-diagram of ADC

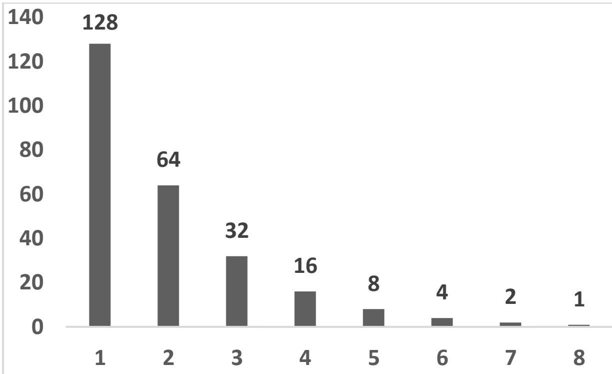

Fig. 4. Operation of ADC with successive approximation

4. System improvement: Fig.5 shows a system improvement with a group of sensors, which could be connected to one multiplexor (MUX), so they could monitor a group of parameters, characterising a certain territory – a mining territory, an environment territory, etc.

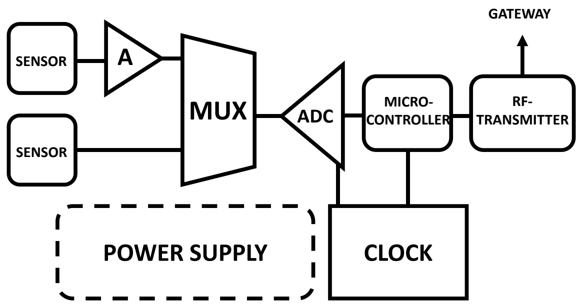

Fig. 5. System improvement: System with a group of sensors

Simulation elements calculation. 1. Sensor choice: A nonlinear resistor is chosen with resistance dependent on the applied pressure: R=f(P). 2. Calculation of dependence pressure-voltage: The voltage is measured as a function of pressure with the Wheatstone bridge: U=f(P). The minimum output voltage of the sensor is 0,1mV=1.10^{-4}V. The maximum output voltage of the sensor is 35mV=$3,5.10^{-2}$V. The maximum applied pressure is 350,25kPa. The pressure for 0,1mV in kPa is:

$$P = \frac{350.25x0.1}{35} = 1\,kPa \quad (1)$$

3. Amplification calculation for the voltage after sensor: ADC works in the range from 0 to 2,2V. Therefore, the voltage after the sensor needs amplification A_U:

$$A_U = \frac{2.2}{3.5x10^{-2}} = 63 \quad (2)$$

4. Calculation of successive approximation step of ADC: For the conversion of the voltage into a digital signal an 8-bit ADC is used. The possible counts are:

$$C = 2^8 = 256 \quad (3)$$

The active counts are:

$$C_1 = 2^8 - 1 = 255 \text{ (From 0 to 255)} \quad (4)$$

The approximation step is calculated from the ADC range and the possible counts are:

$$V = \frac{2.2}{256} = 8.59375.10^{-3}\ V/count \quad (5)$$

Table 1 shows visualization of voltage distribution in Excel.

Table 1: *Voltage Distribution in Excel*

2^8	2^7	2^6	2^5	2^4	2^3	2^2	2^1	Voltage,V	Pressure, kPa	Pressure, mm
0	0	0	0	0	0	0	0	0	0	0
0	0	0	0	0	0	0	1	0.008594	0	0
0	0	0	0	0	0	1	0	0.017188	0	0
0	0	0	0	0	0	1	1	0.025781	0	0
0	0	0	0	0	1	0	0	0.034375	0	0
0	0	0	0	0	1	0	1	0.042969	0	0
0	0	0	0	0	1	1	0	0.051563	0	0
0	0	0	0	0	1	1	1	0.060156	0	0
0	0	0	0	1	0	0	0	0.06875	0	0
0	0	0	0	1	0	0	1	0.077344	0	0
0	0	0	0	1	0	1	0	0.085938	0	0
0	0	0	0	1	0	1	1	0.094531	0	0
0	0	0	0	1	1	0	0	0.103125	0	0
0	0	0	0	1	1	0	1	0.111719	0	0
0	0	0	0	1	1	1	0	0.120313	0	0
0	0	0	0	1	1	1	1	0.128906	0	0
0	0	0	1	0	0	0	0	0.1375	1.45	148
0	0	0	1	0	0	0	1	0.146094	2.9	296
0	0	0	1	0	0	1	0	0.154688	4.35	444
0	0	0	1	0	0	1	1	0.163281	5.8	592
0	0	0	1	0	1	0	0	0.171875	7.25	740
0	0	0	1	0	1	0	1	0.180469	8.7	888

5. ADC scale calculation: The ADC scale is calculated from the possible counts and the ADC range:

$$C_V = \frac{256}{2.2} = 116\ counts/V \quad (6)$$

6. Calculation of Wheatstone bridge offset in V: We suppose that the Wheatstone bridge is not ideally balanced and prior to the pressure application the voltmeter reads 2mV=2.10^{-3}V. The voltage after the amplifier is:

$$V_{offset} = 2x10^{-3}x63 = 126x10^{-3}V = 0.126V \quad (7)$$

7. Calculation of Wheatstone bridge offset in counts:

$$offset = 0.126x116 = 14.6 =\sim 15\ counts \quad (8)$$

8. Calculation of active counts of the ADC reporting the pressure:

$$C_A = 255 - 15 = 240\ counts \quad (9)$$

9. Calculation of the sensor slope in counts/kPa:

$$S_1 = \frac{240}{350.25} = 0.68522\ counts/kPa \quad (10)$$

10. Calculating of the sensor slope in V/kPa:

$$S_2 = 0.68522x8.59375x10^{-3} = 5.88865x10^{-3}\ V/kPa = 5.88865x10^{6}\ V/Pa \quad (11)$$

11. Defining the voltage function: The voltage function is linear from the type:

$$y = ax + b, \tag{12}$$

Where y is the output voltage V_{out} in V, as is the slope S_2 in V/kPa, x is the pressure P in kPa and b is offset V_{offset} in V.

$$V_{out} = S_2 xP + V_{offset} \tag{13}$$

12. Calculation of the dimension on X axe in kPa/count:

$$m= \frac{350.25}{240} = 1.45 \text{ kPa/count} \tag{14}$$

13. Calculation of the dimension on X axis in mm/count: For practical aims let's assume that the fluid height is directly proportional to the pressure:

$$P=\rho gh, \tag{15}$$

Where P is the pressure in kPa, ρ is the fluid density (for water ρ = 1kg/l), g is the standard gravity 9,8m/s^2 и h is the fluid height over the sensor in meters. Then

$$\text{Factor} = \frac{P}{\rho x g} = \frac{1.45}{1x9.8} = 0.147959 \text{ m/count} = 148 \text{ mm/count} \tag{16}$$

Fig.6 shows the dimensions: dimension on X axis in kPa/count and dimension on X axis in mm/count.

The figure shows that 1kPa corresponds approximately to 100 mm.

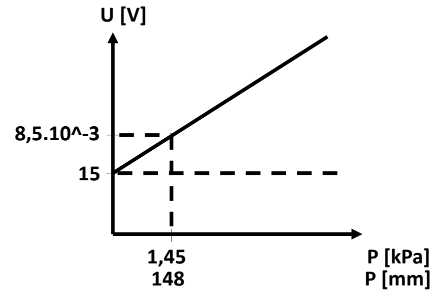

Fig. 6. Dimensions on X axis

Checking: For 117 counts: (117-15)x1.45 = 147.9kPa, $\frac{147.9}{9.8}$ =15.09 m, (117-15)x148 = 15096 mm;

for 219 counts: (219-15)x1.45=295.8kPa, $\frac{295.8}{9.8}$ = 30.184m, (219-15)x148=30192mm. The check shows a difference in the calculations of about 1cm.

14. Definition of the function for fluid height in mm:

$$h = (\text{ncounts} - \text{offset}) * \text{factor}, \tag{17}$$

where ncounts is the number of counts of ADC, corresponding to the analogue value of the sensor voltage.

Service Design

UML diagram synthesis. Fig.7 shows a UML diagram for Managed Objects classes for Maintenance Service.

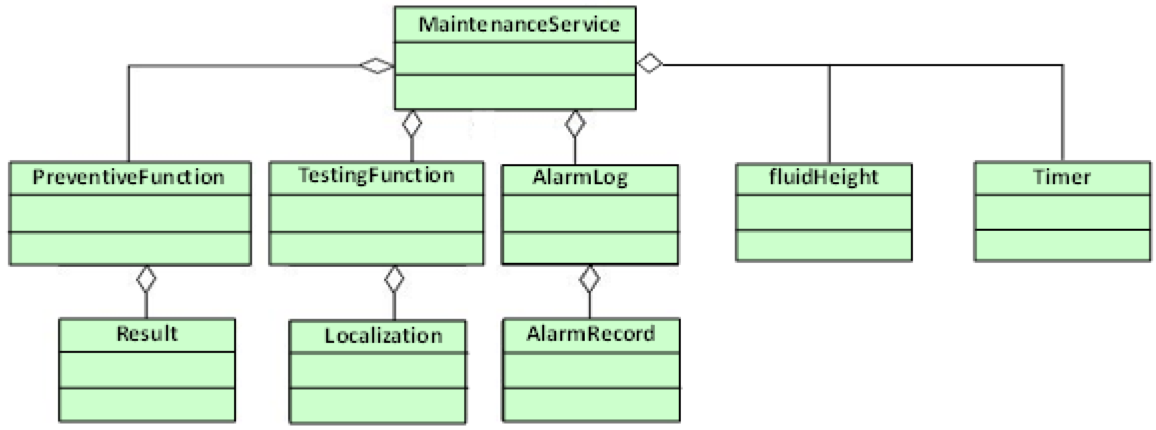

Fig. 7: UML diagram of Managed Objects classes for Maintenance Service

Definitions of Managed Objects (MO) classes with names, attributes, operations and methods.

1. MO **MaintenanceService** represents the information for maintenance service, which helps to monitor the process in normal working conditions and to avoid failures.

2. MO **fluidHeight** represents a function for calculation of sensor constants. A) Attributes: Attribute **gravity** represents gravitational field. Attribute **density_of_water** represents one of the physical properties of water – density. Attribute **ADCrange** shows the maximum voltage of ADC. Attribute **ADCbits** represents the number of ADC bits. Attribute **pressureMaximum** represents the maximum pressure applied on the sensor. Attribute **sensorOutput_min** shows the minimum output voltage of sensor. Attribute **sensorOutput_max** shows the maximum output voltage of sensor. Attribute **WBridgeIntercept** shows the initial voltage in Wheatstone bridge. Attribute **ncounts** represents the number of counts reached by certain pressure. B) Operations: Operation **MinPressure** calculates the minimum pressure measured by the sensor. Operation **Amplification** calculates the necessary amplification so that the sensor range corresponds to ADC range. Operation **ADCcounts** calculates the number of ADC counts. Operation **ADCfactor** calculates the ADC step in V/count. Operation **ADCscale** calculates the ADC scale in counts/V. Operation **InterceptVoltageAfterAmplifier** calculates the initial voltage after amplifier. Operation **offset** calculates the initial voltage, reported from ADC. Operation **ActiveADCcounts** calculates

the ADC counts with pressure. Operation **Slope1** calculates the slope in counts/kPa. Operation **Slope2** calculates the slope in V/kPa. Operation **PressureScale** calculates the dimension on X axis in kPa/count. Operation **Factor** calculates the dimension on X axis in mm/count. Operation **read_ncounts** reads the ADC counts by certain pressure. Operation **fluidHeight** calculates the liquid height over the sensor.

3. MO **Timer** represents a timer, which awakes the processor periodically for fluid height measurement. A) Attributes: Attribute **bHaveLastRead** is a Boolean variable, which shows the processor is awakened. Attribute **BigPeriod** shows the working period of the timer, i.e. 50000000ns=50000us. Attribute **PeriodsNumber** represents the number of periods „asleep-awakened“ of the processor for the timer`s period. B) Operations: Operation **UartStdOutnit** initialises the timer`s turn off. Operation **SysTick_Config** calculates the duration of one period of the timer.

4. MO **PreventiveFunction** represents the programmes for testing the fluid height by normal working conditions.

A) Attributes: Attribute **LastRead** represents the value of the last read. Attribute **mmH2O** shows the value of recent reading. Attribute **permissible_delta** represents the allowed difference in mm, i.e. 500mm=50cm. B) Operations: Operation **delta** calculates the difference between the last and the recent reading. Operation **assign_lastRead** assigns the recent reading as the last reading.

5. MO **Result** represents the result after execution of a preventive function. A) Attributes: Attribute **ID** represents the notification number after the preventive function. B) Operations: Operation **printf** writes a notification after the preventive function.

6. MO **AlarmLog** represents log Alarms, containing the collected maintenance events. A) Attributes: Attribute **ID** represents the log number. Attribute **N** represents the log size, i.e. 1000 records. B) Operations: At this stage operations for the log are not defined.

7. MO **AlarmRecord** represents the Alarm reaction, if a failure occurs. A) Attributes: Attribute **ID** represents the alarm number. B) Operations: Operation **printf** writes an alarm in log by exceeding the allowed difference.

8. MO **TestingFunction** represents the testing programmes for detection of failure: 1.Calculation of the counts number by increasing or decreasing the liquid level over the allowed difference. 2. By reaching a crucial level [mm], i.e. 10000mm=10m, visualisation of the decreasing level speed starts. The crucial level in counts is 83. A) Attributes: Attribute **adc_dac_data** shows the liquid level in counts. Attribute **liquid_level** shows the liquid level in mm. Attribute **gravity** shows the earth gravity. Attribute **density_of_water** shows the water density. Attribute **steadyTime** shows the steady time for procedure execution, i.e. 750 000ns=750us. Attribute **leakingTime** shows the time for leaking simulation, i.e. 10000ns=10us. B) Operations: Operation **Pressure** calculates the pressure by the liquid level in mm and earth gravity. Operation **V_{out}** calculates the output voltage by slope, pressure and initial voltage. Operation **ncount** calculates the counts number by output voltage and ADC scale. Operation **liquid_level** calculates leaking 1% every 1us.

9. MO **Localisation** contains information about the counts by which a failure is reported. A) Attributes: Attribute **ID** represents the number of localisation. B) Operations:

Operation

assign adc_compare assigns the next count smaller than the calculated.

Synthesis of operations` methods. 1. fluidHeight

```
Int fluidHeight (int ncounts) {
        /* model for pressure sensor:
          MinPressure = PressureMaximum * sensorOutput_min / sensorOutput_max
          Amplification=ADCrange/sensorOutput_max
          ADCcounts = 2^ADCbit – 1
          ADCfactor = ADCrange/2^ADCbit
          ADCscale = 2^ADCbit/ADCrange
          InterceptVoltageAfterAmplifier = WbridgeIntercept * Amplification
          offset = InterceptVoltageAfterAmplifier * ADCscale
          ActiveADCcounts = ADCcounts – offset
          Slope1 = ActiveADCcounts / pressureMaximum
          Slope2 = Slope1 * ADCfactor
          PressureScale = PressureMaximum / ActiveADCcounts
          Factor = PressureScale / Density_of_water * gravity
        */

        const int offset = 15;
        const int Factor = 148;

        return (ncounts – offset) * Factor;
}
```

2. Timer

```
Int main (void)

{       bHaveLastRead = 0;

       // UART init
        UartStdOutInit ();

        // set SysTick interrupt timer
        SysTick_Config (50000000/10000);

        // go to sleep
        while (1)
                PreventiveFunction ();
        return 0;
}
```

UART is a Universal Asynchronous Receiver-Transmitter. The period of the timer is 5μs.

3. PreventiveFunction. The method for PreventiveFunction combines attributes and operations for the following objects: **PreventiveFunction, Result, AlarmLog и AlarmRecord**.

```
void PreventiveFunction (void) {
        int n_c = ncounts;
        int mmH2O = fluidHeight(n_c);
```

```
        printf ("ADC reports %d count, %d mmH2O\n", n_c, mmH2O);
        if (!bHaveLastRead) {
                bHaveLastRead=1;
                lastRead=mmH2O;
        }
        else { int delta = mmH2O – lastRead;
                if ((delta < -500) II (delta > 500)) {
                        printf ("***\n*** Significant change in fluid level: %d mm, now %d mmH2O\n***\n", delta, mmH2O);
                        lastRead=mmH2O;
                }
        }
}
```

4. TestingFunction. The method TestingFunction unifies the attributes and operations of the following objects: **TestingFunction** и **Localisation**.

```
module TestingFunction (adc_dac_data, adc_compare)

        input [7:0] adc_dac_data;
        output      adc_compare;

        real        liquid_level, pressure, Vout, ncount;

        initial begin
                liquid_level = 10000; //mm

                // hold steady for the first 750 us
                #750000;

                // start leaking 1% every 1us
                forever begin

                liquid_level = liquid_level * 0,99;
                #10000;
                end
        end // initial begin

        always @(liquid_level)
                begin
                  pressure=liquid_level*9,8;
                  Vout=pressure*5,88865.e-6+0,126
                  ncount=Vout*256/2,2
                end

        assign adc_compare = adc_dac_data < ncount;

endmodule // TestingFunction
```

It could be seen that the fluid level falls with 1 m for 10 μs.

Conclusion

The paper represents an algorithm for the design and service of an IoT-sensor. It contains two parts and meets the requirements of designers and service management. The contributions of paper are as follows:

1. The steps of an algorithm for design and simulation of IoT-sensor are defined with high level of detail.
2. The steps of an algorithm for Maintenance Service are defined. An object-oriented method is used. The Managed Objects (MO) classes, organised in hierarchy, are defined. The attribute, operations and methods of classes are defined.
3. In order to be verified, the algorithm is illustrated with a pressure sensor.
4. The integration of two areas is demonstrated– sensor design and service management – by the interaction of steps from both levels.
5. The steps for reusage are developed: within the frame of one level – for design of different kinds of sensors (for temperature, for humidity, for illumination, etc.) or for service in different functional areas (configuration, security, performance etc.); between the two levels – for sensor design and for service design.
6. A scheme for future work with two or more sensors and a multiplexor is proposed.

The future work could be considered in the following aspects:

1. Development of new functional elements – sensors for different environments;
2. Service modelling for the new elements and development of corresponding information models;
3. Modelling of sensor communications and considering sensors as network elements;
4. Integration of IoT with other platforms, i.e. Smart Grid.

References

Baker, J. 2010. *CMOS circuit Design, Layout, and Simulation, 3rd Edition.* Wiley-IEEE; 1208 p.

Bergeron, J. 2012. *Writing Testbenches: Functional Verification of HDL Models (2nd ed.).* Springer.

Ekelof, S. 2001. The Genesis of the Wheatstone Bridge. *Engineering Science and Education Journal, 10*, 1, 37–40.

Fowler, M. 2004. *UML Distilled: A Brief Guide to the Standard Object Modelling Language. 3rd ed.* Addison-Wesley Professional.

Lienig, J., H. Bruemmer. 2017. *Fundamentals of Electronic Systems Design*. Springer International Publishing. p. 1.

Logan, D. L. 2011. *A first course in the finite element method*. Cengage Learning.

Miller, J. 2018. *Proof-of-concept: The day after*. Mentor® A Siemens Business. www.mentor.com

Perera, C., Mahmoud Barhamgi, Supama De, Tim Baarslag, Massimo Vecchio, Kim-Kwang Raymond Choo. 2018. Designing the Sensing as a Service Ecosystem for the Internet of Things. – *Internet of Things Magazine, December 2018, 1,* 2.

Ruh, W. 2018. Drilling Deep into Digital Industrial Transformation will determine who survives and thrives. – *Internet of Things Magazine*, *September 2018*, *1*, 1.

ENERGY CONTROL ON THE LININGS WEAR OF SEMI-AUTOGENOUS MILLS

Rumen Istalianov, Nikolay Lakov

University of Mining and Geology "St. Ivan Rilski", 1700 Sofia; rgi@mgu.bg

ABSTRACT. A method is proposed for determining the linings wear of semi-autogenous mills using data from the load schedule of the electric motor.

Keywords: semi-autogenous drum mill, specific electricity consumption, wear of linings and lifters

ЕНЕРГИЕН КОНТРОЛ ВЪРХУ ИЗНОСВАНЕТО НА ОБЛИЦОВКИТЕ НА ПОЛУАВТОГЕННИ МЕЛНИЦИ

Румен Исталиянов, Николай Лаков

Минно-геоложки университет "Св. Иван Рилски", 1700 София

РЕЗЮМЕ. Предложен е метод за определяне износването на облицовките на полуавтогенни мелници с използване на данните от товаровия график на електрическия двигател.

Ключови думи: полуавтогенна мелница, специфичен разход на електроенергия, износване на облицовки и лифтери

Introduction

The mills are the main consumers of electricity in the ore processing plants. Considering their installed power capacity, each cease in their operation should be minimised.

A major problem is the wear of linings and lifters. Their control is usually performed by a direct measurement (a mechanical one with template patterns and a roulette, and in some cases more advanced methods are used - for example, with 3D scanners). The periodical ceases of operation of these mills for such measurements in practice result in the stopping of the entire production line.

In this article a method of wear control is proposed through its prediction by the indications of the energy control system, namely by measuring average power for a certain period of time. The wear of linings and lifters is not quick, it is a long-time process within the range of several months. Of course, the weight of the material and the weight of the balls, as well as the RPMs, will influence the instrument readings.

Object of investigation

A semi-autogenous drum mill type METSO-SAG 8.5 X 5.3 is studied, shown in Fig. 1. The indications on the figure are as follows:

- 1 - drum;
- 2 - side bottoms;
- 3 - rear sliding bearing;
- 4 - front sliding bearing;
- 6 - engine;
- 9 - reducer;
- 7 - shaft - tooth gear;
- 5 - tooth ring gear;
- 8 - assistant engine with brake (used for the technical maintenance and the repair of the mill).

The driving engine is asynchronous with a dual power supply of 5.4 MW, a stator voltage of 6 kV, and an additional frequency feed to the rotor to allow the control of RPMs.

As Minin has stated in his paper (Minin, 2011), in accordance with the suggested mathematical model, the wear of the linings and the lifters, which increases the inner diameter and the length of the drum, is almost linearly dependent on the amount of the processed ores.

Results and discussion

The records for three years are taken from the data collection. They include:

- data on energy consumption;
- amount of processed ore;
- periods between measurements of linings wear;
- rotation frequency.

The data on linings wear is presented by Minin (Minin, 2013). After the processing of the obtained results, the average weekly power is calculated for the period before the measurement of lifters wear (Table 1).

The number of the drum diameter measurements is averaged to 1-4 times in one month (the measurements are not in precise periods since all ceases for running repairs, emergency stops, etc. are used).

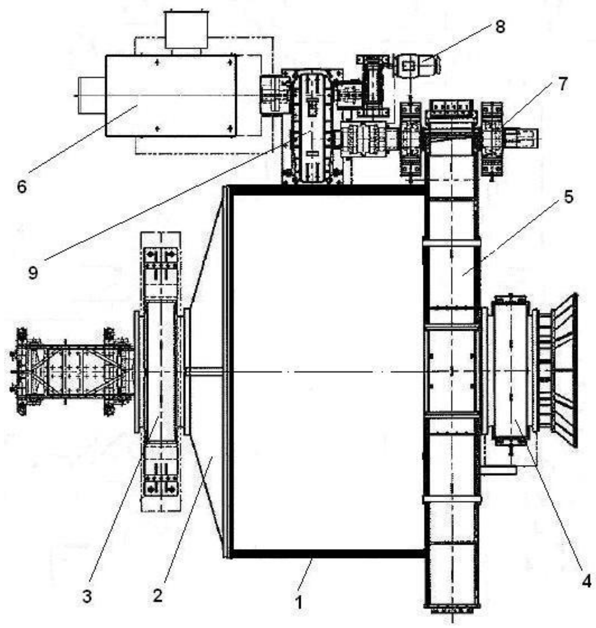

Fig. 1. Overall view of a mill type SAG 8,5 X 5,3

At first sight, the wear of the lifters (made of manganese steel with a density of 7900 kg/m^3), the engine load should be reduced because the grinding media has a lower density (water, steel balls and ore with a density of 3725 kg/m^3) and would fill the volume of worn elements. As Minin has concluded on the basis of his calculations made in (2013), this is exactly the opposite. These conclusions are also confirmed by the results in Table 1 and Figure 2.

Table 1.

№ Of the measure ment	Inner diameter	Average productivity	RPMs	Average power
	m	t/h	min^{-1}	kW
1.	8.268	245	1069.5	4877
2.	8.288	244	1047.7	4991
3.	8.308	243	1052.3	5160
4.	8.334	238	1069	5155
5.	8.354	238	1069	5190
6.	8.374	240	1090	5352
7.	8.385	240	1090.4	5393
8.	8.405	238	1090.6	5383
9.	8.100	255	1069.5	4347
10.	8.120	255	1062.5	4455
11.	8.122	255	1038.3	4616
	8.150	261	1004.3	4669
13.	8.154	261	1004.3	4671
14.	8.150	261	1004.4	4671
15.	8.166	253	1014.4	4833
16.	8.179	254	1014.5	4855
17.	8.186	254	1014.7	4941
18.	8.210	241	1012	5049
19.	8.220	241	1012.9	5060
20.	8.240	241	1013.6	5060
21.	8.250	248	1015.1	5065
22.	8.254	249	1015.3	5065
23.	8.256	249	1015.6	5071
24.	8.257	247	1010.2	5076
25.	8.260	247	1069.5	5049
26.	8.270	247	1011	5092
27.	8.280	248	1011	5173
28.	8.300	231	1017.8	5211
29.	8.330	231	1043.7	5265
30.	8.343	231	1044	5281
31.	8.344	248	1044.2	5319
32.	8.353	248	1017.8	5496
33.	8.390	222	1017.8	5453
34.	8.400	222	1062.6	5493
35.	8.402	222	1062.6	5345
36.	8.100	262	1062.6	4556
37.	8.110	262	1005.3	4613
38.	8.111	262	1005.3	4616
39.	8.120	267	1005.4	4669
40.	8.120	267	951.6	4671
41.	8.122	267	977.4	4671
42.	8.160	262	991.8	4833
43.	8.168	263	963.4	4855
44.	8.169	264	963.3	4941
45.	8.210	253	933.7	5049
46.	8.220	253	971.6	5076
47.	8.222	253	974	5049
48.	8.225	248	964.4	5092
49.	8.230	249	878.6	5173
50.	8.228	250	876	5211
51.	8.260	243	877	5265
52.	8.300	243	1034.5	5281
53.	8.100	272	1033.1	4239

54.	8.110	272	880.6	4347
55.	8.130	272	880.6	4401
56.	8.150	266	879.8	4423
57.	8.159	266	1004.3	4509
58.	8.165	266	1004.2	4715
59.	8.200	258	1004.2	4671
60.	8.221	258	939.6	4833

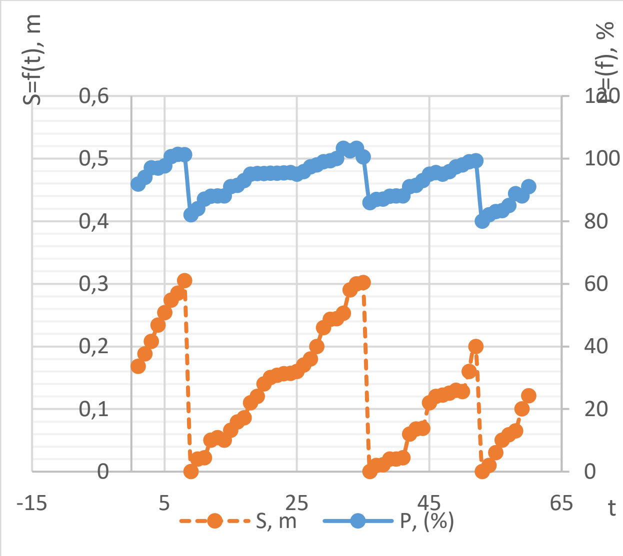

Fig. 2. The dependence of the wear, the average power and the time

The times when the lifters and the linings have been changed could be seen clearly from Figure 2. The electrical power is decreased with about 4% to 7%.

The relation between the electricity consumption and a final product is called a specific power consumption (E). This indicator for semi-autogenous mills has been studied by Hristova (2015). It establishes the dependences between the different factors affecting the specific energy consumption. The methodology for the determination of the lifters replacement period according to the power consumption and the price of processed ore has been proposed by Hristova (2018). In most cases the mining companies prefer to replace the lifters and the linings at a full wear. In our case, the presentation of the specific energy consumption depending on the wear of the lifters in time is presented at Figure 3.

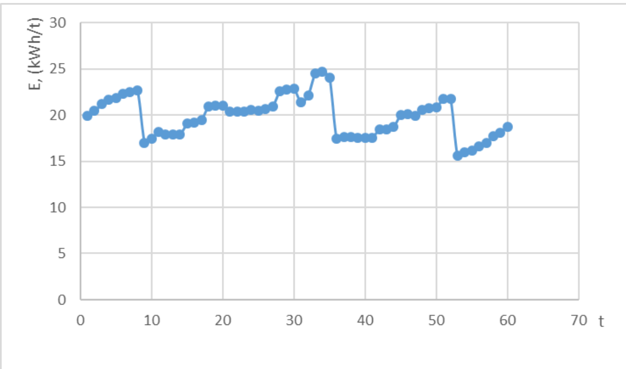

Fig. 3. The dependence of the specific energy consumption on the wear of the lifters in time

Figure 4 shows the relation of the specific electricity consumption to the linings wear.

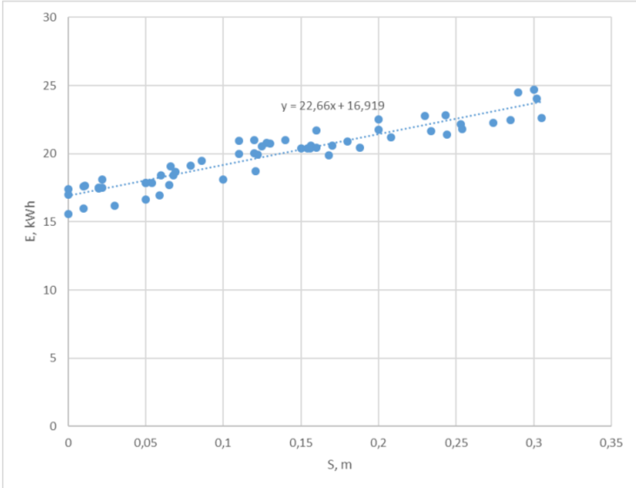

Fig. 4. The dependence of the specific electricity consumption on the linings wear

Conclusion

On the basis of the obtained measurements and results it could be concluded that:

1. It is permissible to control the wear of the lifts of semi-autogenous mills using the readings of the dispatching system.
2. The ceases or stops of the mill can be reduced in order to control the wear.
3. The power averaging time may be longer than the seven days period.
4. The greater interval for averaging will minimise the influence of the variable parameters - water quantity, balls, type of the ore and RPMs of the drum.

References

Hristova, T. 2015. Investigation of specific energy consumption in the sag milling copper ores. − *Annual of the University of Mining and Geology “St. Ivan Rilski”, 58*, III, (in Bulgarian with English abstract).

Hristova, T. 2018. Methodology for determining the replacement period for lifter bars. − *8th International Multidisciplinary Symposium SIMPRO 2018, 11-13 October 2018*, Petroşani, 701−706.

Minin, I. 2013. Determination of the power of tumbling sag mill type sag 8,5 x 5,3 by methods of mathematical statistics. − *Annual of the University of Mining and Geology “St. Ivan Rilski”, 56*, 3, 12−16 (in Bulgarian with English abstract).

Minin, I., A. Yaneva, P. Nedyalkov. 2011. Experimental study of the wear of drum ball mills linings. − *Annual of the University of Mining and Geology “St. Ivan Rilski”, 54*, 3, 99−103 (in Bulgarian with English abstract).

FEATURES OF THE DETERMINATION OF THE OPTIMAL COMPOSITION OF A WIND-SOLAR POWER PLANT WITH DIESEL GENERATORS DURING MULTI-CRITERIAAL SEARCH IN CONDITIONS OF THE RUSSIAN ARCTIC

Alexander Lavrik, Yury Zhukovsky, Aleksandra Buldysko

Saint Petersburg Mining University, 199106 Saint Petersburg; lavrik.alexander@gmail.com

ABSTRACT. The established trend towards decentralisation and the use of renewable energy is reflected in the choice of the composition of the generating complexes in many developed countries. It should be noted that hybrid power plants including two or more renewable sources, as a rule – photovoltaic and wind power plants, become more and more common in the world. Despite the specifics of the development of renewable energy in Russia due to the large reserves of hydrocarbons, such hybrid complexes are relevant also for our country. First of all, their use is advisable to consider in areas where the power supply is traditionally carried out by diesel power plants, working on imported fuel. For Russia, it is primarily the Arctic, the Far East and Siberia. The energy costs of these areas are huge and need to be optimised.

Thus, the issues of determining the optimal composition of autonomous hybrid complexes, consisting of wind generators, solar panels, diesel generators and batteries are an important task, which arises at the design stage of the system.

The article presents the results of a single-purpose optimisation of the composition of a hybrid complex consisting of wind-solar and diesel power plants, according to the criterion of the minimum cost of electricity (COE) for a small settlement in the Arctic. An estimation of the impact of an additional criterion for the total investment cost (TIC) limitation on a result of solving an optimisation problem is given. It is shown that the ratio of the proportions of the solar and wind power is not constant when the TIC changes and it changes when one of the renewable energy sources is excluded from the complex.

Keywords: renewable energy, photovoltaic, wind, power station, optimal composition

ОПРЕДЕЛЯНЕ НА ОПТИМАЛНАТА СТРУКТУРА НА ЕНЕРГИЕН КОМПЛЕКС, СЪСТОЯЩ СЕ ОТ ВЯТЪРНО-СЛЪНЧЕВИ И ДИЗЕЛОВИ ГЕНЕРАТОРИ ЗА УСЛОВИЯТА НА АРКТИЧЕСКИТЕ РАЙОНИ В РУСИЯ, ЧРЕЗ ИЗПОЛЗВАНЕ НА МНОГОКРИТЕРИАЛНО ТЪРСЕНЕ

Александър Лаврик, Юри Жуковски, Александра Булдиско

Санктпетербургски минен университет, 199106 Санкт Петербург

РЕЗЮМЕ. Установената тенденция към децентрализация и използването на възобновяема енергия се отразява при избора на състава на енергийните комплекси в много развити страни. Трябва да се отбележи, че хибридните централи, включващи два или повече възобновяеми източника, като правило - фотоволтаични и вятърни електроцентрали, се срещат все по-често в света. Въпреки спецификата на развитие на възобновяема енергия в Русия поради големите запаси от въглеводороди, такива хибридни комплекси са от значение и за страната ни. На първо място, тяхното използване е препоръчително да се обмисли в райони, в които електроснабдяването традиционно се извършва от дизелови електроцентрали, работещи на вносно гориво. За Русия това са предимно Арктика, Далечният изток и Сибир. Енергийните разходи в тези райони са огромни и трябва да бъдат оптимизирани.

По този начин, въпросите за определяне на оптималния състав на автономни хибридни комплекси, състоящи се от вятърни генератори, слънчеви панели, дизелови генератори и акумулаторни батерии, са актуална и важна задача, която възниква още на етапа на проектиране на системата.

Статията представя резултатите от едноцелева оптимизация на хибриден комплек, състоящ се отвятърно-слънчеви и дизелови електроцентрали, според критерия за минимални разходи за електроенергия за малко населено място в Арктика. Дадена е оценка на въздействието на допълнителен критерий за ограничението на общите инвестиционни разходи върху резултата от решаването на проблем с оптимизацията. Показано е, че съотношението на пропорциите на слънчевата и вятърната енергия не е постоянно, когато критеритерят за ограничение на общите инвестиционни разходи се променя, а той се променя при изключване на един от възобновяемите енергийни източници от комплекса.

Ключови думи: възобновяема енергия, вятър, електроцентрала, оптимален състав

Introduction

The sustainable development of the Arctic, rich in natural, biological and recreational resources, is impossible without creating the appropriate infrastructure, including a reliable and cost-effective power supply system for oil and gas extraction complexes, equipment of main oil and gas pipelines, polar stations, rotation camps, localities. For the Russian Arctic, a relatively new area is the use of renewable energy sources (RES), such as solar and wind energy.

The relevance of the development of renewable energy in the Russian Arctic is due both to the enough potential for solar and wind energy and to the significant material costs and environmental losses when using traditional fuels. And, if it is inappropriate to equip drilling platforms with an installed electrical power up to tens of MW with expensive wind (W) or photovoltaic (PV) power plants, then in the Arctic zone there are quite a few low-power facilities that are currently powered by diesel power plants (DP): particularly, these are small localities, research stations, and rotation camps.

Delivery of essential supplies to the Arctic territories (primarily, food, medicines and petroleum products) is currently carried out through the Northern Supply Haul. Cargo delivery is implemented by rail, air, sea, river and road transport. This, coupled with travel distances and the lack of developed infrastructure, greatly multiplies the cost of goods, placing pressure on the federal budget.

In some cases, such as in the rural locality Lamutskoye in Anadyrsky District of the Chukotka Autonomous Region, the economically feasible cost of 1 kWh is 200 RUB. In 2016, the government allocated about 7 billion dollars at the rate in mid-2016 for the Northern Supply Haul, which amounted to around 2.8% of the expenditure budget for that year.

One of the solutions to reduce economic costs is the use of RES in the Arctic and other energy autonomous regions. At the same time, hybrid wind-solar power plants are becoming increasingly common. Many studies are devoted to study of the optimal composition of autonomous hybrid complexes (Bernal-Agustin at al., 2006; Abdel-Karim at al., 2011; Ayodele and Ogunjuyigbe, 2015), some are carried out by Russian scientists (Marchenko and Solomin, 2016; Popel, 2017; Turovin et al., 2017; Suslov et al., 2018). In the paper (Popel, 2017) the author came to the conclusion that there is a large potential for different kinds of RES in the Arctic.

However, in these and other works, the authors used composition optimisation for plants located in the southern regions of the Earth. At the same time, the use of renewable energy in northern latitudes has its own characteristics that were not noted in the works.

In addition, multi-criteria search seems to be the final decision among the best options for people. It is important to understand how the solution to the optimisation problem changes when additional criteria are taken into account. Thus, the article considers how the optimal composition of a hybrid plant changes when in addition to the cost of generated electricity, an additional limiting criterion is taken into account: initial capital costs.

Characteristics of the Use of PV and W Power Plants in the Arctic

Use of Photovoltaic Plants in the Arctic

Contrary to common belief, the level of solar radiation allows to consider the region as an appropriate place for PV-plants. The map of allocation of average daily values of the direct solar radiation above the Russian Arctic Circle shows, that on average, the regions of the Arctic zone are characterised by a value of direct solar radiation within the range of 2.5-4.5 kWh/m^2/day. In this case, the common criterion for the applicability of PV is the value of annual insolation of 1000 kWh/m2 (Lukutin et al., 2015), corresponding to 2.7 kWh/m^2/day.

It is well known that the duration of light periods throughout the year is identical and it equals the total duration of nights (Popel et al., 2015). In the Arctic, the allocation of these periods has certain peculiarities - if in the equatorial zone the day and night intervals are approximately equal, in the Arctic region most of the light periods occur in the summer when there is full sunlight all day long above the Arctic Circle. It's necessary to consider this natural phenomenon with the geographical location and intended purpose of the complex: for example, the SPS can be very effective when using the complex during the operational season (at meteorological and exploration stations, etc.), even above the Arctic Circle, when the sun does not set below the horizon.

The low temperature, that's typical for the Arctic region, has a positive impact on the efficiency factor of the modules. And the efficiency turns out higher than nominal. The results from the experiment of Serbian researchers show that, in general, the modules work with a higher efficiency in December than in other months (Pantic, 2016).

Essential increase of manufacture of PV-modules is promoted also by radiation reflected by the snow. But it is important to take into account the reduction in production from PV due to snow on the surface of the panels. If necessary, organisational (mechanical snow removal) or technical (for example, the use of special frameless modules[1] shown in Fig. 1,) measures may be applied.

Fig. 1. Experimental PV-panels of the Regional Test Centre in Williston (Vermont, USA) with frameless (foreground) and traditional (in the background) modules for studying the effect of snow on electricity generation and the bearing structure of PV-panels

From a technical point of view, the use of PV-plants in the Arctic is the simplest solution. The key here is the opportunity to construct a plant without moving parts, which greatly simplifies the low-temperature service. The integration of a solar tracking system significantly increases the efficiency of the PV-plant, however, due to large capital costs, such technical solution is not always used in a milder climate, not to mention the Arctic - where this system requires the development of special design solutions, making the construction even more expensive.

In addition, the PV-plant can be located close enough to consumers, because the magnitude of solar insolation does not change abruptly on the ground, in contrast to the wind speed in the case of W-plant.

Use of Wind Plants in the Arctic

In the conditions of the Arctic, the potential of W-plants is noticeably bigger compared to the potential of PV-plants. In most of the Russian Arctic, the average annual wind speed exceeds 5 m/s[2], which is considered to be favourable for the use of wind generation (Lukutin et al., 2015).

The use of W-plants in the Arctic is characterised by the following factors.

[1] How solar panels can thrive in winter weather. [Electronic resource]. Available at: URL: http://poweroverenergy.org/renewables/solar-panels-can-thrive-winter-weather/

[2] Natsionalnyiy atlas Rossii: vetrovoy rejim. [Electronic resource]. URL: национальныйатлас.рф/cd2/172/172.html

Firstly, maximum localisation of W-plant elements is required. A serious problem that has led to the suspending of several promising wind farm projects is the difficult delivery of parts to Russia and their onward transport to the Arctic and the Far East. To some extent, the problem of transport infrastructure is related to this problem. Distance barriers, underdeveloped infrastructure, the absence of specialised equipment in far-flat regions create difficulties in delivery and installation of WPS equipment.

Of course, there are special requirements for W-plants in the Arctic. Lubricants and bearing structures of WPS should be made of low-temperature materials. A reliable and effective system of protection against the action of hurricane winds is necessary in the Arctic and the coastal regions of the Far East. Construction in earthquake-prone areas which have more than 8 points on the MSK-64 scale (the bulk of the coastal areas of the Far East) requires strengthening of bearing structures of WPS, their foundations and power lines. Construction of W-plants of medium and high power (more than 300 kW) is possible only on a pile foundation.

Another problem is the lack of qualified personnel to repair W-plants in far-flat regions.

In addition, in some cases, a refined analysis of the wind potential of a locality may indicate that the W-plants should be located in a place removed from the autonomous consumer, that makes construction irrational due to increasing capital (transmission lines to the consumer, transport infrastructure to the plant) and operational (voltage loss in power lines) costs.

Methods for Optimising the Composition of Hybrid Wind-Solar Power Plants

Existing optimisation methods

Currently, there is a large number of methods for determining the optimal composition of hybrid complexes (Al-Falahi Monaaf at al., 2017): classic (iterative, analytical, graphic, linear), modern (artificial, hybrid), computer (genetic algorithms), etc. Some of them use averaged statistics on the level of insolation, wind speed, daily load, etc.

Some methods, for example, computers, allow to increase the detail of calculations. They involve the use of retrospective data on insolation and wind speed at short intervals (up to every hour of the year), and a set of averaged daily load schedules (Sosnina et al., 2018). Technical and economic parameters are calculated for each period of time throughout the entire period of operation of the hybrid power plant [A1]. The disadvantages of this approach include the need for a large, detailed database of meteorological data for previous years, and the advantages include the possibility of modelling the operation of the complex at any stage of operation, which makes it possible to optimise its modes of operation. Refusal to use a large number of averages can be assessed differently: on one hand, there is a deviation from a statistically verified typical description of weather conditions, on the other, climate change can be taken into account and the probability of using outdated and irrelevant statistical information is generally reduced.

Most of the classical methods use single-purpose optimisation, while more modern methods allow us to determine the optimal composition of the complex based on several criteria.

Method of research

In (Ayodele and Ogunjuyigbe, 2015), the genetic algorithm was used to determine the optimal structure of an autonomous hybrid complex of a PV-W system with DP backup and batteries, and optimisation was carried out according to the criteria of COE, reliability and carbon emissions. On the basis of the mathematical description presented in (Ayodele and Ogunjuyigbe, 2015), the optimal composition of the hybrid system was determined for the selected locality.

The initial data were taken from 12 typical graphs of the electrical load, as well as the hourly values of insolation and wind speed over the last year. In order to simplify the calculations, the values of the array of meteorological data were extended to the entire estimated life of the station according to, the passport of the PV plant - 25 years. The calculation programme was implemented in the MO Excel program and its VBA application. The search for a solution was initially carried out according to the criterion of the lowest COE, which made it possible to use the selection method instead of the more complicated genetic algorithm.

Determination of the Optimal Composition of Wind-Solar Power Plant

Characteristics of the object of study

In the case-study we considered the settlement Nizhneyans in the Yakutia region with a population of about 250 people. The optimal composition of the PV-W power plant with DP was calculated for the urban-type locality of Nizhneyansk.

During the calculation, data about the hourly, monthly averaged, load values in Nizhneyansk in 2016 were used. Thus, 12 typical electrical load curves were taken as a basis. The diagrams of averaged daily loading are characterised by the absence of salient peaks and valleys in electric energy consumption and, in general, correspond to a small settlement with a poorly developed industrial sector. The lowest average value of load per hour is 176 kW (July), the highest is 376 kW (December), the average value of the load per hour during the year was 288 kW. Fig. 2 shows a typical daily load curve for January and July.

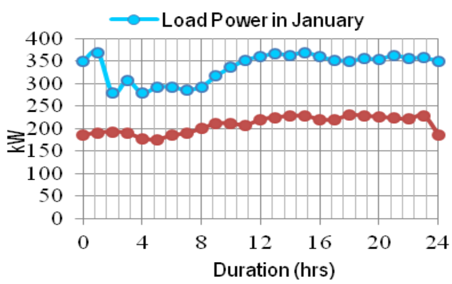

Fig. 2. Typical daily load curve for January and July

Mathematical description of system elements

Solar power plant

Data on hourly wind speeds and solar insolation are taken from the database[3]. For a more detailed analysis, the

[3] Data base Renewables.ninja. [Electronic resource]. Free access: https://www.renewables.ninja, (Date of access 3 June 2019)

meteorological data for all available years should be used, however, in this study, the calculation was made for the life cycle of the HC of PV-W system within 25 years based on data for 2017. The PV modules Quantum KSM 200 were selected as photovoltaic cells for the PV-W system.

The power from the PV module was calculated as

$$P_{pv\_output} = P_{pv\_r} \times H_t \cdot \eta_{pv}, \tag{1}$$

where P_{PV_r} – is the nominal rated power of the module, H_t – is the total solar radiation on a fixed inclined surface, η_{PV} – is the efficiency of the module.

The economic calculation also considers the cost of DC/AC converters required for operation in the PV-W system.

In the course of the calculation, some assumptions were made – for example, the effect of temperature on the power generation of the PV module wasn't taken into account. However, the air temperature averaged over the hourly zone exceeded 20°C only once, reaching 20.4°C. Thus, the decrease in electrical generation by the module due to temperature is negligibly small, since technical parameters of the module are specified by manufacturers of PV modules for air temperature of 20°C.

Fig. 3 shows a diagram of the output power of the PV module for 10 days in the period from 1st to 10th August.

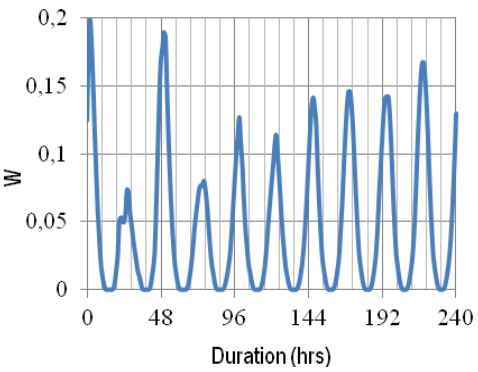

Fig. 3. The output power of the PV module for a 10-days period in August, Kw

Wind power plant

Wind turbine Condor Air WES 380 / 50-50 was chosen as a wind power plant. Fig. 4 shows a diagram of the output power of a wind turbine for 10 days in the period from 1st to 10th August.

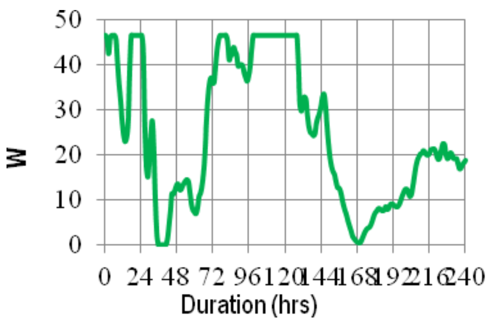

Fig. 4. The output power of the wind turbine for a 10-days interval in August

The power of the wind turbine was calculated using the equation

$$P_w = \begin{cases} 0 & V < V_{ci} \\ P_r \cdot \left(\dfrac{V^3 - V_{ci}^3}{V_r^{\,3} - V_{ci}^3} \right) \cdot \eta_w & V_{ci} < V < V_r \\ P_r \cdot \eta_w & V_r < V < V_{co} \\ 0 & V > V_{co} \end{cases} \tag{2}$$

where V – is the actual wind speed at the height of the tower, V_{ci} – is the initial wind speed (wind turbine switching on), V_{co} – is the limit wind speed (wind turbine switching off), V_r – is the nominal wind speed, P_r – is the nominal wind turbine power; η_{pw} – the electrical efficiency of the wind turbine.

Diesel power plant

In order to ensure reliable power supply to consumers, the total power of a diesel power station was chosen equal to 450 kW, which is almost 20% more than the maximum averaged over the hourly zone power during the year. This margin is required for stable operation of the system.

Usage of several diesel generator sets instead of the big one allows to provide the required level of reliability, and an optimal choice of the nominal rated capacities of the generators - to obtain effective operational factors, as demonstrated in the work [Ogunjuyigbe et al., 2016].

The fuel consumption of DP for a given hour *t* was calculated by the formula:

$$F(t) = \left(0.246 \times E_d(t)\right) + \left(0.08415 \times \frac{P_r}{1\,h}\right), \tag{3}$$

where P_r – is the nominal power of diesel set, kW; *0.246* and *0.08415* – empirical values, taking from (Ayodele and Ogunjuyigbe, 2015), l/kWh; $E_d(t)$ – energy deficit calculated as $E_d(t) = E_{RES}(t) - E_L(t)$, where $E_{RES}(t)$ – electric power from RES at a given hour, $E_L(t)$ – electric power required by consumers and numerically equal load power at a given hour.

Results

The main factors that were used for optimisation during the implementation of the algorithm were certain economic criteria: the cost of electricity (COE) and the related parameter – the life cycle cost (LCC). However, in the process of calculations, other parameters of the complex were also determined - the total investment cost (TIC), carbon dioxide emissions (E_{CO_2}), annual system cost (ASC), dump energy (D).

As a baseline, an optimal configuration without PV-W system was found. Three diesel generator sets have a rated power of 250 kW, 150 kW and 50 kW. Two more types of optimal configurations were determined: DP+W plant and DP+PV plant. Finally, another configuration corresponds to a fully optimal composition and includes DP and PV-W plant. Figure 5 shows the installed capacity in the four options.

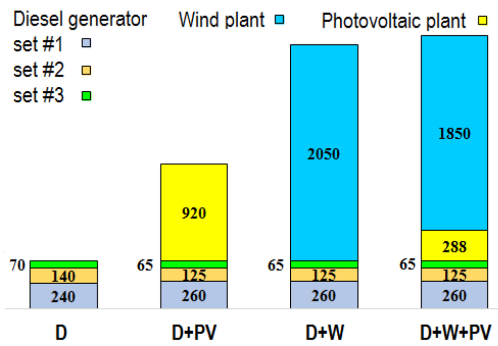

Fig. 5. The installed capacity of four considered configurations

Table 1 shows the cost of electricity (COE).

Table 1. *COE of considered configurations*

	Configurations			
	DP	D+PV plant	D+W plant	D+W+PV plant
COE, rub.	16.58	14.36	7.70	7.51

The main technical and economic parameters of the power plant operation under various configurations are presented in the radar diagram in Fig. 6

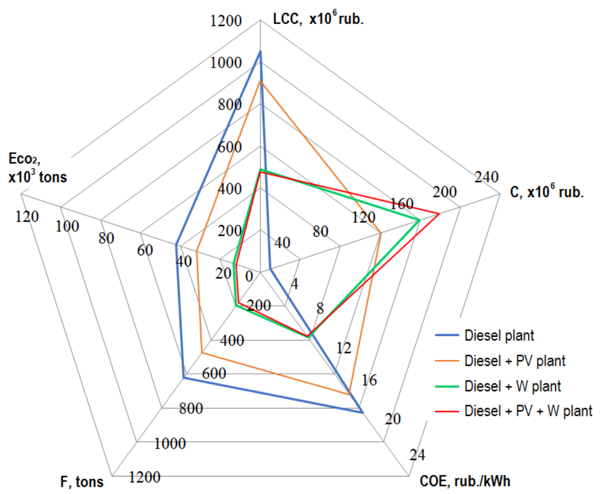

Fig. 6. The main technical and economic parameters of the system operation under considered configurations

The amount of generated electricity in the option #1 is 2533 kWh and it is equal to the demand for electricity. In variants 2-4, energy of dump appears – waste unused energy. In option #4, dump D is large and it is about 55%. However, despite this, the LCC is the smallest in the presence of such a dump value.

On the other hand, a large amount of dump energy can be used for water supplies. According to approximate estimates, the dump energy of about 3.1 million kWh/year is enough to heat 39,400 tons of water from a temperature of 5°C to 70°C. Based on empirical data on the average person's consumption of about 85 litres of hot water per day, this would be enough for hot water supply of more than 1300 people. The population of Nizhneyansk is about 250 people, therefore, dump energy can be used to heat the locality.

Fig. 7 shows the PV-W system behaviour with DPS for 24 hours in May.

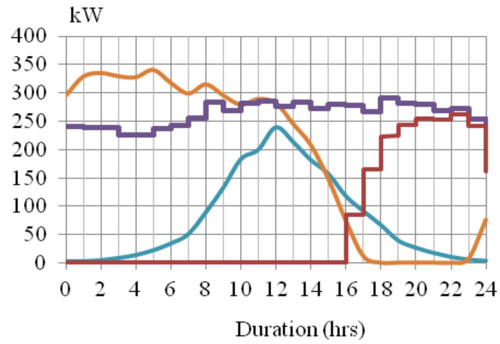

Fig. 7. Demonstration of the work of elements of the HC for 24 hours in May
Curves of generated/consumed power: blue – PV plant, green – W plant, Yellow – load, red – diesel plant

The study also found that the construction of a SPS for a given area is not justified up to a certain level of investment. Fig. 8 shows the dependence of the rate of change of LCC on the level of investment. As indicated in Figure 7, every 1 million rubles invested in W-plant reduce the LCC by approximately 19 million rubles.

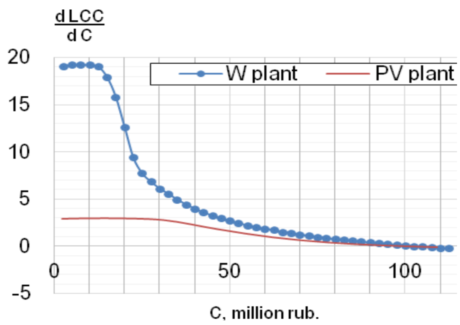

Fig. 8. The dependence of the rate of change of LCC on the level of investment TIC

With the increase in investment, the effect decreases, however, the construction of wind turbines is still preferable to the PV-panels up to a level of investment of about 50 million rubles, which corresponds to 25 wind turbines of the selected capacity. If the investment in the project is 50 million rubles or more, then in order to reduce LCC and COE, it is advisable to include PV-generation in the system. However, beyond the optimal investment point with the optimal configuration found above, LCC and COE begin to grow.

Conclusion

The widespread distribution of wind and solar energy in the Arctic, despite its great potential, is currently constrained by a number of factors. The main problem of using W plants in harsh climatic conditions is reliability – the equipment must be protected from the action of hurricane winds, sudden changes in temperature should be withstood and work should be carried out in conditions of extremely low temperatures. The use of PV plants is limited mainly to the geographical features of the region – with a sufficient level of insolation, on average, there are significant periods of the polar night during the year (up to half a year at the North Pole); However, it is worth noting that the potential of solar energy is still noticeably inferior to the wind one.

At the same time, most of the power supply facilities are located in areas with a milder climate. However, the development of technologies cannot be ignored and as a result of this an increasing number of facilities based on RES appear in the Arctic region.

The construction of the PV-W systems should be carried out based on the latest global trends in the design of such objects. The need for deep reconstruction of many power supply systems of remote low-power consumers in the Russian Arctic due to their low efficiency establishes excellent conditions for creating "from scratch" high-tech and efficient systems with intellectualisation elements.

In the work, the optimal structure and parameters of the D-PV-W plant for the settlement Nizhneyansk of the Yakutia region are determined. An estimation of the impact of an additional criterion for the total investment cost (TIC) limitation on a result of solving an optimisation problem is given. It is shown that the ratio of the proportions of the solar and wind power is not constant when the TIC changes and it changes when one of the renewable energy sources is excluded from the complex.

References

Abdel-Karim, D., M. Ismail, W. Kukhun, M. M. Marwan. 2011. Simulation of a hybrid power system consisting of wind turbine, PV, storage battery and diesel generator: design, optimization and economical evaluation. – *International Journal of Energy Engineering*, 1, 56–61.

Al-Falahi Monaaf, D. A., S. D. G. Jayasinghe, H. Enshaei. 2017. A review on recent size optimisation methodologies for standalone solar and wind hybrid renewable energy system. – *Energy Conversion and Management, 143*, 252–274.

Ayodele, T. R, A. S. O. Ogunjuyigbe. 2015. Increasing household solar energy penetration through load partitioning based on quality of life: the case study of Nigeria. – *Sustainable Cities and Society, 18*, 21–31.

Baza dannyih Renewables. ninja. [Elektronnyiy resurs]. Rejim dostupa: https://www.renewables.ninja, svobodnyiy (in Russian).

Bernal-Agustin, J. L., R. Dufo-Lopez, D. M. Rivas-Ascaso. 2006. Design of isolated hybrid systems minimising costs and pollutant emissions. – *Renewable Energy, 31 (14),* 2227–2244.

Dunikova, D. O., O. S. Popelya. 2018. – Obyedinennyiy institut vyisokih temperatur Rossiyskoy akademii nauk, Moscow, 114–120. (in Russian)

How solar panels can thrive in winter weather. [Electronic resource]. http://poweroverenergy.org/renewables/solar-panels-can-thrive-winter-weather/.

Lukutin, B. V., I. O Muravlëv, I. A. Plotnikov. 2015. *Sistemyi elektrosnabjeniya s vetrovyimi i solnechnyimi elektrostantsiyami: uchebnoe posobie*. Izd-vo TPU. Tomsk, S. 32. (In Russian)

Marchenko, O. V., S. V. Solomin. 2016. Analiz sovmestnogo ispolzovaniya energii solntsa i vetra v sistemah avtonomnogo elektrosnabjeniya. – *Promyishlennaya energetika, 9,* 39– 43 (in Russian).

Natsionalnyiy atlas Rossii: vetrovoy rejim. [Elektronnyiy resurs]. natsionalnyiyatlas.rf/cd2/172/172.html (in Russian).

Ogunjuyigbe, A. S. O., T. R. Ayodele, O. A. Akinola. 2016. Optimal allocation and sizing of PV/Wind/Split-diesel/Battery hybrid energy system for minimising life cycle cost, carbon emission and dump energy of remote residential building. – *Applied Energy, 171,* 153–171.

Pantic, L. S., T. M. Pavlovic, D. D. Milosavljevic. 2016. The assessment of different models to predict solar module temperature, output power and efficiency for Nis, Serbia. – *Energy, 109,* 38–48.

Popel, O. S., S. V. Kiseleva, M. O. Morgunova. 2015. Ispolzovanie vozobnovlyaemyih istochnikov energii dlya energosnabjeniya potrebiteley v Arkticheskoy zone Rossiyskoy Federatsii. – *Arktika: ekologiya i ekonomika*. 1 (17), 67 (in Russian).

Popel, O. S. 2017. Perspektivnyie tehnologii maloy i vozobnovlyaemoy energetiki dlya osvoeniya i razvitiya arkticheskoy zonyi Rossiyskoy Federatsii. – *Gosudarstvennyiy audit. Pravo. Ekonomika,* 1, 44–52 (in Russian).

Sosnina, E. N. 2018. Analiz harakteristik vozobnovlyaemyih istochnikov energii i faktorov vliyayuschih na sebestoimost vyirabotki elektroenergii. *Vozobnovlyaemaya energetika XXI vek: energeticheskaya i ekonomicheskaya effektivnost: materialyi IV Mejdunarodnogo kongressa REENCON-XXI pod red* (in Russian).

Suslov, K. V. 2018. Ispolzovanie vozobnovlyaemyih istochnikov energii dlya pitaniya sobstvennyih nujd nefteprovoda. – *Izvestiya vyisshih uchebnyih zavedeniy. Problemyi energetiki*, *20*, 1-2, 70–79 (in Russian).

Turovin, O. A., E. N. Ognev, A. E. Kochnev. 2017. Primenimost vetro-solnechnoy energetiki v kachestve alternativnogo istochnika elektrosnabjeniya neftyanyih obyektov kompanii. – *PRONEFT. Professionalno o nefti,* 2, 69–74 (In Russian).

A METHOD FOR DIMENSIONING THE LIGHTNING PROTECTION OF PHOTOVOLTAIC MODULES, PLACED ON THE ROOFS OF BUILDINGS

Petar K. Petrov, Georgi Ts. Velev, Krasimir M. Ivanov

Technical University of Gabrovo, 5300 Gabrovo; g.velev@gmail.com

ABSTRACT. The installation of photovoltaic modules on the roofs of buildings is appropriate, but the issue of their protection against the effects of lightning is becoming more and more relevant. The design of lightning protection implies different methodologies and constructive solutions. With static installation of photovoltaic modules, the design approaches used ensure effective protection according to the selected lightning protection level. Some manufacturers offer photovoltaic modules which allow adjustment of optimal vertical alignment to maximise solar radiation use depending on the geographical location and season. In this case, additional design checks and updates are required to guarantee the lightning protection zone.
The paper proposes a methodology, basic analytical dependencies are derived and the sequence of activities to solve the problem are shown.

Keywords: lightning protection, dimensioning, protection zone

МЕТОД ЗА ОРАЗМЕРЯВАНЕ МЪЛНИЕЗАЩИТАТА НА ФОТОВОЛТАИЧНИ МОДУЛИ, РАЗПОЛОЖЕНИ НА ПОКРИВА НА СГРАДИ

Петър К. Петров, Георги Ц. Велев, Красимир М. Иванов
Технически университет, Габрово, 5300 Габрово

РЕЗЮМЕ. Монтирането на фотоволтаични модули на покривите на сгради е удачно, но заедно с това става актуален въпроса за тяхната защита от действието на мълнии. При проектирането на мълниезащитата се използват различни методики и конструктивни решения. При статичен монтаж на фотоволтаичните модули използваните подходи за проектиране гарантират ефективна защита, съобразно избраното ниво на мълниезащита. Някои от фирмите производители предлагат фотоволтаични модули позволяващи завъртане на оптимален ъгъл с цел използване в максимална степен на слънчевата радиация в зависимост от географско разположение и годишен сезон. В този случай се налага да се направят допълнителни проектни проверки и актуализации, имащи отношение към гарантиране на защитната зона.
В тази статия е предложена методика, изведени са основните аналитични зависимости и е показана последователността от действия за решаване на посочения проблем.

Ключови думи: мълниезащита, проектиране, защитна зона

Introduction

During the last decades the use of renewable energy sources, such as sun, wind, tides, thermal springs, etc. has become particularly relevant. Without any doubt, the photovoltaic (PV) systems are the most popular among them, because they can be used not only in industrial companies, but also in everyday life. A number of leading companies (relevant to 2019), such as Trina Solar, Canadian Solar, Jinko Solar, JA Solar etc. develop and offer photovoltaic modules and power inverter equipment for obtaining of sinusoidal voltage, microprocessor control and interconnection with the power grid (website: www.power-technology.com).

Along with the large-scale studies with regard to these systems, the problem for the lightning protection of photovoltaic modules, and electronic power equipment interconnected to them remains completely unresolved.

There are a number of regulations and standards, dealing with lightning protection design of buildings, structures and open-areas, including international standards (IEC 62305-1, 2, 3, 4, 2010) and local Bulgarian regulations (Ordinance № 4 of 22nd December 2010 on the Lightning Protection of Buildings, External Equipment and Open Spaces). All of these regulations do not reflect the fact that the PV modules are tilted in order to efficiently absorb the solar radiation, and often their tilt angle is adjustable.

Another problem is related to the efficiency of grounding systems and the dissipation of lightning current through earth (Stefanov, Hristova and Atanasov, 2009).

The probability of direct lightning strikes is significant, because in most cases photovoltaic panels are placed on the roofs of buildings. This problem is particularly relevant for mountain areas with strong lightning activity.

The development proposed here is indicated to solve some existing problems in the following areas:

- Based on the constructional characteristics and requirements for the installation of photovoltaic systems, a method for protection against the effects of lightning has been offered;
- Analytical expressions have been derived, which can be used at the preliminary design stage ;

- An overall methodical sequence of activities to solve problems with lightning protection by the designer has been proposed.

Special points with regard to the installation of photovoltaic modules on the roofs of buildings

Photovoltaic modules have a rectangular shape with dimensions (***a*** x ***b***, Fig. 1) and are covered by a non-conductive or metal frame. They are mounted statically and are able to rotate in order to optimally absorb solar radiation. Figure 1 shows two variations of their attachment.

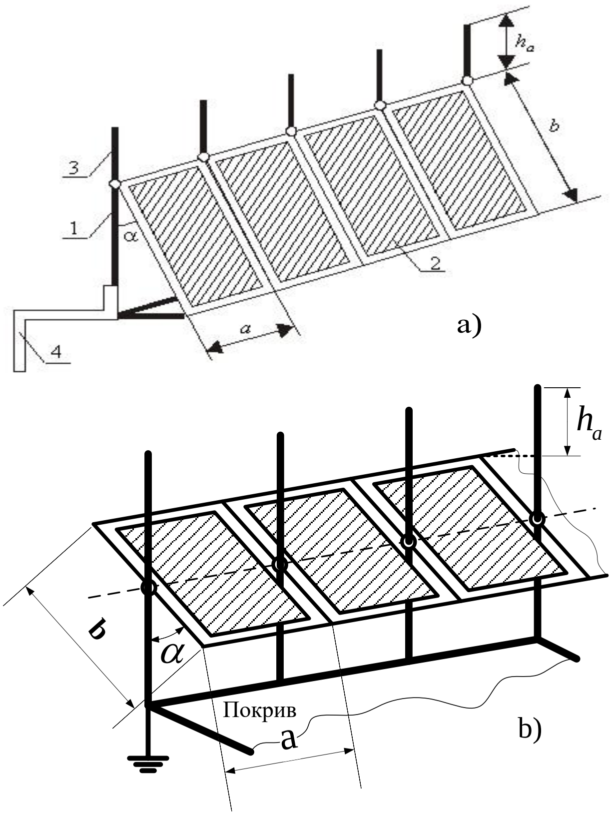

Fig. 1. Alignment of PV modules and installation of the lightning rods, where: a) upper suspension; b) suspension in the middle

The construction from Fig.1 consists of the steel frame 1 on which the PV modules 2 are fixed. In both cases in Fig.1 (upper suspension and suspension in the middle of PVs) rotation and locking of PV modules have been realized at a desired tilt angle. The vertical steel rods 3 are used in order to protect the PV modules against lightning. These rods are mounted on the metal frame by welding. The zinc-plated steel buss-bar 4 connects the metal frame with the grounding system. Using a lightning protection of this type is suitable since the lightning rods create a small and limited shaded area on the modules.

In our case of a lightning protection system, the following input parameters are used for designing needs:

- h_X - building height of the roof, on which the modules are installed;
- Geometric dimensions of the modules (***b*** - height; ***a*** - width);
- α - the maximum angle of tilt rotation relative to the vertical axis.

The main question that a designer should answer is related to defining the lightning rod's active height h_a in order to ensure effective protection of the modules from a direct lightning strike at the selected rotation tilt angle α .

Deriving of basic analytical dependencies needed for the lightning protection design

The protection of PV modules is realized by vertical lightning rods, located on the metal support frame (the connection is made by welding).

The protection area of a vertical lightning rod comprises a tent-shaped volume with a peak at the tip of the lightning rod. The wrapping curve of this volume is described by the equation (Petrov, Venkov, 2002):

$$r_x = \frac{1,6}{1+h_x/h}\left(h-h_x\right) p = \frac{1,6p\cdot h_a}{1+h_x/h} \qquad (1)$$

, where:

h_x – Height of the protected object;

r_x – Radius of the protection zone with a height h_x;

h_a – Active height of the lightning rods;

$h=h_a+h_x$

$p=1$ for $h\leq 30$ m; $p=5,5/\sqrt{h}$ for $h>30$ m

This protection area has been determined experimentally with a reliability of protection up to 0.999. (Valchev, et al., 1980)

Equation (1) can be transformed precisely in relation to the active height h_a for the following cases:

- $p=1$ when $h\leq 30$ m;

$$h_a = \frac{\left(r_x-1,6h_x\right)+\sqrt{2,56h_x^2+9,6h_xr_x+r_x^2}}{3,2} \qquad (2)$$

- $p=5,5/\sqrt{h}$ when $h>30$ m;

$$h_a = \frac{\left(r_x-1,6p\cdot h_x\right)+\sqrt{2,56p^2\cdot h_x^2+9,6p\cdot h_xr_x+r_x^2}}{3,2\cdot p} \qquad (3)$$

, where:

p - Length of the horizontal part of the structure on which the modules are arranged;

In dependencies (2) and (3), the radius of the protection area r_x is selected to be one half of the width of the photovoltaic module i.e. $r_x = \frac{a}{2}$.

Since PV modules are not located tight-close to each other and in order to provide overlapping of their protection areas it is necessary the value of r_x to be increased. For this purpose, we must take into account the length of the horizontal part of the structure on which the modules are arranged ***p*** and their number ***n***:

$$r_x = \frac{p}{2 \cdot n} \tag{4}$$

In dependences (2) and (3) it is necessary to add the height of the modules to the height of the building, i.e.:

$$h'_x = h_b + b \tag{5}$$

Fig. 2 illustrates the maximum allowable rotation angle $\alpha_{\max}$ of PV modules in order to guarantee efficient lightning protection.

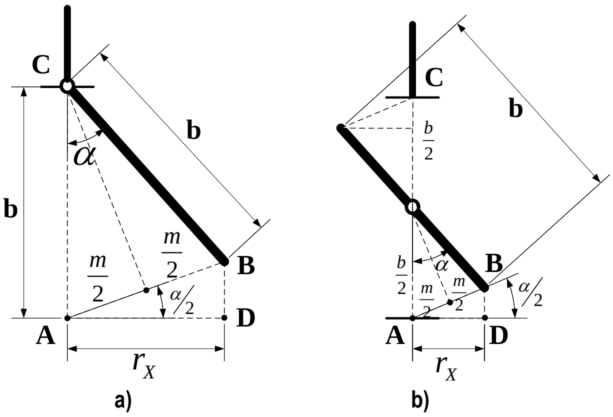

Fig. 2. Principle diagram of modules' rotation for the various cases of suspension, wherein:
a) upper suspension; b) suspension in the middle

For both cases the following analytical relationships are valid:

- For the case of Fig. 2 a) - From triangle ABC it is defined: $m = 2b \cdot \sin\left(\frac{\alpha}{2}\right)$, and from triangle ABD: $r_x = b \cdot \sin(\alpha)$. Then the maximum allowable angle of rotation $\alpha_{\max}$ is obtained as:

$$\alpha_{\max} = \arcsin\left(\frac{r_x}{b}\right) \tag{6}$$

, where $r_x \le b$

- For the case of Fig. 2 b) – Analogically, the maximum allowable angle of rotation $\alpha_{\max}$ is:

$$\alpha_{\max} = \arcsin\left(\frac{2 \cdot r_x}{b}\right) \tag{7}$$

, where $r_x \le \frac{b}{2}$

The obtained analytical expressions (6) and (7) allow the determination of the magnitude of the maximum allowable rotation of PVs $\alpha_{\max}$ for a predefined radius of the protective zone r_x (4).

In case $\alpha_{\max}$ is higher than required, r_x is additionally increased and calculations (6) and (7) are repeated. The final value for the active height of the lightning rod h_a is calculated by (3), where the chosen value for $\alpha_{\max}$ has to satisfy equations (6) and (7).

The protection area of a group of two lightning rods has substantially larger dimensions compared to the single rods' protection areas, taken together.

In our specific case, the lightning protection consists of vertical lightning rods, having the same heights and arranged in one and the same plane. Therefore, it can be concluded that the proposed method for lightning protection design has a significant coefficient of reserve, which guarantees a reliable protection of PV modules.

Example: *On a building roof PV modules are mounted with dimensions respectively: b = 1,5* m*; a = 1,2* m*, the number of modules n = 3 and the length of the support frame p = 4,2 m. The height of the building is* $h_X = 20$ m *.*

The lightning protection design will include the steps:

1) The corrected building height is:
$h'_X = h_X + b = 20 + 1,5 = 21,5$ m
2) The radius of protection area is:
$$r_x = \frac{p}{2 \cdot n} = \frac{4,2}{2 \cdot 3} = 0,7 \text{ m}$$
3) Using (2), the lightning rods active length will be:

$$h_a = \frac{(r_x - 1,6h_x) + \sqrt{2,56h_x^2 + 9,6h_x r_x + r_x^2}}{3,2}$$

$$h_a = \frac{(0,7 - 1,6 \cdot 21,5) + \sqrt{2,56 \cdot 21,5^2 + 9,6 \cdot 0,7 \cdot 21,5 + 0,7^2}}{3,2}$$

$h_a = 0,86 \text{ m} = 86 \text{ cm}$

4) For the maximum allowable rotation the angle $\alpha_{\max}$ is obtained:

- In case of upper suspension via (6):

$$\alpha_{\max} = \arcsin\left(\frac{r_x}{b}\right) = \arcsin\left(\frac{0,7}{1,5}\right) = 27,8°$$

- In case of suspension in the middle via (7):

$$\alpha_{\max} = \arcsin\left(\frac{2 \cdot r_x}{b}\right) = \arcsin\left(\frac{2 \cdot 0,7}{1,5}\right) = 43,03°$$

4) In case when the optimal rotation angle of PV modules exceeds $\alpha_{\max}$ the calculation procedure has to be repeated with a larger value for the protection radius r_x .

Conclusions

The proposed methodology for a lightning protection design of photovoltaic modules can be used in practice. The following conclusions with regard to it can be made:

- The vertical lightning rods appear to be suitable for lightning protection of PV modules located on the roofs of buildings. They are of relatively small dimensions, allowing their installation without extra reinforcement. Most often this is realized by welding. The installed lightning rods do not affect the overall lightning protection of the building;
- When the PV modules are installed with suspension in the middle, the active length of lightning rods is smaller, which

allows larger angles of PV modules' rotation. Therefore, for higher buildings, it is preferable PV modules to be suspended in the middle.

- The proposed methodology is based on derived analytical dependencies for the different variants of suspension of PV modules, allowing the determination not only of the geometric dimensions of the lightning rods, but also the evaluation of the impact of different angles of PV modules rotation.

References

IEC 62305-1 Part 1: Protection of structures against lightning - General principles. 2010.

IEC 62305-2 Part 2: Protection of structures against lightning - Risk management. 2010.

IEC 62305-1 Part 3: Protection of structures against lightning - Protection of structures and people. 2010.

IEC 62305-2 Part 4: Protection of structures against lightning - Electrical and electronic systems within structures. 2010.

Naredba № 4 ot 22 dekemvri 2010 g. za malniezashtitata na sgradi, vanshni saorazhenia i otkriti prostranstva (in Bulgarian).

Petrov, P. K., G. I. Venkov. 2002. Metod za parvonachalna otsenka broya, razpolozhenieto i geometrichnite razmeri na pratovi malniepriemnitsi. – *Mezhdunarodna nauchna konferentsia "Uniteh02",* Gabrovo (in Bulgarian).

Stefanov, S., T. Hristova, L. Atanasov. 2009. Otnositelna platnost na elektricheskia tok sazdaden ot dva raznopolyarni iztochnika na tok (zazemiteli) vav funktsia ot razstoyanieto mezhdu tyah i ot dalbochinata na razprostranenieto na toka v zemiata. – *Annual of the University of Mining and Geology "St. Ivan Rilski", 52*, 123–128 (in Bulgarian).

Valchev, M., et al. 1980. *Tehnika na visokite naprejenia.* PK Tehnika, Sofia (in Bulgarian).

https://www.power-technology.com/features/featurethe-worlds-biggest-solar-photovoltaic-cell-manufacturers-4863800/

EVALUATION OF THE OPPORTUNITIES FOR ELECTRICITY AND HEAT GENERATION FROM GENERATED BIOGAS

Nikolay Savov, Petya Gencheva

University of Mining and Geology "St. Ivan Rilski", 1700 Sofia; nsawow@abv.bg

ABSTRACT. The possibilities for the generation of energy from generated biogas are studied in this article, and the quantities of biowaste that have to be treated are determined. An energy efficiency analysis has been carried out at different bio-waste ratios, whereby the calorific value of the biogas has been assessed. The amount of methane contained therein is determined, as well as that of the other combustible components (including H_2), for the purpose of more efficient heat and electricity generation. The lower calorific value or calorific value for methane is determined which is 36 MJ/m³N (8560 kkal/m³N) or 50 100 kJ/kg or 9.7 kWh/m³N. The average calorific value of biogas is about 18 000 kJ/m³N (4 280 kkalm³N) or 5 kW/m³N. The efficiency coefficient of the cogeneration system is determined. An analysis is made and the results for the annual electricity generation are presented, depending on the annual load of the fermenters.

Keywords: electricity, heat generation, biogas, cogeneration

ОЦЕНКА НА ВЪЗМОЖНОСТИТЕ ЗА ПРОИЗВОДСТВО НА ЕЛЕКТРОЕНЕРГИЯ И ТОПЛОЕНЕРГИЯ ОТ ГЕНЕРИРАНИЯ БИОГАЗ

Николай Савов, Петя Генчева

Минно-геоложки университет "Св. Иван Рилски", 1700 София

РЕЗЮМЕ. В настоящия научен труд са проследени възможностите за производство на енергия от генериран биогаз, като са определени количествата биоотпадъци които подлежът на обработка. Направен е анализ на енергийната ефективност при различни съотношения на биоотпадъците вследствие на което е направена оценка на калоричността на биогаза. Определено е количественото съдържанието на метан в него, определени са и другите горими компоненти (в това число и H_2), с цел по – ефективно генериране на топлинна и електроенергия е определена долната топлина на изгаряне или калоричност за метана, която е 36 MJ/m³N (8560 kkal/m³N) или 50 100 kJ/кг или това са 9.7 kWh/m³N. Средната калоричност на биогаза е около 18 000 kJ/m³N (4 280 kkal/m³N) или 5 kW/m³N. Определен е коефициента на ефективност на когенериращата система. Направен е анализ и са представени резултати за годишно ел. производство в зависимост от годишното натоварване на ферментаторите.

Ключови думи: електроенергия, топлоенергия, биогаз, когенератор

Introduction

Natural decomposition or degradation of organic material results in the production of biogas by microorganisms under anaerobic conditions. Anaerobic digestion converts organic material into biogas, a renewable fuel that could be used to produce electricity, heat, or as vehicle fuel. In recent years, Anaerobic Digestion (AD) of waste and residues from agriculture and industry, municipal organic waste, sewage sludge, etc. has become one of the most attractive ways of generating renewable energy. The energy and climate policies in the EU and the introduction of various support schemes for promoting the utilisation of renewable resources have encouraged the development of biogas plants for energy production. The energy efficiency of different biogas systems, including single and co-digestion of multiple feedstock, different ways of biogas utilisation, and waste-stream management strategies have all been evaluated (Pöschl et al., 2010). The input data were derived from the assessment of the existing biogas systems, present knowledge on the management of anaerobic digestion processes, and technologies for biogas system operating conditions in Germany. The energy balance was evaluated as Primary Energy Input to Output (PEIO) ratio, to assess the process energy efficiency, hence, the potential sustainability. Results indicated that the PEIO corresponded to 10.5–64.0% and 34.1–55.0% for single feedstock digestion and feedstock co-digestion, respectively. The energy balance depended on the biogas yield, the utilisation efficiency, and the energy value of the intended fossil fuel substitution. For example, the obtained results suggest that the upgrading of biogas to biomethane for injection into the natural gas network potentially increased the primary energy input for biogas utilisation by up to 100%; also, the energy efficiency of the biogas system improved by up to 65% when natural gas was substituted instead of using electricity. Energy balances have been analysed from a life-cycle perspective for biogas systems based on 8 different raw materials. The analysis was based on published data and relates to Swedish conditions. The results show that the energy input into the biogas systems (i.e. large-scale biogas plants) corresponds to 20–40% (on average, to approximately 30%) of the energy content in the biogas produced. Large variations exist in energy efficiency among the biogas systems studied. These variations depend both on the properties of the raw materials studied and on the system design and the allocation methods chosen. The net energy output from biogas systems based on raw materials that have high water content and low biogas yield (e.g. manure) is relatively low. When energy-demanding handling of the raw materials is required, the energy input increases significantly. For instance, in a ley crop-based biogas system, the ley cropping alone corresponds to approximately 40% of the energy input. Overall, the operation of the biogas plant is the most energy-demanding process, corresponding to 40–80% of the energy input into the systems. Thus, the results are substantially affected by the assumptions made about the allocation of a plant's entire energy demand among raw materials, e.g. regarding the biogas yield or the need of additional water for dilution (Berglund et al., 2006). From the point of view of the application, what is unfavourable for the internal combustion engines (ICE) operating on biogas instead of on natural gas, is hydrogen sulphide and moisture. These ingredients are due to the way biogas is formed and are inevitable. This also determines the need for equipment and technologies to reduce emissions. Concentration of hydrogen sulphide depends on the type of waste and the time of biogas formation, i.e. these factors cannot be influenced. In the bioreactor, the timing of creating biogas conditions for the generation of biogas is about 21 days. Moisture removal will use a cycle equipped with heating.

Energy capacity (calorific value) of biogas

The calorific value of biogas is determined by the content of methane in it. Other combustible components (including H_2) are in small quantities and do not affect its calorific value. According to the literature and observations of such installations, the biogas composition is given in Table 1.

Table 1. *Average composition of biogas*

NAME	GAS	v/v percent
Methane	CH_4	54
Carbon dioxide	CO_2	42
Ammonium	NH_3	3
Others		1

Lower combustion heat, or calorific value, for methane is 36 MJ/m^{3}N (8,560 kkal/m^{3}N) or 50,100 kJ/kg or 9.7 kWh/m^{3}N.

Therefore, the calorific value of biogas is about 18,000 kJ//m^{3}N (4,280 kkal/m^{3}N) or 5 kW/m^{3}N.

The specific weight of the individual components of biogas is:

• methane 0.716 kg/m^{3}N

• carbon dioxide 1.93 kg/m^{3}N

When using anaerobic plants for biodegradable waste, the biogas process is limited to a few-week cycle. This is due to the fact that technologically favourable conditions are created for the biogas generation from biodegradable waste. This produces biogas quantities that are controlled and utilised. The most common way of doing so is the combined generation of electricity and heat. For the implementation of this technology, a system is necessary for the separate collection of biodegradable waste, as well as an anaerobic installation developed in which to generate biogas from the collected biodegradable waste.

From an energy point of view, the biogas from anaerobic plants is a renewable energy source (RES). This means that its use as a primary energy source is a priority. Undoubtedly, the generation and use of biogas from waste brings significant benefits. Despite the obvious benefits to society, it is very important to determine the exact capacity of the installation and the choice of technology, respectively.

The most common way to exploit the biogas generated in bioreactors and used to generate electricity is provided by the following:

□ Spark ignition ICE;

□ Generator;

□ Cooling and heat recovery system;

□ Increasing transformer;

□ Connection to the electricity distribution system.

The difference between the cogeneration scheme and that for the generation only of electricity is that in the latter case, the released heat is taken to the atmosphere.

This recovery scheme has the following advantages:

- It is implemented directly next to the biogas source, i.e. there is no gas transport at a distance;
- Easy transmission and low-loss electricity;
- Small running costs.

The drawbacks of this method are limited to the more difficult realization of the excess heat (especially in summer periods).

Quantity of biodegradable waste

In the analysis, only the biodegradable waste is considered that can be used as feedstock in an anaerobic treatment plant for biodegradable municipal waste - from food, paper, and green waste. Other biodegradable waste exists, such as that classified as wood waste whose biogas potential for anaerobic digestion is greater, yet the degradation process time is much larger and also, it cannot be used in bioreactors (fomenters) without pre-treatment.

Table 2. *Amount of biodegradable waste by municipalities used as feedstock for the anaerobic installation*

		Ruse	Vetovo	Ivanovo	Slivo pole	Tutrakan	TOTAL
Nutritional	t/y	4536	114	367	257	434	5708
Gardening	t/y	6142	289	771	714	392	8308
Timber	t/y	571	19	43	114	40	787
Paper and cardboard	t/y	1147	27	82	45	86	1387
TOTAL	t/y	12396	449	1262	1130	952	16190

For the period 2023-2050, the average value of biodegradable waste collected separately and fed to the anaerobic installation will be 17,206 t/y; for the first 10 years of operation it will be 17,045 t/y with a maximum of 17,845 t/y.

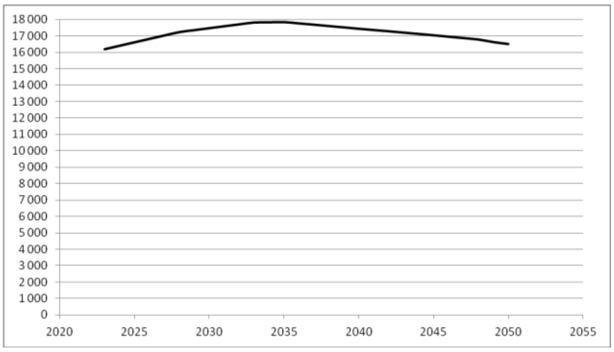

Fig. 1. Quantities of biodegradable CBT fed to the anaerobic plant in t/y

Regarding the seasonality of biodegradable waste, Fig. 2 illustrates the change of the individual components by seasons.

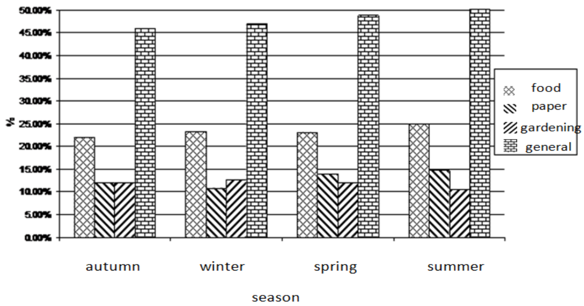

Fig. 2. Seasonality of biodegradable waste

There is an obvious seasonality of waste which is easy to explain. For this reason, the design of the plant should allow it to operate over a wide load range, with a minimum capacity of 30%.

Figure 3 shows the main flows in the adopted flow diagram according to the requirements of the "National Technical Requirements for Biodegradable Anaerobic Biodegradation Facilities (Guidance on Good Practices)".

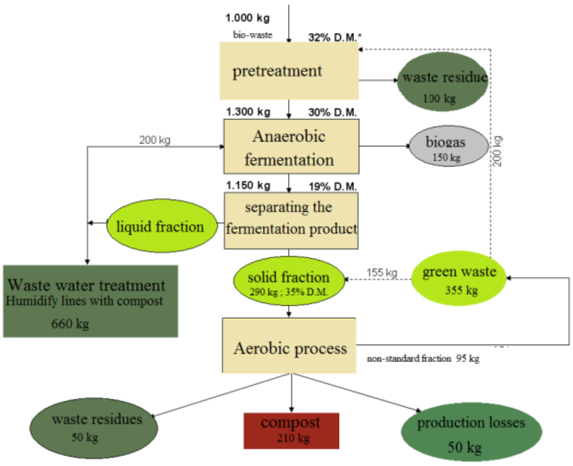

Fig. 3. Material balance of the technology for dry, continuous fermentation of biodegradable waste

From the data presented, the following capacity of the anaerobic installation for biodegradable waste collected separately can be determined.

□ Maximum installation capacity - 17,845 t/y;

□ Maximum capacity of biodegradable waste to fermenters - 13,934 t/y;

□ Type of installation - modular with 3 fermenters, dry type;

□ Capacity of 1 digester/fermenter - 6,040 t/y;

□ Operating range of the installation - from 30% to 100% of the maximum load;

□ Permissible waste: Biodegradable collected separately - food, paper and cardboard, green, garden.

To accelerate the biodegradation processes, especially for the slowly degradable components, primary treatment of the incoming material will be carried out in order to eliminate the retarding action of the cellulose on the biodegradation process.

Before the material enters the fermenter, it undergoes ultrasonic treatment (US). The purpose of this operation is the easier degradation of the cellulose and other constituents of the waste and, accordingly, the increase of the biogas yield.

Using ultrasound is another bio-waste pre-treatment technology that has not been used in anaerobic bioreactors so far. With wave frequencies above 20 kHz, cavitation and destruction of microbial cell walls is induced in the liquid. This leads to an increase in the yield of biogas of up to 25%. The substrate thus obtained is transported to the bioreactor where mesophilic or anaerobic fermentation is carried out at a temperature not exceeding 35-37° Celsius.

Figure 4 illustrates the principle of operation of ultrasound waste treatment.

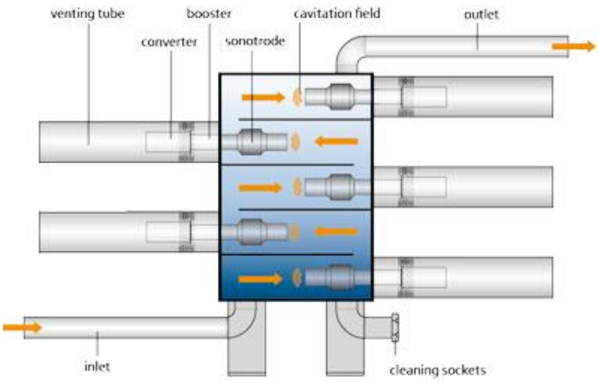

Fig. 4. Principle of operation of US waste treatment

In addition, the material that has undergone US treatment has the following advantages:

• Reduced viscosity of the material; therefore, less technical water needs to be added, which reduces the transport costs and the volume it occupies in the fermenter;

• Increased methane yield by up to 10%;

• Increased concentration of methane by 1-2%.

The expected effect of the use of US is an increase in the generated electricity and heat by about 12%, while reducing electricity costs for transporting bio-waste and for separating the liquid from the solid fraction of the fermentation product.

The energy consumption for the US treatment of a cubic meter of waste is 4 kWh/m^3.

The resulting biogas is a function of the amount of waste that is fed to bioreactors.

Figures 5 and 6 illustrate the various technological diagrams.

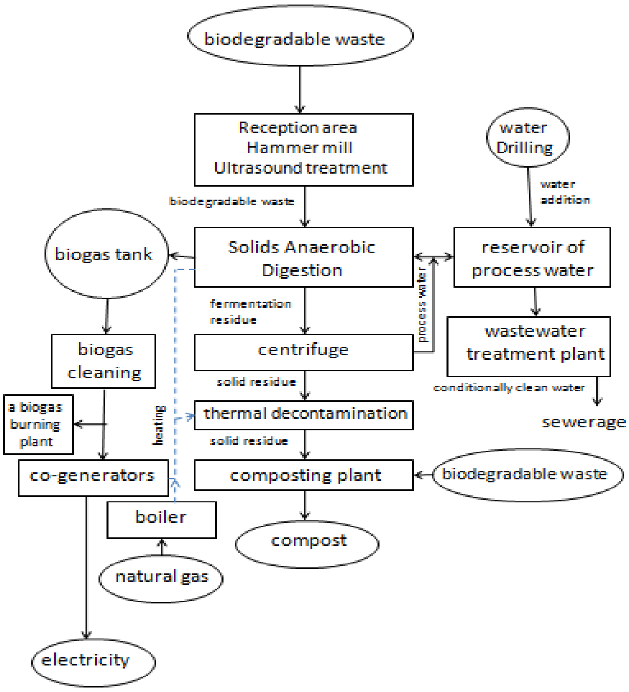

Fig. 5. Technological diagram of an anaerobic facility with one fermenter and one co- generator

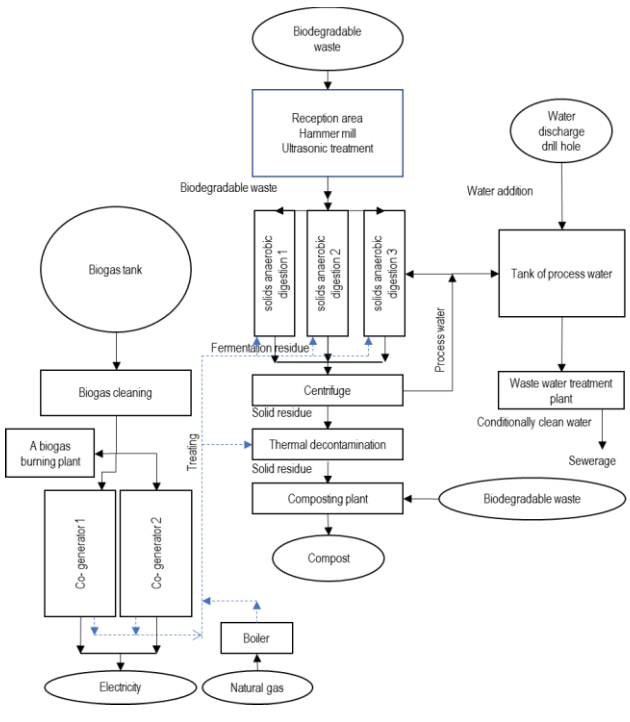

Fig. 6. Technological scheme of an anaerobic facility with three fermenters and two co-generators

Selection of bioreactors

With regard to bioreactors

An analysis has been carried out of the similar installations existing in Bulgaria and a literature reference has been made for such installations in the EU countries.

Installations with one bioreactor have advantages at constant amounts and composition of the feedstock due to the relatively more compact overall facility. The deficiencies of anaerobic facilities with one bioreactor are significant because any maintenance action, fermenter repair or a compromised mixture means stopping the anaerobic process, and the cycle to restore the biogas production is about a month long; therefore, the amount of unprocessed biogas is significant; respectively, the non-generated electricity, plus the additional costs of natural gas for heating and maintaining the temperature in the bioreactor. In other words, from the operational point of view, each stop of the anaerobic installation from being able to generate biogas, respectively electricity and revenues from its realization and at the same time the additional costs of natural gas within one month. Another feature of single bioreactor plants is that much of the equipment needs to be reserved.

With regard to multiple bioreactor plants

The proposal is for the anaerobic installation to be with three bioreactors, each with a capacity of 1/3 of the total load. What are the benefits of this scheme? The use of the anaerobic installation is significantly more flexible because, due to different seasonal loads, the installation will be able to work with one, two or three fermenters, depending on the available raw material. This allows organising and performing maintenance and repairs of the fermenters to be carried out without disturbing the production of biogas. In the installation with three fermenters, even if a problem arises in one of the reactors, that is associated either with the equipment or with the mixture, the production biogas will be, in the worst case, about 2/3 of the nominal one and will not necessitate natural gas supply. In other words, there will be no period when the installation will not generate revenues. The following table presents the comparison of the two variants of electricity sales revenues for a period of one year with a single bioreactor shutdown.

Table 4. *Comparison of variants with one and three bioreactors with one hypothetical reactor shutdown in a given year*

		1 bioreactor	3 bioreactors
Amount of biowaste to bioreactors	t/y	12000	12000
WITHOUT bioreactor shutdowns			
Generated biogas	m^3/y	1365181	1365181
Electricity produced	kWh/y	3559518	3559518
Revenue from electricity	BGN	833248	833248
With ONE bioreactor shutdown			
Generated biogas	m^3/y	1023886	1296922
Electricity produced	kWh/y	2669639	3381542
Revenue from electricity	BGN	624936	791585
Decrease in revenue	BGN	208312	41662
Decrease in revenue	%	25%	5%

Table 5. *Comparative table of variants with one bioreactor and with three bioreactors*

№	Criterion	1 Bioreactor	3 Bioreactors
1	Amount of the investment	36244774.25 BGN	31517195.00 BGN
2	Staff costs per shift per year	306800.00 BGN	306800.00 BGN
3	Capacity of the installation	17845 t/y	17845 t/y
4	Electricity produced, kWh/r	2669639	3381542
5	Minimum amount of bio-waste required	5500 t/y	5500 t/y
6	Installation time after emergency repairs	1 month	0 month
7	Time to restart the installation	2 months	0 month
8	Revenue from electricity	624936.00 BGN	791585.00 BGN
9	Service shutdown - times per year	1	0

From the table above, it is clear that the 3-bioreactor option is the one that is appropriate, both in terms of maintenance and service.

Selection of generating modules

The main consideration for choosing the number of generators is that they should be able to provide a continuous generation of electricity. The generators can operate at a mode of 50 to 110% of the nominal load. In addition, this kind of generators usually operates up to 7,000 hours/year. The other option is used for maintenance and repairs. In other words, with the right choice of power of the generator, the maximum utilisation of the works can be achieved. It should be noted that the seasonality of collected biodegradable waste is determined by the different amount of biogas to be generated. The practice of choosing such type of power equipment is to select one generator that has a rated output of 35-40% of the total load, and another one that has 60-65%.

From the examined alternative technologies, a conclusion is drawn that the Rousse anaerobic installation will be constructed with three bioreactors, each of which having a capacity of 1/3 of the maximum, and with two generators, one at about 40% and the other at about 60% of the nominal value of the one offered by the manufacturers.

Efficiency / efficiency ratio

Spark-ignition ICE is used as an engine.

The efficiency in the generation of energy is the efficiency obtained by the flywheel of an ICE multiplied by the efficiency of the generator. Generally, an ICE has better electrical efficiency than gas turbines, especially for small capacities. It depends on the type of ICE used.

The presented study is based on the data provided by the major manufacturers of such equipment: GE Jenbacher - Austria, Tedom - Czech Republic, Accorroni - Italy and ENER G - Great Britain.

The electrical efficiency of the generating installations depends on the power of the engine and is shown in Figure 7.

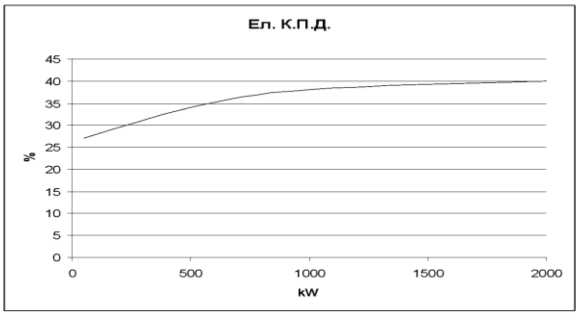

Fig. 7. Efficiency ratio of generators with Otto engines

The efficiency factor ranges from 27% for low-power plants, normally reaching 34-36% for those with a power output of 500 to 1000 kW.

If the system is co-generating, the thermal efficiency ratio is usually about 1/3 greater than the electrical efficiency. The total efficiency factor (thermal + electric) is about 80-85%. For the purposes of the preliminary analysis, an average electrical efficiency ratio of 28% and a thermal efficiency of 52% can be adopted. The efficiency factor of the generator should be taken into account, which can be assumed as 96% for the purposes of this analysis.

From the calculations made on the basis of the forecast data on the biowaste entering the installation, the extraction of biogas and methane at different installation loads has been obtained and is given in Table 6.

Table 6. *Methane obtained at different installation loads*

		Waste to fermenters - t/y				
GAS	dimension	2,500	5,000	7,500	10,000	12,000
CH_4	%	53.89%	53.89%	53.89%	53.89%	53.89%
CO_2	%	41.75%	41.75%	41.75%	41.75%	41.75%
NH_3	%	4.29%	4.29%	4.29%	4.29%	4.29%
H_2S	%	0.07%	0.07%	0.07%	0.07%	0.07%
CH_4	Nm^3	28441	56882	853238	113765	136518

Based on the data in the table, the energy indicators of the generated biogas and the installed generation capacities are set and are presented in Table 7.

Table 7. *Generated biogas and installed generating capacity*

Parameters of the generated biogas	value	dimension
Methane - at a nominal load of the fermenters of 12000 t/yr.	1365181	m^3/y
Energy capacity of the biogas	13242256	kWh/y
Annual usability of the installation	8760	h
Heat output received	1512	kWh
Theoretical installed power	406	kW

Selection of the type of equipment for electricity generation

It is recommended to install two modules in order to exploit the resulting biogas under a different load of anaerobic installations with capacities of:

• 150 kW;

• 250 kW.

or a total installed power of 400 kW.

The considerations for this choice are as follows:

□ The biogas flow is not constant and depends on the load of the installation, etc.;

□ Each co-generation unit can operate within the range of 50 to 110% of the nominal load. With the chosen configuration, it can cover a working range of 75 to 440 kW.

The theoretical quantities of electricity generated, depending on the annual load of the fermenters, are shown below.

Table 8. *Annual electricity production at different installation loads*

Biowaste	Electric energy
t/yr	KWh
2500	741566
5000	1,483132
7500	2224699
10000	2966265
12000	3559518

The produced electricity is bought at preferential prices, determined by the State Agency of Energy Regulations, and is part of the group of renewable energy sources (RES).

Electrotechnical part

The development of the project will meet the requirements of Ordinance No. 3 on the Layout of Electrical Systems and Power Lines of 2004. The electrical part covers the following types of installations and facilities to ensure the normal operation of the facility:

- External power supply;
- Area lighting;
- Power supply to all technological consumers;
- Internal electrical installations in the building - motor, lighting and earthing;
- Lightning protection of buildings and facilities.

With respect to the security of the power supply, the object falls into the third category.

Power supply

It is planned to build new 20/0.4kV switchgear, which will be located at a suitable place. The required electrical power for the site lighting will be about 610 kW, which means that the power of the switchgear should be 630 kVA. The 20/0.4kV switchgear will consist of the following devices:

- 20kV Distribution system. This will be built with switchgear cabinets and the number of 20 kV cable cabinets will be determined by the power distribution company, cabinet measurement and cabinet for protection of a 20/0.4kV power transformer; 630kVA. The cabinets will be equipped with electric switches, current and voltage transformers, high-power fuses, and electronic protections;
- 20/0.4kVA Power transformer. The transformer will be dry, located in a separate room with natural ventilation. Grounding of the star centre of the power transformer will be provided by means of a grounding system made of two rods of 60/60/6mm galvanised steel bridges and a 40/4mm galvanised steel bus.

External 20kV power supply

The 20kV external power supply will be executed in compliance with the requirements of the local power distribution company. Three single-core cables type CXekt - 20 kV will be laid to the CTS (complete transformer station). The cable cross section will be determined according to the current load and to the resistance under short-circuit conditions.

Conclusion

A three bioreactors system is proposed for the production of energy from generated biogas. An analysis of the composition and quantities of bio-waste has been made, their effectiveness at different bio-waste ratios, and a biogas calorific value is subsequently assessed. The amount of methane in the biogas is determined as well as other combustible components (including H_2) in order to more efficiently generate heat and electricity. The average calorific value of the biogas is about 18 000 kJ / m^3N (4 280 kkal / m^3N) or 5 kW / m^3N. The coefficient of efficiency of the cogeneration system is determined. An analysis is made and the results for annual electricity production are presented, depending on the annual load of the fermenters.

References

Berglund, M., P. Börjesson. 2006. Assessment of energy performance in the life-cycle of biogas production. – *Biomass and Bioenergy, 30*, 3, 254–266.

Pöschl, M., Sh. Ward, P. Owende. 2010. Evaluation of energy efficiency of various biogas production and utilization pathways. – *Applied Energy, 87*, 11, 3305–3321.

LABORATORY TESTS OF AN INSULATION MONITORING DEVICE

Radi Tenev

Kardzhali Branch of the University of Mining and Geology "St. Ivan Rilski" - Sofia, 6600 Kardzhali; raditenev@abv.bg

ABSTRACT. The IT system is safe only in the presence of an insulation monitoring device which monitors the level of insulation resistance and turns off the voltage, if it is lowered below a pre-set value. The Insulation Monitoring Device ensures the safety of a person in contact with a live conductive part only, if it is triggered at the moment and switches off the voltage. That is why, time response is an important parameter of the device.
This article examines the response time of an apparatus in laboratory conditions. The operation of the device in a three-phase network is presented. Statistically, the most common electrical injury from is the when is a person is in contact with a live conductive part. The resulting single-phase leakage is described for the three possible cases: with a small network length or negligible capacity, with a large network length or high capacity and operating the device together with a compensator, that reduces the capacitive leakage current.
The experiments were carried out with an insulation monitoring device, which was made on universal board with electronic components

Keywords: IT system, Insulation Monitoring Device, Insulation resistance.

ЛАБОРАТОРНИ ИЗСЛЕДВАНИЯ НА АПАРАТ ЗА КОНТРОЛ НА ИЗОЛАЦИЯТА

Ради Тенев
Филиал Кърджали на Минно-геоложки университет "Св. Иван Рилски" – София, 6600 Кърджали

РЕЗЮМЕ. Мрежата с изолиран звезден център е безопасна само при наличието на апарат за контрол на изолацията, който следи нивото на изолационното съпротивление и изключва напрежението, ако то се понижи под предварително зададена стойност. Апаратът за контрол на изолацията осигурява безопасност на човек допрял се до тоководеща част единствено, ако се задейства на момента и изключи напрежението. Ето защо времето за което сработи апарата е основен параметър.
Статията разглежда определянето на бързодействието на апарата в лабораторни условия. Показана е работата на устройството в трифазна мрежа. Статистически най-често срещаното поражение от електрически ток е допир на човек до тоководеща част. Получената еднофазна утечка е експериментирана при трите възможни случая: при малка дължина на мрежата или незначителен капацитет, при голяма дължина на мрежата или наличие на голям капацитет и работа на устройството съвместно с компенсатор, който намаля капацитивния ток на утечка.
Експериментите са проведени с апарат за контрол на изолацията, който е събран на универсални платки и е изпълнен изцяло с електронни компоненти.

Ключови думи: мрежа с изолиран звезден център, апарат за контрол на изолацията, изолационно съпротивление

Introduction

The task of an insulation monitoring device is to shut down the controlled network voltage when its insulation resistance drops below a pre-set value. The most common electrical injury is when a person is in contact with a live conductive part. This is single–phase leakage for the IT network, and the less time the current passes through the person, the smaller the risk of injury. It is assumed that the body resistance is about 1 kΩ and the response time of an insulation monitoring device is regulated according to BDS 10880-83 (Table 1).

Table 1. *Response time according to BDS*

Nominal network voltage [V]	Response time [s], not more than
To 1000	0.1

Exposition

The device is connected to a 220 V network. To determine the performance of the device the circuit shown in Fig. 1 is used. The timer uses a pulse counter МЭС-54. The device system is vibrational with a polarised relay acting as a drive unit. When the AC current flows through the polarised relay, the anchor of the electromagnet starts to vibrate between the poles of a permanent magnet at 50 Hz. The anchor of the electromagnet is connected to an axis that actuates the gearing drive mechanism. Before the measurement, the counter is reset. When the instrument is turned off, the arrows are read. The big arrow shows the tenths and hundredths of a second, the small arrow shows the seconds. If the measurement is carried out at a frequency other than 50 Hz, a correction should be made according to the formula:

$$t = \frac{t_1 50}{f} \quad (1)$$

where: t_1 - the indication of the instrument;

f - is the frequency of the network under which the measurement is performed.

A drawback of the network diagram thus realized is a certain increase in the measurement error at the expense of the inertia of the transformer, which is an inductive element of the circuit.

Technical characteristics of the МЭС-54 counter:

- reading error, not more than 0.1% of the reading;
- coil resistance of the МЭС-54 2200 plus minus 220 Ω counter;
- electric insulation strength 500 V;
- insulation resistance of not less than 20 MΩ;
- pulse count МЭС-54 starts counting the pulses at power +6 V.

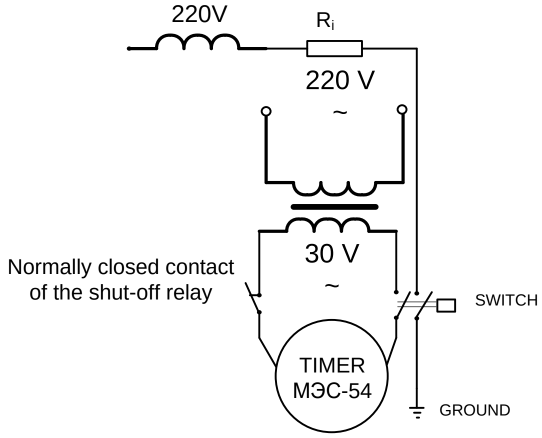

Fig. 1. Connection scheme of the МЭС-54 counter to measure performance

The counter is powered by an AC voltage of 30 V, which is produced by a transformer. The normally closed contact of the relay and the double switch are connected to the counter. One contact of the open switch is connected to the voltage source, in this case the transformer and the counter, respectively. The second contact is connected to the network that is being controlled and ground. When the circuits is closed, a low insulation resistance is simulated and the counter begins counting from that moment, the isolation monitoring device is triggered, the relay switches on, and the normally closed contact interrupts the operation of the counter. Time is reported. The following data were obtained from the experiment (Table 2).

Table 2. *Response time of the apparatus*

Insulation resistance, R_F	Response time [ms]
40 kΩ	200
30 kΩ	140
20 kΩ	120
10 kΩ	90

Operating the device in a three-phase network. Laboratory tests

The device is plugged into a three-phase network to test its functional capabilities. A dangerous event exemplifying the touching of a person to a live conductive part is simulated with a resistor with a value of 1000 Ω. Statistically, this is the most common case of injury and represents a one-phase leak to ground.

The current flowing through the human body can be considered as being composed of two components: I_a - active current determined by the insulating resistance of the phases of the network and the capacitive component I_c. Capacitive leakage current develops because any two conductors separated in space have a certain amount of capacitance between them. The electrical capacity of the network depends linearly on its length or on an average of 1 km of network, the capacity of each phase on earth is approximately 1 μF. According to the BDS, the insulation control devices operating in a three-phase IT network must be equipped with a compensating device. The principle of compensation is illustrated in Fig. 2. A choke coil is used whose inductance is sized relative to the network to which the apparatus is connected.

It is assumed $r1 = r2 = r3 = \infty$. If a person touches one of the phases of the network, the current that passes through his body is determined by the total capacity of the network C and the inductance L of the compensating choke coil which is connected to the neutral point of the secondary winding of the power transformer T. The total current passing through the man is the geometric sum of the capacitance current and the inductive current.

$$\dot{I}_h = \dot{I}_c + \dot{I}_L \tag{2}$$

To fully compensate the capacitive current it is necessary:

$$\dot{I}_C + \dot{I}_L = 0 \tag{3}$$

A condition for this is the current resonance:

$$\omega C = \frac{1}{\omega L} \tag{4}$$

In this case, the currents have a phase difference of 180 degrees and as a result the current through the human body is I_h=0. The condition I_h=0 is purely theoretical. Due to losses in the coils there is always some capacitive current that is not compensated (Fig. 2c). In practice, the total current passing through a person in contact with a live conductive part, is a geometric sum of the active, capacitive and inductive currents.

$$\dot{I}_h = \dot{I}_a + \dot{I}_c + \dot{I}_L \tag{5}$$

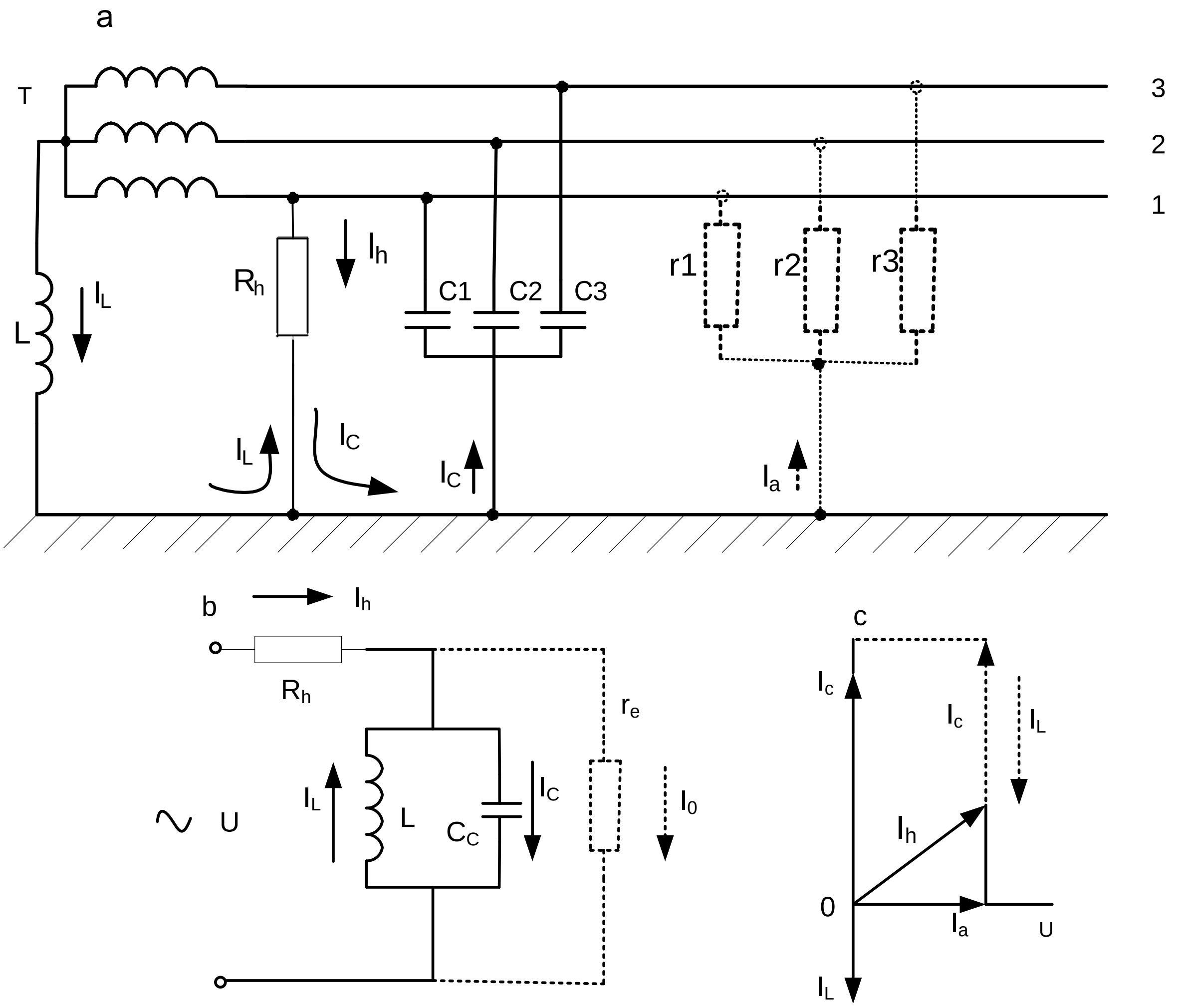

Fig. 2. Capacity compensation principle: (a) network scheme: (b) substitution scheme (c) vector flow diagram

To limit the capacitive current when changing the network capacity, it is necessary to change the inductance of the choke so that the residual current is minimal.

Experiment Description

In the experiments three identical divided coils were used. The following scheme (Fig. 3) is applied to measure their inductance.

The active resistance of the windings is measured by an ohmmeter. The network voltage measured by a voltmeter showed 225 V. The data are given in Table 3.

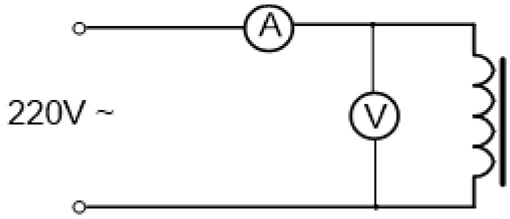

Fig. 3. Determination of coil inductance by ammeter and voltmeter method

Table 3. *Choke coil parameters and the corresponding capacity that compensates*

R [Ω]	I [mA]	$Z = \frac{U}{I}$ [Ω]	$X_L = \sqrt{Z^2 - R^2}$ [Ω]	L [H]	C [μF]
441	40	5625	5608	18	0.567
345	65	3460	3443	11	0.925
260	115	1956	1939	6	1.64
225	150	1500	1483	5	2.15

To measure the current passing through a person in contact with a live conductive part, the circuit shown in Fig. 4 is used. The insulation monitoring device is connected to a three phase network through a 200 kΩ limiting resistor. The body resistance is simulated with R_h. In series with R_h an ammeter is connected to measure the current.

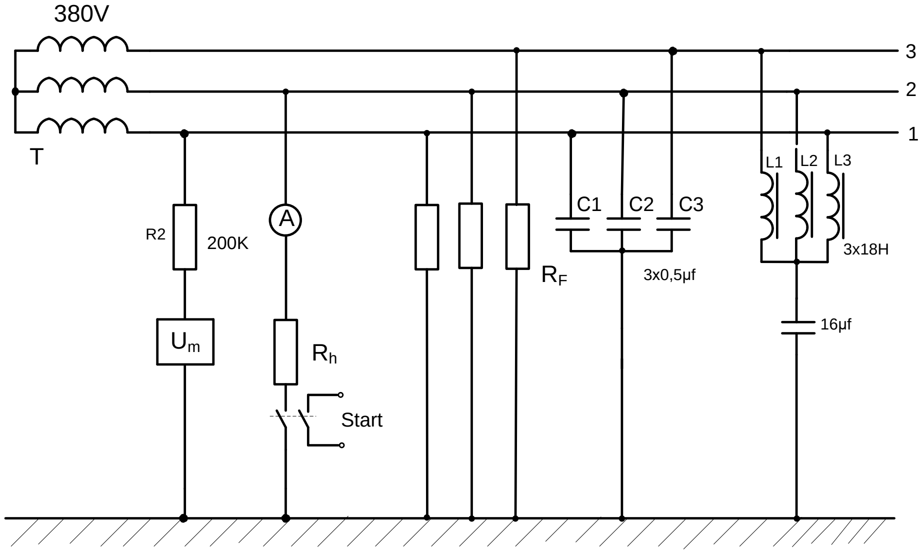

Fig. 4. A scheme that determines the current through the person

When the IT network is of a small length, the capacity of the network may be disregarded. The current passing through a person in contact with a live conductive part is determined only by the active resistance of the network. The value of R_h = 1000 Ω, in this case simulates the body resistance. In this measurement, the components C1, C2, C3 as well as L1, L2, L3 are not included in the network.

The second measurement was carried out with three connected capacitors, one for each phase with a capacity of 0,5 μF. In this case capacitors carry capacitive conductivity and the scheme simulates a network with a long length (a network of significant capacity).

In the third measurement, three chokes with an inductance of 18 H, one for each phase, whose purpose is to compensate for the capacitive conductivity of the network, are added to this scheme. The data are tabulated in Table 4. An increase in current through the R_h resistance is seen when the capacitors that introduce capacitive conductivity are added to the circuit. In the presence of inductance coupled in parallel to the capacitors, the current through R_h decreases as the currents through the capacitor and the inductance are in antiphase. Full compensation of the capacitive component of the current is virtually impossible due to losses in the core and windings of the coils.

Table 4. *Current through a person*

Insulation resistance [kΩ]	40	30	20
Not count the capacitive current [mA]	26	35	49
Taking into account the capacitive current [mA]	154	165	150
With compensation [mA]	62	64	78

Determining response time

Fig. 5 is a schematic diagram for determining the performance of the apparatus when it is connected to a three-phase network. The reported data is shown in Table 5.

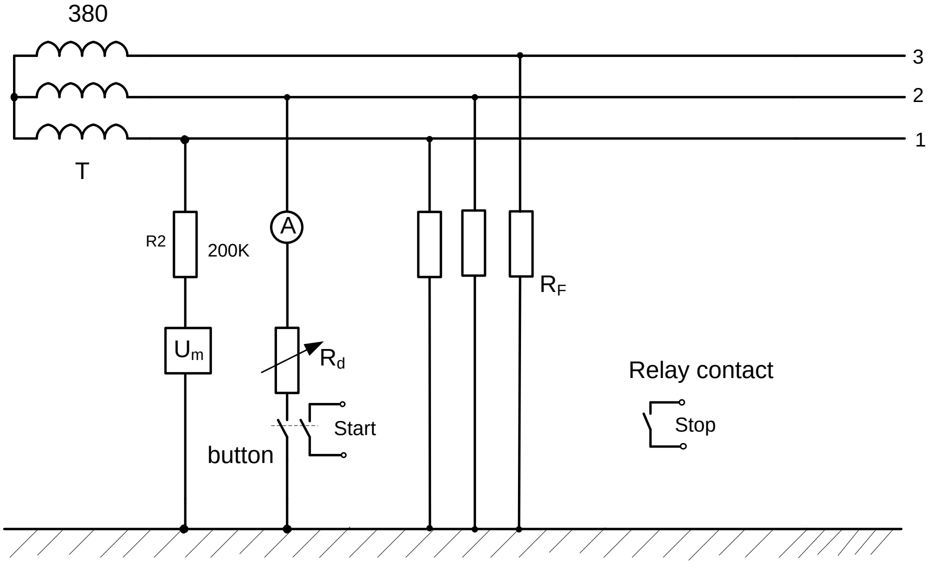

Fig. 5. Determining response time

Table 5. *Response time at different insulation resistance values*

Rd [kΩ]	40	30	20	10	1
ΔT [ms]	150	150	120	110	95

For the determination of the response time, an interval meter is used - L23. The change of R_d simulate a single-phase leakage at different values of the insulation resistance. The double button gives earth to one phase through the corresponding resistor (single-phase leakage) and simultaneously includes the interval meter.

The normally open contact of the relay closes the meter at intervals. The data obtained are shown in Table 5.

When changing the insulation resistance, with its decrease, the time for triggering the apparatus also decreases.

Conclusion

The experiments were carried out with an insulation monitoring device that was assembled on universal boards and made entirely of electronic components, which allows for a device with a small mass and gauge. With single-phase leakage of 1 kΩ (simulation of a person in contact with a live conductive part), the device fits into BDS 10880-83 regarding trigger time. When connected to a three-phase network, the device works successfully with a compensator.

Acknowledgements. The paper was implemented with the support of Research Project FK-018 / 11.03.2019 of UMG "St. Ivan Rilski" - Sofia.

References

BDS 10800-83. 1983. Suoruzeniya electricheski rudnichni. Aparati za zashtita ot tokove na utechka za mrezhi na naprezeniya do 1200 V s izoliran zvezden tsentur. Sofia, (in Bulgarian).

Kolosyuk, V. P. 1980. *Zashcitnoe otklyucheniye rudnichnykh elektroustanovok*. Nedra, Moscow (in Russian).

IMPROVING THE RELIABILITY OF POWER SUPPLY OF INDUSTRIAL ENTERPRISES THROUGH THE APPLICATION OF HYBRID ENERGY STORAGE DEVICES

Oleg Vasilkov

Saint Petersburg Mining University, 199106 Saint Petersburg; s175070@stud.spmi.ru

ABSTRACT. The article presents a comparative analysis of various types of energy storage devices, considers the possibility of using a hybrid energy storage device as a compensator of short-term oscillations of active power. The features of the joint use of batteries and supercapacitors are presented. A simulation model of a hybrid energy storage device was built to evaluate the efficiency of sharing and determining the applications of such storage devices.

Keywords: supercapacitor, battery, hybrid energy storage system

ПОДОБРЯВАНЕ НА НАДЕЖДНОСТТА НА ЕЛЕКТРОСНАБДЯВАНЕТО НА ПРОМИШЛЕНО ПРЕДПРИЯТИЕ ЧРЕЗ ИЗПОЛЗВАНЕ НА ХИБРИДНИ УСТРОЙСТВА ЗА СЪХРАНЕНИЕ НА ЕЛЕКТРОЕНЕРГИЯТА

Олег Василков

Санктпетербургски минен университет, 199106 Санкт Петербург

РЕЗЮМЕ. Статията представя сравнителен анализ на различни видове устройства за съхранение на енергия, разглежда възможността за използване на хибридно устройство за съхранение на енергия като компенсатор на кратки трептения на активната мощност. Представени са характеристиките на съвместната употреба на акумулаторни батерии и суперкондензатори. Създаден е симулационен модел на хибридно устройство за съхранение на енергия, за да се оцени ефективността на споделянето и определянето на приложенията на такива устройства за съхранение.

Ключови думи: суперкондензатор, акумулаторна батерия, хибридни устройства за съхранение на електроенергия

Introduction

The most significant indicator of the quality of electricity, which occurs when there is a sudden decrease in the voltage of the electric network below 0.9 Unom (Unom – rated voltage) – is a voltage failure. After the failure, the voltage is restored to the initial or close level after a certain period of time - from 10 ms to several tens of seconds. Its reduction can vary from 10 to 100% of the nominal. A voltage drops of 100% can be considered as a short-term power interruption. Failures are the most critical emergency violations. They lead to shutdowns and overloading of electrical equipment and electricity consumers.

The easiest way to protect sensitive processes from failures is installation of energy-intensive storage between energy sources and the consumer.

Comparative analysis of energy storages

So far, a wide range of drives has been created. They are built on different principles, differing both in technical and economic indicators as well as in functional purpose. Among these devices, batteries should be distinguished. The analysis of the data of energy storage devices is presented in Table 1.

Table 1. *Characteristics of various types of batteries*

	Capacity of one element, A*h	Energy density, W*h / kg	Number of cycles charge / discharge	Allowable charge temp. range,°C	Allowable discharge temp. range,°C
Lead Acid	26–3000	30–60	200–1200	-20–50	-20–50
Li-ion	40–800	80–160	700–3000	0–45	-20–60
NiCd	10–1100	45–80	1500	0–45	-20–65
Ni-NaCl	40–200	140–190	3000–7000	0–45	-20–65
NiMH	0,3–7	60–120	300–500	0–45	-20–65

The disadvantages of lithium-ion and nickel-cadmium batteries are the high cost and service life, which directly depend on the number and nature of the charge-discharge cycles in operation. These are the most widely used storage devices for industrial energy. Exactly these characteristics are the main limiting factors in the widespread use of electric power storage devices. Devices based on fully controlled semiconductor devices, such as dynamic voltage distortion compensator or static reactive power compensator (STATCOM), are widely used.

There is another limiting factor of battery application, namely the response time of the drive. The response time of the batteries is up to 60 ms according to the Electric Power Research Institute, USA. This factor can have a significant impact when choosing a power storage device, as for some technological processes power outages even at 20 ms are critical.

However, supercapacitors (SC) practically lack the above-mentioned disadvantages. The distinctive features of supercapacitors are their ability to quickly charge an unlimited number of times and discharge over time from a few milliseconds to tens of minutes, giving high power to the load. The disadvantages and limiting factors of SC application are the relatively low energy density and the high self-discharge. It is also worth noting that the response time of the SC is from 1 μs. More detailed characteristics of the SC are presented in Table 2.

Given these factors, it is currently promising to use the battery in conjunction with the SC to compensate for the shortcomings and combine the advantages and to create a hybrid energy storage system (HESS).

Table 2. *Characteristics of supercapacitors*

	Capacity of one element, kF	Energy density, W*h / kg	Number of cycles charge / discharge	Allowable charge temp. range,°C	Allowable discharge temp. range,°C
SC	0.5–12	1–10	>500 000	-40–65	-40–65

Simulation model of hybrid energy storage

The present study developed a simplified model of hybridisation of a battery and a supercapacitor, presented in Figure 1.

This model involves a lithium-ion battery and a block of capacitors with the appropriate characteristics. The simulation did not take into account the temperature effect and the aging effect of batteries. Battery self-discharge is not presented.

The Boost and Buck/Boost converter model is shown in Figure 2.

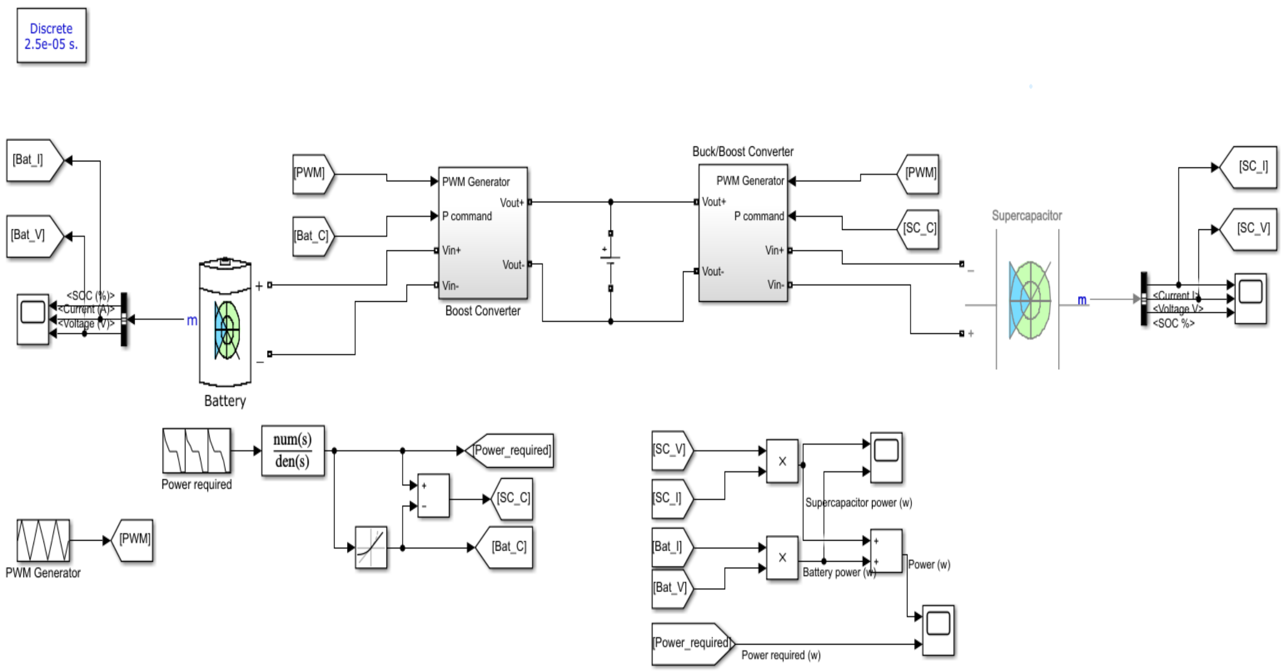

Fig. 1. Battery and supercapacitor hybridisation model

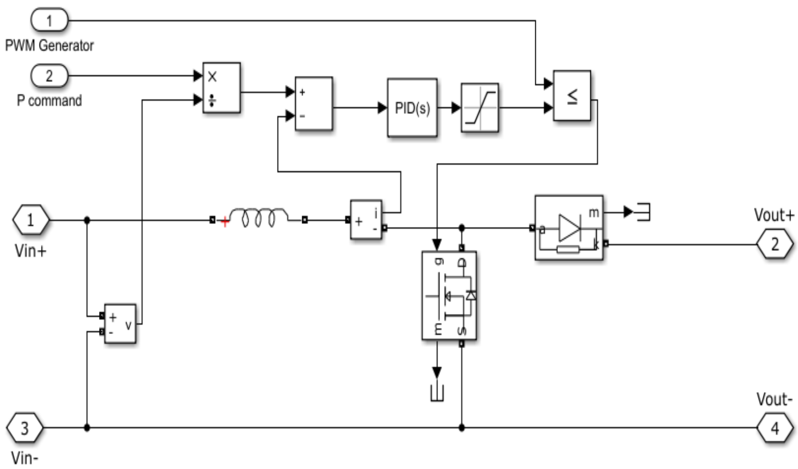

a)

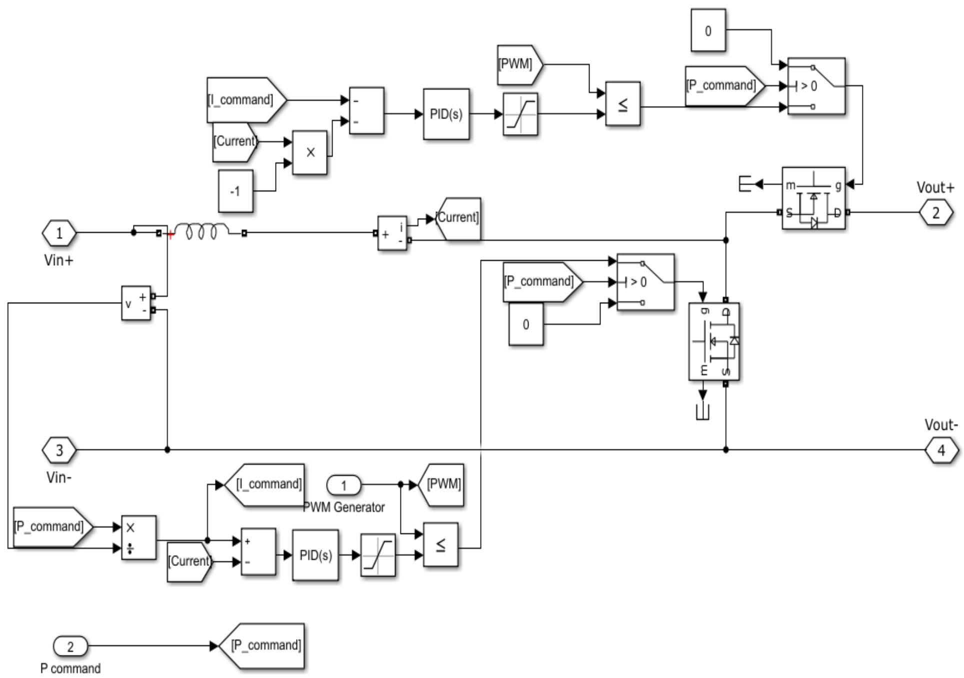

b)

Fig. 2. a) the Boost converter model; b) The Buck/Boost converter model

Using the simulation, the following results were obtained (Figure 3):

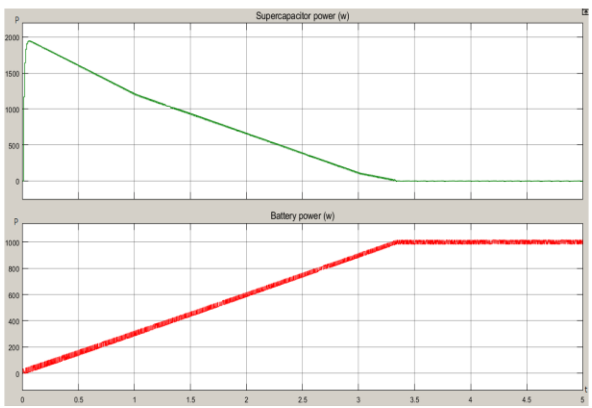

Fig. 3. The graph of the power generated by the battery and the block of supercapacitors

After analysing the data dependencies, the differences in the nature of the power output to the network were noted. Since the feature of the SC is a fast discharge with a large amount of power output to the network, it is logical to use this drive to compensate for peak loads. Rechargeable batteries are inherently slow to discharge, gradually giving power to the network, which will allow compensation for long-term power dips. It is also worth noting the increase in the life cycle of batteries by reducing the impact of peak loads when used together with supercapacitors.

Figure 4 below shows the graph of the power supplied to the network by the hybrid energy storage.

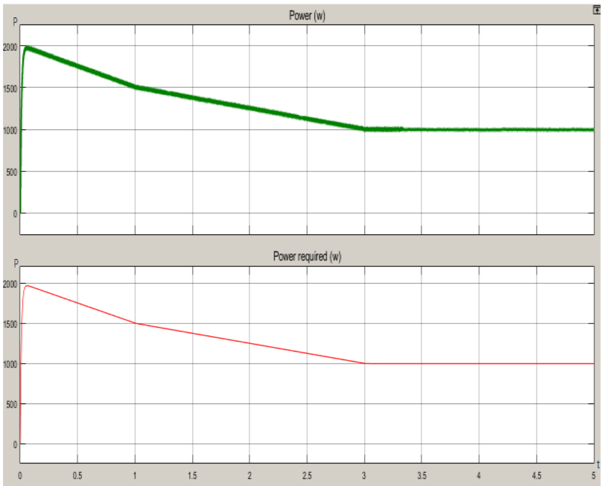

Fig. 4. The graph of the power generated by the hybrid energy storage system

Conclusions

Based on the obtained results, it is possible to conclude that joint application of batteries and blocks of supercapacitors can perform a number of important functions:

- alignment of load graphs in the network;
- damping of short-term oscillations of active and reactive power and frequency;
- ensuring uninterrupted power supply of substations and especially responsible consumers;
- ensuring stable and sustainable operation of decentralised and non-traditional sources operating both autonomously and as part of a unified power supply system.

However, a number of issues that are not addressed in the article remain, namely, when creating hybrid energy storage devices, the issue of balancing the SC remains relevant [8]. As it is known, due to the low rated voltage of supercapacitors, the use occurs when they are connected in series. In the production of supercapacitors there is some variation in the parameters of the capacitance. In this regard, the problem arises from the different charge rates of supercapacitors, since there is a probability of overcharging the supercapacitor, which can cause its breakdown. There is a need to limit the voltage of the supercapacitor when charging. It is also necessary to take into account that the electric power output to the load from the storage device is carried out under the condition that the electric power quality parameters are observed. This requires solving the issue of electromagnetic compatibility of objects with regard to their economic efficiency.

Acknowledgments. This research has been conducted with the financial support of the Russian Science Foundation (project No. 18-79-00127).

References

Bakhteev, K. 2017. The use of power storage to prevent short-term power interruption. – *"Youth and the XXI century – 2017": Mat. VII International Youth Scientific Conference, Kursk.* 4, 216–219.

Berdnikov, R., V. Fortov, E. Son, K. Delshchikov, A. Zhuk, N. Novikov, Yu. Shakaryan. 2013. Hybrid power storage for UNEG based on accumulators and supercapacitors. – *Energy of a unified network,* 2 (7), 41–51.

Razuvaev, Yu. Yu., M. Yu. Chayka, V. V. Agupov, V. S. Gorshkov, D. E. Silyutin. 2011. Features of active voltage balancing of supercapacitors. – *Bulletin of the Voronezh State Technical University*, Publishing house of Voronezh State Technical University, Voronezh, 85–88.

Zhezhelenko, I. V. 2014. *Electricity quality indicators and their control at industrial enterprises*. Energoatomizdat, Moscow, 167 p. (in Russian)

LIGHTING SYSTEM FOR STUDYING PLANT GROWTH

Svetlana Velinova

University of Mining and Geology "St. Ivan Rilski", 1700 Sofia; svetliv@mail.bg

ABSTRACT. The cultivation of plants on artificial light has gained special popularity in recent years. On one hand, it is economically advantageous for places with low sunshine - in the winter months or in places above the 50th parallel. Even in the conditions of our country, in the winter it is economically advantageous to grow some plants on artificial light. On the other hand, it is also relevant to the growing of plants in space - for longer stays outside the Earth where, besides providing oxygen, cosmonauts will need vegetation as a food and an environmental factor.

It is well known that plant photosynthesis has maximum effectiveness in irradiation with blue and red light. In order to investigate which part of the spectrum of visible light has the greatest impact on the growth and development of plants, the Scientific and Research Laboratory (SRL) "Lighting Equipment" at the University of Mining and Geology "St. Ivan Rilski" a specialised lighting system was created. It is an improved version and a functional extension of the lighting system from 2015. It consists of 7 cabins with dimensions 600x600x1250mm, illuminated by LED modules, each radiating in a narrow range of the visible spectrum. The cabin sizes are suitable for plant growing and full life cycle research, which includes biomass in addition to qualitative indicators such as colour, smell, taste, etc. With the help of the newly created lighting system, the influence of light of different wavelengths on the effectiveness of photosynthesis can be investigated. Research will allow plants to grow under artificial light with minimal energy consumption.

Keywords: LED, photosynthesis, photosynthetic active radiation (PAR), growth of plants, light spectrum

ОСВЕТИТЕЛНА УРЕДБА ЗА ИЗСЛЕДВАНЕ РАСТЕЖА И РАЗВИТИЕТО НА РАСТЕНИЯ

Светлана Велинова

Минно-геоложки университет "Св. Иван Рилски", 1700 София

РЕЗЮМЕ. Отглеждането на растения на изкуствена светлина в последните години доби особена популярност. От една страна това е икономически изгодно за места със слабо слънчево греене – през зимните месеци или на места над 50–ия паралел. Дори в условията на нашата страна, през зимата е икономически изгодно да се отглеждат някои растения на изкуствено осветление. От друга страна, интерес представлява също и отглеждането на растения в Космоса - при по-продължително пребиваване извън Земята, където освен за снабдяването с кислород, на космонавтите ще бъде нужна растителността като храна и средообразуващ фактор.

Известно е, че фотосинтезата при растенията има максимална ефективност при облъчване със синя и червена светлина. За да се изследва коя част от спектъра на видимата светлина влияе най-силно върху растежа и развитието на растенията, в НИЛ "Осветителна техника" към Минно-геоложки университет "Св. Иван Рилски" беше създадена специализирана осветителна уредба. Тя е подобрен вариант и функционално продължение на осветителната уредба от 2015 г. Съставена е от 7 кабини с размери 600x600x1250мм, осветявани от светодиодни модули, всеки излъчващ в тясна област от видимия спектър. Размерите на кабините са подходящи за отглеждане на растения и изследването на пълния им жизнен цикъл, което включва освен получената биомаса, така и качествени показатели като цвят, мирис, вкусови качества и др. С помощта на новосъздадената осветителна уредба може да се изследва влиянието на светлина с различна дължина на вълната върху ефективността на фотосинтезата. Изследванията ще позволят да се отглеждат растения при изкуствена светлина с минимален разход на енергия.

Ключови думи: LED, photosynthesis, photosynthetic active radiation (PAR), growth of plants, light spectrum

Introduction

In recent years cultivation of artificial light plants has gained special popularity. On one hand, it is economically advantageous for places with low sunshine - in the winter months or in places above the 50th parallel. Even in the conditions of our country, in the winter months it is economically advantageous to grow some vegetables in artificial lighting. Plant growing in space is also of interest - for longer stays outside the Earth where, besides supplying oxygen and carbon dioxide, cosmonauts will need vegetation as a food and a place to rest.

To achieve photosynthesis, a critical level of illumination is required. Photosynthesis in plants has maximum efficacy in irradiation with blue and red light. (For comparison, the human eye has a maximum sensitivity in the yellow-green range, about 555 nanometres.) (Fig. 1).

Blue and red rays affect photosynthesis directly and indirectly. Blue beams (70 kcal / mole) have about 1.5 times more energy than red (40 kcal / mole). According to quantum theory, once a photon replaces only one electron of the pigment molecule, the blue loses more unproductive energy. It was observed that in normal illumination with the same energy of blue and red light, photosynthesis is more effective with red rays. This can be explained by the fact that, with the same energy, more red quanta will fall on the leaves and therefore more pigment molecules will be excited.

At a high level of brightness, however, blue rays have the advantage because they activate protein synthesis and this has a stimulating effect on the carboxylating enzymes, while the red rays - enhance the formation of carbohydrates. The addition of blue light (about 20%) to the red, significantly enhances photosynthesis and can be used in greenhouse production.

The efficiency of conversion of light energy into chemical energy in plants is estimated to be between 3 and 6%. The actual effectiveness of photosynthesis varies greatly with changes in the light spectrum, intensity of light, temperature and carbon dioxide concentration. This part of the solar radiation spectrum (400-700 nm) is called photosynthetic active radiation (PAR) (Fig. 1). In the process of photosynthesis, practically only 1-3% of PHARE is used. Typically, PAR is expressed in μmol photons m-2s-1.

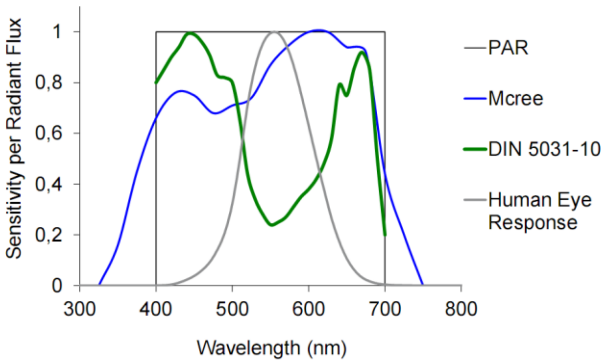

Fig. 1. Different methods of weighting the light spectrum

McCree measured three physiological parameters, including the quantum yield of photosynthesis, action, and absorptance. Physiologically, it describes the maximum photosynthetic efficiency with which light can be converted into chemical energy at low light (Fig. 1).

It is also possible to calculate the effective spectrum of photosynthesis, as its values are taken from DIN 5031-10 (Fig. 1).

The superior plants (Embryophyta) photosynthesise through leaves and stems that are rich in photosynthetic structures – chloroplasts. (Although they do not participate directly in photosynthesis, the roots are also involved.)

Photosynthesis (air feeding) is performed in the tilacloid membranes of the chloroplasts. (Fig. 2).

The chloroplasts perform: absorption of light from chlorophyll; transformation of light energy into chemical; fixing and reducing CO2; photolysis of the water.

The main role in photosynthesis plays the plant pigments, which act as primary acceptors of the light quanta and carry out the further transformation of the chemical energy.

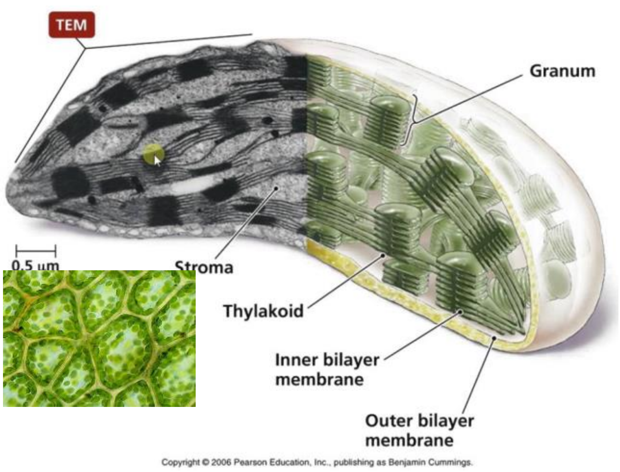

Fig. 2. Structure of the chloroplast

Plant pigments are divided into 4 types: chlorophylls, carotenoids, phycobiliens, and anthocyanins.

The main property of chlorophyll is to selectively absorb the light rays - a maximum absorption in the red area at a wavelength of 668 nm; fluorescein - dissolved in organic solvents emit red light (Krumov, A.).

Chlorophyll a and b is mainly responsible for the photosynthesis and for the definition of the area for PAR. Carotenoid are further photosynthetic pigments also known as antenna pigments like carotenoids-carotene, zeaxanthin, lycopene and lutein etc. (Fig. 3).

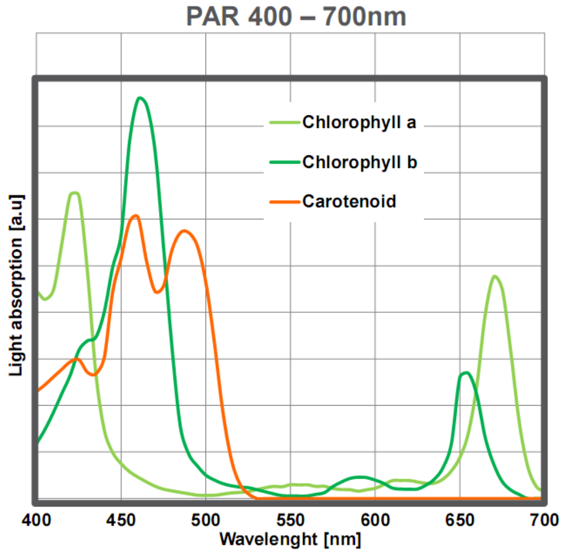

Fig. 3. Spectral sensitivity in photosynthesis (portions of the light spectrum used by the main pigments)

For some time, leading light source manufacturers have been working hard to create effective photosynthesis lamps by producing high-pressure sodium, metal halide, luminescent sodium lamps, and so on.

In recent years, due to the rapid development of LED technology, specialised photoinitiator luminaires are already available from many companies. Examples of emission spectra of such light sources are shown in Figure 4.

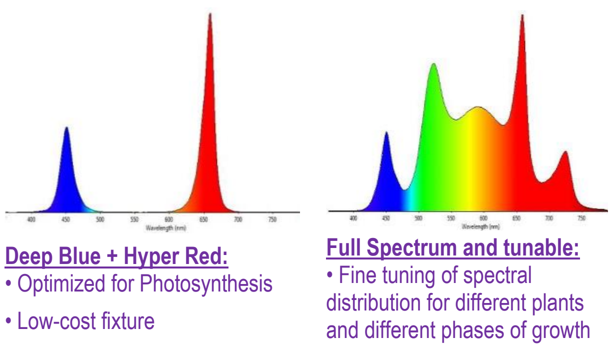

Fig. 4. Variations of radiation spectra of specialised photosynthesis luminaires

The advantage of horticultural lighting of LEDs is that a single-color LED emits light in a narrow spectral band, resulting in a saturated colour. There is also the possibility to reproduce several spectra with single-colour LEDs.

Realization

In order to investigate which part of the spectrum has the greatest influence on the photosynthesis at SRL "Lighting Engineering" at the University of Mining and Geology "St. Ivan Rilski" (UMG), a specialised lighting system was set up in 2015. It consists of 18 LEDs, each of which emits in a narrow area of the spectrum and has an intensity of photosynthetic radiation of 300-500 µmol / m3 (Table 5 and Fig. 6) and Table 1 (Velinova, 2015).

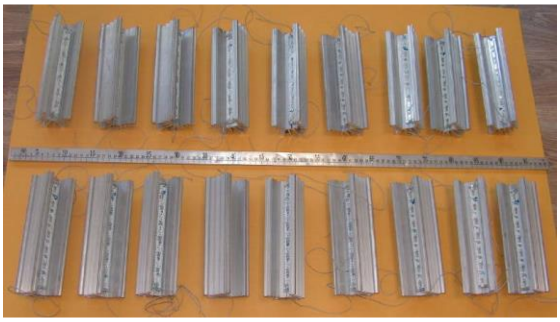

Fig. 5. 18 luminaires, each of which radiates in a narrow area of the visible spectrum

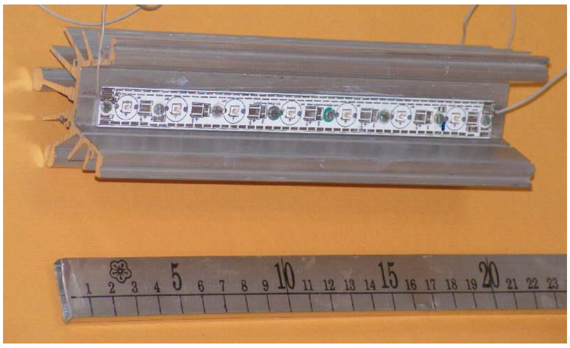

Fig. 6. One of the LED luminaires

The purpose of this system is to investigate the influence of particular parts of the light spectrum on the quantitative and qualitative characteristics of photosynthesis in different plant species, while tracking their growth and development.

Table 1.

LED №:	LED type	Length on wave λ / nm
1.	INDIGO BLUE	402 +/-3
2.	INDIGO BLUE	407 +/-3
3.	DEEP BLUE	422 +/-2
4.	DEEP BLUE	427 +/-2
5.	ROYAL BLUE	452 +/-2
6.	ROYAL BLUE	457 +/-2
7.	BLUE 1	462 +/-2
8.	BLUE 2	472 +/-2
9.	CYAN 1	497 +/-2
10.	CYAN 2	502 +/-2
11.	GREEN 1	522 +/-2
12.	GREEN 2	527 +/-2
13.	AMBER	592 +/-2
14.	RED 1	616 +/-3
15.	RED 2	625 +/-5
16.	TRUE RED 1	652 +/-2
17.	TRUE RED 2	663 +/-2
18.	DEEP RED	730 +/-10

The following species were selected as test subjects: salad (Lactuca sativa), cloves (Dianthus caryophyllus), French marigold (Tagetes patula), and tomato (Solanum lycopersicum). The following morphological indicators were examined: plant height; foliage development; number of developed leaves; stem length; length and width of the leaves; length and development of the root system.

The results of these studies are published in (Velinova, 2017a; 2017b; 2018).

Fig. 7. Test facility - mounted luminaires and plants

In the above-mentioned LED lighting system, the volume of the chambers and the size of the plants examined is limited to the dimensions of about 30x30x40 cm (Fig. 7). That is why, in 2019, another specialised lighting system was set up at the SRL "Lighting equipment" at the UMG. It is an improved version and a functional continuation of the lighting system from 2015. It consists of 7 cabins with dimensions 60x60x125 cm, illuminated by LED modules, each emitting in a narrow area of the visible spectrum. (Fig. 8 - 9 and Table 2).

Fig. 8. Specialised lighting system 2 in 2019 - cabins with illuminators and studied plants

The luminaires are made of aluminium, donated by BSM. In the first five chambers 3 luminaires with a light emitting module are housed (Figure 10, Table 2). In each module 40 LEDs are mounted GA type CS8PM1.23, GB + CS8PM1.13, GH CSSPM1.24, GT CS8PM1.13, GY CS8PM1.23. The drivers are part of a donation by OSRAM. The total power of the luminaires for each cab is about 160W.

A specialised LED light for photosynthesis is installed in chamber № 6.

In chamber № 7 is installed a LED luminaire emitting a neutral white light - 4337 K, which will be used as a cabin with control measurement samples (Fig. 9, 11 and 12; Table 2).

Table 2.

Camera №	Luminaire	Length on wave λ / nm	PAR/ mmol	Power/ W
1.	BLUE	467 +/-3	298	150
2.	GREEN	523 +/-3	219	150
3.	AMBER	601 +/-2	77	150
4.	RED	626 +/-2	237	150
5.	DEEP RED	658 +/-2	333	150
6.	BLUE / RED	447 / 650	333	160
7.	WHITE	4337 K	188	180

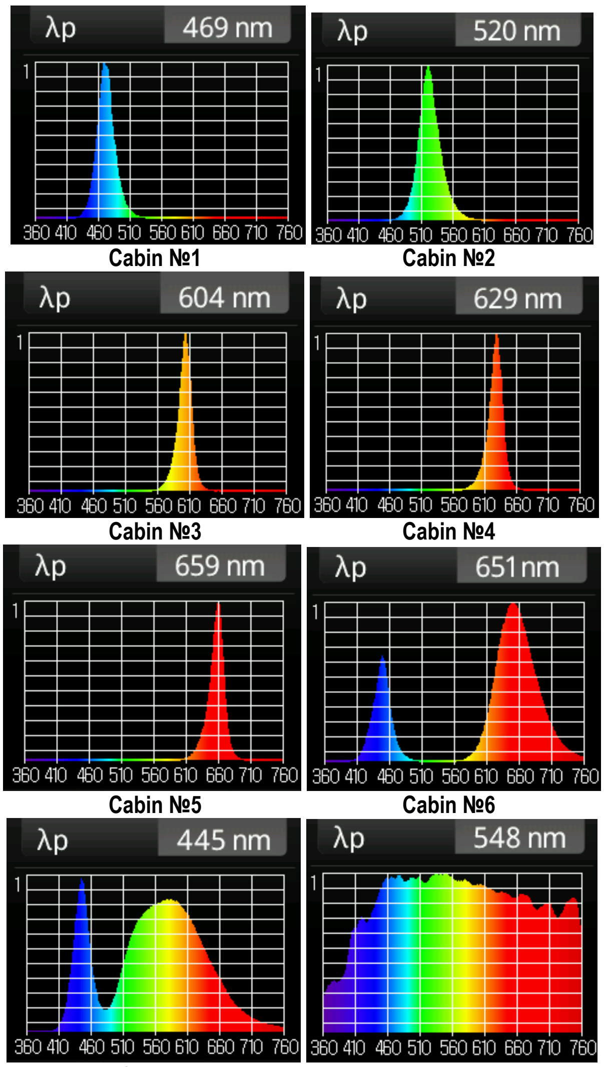

Fig. 9. Radiation spectra of each of the cameras and a spectrum of daylight (as a control)

Cabin sizes are suitable for plant growing and their full life cycle research, which includes biomass in addition to qualitative indicators like colour, smell, taste, etc.

With the help of the newly-created lighting system, the effects of light of different wavelengths on the effectiveness of photosynthesis as well as the growth and development of plants can be studied. Research will allow plants to grow under artificial light with minimal energy consumption.

Fig. 10. Cabins № 1 to 5. Lights, each of them emitting in a narrow range of the spectrum

Fig. 11. Cabin No 6 - Specialised luminaire designed for photosynthesis

Fig. 12. Cabin No 7 - Illumination light emitting neutral white light - 4337 K (control)

So far, some preliminary experiments have been made in the newly created chambers to study the impact of the light spectrum. As an experimental species the tomatoes (Solanum lycopersicum) - interdimensional strain "Milliana" are chosen and the strawberries (Fragaria sp.) - self-pollinating variety are used. (Fig. 13).

The nourishment of the plants is hydroponic using food solutions according to recipes recommended by Prof. Hristo Simidchiev (Simidchiev, Kanazirska, 2017). Other important parameters influencing their growth and development are temperature, humidity, CO2, etc., which are maintained at constant rate.

Growth assessment is done by measuring certain parameters (plant height, stem thickness, number of leaves, leaf size, number of cobs or runners, number of flowers, number of worms, number of fruits ripened, quality evaluation of fruits, etc.); visually - by assessing the total plant habit and assessing their health status.

Additionally, the chlorophyll content of plant leaf samples (in relative units) was measured using the Chlorophyll Content Meter CCM-200.

Initial results of the first samples in these chambers can be seen in Fig. 13 and 14.

Fig. 13. Cabin No 7 - Test plants on 06.06.19 (control)

Fig. 14. Cabin No 7 - Test plants on 12.07.19 (control)

It is envisaged to carry out experiments with the following types of plants: salads (Lactuca) and other leafy vegetables, spices and essential oil plants, wheat and others. Poaceae, Fabaceae, Orchidaceae, other members of the Solanaceae family, some suitable representatives of tree-shrub species. (Kalinkov, Pavlov, 1993).

The pursuit of plant selection is to use those that have a strong light response as a factor; to be suitable both as indicators and for growing in the conditions of existing cabins, if possible self-pollinating (or at least one-domed) and last but not least, suitable for consumption.

It is planned to carry out similar experiments with representatives of unicellular algae together with the Department of Engineering Geoecology, and for this purpose special containers will be made which will be illuminated with the same types of diodes mentioned above.

Acknowledgements. Scientific and Research Laboratory "Lighting Equipment", Assoc. Prof. Dr. Eng. Krasimir Velinov, Prof. Dr. Veselina Ilieva, Prof. Dr. Hristo Simidchiev, Prof. Dr. Vasily Goltsev, Assoc. Prof. Dr. Eng. Svetlana Bratkova.

References

Aleksandrov, N. 2012. *Fundamental theory of colors*. East-West, 255 p.

Angelov, V. 2018. Irradiator for growing plants without sunlight. – *VII Balkan conference on lighting - Balkanlight 2018, 04-06 june, Sofia*, 161–164.

Blankenship, R. 2014. *Molecular mechanisms of photosynthesis.* Wiley Blackwell, Washington University in St. Louis, Missouri, USA, 314 p.

Bula, R. J., D. Tennessen et al. 1994. Light emitting diodes as a plant lightning source. – *International Lightning in Controlled Environments Workshop, NASA-CP-95-3309*, 225–267.

DIN 5031-10, Deutsche norm, 2000. 03, 16-18.

Goltsev, V., M. Kaladzhi, M. Kuzmanova, S. Allahverdiev. 2014. Chlorophyll fluorescence in studies of the physiological state of plants. – *Izhevsk Moscow, Institute for Computer Studies*, 197 p.

Howell, C. H. 2009. *Flora mirabilis – how plants have shaped world knowledge, health, wealth, and beauty*. – National Geographic Society, Washington, D.C., 175 p.

Ilieva, I., Y. Naydenov. 2012. Influence of green/blue light ratio on leaf chicory physiology in rgb light. – *Eighth Scientific Conference With International Participation – Space, Ecology, Safety, 4-6, 12, Sofia, Bulgaria*, 239–243.

Ilieva, I., Y. Naydenov. 2011. Morphometric characteristics and photosynthetic activity of leaf chicory in RGB LED lighting. – *Seven Scientific Conference with International Participation, SES*, *Sofia, Bulgaria, 29.11-01.12*, 119–124.

Ilieva, V. 2013. Impact with optical radiation on plant and microbiological sites. – In: *Impact and study with electromagnetic fields in agriculture,* under No. 82/93 in the Central Technological Library, Sofia, 39–180.

Ilieva, V., S. Velinova. 2017. Photosynthetic active radiation - Theoretical prerequisites, basic systems and measuring units for it's measurement. *XVI National Conference with International Participation Bullight / Bulgaria Light 2017 and BalkanlightJunior 2017, 25–27 may, Sozopol*, 62–64.

Ilieva, V., S. Velinova. 2017. On some specific aspects of photosynthesis and photosynthetic active radiation. – *International Scientific Conference Uniteh 2017, 17-18 November, Gabrovo*, *1*, 154–159.

Ilieva, V., S. Velinova. 2018. LED-technology in greenhouse horticulture. *VII Balkan conference on lighting - Balkanlight 2018, 04-06 june, Sofia*, 157–160.

Ilieva, M. 2017. LED Development trends – functions, management, applications. – *Bullight 2017 – Balkan Light Junior 2017, 27.05.2017, Sozopol*, 130–135.

Ilieva, M., V. Ilieva. 2014. LED Irradiation systems for plant growing. – *XV National Conference with International Participation Bullight / Bulgaria LIGHT 2014, 10–13 June, Sozopol*, 184–187.

ISBN 978-954-765-064-0, 167-184

Kalinkov, V., D. Pavlov. 1993. *Botany*. Martilen Publishing House, Sofia, 37–43; 428–429.

Krumov, A., N. Nikolova, V. Vassilev. Biocamera for the study of fluorescence in plants.

Kudryumov, N., K. Malishevski. 2008. *The Smart Greenhouse.* Ed. Allivgo, Sofia, 173 p.

Lalayants, I., I. S. Milovanova. 1989. Green, green grass. *Quantum, 7*, Nauka, Moscow, 6–9.

Massa, G. D., J. Emmerich. 2006. Plant-growth lighting for space life support: a review. – *Gravitational and Space Biology 19 (2)*, 8, 19–29.

Mitchell, C., A. Jan Both. 2012. LEDs: The Future of Greenhouse Lighting! – *Chronica horticulturae, 52*, 1, 6–12.

OSRAM Horticultural Lighting with LEDs Presentation. – Seminar Bulgarian National Committee on Illumination (BNCI) 2019-04-09.

Pavlov, D. 2006. *Phytocenology*. ED. House LTU, Sofia, 250 p.

Poryazov, I., V. Petkova, N. Tommekova. 2013. *Vegetable production.* Publishing House "DIMI 99", Sofia.

Rittershausen, B. and W. 2002. *Orchids a practical handbook*. Hermes House.

Rossi, M., D. Casciani. 2018. Lighting design research for horticultural vegetables growing: A case study. – *VII Balkan Conference on Lighting - Balkanlight 2018, 04-06 june, Sofia,* 145–149.

Simidchiev, H., V. Kanazirska. 2017. *For hydroponics from A to Z*. Kota publ., 496 p.

Velinova, S. 2015. LED Lighting system for the study of the photosynthesis. – *Annual of Mining and Geological University "St. Ivan Rilski", 58*, 3, 105–109.

Velinova, S. 2017. Possibilities for using of mining galleries for growing plants on artificial lighting. – *International Scientific Conference UNITECH 2017, November 17-18, Gabrovo*, *1*, 148–153.

Velinova, S. 2018. Growing plants on artificial lighting. – *VII Balkan Conference on Lighting - Balkanlight 2018, 04-06 June, Sofia,* 150-156.

Velinova, S., V. Ilieva. 2017. Influence of the spectrum of light on plant growth. – *XVI National Conference with International Participation Bullight / Bulgaria Light 2017 and BalkanlightJunior 2017, 25 - 27 May, Sozopol*, 55–61.